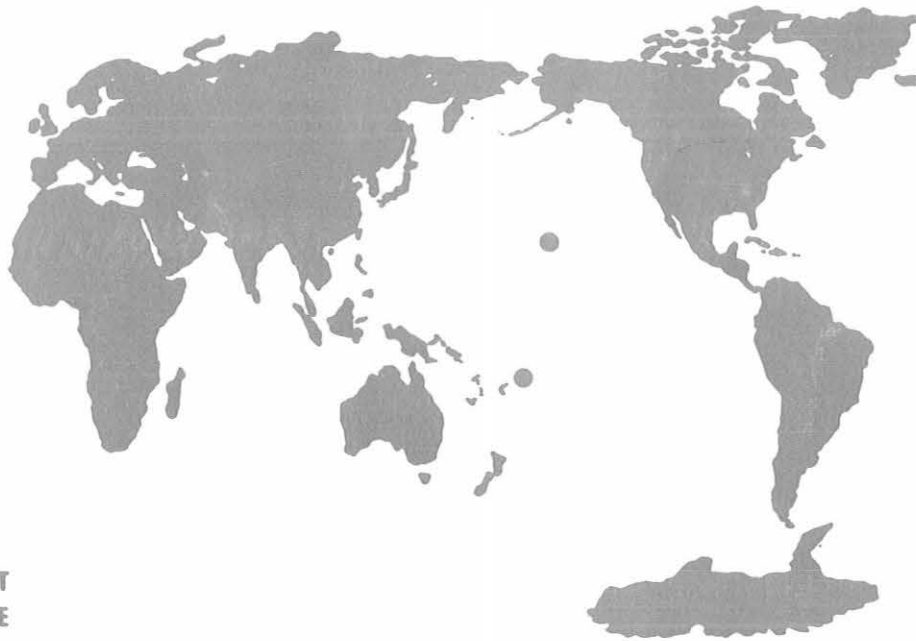


Climate Monitoring and Diagnostics Laboratory

No. 18

Summary Report 1989



U.S. DEPARTMENT
OF COMMERCE

NATIONAL
OCEANIC AND
ATMOSPHERIC
ADMINISTRATION

ENVIRONMENTAL
RESEARCH
LABORATORIES





Climate Monitoring and Diagnostics Laboratory No. 18

Summary Report 1989

Walter D. Komhyr, Editor
Rita M. Rosson, Assistant Editor

Boulder, Colorado

December 1990

U.S. DEPARTMENT OF COMMERCE

Robert A. Mosbacher, Secretary

National Oceanic and Atmospheric Administration

John A. Knauss, Under Secretary for Oceans and Atmosphere/Administrator

Environmental Research Laboratories

Joseph O. Fletcher, Director

NOTICE

Mention of a commercial company or product does not constitute an endorsement by NOAA Environmental Research Laboratories. Use for publicity or advertising purposes of information from this publication concerning proprietary products or the tests of such products is not authorized.

ACKNOWLEDGMENT

The editors appreciate the excellent response from the cooperative programs in contributing to this report. The editors also thank Christine Sweet for her outstanding editorial assistance.

For sale by the National Technical Information Service, 5285 Port Royal Road
Springfield, VA 22161

Contents

CMDL Staff, 1989	vi
CMDL Station Information	vii
1. Introduction	1
2. Observatory Reports	2
2.1. Mauna Loa	2
2.1.1. Operations	2
2.1.2. Programs	2
2.2. Barrow	7
2.2.1. Operations	7
2.2.2. Programs	8
2.3. Samoa	10
2.3.1. Operations	10
2.3.2. Programs	11
2.4. South Pole	13
2.4.1. Operations	13
2.4.2. Programs	13
2.5. References	15
3. Aerosols and Radiation Monitoring Group	16
3.1. Continuing Programs	16
3.1.1. Surface Aerosols	16
3.1.2. Solar and Thermal Radiation	18
3.1.3. Solar Radiation Facility	21
3.2. Special Projects	22
3.2.1. CN Counter Comparison at MLO	22
3.2.2. Radiative and Meteorological Effects of Transient Weather Disturbances at the South Pole During Winter	24
3.2.3. Confirmation of Ground-Based Measurements of Ozone and Stratospheric Aerosol and Computations of Umkehr Profile Aerosol Errors	27
3.3. References	30
4. Carbon Cycle Group	31
4.1. Continuing Programs	31
4.1.1. Continuous In-Situ and Flask Sample Carbon Dioxide Measurements	31
4.1.2. Flask Sample Methane Measurements	34
4.1.3. In-Situ Methane Measurements at MLO	35
4.1.4. In-Situ Methane Measurements at BRW	35
4.1.5. Flask Sample Carbon Monoxide Measurements	36
4.2. Special Projects	38
4.2.1. AGASP III	38
4.2.2. Shipboard Sampling	38
4.3. References	39
5. Ozone Group	40
5.1. Continuing Programs	40
5.1.1. Total Ozone Observations	40
5.1.2. Dobson Spectrophotometer Calibrations	41
5.1.3. Umkehr Observations	41
5.1.4. Tropospheric Ozone	43
5.1.5. Ozonesonde Observations	43
5.1.6. Validation of Satellite Instrument Ozone Data	44

5.1.7.	Stratospheric Water Vapor	44
5.2.	Special Projects	47
5.2.1.	Stratospheric Ozone Intercomparison Campaign	47
5.2.2.	Ozonesonde Observations at Mirny, Antarctica	48
5.2.3.	Ozonesonde Observations at BRW	48
5.3.	References	49
6.	Acquisition and Data Management	50
6.1.	Continuing Programs	50
6.1.1.	Station Climatology	50
6.1.2.	Data Management	54
6.2.	Special Project: Atmospheric Trajectories	57
6.3.	References	59
7.	Air Quality Group	60
7.1.	Continuing Programs	60
7.1.1.	Introduction	60
7.1.2.	Atmospheric Lidar Validation Experiment	60
7.2.	Special Project: Sulfur Monitoring at MLO	62
7.3.	References	63
8.0	Nitrous Oxide and Halocarbons Group	64
8.1.	Continuing Programs	64
8.1.1.	Flask Samples	64
8.1.2.	RITS Continuous Gas Chromatograph Systems at CMDL Baseline Stations	64
8.1.3.	Low Electron Attachment Potential Species	67
8.1.4.	Gravimetric Standards	67
8.2.	Special Projects	69
8.2.1.	RITS <i>Discoverer</i> Cruise	69
8.2.2.	FT-IR Spectrometer Archive Project	69
8.2.3.	Airborne Gas Chromatograph	71
8.3.	References	72
9.	Director's Office	73
9.1.	A Joint U.S./U.S.S.R. Experiment for the Study of Desert Dust and its Impact on Local Meteorological Conditions and Climate	73
9.1.1.	Introduction	73
9.1.2.	Purpose	73
9.1.3.	Activities	73
9.1.4.	Summary	74
9.2.	Annual Ozone Cycle and Decade Trend at South Pole	75
9.2.1.	Introduction	75
9.2.2.	Seasonal Ozone Variations at South Pole	75
9.2.3.	Long-Term Decreasing Ozone Trend at South Pole	75
9.2.4.	Summary and Conclusions	76
9.3.	Wintertime Black Carbon Aerosol Measurements Over the Southwestern United States, December 1989	77
9.3.1.	Introduction	77
9.3.2.	Experimental Methods	77
9.3.3.	Results and Discussion	77
9.4.	References	80
10.	Cooperative Programs	81
	Precipitation Chemistry	
	<i>R.S. Artz</i>	81

Continuous Aerosol Monitoring with the Epiphaniometer at MLO <i>U. Baltenperger, H.W. Gaeggeler, and D.T. Jost</i>	83
Antarctic Ultraviolet Spectroradiometer Monitoring Program <i>C.R. Booth, T. Lucas, J. Yeh, and D. Neuschuler</i>	85
Chemical Resolution of Fine Aerosol Mass at MLO: The Role of Organic Matter <i>T.A. Cahill, L.K. Wilkinson, and R.A. Eldred</i>	88
Artificial Windshielding of Precipitation Gauges in the Arctic <i>G.P. Clagett</i>	92
UVB Monitoring Data from Rockville, Maryland <i>D.L. Correll, C. Clark, R. Goodrich, and D. Hayes</i>	93
Roberston-Berger UVB Meter <i>G.F. Cotton</i>	95
The CSIRO Latitudinal Gradient Study: Methane Data from Air Samples Collected at CMDL Baseline Observatories and at Cape Grim, Tasmania <i>P. Fraser, P. Steele, R. Francey, and G. Pearman</i>	97
Secular Variation in the Carbon-13 Content of Atmospheric Carbon Dioxide <i>I. Friedman, J. Gleason, and A. Warden</i>	101
Snow Bunting Nesting Study at Barrow, Alaska <i>J.C. George, K. Bagne, and M. Leinberger</i>	104
A New Look at Optical Depth Retrieval With the Multiple Field of View Sunphotometer <i>P.F. Hein, J.M. Davis, and S.K. Cox</i>	105
Tropospheric Nitrogen Oxide Measurements During Spring at Barrow <i>R.E. Honrath and D.A. Jaffee</i>	107
Chemical Analyses of Atmospheric Particulates and Gases at MLO <i>C.R. Jensen, X. Cal, and W.H. Zoller</i>	110
A Temperature Inversion Climatology for Barrow: 1976-1985 <i>J.D. Kahl</i>	112
The Global Precipitation Chemistry Project <i>G.E. Likens and J.M. Miller</i>	115
Radioactivity in the Surface Air at BRW, MLO, SMO, and SPO <i>R. Larsen and C. Sanderson</i>	117
Total Nitrate Variations at Mauna Loa <i>G. Lee and B.J. Huebert</i>	119
Seasonal and Latitudinal Trends in the ¹³ C/ ¹² C Ratio of Methane <i>P. Quay, S. King, J. Stutsman, and D. Wilbur</i>	121
Aerosol Constituents at American Samoa, November 1989 <i>D.L. Savoie, J.M. Prospero, R. Arimoto, and R.A. Duce</i>	123
Update on the O-Ring Bias as Determined from MLO Precipitation Chemistry Samples <i>G.J. Stensland</i>	125
Trends of the Carbon Isotopi Composition of Atmospheric Methane in the Southern Hemisphere <i>C.M. Stevens and A. Engelkemeir</i>	126
Bromine and Surface Ozone Atmospheric Chemistry at Barrow, Alaska, During Spring 1989 <i>W.T. Sturges, R.C. Schnell, S.J. Oltmans, S. Landsberger, and S.-M. Li</i>	127
USGS Barrow Observatory <i>J. Townshend</i>	130
Radon from Distant Continents Detected at the Mauna Loa Observatory <i>S. Whittlestone</i>	131
11. International Activities 1989	134
12. Publications and Presentations by CMDL Staff, 1989	136
13. Acronyms and Abbreviations	139

CMDL Staff, 1989

Director's Office

James Peterson, Director
Bernard Mendonca, Deputy Director
Ellen Hardman, Secretary
Antonio Diaz, Guest Scientist
Dale Gillette, Physical Scientist
Jon Kahl, NRC Post Doctorate
Tezz Marquardt, CIRES
Karen McSwain, CIRES Student
Ted Mullen, Electronic Technician
Rita Rosson, Editorial Assistant
Russell Schnell, CIRES
Patrick Sheridan, NRC Post Doctorate
Donna Smith, CU Work Study
Matthew Steiman, CU Work Study
William Sturges, CIRES
Denise Theede, Program Clerk
Mark Vanderiet Elect. Tech.
Bill Van Leeuan, CU Work Study

Acquisition and Data Management Group

Gary Herbert, Chief
Dee Dee Mitchell, Secretary
Mark Bieniulis, CIRES
Michael Ellis, Physical Science Aid
Joyce Harris, Computer Specialist
James McCutcheon, CIRES
Steve Roughton, Computer Assistant
Kenneth Thaut, Electronic Technician

Aerosols and Radiation Monitoring Group

John DeLuisi, Chief
Marilyn Van Asche, Secretary
Larry R. Arnold, Physical Science Aid
Barry Bodhaine, Meteorologist
Ellsworth Dutton, Meteorologist
Rudy Haas, Mathematician
Fred Kreiner, CIRES
David Longenecker, CIRES
Donald Nelson, Meteorologist
Gayland Pounder, Physical Science Aid
Patrick Reddy, CIRES
Kevin Schlatter, CIRES
Michael Shanahan, Physical Science Aid
Scott Siao, Physical Science Aid
Robert Stone, CIRES
Barbara Thomson, Physical Science Aid

Air Quality Group

Joseph Boatman, Chief
Dee Dee Mitchell, Secretary
Cynthia Crouch, CIRES
Laureen Gunter, Meteorologist
Young Kim, CIRES
Menachem Luria, CIRES
John Ray, CIRES
Herman Sievering, CIRES
Timothy Straube, Physical Science Aid
Charles Van Valin, Research Chemist
Dennis Wellman, Engineer
Stan Wilkison, Computer Programmer

Carbon Cycle Group

Pieter Tans, CIRES
Lee Prendergast, Secretary
Todd Aten, CIRES
Thomas Conway, Research Chemist
Brian Hirsch, CO-OP
Darryl Kaurin, CO-OP
Duane Kitzis, CIRES
Patricia Lang, CIRES
Amy Lee, Data Analyst Technician
Terry Lesoing, CO-OP
Russell Martin, CIRES
Kenneth Masarie, CIRES
Paul Novelli, CIRES
Vernon Preston, CO-OP
L. Paul Steele, CIRES
Gregory Summers, CO-OP
Kirk Thoning, CIRES
Anthony Vaughn, Physical Science Aid
Lee Waterman, Research Chemist

Ozone Group

Walter Komhyr, Chief
Lee Prendergast, Secretary
Brandon Bird, Physical Science Aid
Robert Evans, CIRES
Robert Grass, Physicist
Gloria Koenig, Computer Programmer
Jeffrey Lathrop, CO-OP
Kent Leonard, CIRES
Samuel Oltmans, Physicist
Dan Opperman, CO-OP
Christopher Platt, Physical Science Aid
Frank Polacek, III, Meteorological Technician
Dorothy Quincy, CIRES
Jim Wendell, Electronic Technician
LaRae Williams, Physical Science Aid

Nitrous Oxide and Halocarbons Group

James Elkins, Chief
Marilyn Van Asche, Secretary
Christina Brunson, CIRES
James Butler, Research Chemist
Thomas Baring, Physical Science Aid
Scott Cummings, Physical Science Aid
Keith Egan, CIRES
Brad Hall, CIRES
Bradley Halter, CIRES
Thayne Thompson, Physicist
Jeffrey Sczechowski, CIRES
Thomas Swanson, CIRES

Barrow Observatory

Daniel Endres, Station Chief
Timothy Quakenbush,
Electronic Engineer

Mauna Loa Observatory

Elmer Robinson, Director
Judith Pereira, Program Support Technician
Ame Astring, Physical Scientist
Lynne Borman, Physical Science Aid
John Chin, Physicist
Thomas DeFoor, Electronic Engineer
Barbara Kerecman, Data Clerk
Darryl Kuniyuki, NOAA Jr. Fellow
Steven Ryan, Physical Scientist
Mamoru Shibata, Electronic Technician
Alan Yoshinaga, Chemist

Samoa Observatory

Steven Ryan, Station Chief
Carl Farmer, Station Chief
M. Emily Wilson-Godinet,
Electronic Technician

South Pole Observatory

Elizabeth Crozer, NOAA Corps
Mark Winey, Elect. Engineer
Carl Groeneveld, NOAA Corps
Fred Schrom, Elect. Technician

CMDL Station Information

Name:	Barrow (BRW)	Mauna Loa (MLO)
Latitude:	71.3233	19.533
Longitude:	156.6067	155.578
Elevation:	0 km	3.4 km
Time Zone:	GMT -9	GMT -10
Office Hours:	8:00 am-5:00 pm	8:00 am-5:00 pm
Telephone		
Office hours:	(907) 852-6500	(808) 961-3788
After hours:	(907) 852-6500	(808) 961-3788
Postal Address:	Officer in Charge NOAA/ERL/CMDL Pouch 8888 Barrow, AK 99723	U.S. Dept. of Commerce NOAA - Mauna Loa Observatory P.O. Box 275 Hilo, HI 96720
Freight Address:		U.S. Dept. of Commerce NOAA - Mauna Loa Observatory 154 Waiianuenue Ave. Hilo, HI 96720
Name:	Samoa (SMO)	South Pole (SPO)
Latitude:	-14.2522	-90.000
Longitude:	170.5628	0.000
Elevation:	0.03 km	2.8 km
Time Zone:	GMT -11	GMT +12
Office Hours:	8:00 am-5:00 pm	8:00 am - 5:00 pm
Telephone:		
Office hours:	011-(684) 622-7455	Relayed through CMDL Boulder
After hours:	011-(684) 699-9953	
Postal Address:	U.S. Dept. of Commerce NOAA - CMDL Samoa Observatory P.O. Box 2568 Pago Pago, American Samoa 96799	Officer in Charge, CMDL Program Box 400 USARP C/O NAVSUPFORANTARCTICA FPO San Francisco, CA 96692 ATTN: South Pole #S-257 J.Lowell

CLIMATE MONITORING AND DIAGNOSTICS LABORATORY

NO. 18

SUMMARY REPORT 1989

1. Introduction

The year 1989 marked several significant events in the history and organization of NOAA's Geophysical Monitoring for Climatic Change (GMCC) program that was formed in 1972. The most important was the retirement of Dr. Lester Machta as the Director of NOAA's Air Resources Laboratory, GMCC's parent Laboratory. Lester was the force behind the formation of GMCC, and he served as its Laboratory Director continuously through 1989. In the beginning there were only two GMCC Observatories—Mauna Loa and the South Pole—and only a handful of scientists in Boulder. Under Lester's guidance and direction, GMCC grew to a \$5 million per year program with nearly 100 staff, four primary observatories, and many secondary sampling sites scattered over the globe. We continue to be gratified that the work we do has immediate application to international concerns about greenhouse gas climate warming and stratospheric ozone depletion.

In January 1990, as part of an ERL reorganization, GMCC activities were transferred, along with those of the NOAA Climate Research Group, to a newly formed NOAA Laboratory, the Climate Monitoring and Diagnostics Laboratory (CMDL). Dr. Eldon Ferguson was named the CMDL Director. Eldon has many years of experience in the NOAA research laboratories, including previous direction of the Aeronomy Laboratory. With our new structure, we look toward the future with a positive view of the usefulness of our long-term monitoring activities and their application to research in climate and global change.

The title change this year for our annual report reflects the reorganization described above. Note that although the title has changed, the numbering of the reports has continued. The research summary for 1989 of the Climate Research Group is not included in this report.

2. Observatory Reports

2.1. MAUNA LOA

E. ROBINSON

2.1.1. OPERATIONS

In January 1989, the eruption of Kilauea Volcano on the Island of Hawaii passed its sixth "birthday." During 1989 the eruption activity caused an increasing amount of damage in Kalapana and coastal areas of the Hawaii Volcanoes National Park. Because of the attention given to this eruption by the media, it is useful to evaluate the eruption activity relative to the MLO operations and programs. First, these Kilauea lava flows originate from a site on the east rift zone of Kilauea 35 km south of Hilo and 58 km east-southeast of MLO at an altitude of 670 m MSL. The fumes produced by this eruption typically move toward the southwest from the emission site and are limited primarily to the marine boundary layer. Prevailing winds bring the volcanic plume haze to the western or Kona side of the island and from there the plume occasionally reaches MLO as part of the typical afternoon boundary layer upslope wind regime. The program of sulfur gas monitoring was able to document incidents of this nature. However, with regard to the long-term atmospheric background monitoring program conducted at MLO, no significant impact is believed to result from the Kilauea eruption because the Kilauea plume is mixed into the marine boundary layer and marine boundary layer upslope flow periods with or without volcanic constituents are generally excluded from the MLO record. Marine boundary layer events have always been of concern because they may have been influenced by biological effects (e.g., CO₂ vegetation exchange) or a wide variety of urban anthropogenic emissions. Thus we conclude that at present the additional presence of volcanic plume constituents in the marine boundary layer does not pose a problem for the MLO record.

The 1989 winter meeting of the AGU held in San Francisco in December had a major symposium devoted to the photochemical field experiment (MLOPEX) conducted at MLO in May and June 1988 by NCAR and other atmospheric research groups. NCAR organized both the 1988 experiment and the 1989 AGU symposium.

2.1.2. PROGRAMS

The major CMDL and cooperative programs carried out at MLO in 1989 are shown in Table 2.1, which is similar to Table 2.1. of the 1988 Summary Report [Elkins and Rosson, 1989], with the following exceptions. Three programs were added (one CMDL and two cooperative) and three programs were dropped (one CMDL and two cooperative). The CMDL aerosol measurement program was expanded to include continuous monitoring of carbon aerosol concentrations using an aethalometer. This instrument was installed in May, although difficulties in matching the output signal to

the CAMS delayed its full operation. In April 1989, the CMDL microbarograph at MLO was removed from service. In May, continuous monitoring of radon was begun with the installation of an instrument by ANSTO, and in December The Paul Scherrer Institute of Switzerland installed an epiphaniometer at MLO, a device that measures the total surface area of the atmospheric aerosol particles. Sun-photometer observations of turbidity for AES Canada and the collection of flask air samples for USGS, Denver, for ¹³C measurements were discontinued. Further information about some of the MLO programs is given next and also in subsequent sections where the technical results of CMDL groups and cooperative investigators are presented.

Carbon Dioxide

The CMDL Siemens Ultramat-3 and the SIO Applied Physics IR CO₂ analyzers were operated side by side without significant downtime throughout the year. Routine maintenance and calibrations were done on both instruments as required and according to schedule. The Ultramat-3 instrument has been in operation continuously since August 5, 1987.

The preliminary average MLO CO₂ concentration for 1989 was 352.8 ppm. The growth rate between 1988 and 1989 was approximately 2.0 ppm yr⁻¹. This is an increase in the CO₂ growth rate compared with that of the early 1970s when it was only 0.7 ppm yr⁻¹. Outgassing from the volcanic vents at the caldera and along the northeast rift of Mauna Loa continued to cause periodic observable peaks in some of the CO₂ records. These events occurred primarily between midnight and 0800 LST of the following day, during the downslope wind regime. The erratic traces in the CO₂ records caused by these events were easily identified by visually scanning the chart records or by setting up a computerized data screening procedure. Table 2.2 gives the estimated frequency of Mauna Loa venting for 1989. Such venting episodes were detected and excluded from the MLO CO₂ record mainly on the basis of criteria for CO₂ concentration, CO₂ variability, and wind sector. The annual total of 84 hours for these events in 1989 was 1.0% of the total time when CO₂ was measured at MLO. The criterion for the CO₂ standard deviation screening was 1.0 ppm, which is the value suggested by Thoning *et al.* [1989]. Estimated venting episode frequencies reported in previous *Summary Reports* [e.g., Elkins and Rosson, 1989; Bodhaine and Rosson, 1988], used other and sometimes less definitive criteria than were used to obtain the estimates of Table 2.2.

Methane

CH₄ concentrations were available throughout the year from two types of observations: the continuous operation of a Carle automated GC, and weekly collection of air samples in 0.5-L glass flasks. The CH₄ GC is at MLO, and flask air samples are collected at both MLO and Cape Kumukahi at sea level on the easternmost point of the island. Although the Carle automated GC system can potentially monitor CO

TABLE 2.1. Summary of Measurement Programs at MLO in 1989

Program	Instrument	Sampling Frequency
<i>Gases</i>		
CO ₂	Siemens Ultramat-3 IR analyzer 3-L glass flasks†	Continuous 1 pair wk ⁻¹
CO ₂ , CH ₄	0.5-L glass flasks, through analyzer	1 pair wk ⁻¹
CH ₄	0.5-L glass flasks, P ³ pump unit†	1 pair wk ⁻¹
Surface O ₃	Carle automated GC	1 sample (24 min) ⁻¹
Total O ₃	Dasibi ozone meter	Continuous
O ₃ profiles	Dobson spectrophotometer no. 76	3 day ⁻¹ , weekdays
	Dobson spectrophotometer no. 76 (automated Umkehr method)	2 day ⁻¹
CFC-11, CFC-12, N ₂ O	Balloonborne ECC sonde	1 wk ⁻¹
CFC-11, CFC-12, N ₂ O, CCl ₄ , CH ₃ CCl ₃	300-mL stainless steel flasks	1 pair wk ⁻¹
N ₂ O	HP5890 automated GC	1 sample (3h) ⁻¹
Total sulfur gases	Shimadzu automated GC	1 sample (3h) ⁻¹
SO ₂	CSI flame photometric analyzer*	Continuous
	TECO pulsed fluorescence analyzer*	Continuous
<i>Aerosols</i>		
Condensation nuclei	Pollak CNC	1 day ⁻¹
	G.E. CNC*	Continuous
	TSI CNC*	Continuous
Optical properties	Four-wavelength nephelometer*: 450, 500, 700, 850 nm	Continuous
Stratospheric aerosols	Lidar, 694.3 nm	1 profile wk ⁻¹
Black carbon	Aethelometer	Continuous
<i>Solar Radiation</i>		
Global irradiance	Eppley pyranometers with Q, OG1, and RG8 filters	Continuous
Direct irradiance	Eppley pyrhelimeter (2) with Q filter* Eppley pyrhelimeter with Q, OG1, RG2, and RG8 filters	Continuous 3 day ⁻¹
	Eppley/Kendall active cavity radiometer	1 mo ⁻¹
Diffuse irradiance	Eppley pyrgeometer with shading disk and Q filter*	Continuous
Turbidity	J-202 and J-314 sunphotometers with 380-, 500-, 778-, 862-nm narrowband filters	3 day ⁻¹
	PMOD three-wavelength sunphotometer*: 380, 500, 778 nm; narrowband	Continuous
Solar spectroradiometry	Solar spectroradiometer	Discrete
<i>Meteorology</i>		
Air temperature	Aspirated thermistor*, 2- and 40-m heights	Continuous
	Max.-min. thermometers, 2-m height	1 day ⁻¹
	Hygrothermograph‡	Continuous
Temperature gradient	Aspirated thermistors*, 2- and 40-m heights	Continuous
Dewpoint temperature	Dewpoint hygrometer*, 2-m height	Continuous
Relative humidity	Hygrothermograph‡	Continuous
Pressure	Capacitance transducer*	Continuous
	Microbarograph	Continuous
	Mecurial barometer	5 wk ⁻¹
Wind (speed and direction)	Bendix Aerovane*, 8.5- and 40-m heights	Continuous
Precipitation	Rain gauge, 8-in	5 wk ⁻¹
	Rain gauge, 8-in§	1 wk ⁻¹
	Rain gauge, weighing bucket	Continuous
	Rain gauge, tipping bucket*	Continuous
Total precipitable water	Foskett IR hygrometer*	Continuous
<i>Precipitation Chemistry</i>		
pH	pH meter	Daily
Conductivity	Conductivity bridge	Daily
Chemical components	Ion chromatograph	Daily

TABLE 2.1. Summary of Measurement Programs at MLO in 1989—Continued

Program	Instrument	Sampling Frequency
<i>Cooperative Programs</i>		
CO ₂ (SIO)	Applied Physics IR analyzer	Continuous
CO ₂ , ¹³ C, N ₂ O (SIO)	5-L evacuated glass flasks†	1 pair wk ⁻¹
Surface SO ₂ (EPA)	Chemical bubbler system	Every 12 days; 24-h (0000-2400) sample
CO ₂ , CO, CH ₄ , ¹³ C/ ¹² C (CSIRO)	Pressurized glass flask sample	1 mo ⁻¹
CO ₂ , CH ₄ , other trace gases (NCAR)	Evacuated stainless steel flasks†	1 pair wk ⁻¹
Total suspended particles (DOE)	High-volume sampler (1 filter wk ⁻¹)	Continuous
Turbidity (AES Canada)	Sonotek sunphotometer no. 5698	1-3 day ⁻¹
CH ₄ (¹³ C/ ¹² C) (Univ. of Washington)	35-L evacuated flask	1 mo ⁻¹
Total suspended particles (EPA)	High-volume sampler	Every 12 days; 24-h (0000-2400) sample
Ultraviolet radiation (Temple Univ.)	UV radiometer (erythema)	Continuous
Ultraviolet radiation (Smithsonian)	8-wavelength UV radiometer: 290-325 nm; narrowband	Continuous
Solar aureole intensity (CSU)	Multi-aperture tracking photometer: 2, 5, 10, 20, 30° fields of view	Continuous
Precipitation collection (DOE)	Exposed collection pails	Integrated monthly sample
Precipitation collection for ⁷ Be and ¹⁰ Be analysis (ISWS)	Aerochemetric automatic collector	Integrated 7-day sample
Precipitation collection for organic acid analysis (Univ. of Virginia)	Aerochemetric automatic collector	Collection after each rain event
Wet-dry deposition (ISWS, NADP)	Aerochemetric automatic collector	Integrated 7-day sample
Aerosol chemistry, upslope-downslope discrimination (Univ. of Washington)	Nuclepore filters	Continuous
Aerosol chemistry (Univ. of Calif.-Davis)	Programmed filter sampler	Integrated 3-day sample 1 continuous and 1 down-slope sample (3 days) ⁻¹
¹³ C(USGS, Denver)	10-L stainless steel flasks	Biweekly
Various trace gases (OGC)	Stainless steel flasks†	1 set wk ⁻¹ (3 flasks)
HNO ₃ , HCl vapor, aerosols (URI)	Filter system	Daily, 2000-0600 LST
Radon (ANSTO)	Aerosol scavenging of Rn	Continuous; integrated 30-min samples
Aerosol surface area (PSI)	Epiphaniometer	Continuous; integrated 30-min samples

All instruments are at MLO unless indicated.

*Data from this instrument recorded and processed by CAMS.

†MLO and Kumukahi.

‡MLO and Kulani Mauka.

§Kulani Mauka.

TABLE 2.2. Estimated Frequency of MLO Venting Effects*

	Jan.	Feb.	March	April	May	June	July	Aug.	Sept.	Oct.	Nov.	Dec.	Year
Total time (hours)	11	3	2	3	7	3	11	11	8	10	6	9	84

*Criteria: CO₂ SD ≥1.0 ppm; wind direction sector 135°-225°; wind speed >1.35 m s⁻¹.

and CO₂ concentrations as well as CH₄, these species have not been analyzed with the MLO instrument.

Ozone

As in prior years, the MLO ozone measurement program consisted of three major phases: continuous surface air monitoring at MLO using a Dasibi model 1003-AH ozone

monitor; daily total ozone observations and Umkehr ozone profile measurements using automated Dobson instrument no. 76; and ozone profile measurements using balloonborne ECC ozonesondes launched from the Hilo NWS station.

The MLO-Hilo ECC ozonesonde program through September was on a nominal weekly flight schedule using large 9-kg plastic balloons. Beginning in October, the

schedule was reduced to three soundings per month using 2-kg rubber balloons. During 1989, 45 flights were launched; 44 of these passed through the region of ozone maximum, and 39 were successful in providing data to burst altitude. The six flights that did not reach the expected peak altitude occurred in midsummer; the problem was diagnosed to be radiosonde battery failure occurring about 2 hours after launch. Obtaining a replacement batch of batteries corrected this problem. Of the 39 fully successful flights, 23 were made using the 9-kg plastic balloons and 16 using 2-kg rubber balloons. For the 23 plastic balloons, the average maximum altitude was 41.4 km; only three failed to reach the 40-km target altitude. For the 16 successful flights using 2-kg balloons, the average maximum altitude was 34.1 km. The average height of the ozone maximum from the total of 44 flights was found to be 25.6 km with a standard deviation of 2 km. No major trends were discernible in stratospheric ozone over Hawaii from the ozonesonde data.

Total column ozone and Umkehr observations were made using automated Dobson instrument no. 76 whenever weather conditions permitted. The total ozone observations were made on 160 of the 235 MLO observation days, for an observational frequency of 68%. Cloudy weather was especially frequent through June, causing the 1989 observing frequency to be less than the 80% observing frequency of 1988. During the year the MLO Dobson instrument was out of service 15 days, mainly due to computer control problems. From June 13 to August 15, a program of Langley plot calibrations was carried out for the WMO standard Dobson instrument no. 83 and for Dobson instrument no. 65 from Boulder. This calibration program included intercalibrations of Dobson instrument no. 83, MLO Dobson instrument no. 76, and Japanese secondary or regional standard Dobson instrument no. 116. In addition, part of this summer study included simultaneous ozone observations from MLO and from a sea-level site on the western, or Kona, side of the island. This phase of the program was designed to evaluate possible influences of the atmospheric boundary layer on Dobson instrument ozone measurements and, in particular, on the Langley plot calibrations.

The Dasibi ozone monitor operated continuously throughout the year and experienced only minor problems. Routine maintenance and calibrations were carried out on schedule. The air sample for the Dasibi is taken from the MLO main gas sampling stack through Teflon tubing about 2-m long.

Halocarbons and Nitrous Oxide

Monitoring of atmospheric concentrations of N_2O , CFC-11, CFC-12, CCl_4 , and CH_3CCl_3 continued at MLO using an automated RITS GC system and through the weekly collections of pressurized 300-mL air samples in stainless steel flasks. The flasks, as in prior years, were sent to the CMDL Boulder laboratory for analysis. The RITS GC provided ambient atmospheric air concentrations of the trace gas species every 3 hours. Although this rather complex monitoring system experienced a variety of problems during the year, usually resulting in short periods of downtime,

these conditions could usually be dealt with readily so that there were no prolonged or serious breaks in the RITS monitoring record.

Sulfur Gases

Sulfur gas monitoring continued throughout 1989, following the procedures described in the 1988 report [Elkins and Rosson, 1989]. The two monitoring instruments include a CSI flame-photometric total sulfur analyzer (i.e., SO_2 plus any other sulfur gases but not sulfur compound aerosol particles) and a TECO pulse fluorescence SO_2 monitoring analyzer. The data from both of these instruments showed that the highest concentrations of both SO_2 and total sulfur typically occurred during midday upslope wind conditions. These events occurred, presumably, because of the entrainment of Kilauea volcanic emissions into the marine boundary layer followed by the transport of this contaminated boundary layer air around the south end of the island and then north to the Kona area. Southerly downslope winds, which can contain evidence of CO_2 volcanic gas venting from the Mauna Loa summit (Table 2.2), were found to have little if any characteristic sulfur gas signature. More details of this sulfur monitoring program, which received major support from the ARL Air Quality Group, are given in Section 7.2.1 of this Summary Report.

Aerosols

The MLO aerosol program consisted of a set of in-situ atmospheric monitoring instruments and a remote sensing ruby lidar system. In May 1989, the program added an aethalometer. This instrument monitors the atmospheric concentration of black carbon, i.e., soot or similar dark-colored particles, by tracking the changing optical density of a filter surface through which an air sample is drawn continuously. Although the aethalometer was originally installed in May and data were recorded subsequently by the CAMS, it became evident after a short period that extraneous signals were being included in the aethalometer CAMS record. Modifications requested from the manufacturer were made, and a fully usable instrument began operation early in 1990. The aethalometer supplements the aerosol instruments already in operation at MLO, namely, the G.E. and TSI CNCs and the four-wavelength nephelometer, by monitoring specifically for black carbon aerosol concentrations. The Pollak CNC was used as a calibration standard for the G.E. and TSI CNCs as in prior years.

The MLO ruby lidar system was used throughout the year to monitor aerosol concentrations in the stratosphere. During 1989, 31 lidar aerosol profiles were obtained. Figure 2.1 shows the integrated non-Rayleigh backscatter (NRBS) coefficient results for 1989 as well as for years back to January 1985. These data are for the stratospheric layer between 16 and 33 km.

As is apparent from Figure 2.1, the decrease in NRBS that began in 1987, following a period of increasing stratospheric aerosol scattering in 1986, continued during 1989. The average NRBS for the 31 observations of 1989 was $0.70 \times 10^{-4} \text{ sr}^{-1}$. This can be compared with the 1988 average NRBS



Fig. 2.1. Integrated NRBS coefficient profile for the stratospheric layer between 16 and 33 km at MLO, January 1985-December 1989.

of $0.83 \times 10^{-4} \text{ sr}^{-1}$ for 37 observations. Thus there was an apparent 16% decrease in yearly averages between 1988 and 1989. This expected decrease follows from observations that no new volcanic perturbations of the stratosphere were detected during 1989. Considering the relatively small NRBS trend during 1989, it appears that the stratosphere may be close to an aerosol base-level concentration value.

Solar Radiation

The complement of MLO solar radiation measurements continued unchanged in 1989. Instruments exchanged during 1989 included quartz pyronometer no. 1261 in May and RG8 pyronometer no. 10153 in November. Replacement units were quartz pyronometer no. 12271 and RG8 pyronometer no. 12616. The active cavity radiometer was in Boulder for calibration during September and October. In July the pyrliometer began to indicate a 1% degradation of output relative to the output of the active cavity radiometer. (The unit was subsequently replaced in early 1990).

Sunphotometer calibrations were performed frequently, for a yearly total of 17. In June the efficiency of the calibration procedure was improved significantly by the development of a computerized data entry process using a small portable computer.

The development program in solar spectroradiometry continued throughout the year, and numerous changes were made in both the mechanical components and the computer control system. A major goal for the coming year is the

implementation of a calibration system that will be compatible with the long-term solar spectroradiometric goals of the program.

Meteorology

Several changes were made in the meteorological sensors during 1989. In September a new pressure sensor, SN 225, was installed. The old sensor, SN 109, had begun to show indications of a very slow leak. Some past reports regarding below-average annual mean pressure at MLO [e.g., *Bodhaine and Rosson, 1988; Schnell and Rosson, 1987*] may have resulted in part from this faulty sensor as well as from the relatively short MLO climatological barometric pressure record. The MLO microbarograph was taken out of service in April 1989, leaving only the CAMS record to indicate pressures and patterns of pressure change. The mercury barometer is read daily and used as a check on the continuous CAMS pressure record. In November, the 2-m temperature and dewpoint sensors were replaced by a TSL hygrothermometer, model no. 1063, SN 46. The TSL was mounted on the 40-m tower at 2 m above the ground surface approximately 30 m west of the previous sensor location. Since the TSL system displays maximum and minimum temperatures, as well as current temperature and dewpoint, less reliance is now placed on the conventional alcohol and mercury thermometers and the hygrothermograph in the standard NWS temperature shelter to provide for independent spot checks of atmospheric temperature and the daily high and low temperatures.

Other than these changes, the standard set of meteorological observations as listed in Table 2.1 continued throughout the year without significant problems. The regular schedule of maintenance and calibrations was accomplished.

During 1989 the MLO and NWS climatological files were searched and the monthly average precipitation record was compiled for the 34-yr period since MLO was established. Table 2.3 shows the MLO precipitation climatology for this period from January 1956 through December 1989. The average annual precipitation was 522 mm. The maximum annual total of 1249 mm occurred in 1982. The minimum annual precipitation was 155 mm, which occurred in 1983. January is the month with the highest average precipitation, 70 mm, whereas June, with an average of only 15 mm, has the lowest monthly average. During this 34-yr period only 26 months or 6% of the total number of months experienced no measurable precipitation. Only September and November did not have at least 1 month in this 34-yr period during which only a trace or less of rain was recorded.

TABLE 2.3. Precipitation Climatology at MLO, 1956-1989

	Jan.	Feb.	March	April	May	June	July	Aug.	Sept.	Oct.	Nov.	Dec.	Annual
Average (mm)	70	42	60	46	35	15	31	45	41	33	51	53	522
Maximum (mm)	327	257	395	239	148	63	120	163	127	115	185	420	1249
Year of maximum	1956	1982	1980	1986	1965	1983	1982	1957	1957	1979	1978	1987	1982
Months \leq Trace	5	4	2	1	3	5	2	1	0	1	0	2	26

Precipitation Chemistry

The precipitation chemistry program consisted of daily rainfall collections 5 days per week (or the replacement of exposed collectors in the case of no rain) at three stations: Hilo, 35 km on the Saddle Road, and MLO. In October, sample collections at Hilo and 35 km were terminated, but MLO was kept on a daily collector change schedule. The MLO precipitation chemistry laboratory kept to its analytical schedule and performed the required analyses on the samples collected locally as well as on precipitation samples received from SMO, BRW, and SPO.

Cooperative Programs

As shown in Table 2.1, 23 studies were carried out on a continuous basis at MLO under the CMDL Cooperative Investigator Program. Most of these were ongoing studies which have been operated within the MLO program for one or more years. At least one of these, the SIO CO₂ investigations, predates the 1972 establishment of the NOAA/CMDL program.

The cooperative program for 1989 includes two new investigations. In May, ANSTO put into operation a continuous ambient atmospheric radon monitor. The radon air sample inlet is at the 40-m level of the MLO tall tower. Section 10 of this Summary Report describes some initial results from this experiment. The second new program was installation of an instrument in December to monitor total atmospheric aerosol particle surface area with an epiphaniometer. This instrument was installed by the Paul Scherrer Institute, Switzerland. It is situated in the small building near the base of the 40-m tower. The air sample is obtained through a 6-m-high inlet adjacent to the building. Section 10 gives more details about this program.

Two cooperative programs were discontinued during the year: Canadian AES turbidity observations using a sunphotometer were discontinued in June, and the USGS (Denver) flask air sample collection program for ¹³C determinations was discontinued in March.

The MLO cooperative programs in 1989 also included several short-period studies (not listed in Table 2.1) during which individual investigators set up and operated their experiments more or less independently of MLO operations. The most extensive program of this type was a study of atmospheric ions performed by Georgia Institute of Technology during the summer months of June through August. Section 10 gives a more detailed description of this experiment. Another short-period study was conducted by DOE HASL, New York City, during March. The objectives of this program were to measure both radon and radon daughters at MLO, to identify possible daily concentration cycles of these species, and to bracket their limiting concentrations. Two other short-period projects were carried out by scientists from the NASA Ames Laboratory, Mountain View, California. These studies were directed toward obtaining absolute calibrations of sunphotometer systems.

2.2. BARROW

D. ENDRES

2.2.1. OPERATIONS

BRW maintained a full schedule of data collection in 1989, including increasing measurement frequency for some programs and the addition of several new programs. A 3-mo project requiring an increase in ozonesonde balloon flights was conducted to detect possible stratospheric ozone depletion during the Arctic winter and early spring. A program to measure background levels of NO and NO_y was begun by the University of Alaska, Fairbanks. Aerosol filter samples were obtained by personnel in residence at the observatory from CIRES and NCAR during the Arctic haze season. The observatory's Temple UV-B meter was put back in service after being refurbished and checked at CMDL in Boulder. The 1989-1990 two-person CMDL/SPO crew was detailed to BRW in the summer, and each member of the crew underwent 2 weeks of intensive training in observatory operations before leaving for the South Pole in October.

The normal Arctic weather experienced at Barrow caused numerous vehicle breakdowns that disrupted the observatory routine throughout the year, and in particular, in the winter. Problems from broken shock absorbers to wheel bearings locking up were encountered. A new pickup truck arrived in November, and it helped alleviate some of the vehicle problems.

A new electrical outlet was installed on a pole on the road to the station so that vehicles could be plugged in to it to keep them warm during the winter when road and power line maintenance was required. Road access to the observatory continues to be a major problem because of snow drifting during winter storms. Snow removal was done by DEW Line personnel and equipment whenever possible, especially when major drifting occurred.

As with vehicle repairs and road maintenance, severe weather caused power line breakdowns that required repair efforts by observatory personnel to maintain good electrical power to the observatory. A major power failure occurred when a power line cutout blew apart during one storm. Repairs took several days before power was restored.

The clean room at the observatory was rewired when it was noted that one of the two electrical circuits feeding the room was loaded to maximum capacity. New circuits were added during the rewiring.

A double-wide trailer was obtained from NWS, Barrow, to provide for CMDL housing after government housing for CMDL personnel was cut back from two units to one by NWS. This trailer unit was reconfigured into two apartments. By the end of the year, remodeling of apartment B was finished and work began on apartment A. Walls were erected, floors installed, Sheetrock hung and textured, and some plumbing and electrical work done. A new boiler for

the trailer heating unit was installed during December by station personnel when the old boiler broke down and was unrepairable.

Numerous autorestarts in the solar/aerosol CAMS box were experienced throughout the year. Several attempts were made to locate the source of the problem. At one time an error in the clock reading of over 5 years, several months, and several hours was noted. The data acquisition system experienced no other problems.

2.2.2. PROGRAMS

Table 2.4 summarizes the 1989 measurement programs at BRW. Operational highlights were as follows:

Carbon Dioxide

BRW is still operating an old Uras 2T NDIR CO₂ analyzer. Plans are being made to replace it. A chopper motor was replaced in the instrument when the old one failed. A new power line conditioner was installed after several power-related problems occurred. An old Cryocool H₂O freezer unit failed and was replaced with a new FTS Systems freezer. No other problems were noted. Flask air samples were collected as scheduled with no problems.

Methane

A disk drive of the Carle GC data acquisition system was damaged by a power spike and was replaced in January. A new UPS was installed, replacing the old unit whose power capacity was underrated. A stream selection valve of the GC system plumbing was replaced when the old valve became misaligned.

Surface Ozone

A pinched air hose and a bad data display were the only problems experienced with the Dasibi instrument in 1989. The instrument operated well and was cleaned and calibrated as needed.

Total Ozone

Observations were made with Dobson spectrophotometer no. 91 on a routine schedule. The instrument was sent to Boulder for calibration in February, being temporarily replaced by Dobson instrument no. 86. In October, instrument no. 86 was returned to Boulder after replacement with Dobson instrument no. 91, which has a history of observations in BRW.

Ozone Profiles

ECC ozonesonde soundings were made during January 16-April 19, 1989, from the NWS balloon facility at Point Barrow by a Boulder CMDL staff member with assistance from BRW staff. Instrument launches were conducted at approximately 3-day intervals for a total of 33 successful flights. Total ozone amounts measured by the ECC sondes ranged from about 340 to 520 Dobson units, except for one low ozone value of 307 Dobson units. The lower ozone amounts occurred on days of high tropopause. No evidence

was present in the measured ozone profiles of ozone depletion similar to that which occurs in Antarctica during the austral late winter and early spring.

Halocarbons

An ECD of the HP-5890 chromatograph failed in February and was replaced. The old detector was sent to Boulder. Several leaks developed in the system and were fixed, and a bad pump was repaired. The program was updated in April by visiting CMDL personnel, and the system underwent routine maintenance. In August a printer and a hard disk malfunctioned. These were replaced and the system was returned to service. CMDL staff returned in October to service and upgrade the system. A burned-out flow controller was found in December and replaced.

Aerosols

Plastic tubing in the vacuum system of the G.E. CNC had become worn and would no longer hold a vacuum. The tubing was replaced with copper tubing and tube connectors. A small amount of bleach was added to the water reservoir in the G.E. CNC. This has kept algae from growing in the water lines. Routine maintenance and calibrations were performed on schedule, and no other problems were noted.

The aethalometer required several pump replacements. Installation of a new type of pump solved the problem. Several light bulbs for the aethalometer were incorrectly marked and found to be inadequate. They were replaced and no further problems were noted.

The nephelometer power switch was replaced along with several chips. No other problems were noted, and the system operated well the rest of the year with only routine maintenance and calibrations.

Solar Radiation

Solar radiation measurements began at BRW March 2, 1989, with receipt from CMDL, Boulder, of newly calibrated instruments, except for a NIP, which was temporarily lost in the mail. The "lost" NIP arrived in BRW 2 weeks later and was placed into operation shortly thereafter. During May a drive cable in the HP data logger system printer twisted and had to be adjusted and cleaned.

During September the albedo rack was dismantled and cleaned. Several rusted bolts were replaced. The rack was leveled and several modifications were made to prevent the rack from sinking into the thawing tundra. Connectors were cleaned and all instruments were returned to service.

The operational amplifiers driving the solar instrumentation amplifier board were replaced with upgraded operational amplifiers to correct a persistent noise problem. The old system had an unacceptable level of noise, and the new amplifiers appear to have reduced the noise.

Meteorology

The worst wind storm in the recorded history of Barrow occurred in February when winds averaged 33.6 ms⁻¹ for several hours. A peak gust of 43.5 ms⁻¹ was recorded at

TABLE 2.4. Summary of Measurement Programs at BRW in 1989

Program	Instrument	Sampling Frequency
<i>Gases</i>		
CO ₂	URAS-2T IR analyzer 3-L glass flasks	Continuous 1 pair wk ⁻¹
CO ₂ , CH ₄ , CO CH ₄ , CO, CO ₂	0.5-L glass flasks, through analyzer 0.5-L glass flasks, P ³ pump unit	1 pair wk ⁻¹ 1 pair wk ⁻¹
Surface O ₃	Carle automated GC	1 sample (24 min) ⁻¹
Total O ₃	Dasibi ozone meter	Continuous
O ₃ profiles	Dobson spectrophotometer no. 91	3 day ⁻¹
CFC-11, CFC-12, CFC-113, N ₂ O	Balloonborne ECC sonde	1 (3 days) ⁻¹ , winter
CFC-11, CFC-12, CFC-113, N ₂ O, CCl ₄ , CH ₃ CCl ₃	300-mL stainless steel flasks HP5890 automated GC	1 pair wk ⁻¹ 1 sample (3 h) ⁻¹
N ₂ O	Shimadzu automated GC	1 sample (3 h) ⁻¹
<i>Aerosols</i>		
Condensation nuclei	Pollak CNC G.E. CNC	1 day ⁻¹ Continuous
Optical properties	Four-wavelength nephelometer	Continuous
Black carbon	Aethelometer	Continuous
<i>Solar and Terrestrial Radiation</i>		
Global irradiance	Eppley pyranometers with Q and RG8 filters	Continuous
Direct irradiance	Tracking NIP Eppley pyrhemliometer with Q, OG1, RG2, and RG8 filters	Continuous Discrete
Terrestrial (IR) radiation	Eppley pyrgeometer	Continuous
Turbidity	Sunphotometers with 380-, 500-, 778-, and 862-nm narrowband filters	Discrete
Albedo	Eppley pyranometer and pyrgeometer	Continuous
<i>Meteorology</i>		
Air temperature	Thermistor, 2 levels Max.-min. thermometers	Continuous 1 day ⁻¹
Dewpoint temperature	Dewpoint hygrometer	Continuous
Pressure	Capacitance transducer Mercurial barometer	Continuous Discrete
Wind (speed and direction)	Bendix Aerovane	Continuous
Precipitation	Rain gauge, tipping bucket	
<i>Precipitation Chemistry</i>		
pH	pH meter (samples analyzed at MLO)	Discrete
Conductivity	Conductivity bridge (samples analyzed at MLO)	Discrete
<i>Cooperative Programs</i>		
Total surface particulates (DOE)	High-volume sampler (1 filter wk ⁻¹)	Continuous
Aerosol chemistry (URI)	High-volume sampler (1 filter wk ⁻¹)	Continuous
Precipitation gauge (ASCS)	Wyoming shielded precipitation gauge	2 mo ⁻¹
Magnetic fields (USGS)	Magnetometer	Continuous
Various trace gases (OGC)	Stainless steel flasks	1 set wk ⁻¹ (3 flasks set ⁻¹)
CO ₂ , CH ₄ , other trace gases (NCAR)	3-L stainless steel flasks	1 pair wk ⁻¹
¹³ C, ¹⁸ O, CO ₂ (CSIRO)	5-L glass flasks	1 pair (2 wk) ⁻¹
CO ₂ , ¹³ C, N ₂ O (SIO)	5-L evacuated glass flasks	1 pair wk ⁻¹
Halocarbon monitoring (Univ. of Calif., Irvine)	Various stainless steel flasks	1 set (3 mo) ⁻¹
Earthquake detection (Univ. of Alaska)	Seismograph	Continuous, check site 1 wk ⁻¹ , change tape 1 mo ⁻¹
¹³ CH ₄ (¹³ C/ ¹² C) (Univ. of Washington)	35-L stainless steel flasks	1 (2 wk) ⁻¹
NO, NO _y (Univ. of Alaska)	Chemiluminescence	Continuous
Ultralow frequency waves (Univ. of Tokyo)	Magnetometer	Continuous
UVB (ARL)	Robinson-Berger meter	Continuous
Air chemistry ions, organic acid, halogens, nitrous oxides (CIRES)	Sample tubes and filters	1 day ⁻¹
Air chemistry (Florida State Univ.)	24 filters	1 day ⁻¹

BRW as well as at the NWS office in town. Several villages along the coast reported winds in excess of 44.8 ms^{-1} . The old BRW wind speed observatory record was 29.6 ms^{-1} set in 1986. BRW set five new record temperature lows during the last week in January and seven new temperature highs during the first week in February.

A new synchro was installed in the Aerovane anemometer after it was determined that the old one had worn enough to give inaccurate readings.

Several times during the year erratic readings were noted on the TSL dewpoint hygrometer. The problem was traced to bad connections in the wiring to the sensor card and to badly soldered joints of some components on the cards. Several printed-circuit boards were replaced throughout the year as connectors corroded.

All maintenance was performed as scheduled and no further problems were noted.

Precipitation

Samples were collected routinely and sent to MLO for analysis. Even though July 1989 was the wettest July on record, few samples were collected. The cause was the low rate of precipitation during most 24-h periods. A light drizzle fell most of the month.

Cooperative Programs

Personnel from University of Alaska, Fairbanks, arrived at BRW to install an NO , NO_y chemiluminescence converter into the instrument measuring these trace gases. NO_y compounds are converted to NO using reduction with CO in a gold tube maintained at a temperature of 300°C . The instrument operated generally satisfactory with no major down time.

The DOE high-volume air pump was replaced in May because the old pump was damaged during the February wind storm. The wind knocked the entire pump and housing onto its side.

High winds caused drifting snow to enter the door of the USGS observatory building. The winds also caused the power lines to slap together, and a fuse was blown in the protonmagnetometer. A tape data acquisition unit also developed problems during this time.

Several new rain gauges were installed in 1989 by the Alaska Soil Conservation Service as part of an experiment to determine the efficiency of different types of collectors. The project involves several sites across the state. It has been shown that errors of up to 300% can be induced by some of the collection methods.

Several types of air filter samples were obtained for and with personnel from NCAR during the spring Arctic haze episode. The program operated for 2 months, after which time all equipment was sent back to NCAR in Boulder.

Several filter packs, known as "jet packs" were obtained for and with CIRES personnel to study the spring bromine injection from the ocean into the atmosphere when ice breakup occurs. The duration of this project was about 2 months.

Argonne National Laboratory set up a small Shimadzu GC at BRW to search for non- CH_4 hydrocarbons. The GC was

damaged in shipping and never worked the way it was supposed to.

The URI filter pump blew completely off the filter unit platform during the high winds in February. The pump was packed with snow and was moved indoors for servicing. After the pump was cleaned it ran well the rest of the year.

The ultralow-frequency magnetometer recorder had several recurring problems. A drive belt tended to become loose and would not grip the drive gear. Personnel from the University of Tokyo were in BRW during August to replace the unit and install a new sensor.

The Temple University UV meter was returned to service in July. Responsibility was turned over to CMDL for maintenance of the sensor/data logger unit. Data will be sent to ARL in Silver Spring for final analysis.

NCS International installed an offshore navigation antennae near the BRW observatory during the summer. It was used as one part of a number of antennae set up to help ships navigate to Prudhoe Bay during the summer. BRW was chosen because of its remoteness and because of its proximity to a baseline survey marker.

During September an acoustic sounder, or SODAR, system was installed by NOAA/WPL personnel. It is used to study inversion layer formation. Useful information will be gathered to enable the investigators to learn more about how surface inversions form in the Arctic, how they break up, how strong they get, and how long they last during the Arctic winter and spring.

2.3. SAMOA

J. C. FARMER

2.3.1. OPERATIONS

During 1989 there were many changes at SMO. A new station chief was hired in April. During this same period, the electronics technician was on maternity leave. The observatory was able to operate quite successfully, however, with the use of some temporary help. There were also many changes with the observatory facilities and the government housing. After the new station chief arrived, a major effort was put into upgrading the houses used by the CMDL observatory staff. The houses suffered from some neglect and limited budgets. New furniture was purchased, termite damage was repaired, and remodeling was done on the kitchens, bathrooms, and living-room windows.

At the beginning of the year new power lines were installed at Matatula Point to help remedy recurring power outages, surges, and brownouts that periodically hindered the measurement programs. Trees were trimmed that were beginning to block some of the solar radiation instruments. Minor, but necessary repairs, were made to the main observatory building to improve the observatory's operation and maintain a safer measurement environment. The installation of new CO_2 sampling lines to Matatula Point began in late October. It was also decided to renovate the old Ekto building, since the small building at the base of the

tower was in very bad shape. This work was nearly completed by the end of the year. The hardwood posts around the outside of the observatory were stripped of the old varnish and two coats of marine varnish were applied. The generator failed to operate properly during November. A new battery and cable corrected the problem.

2.3.2. PROGRAMS

Table 2.5 summarizes the programs at SMO for 1989. Further descriptions of some of the programs follow.

Carbon Dioxide

Continuous CO₂ measurements were interrupted for most of April because of power problems at Matatula Point. A problem with the Air Cadet pumps used in the CO₂ analyzer system began surfacing in August. Apparently, because of the heavy load put on the pumps, the plastic heads were cracking on a regular basis, causing small leaks. This problem continued throughout the remainder of the year, necessitating frequent replacement of the damaged pump heads with new ones. A new cooler from FTS Systems was installed in place of a worn-out Cryocool unit; it has worked well, although a new design for a lid for the cooler is badly needed to prevent the accumulation of water within the cooler's alcohol bath. The installation of two new air sampling lines to Matatula Point was under way in late October and neared completion by the end of the year. The old Ekto building at the point was refurbished to house the water-trap system for the CO₂ sampling lines.

Surface Ozone

Observations continued during 1989 with no significant problems or downtime.

Total Ozone

Observations were conducted throughout the year without difficulty using Dobson instrument no. 42. The instrument was calibrated relative to secondary standard Dobson instrument no. 65 in May 1989.

Ozone Profiles

ECC ozonesonde soundings that had been made at SMO at a frequency of one per 2 weeks in 1988 were discontinued in July 1989. Six soundings were made during 1989.

Halocarbons and Nitrous Oxide

The HP-5890 and the Shimadzu gas chromatographs operated all year with relatively minor problems. There was a continual problem with the Shimadzu GC not coming up online after a power failure. The only other problem during the year was loss of calibration gas in one tank during November. An old tank of calibration gas was found at the observatory and installed to maintain the system in operation pending receipt of new calibration gas from Boulder. The new tank of calibration gas arrived in late December and was put into use. The old calibration gas tank was then returned to Boulder so that it could be recalibrated. The chromatograph

systems were operating on only one tank of calibration gas at the end of the year. The chromatograph systems' software was upgraded in April.

Flask air sampling continued on a weekly basis when flasks were available. LEAPS flasks were substituted for the CMDL 300-mL flasks once per month when possible.

Aerosols

The G.E. CNC had several problems during the year. It was sent to Boulder for repair on two occasions and was there at year's end. The nephelometer worked well throughout the year. The contacts on the two rotary switches of the nephelometer were cleaned in July when certain switch positions began giving erroneous readings. The aerosol air sampling stack showed signs of wear. Cracks were found in several places, including the sample ports. These were all repaired successfully. Severe corrosion was also noted on the frame for the stack.

Solar Radiation

The pyranometers and pyrhelimeter were operated without difficulty. The filter-wheel NIP also operated well. One of the sunphotometers had a broken reset switch during the last half of the year. No replacement was received from Boulder.

Meteorology

The meteorology program added a dewpoint sensor to its list of instruments during 1989. The driest month and wettest month on record were recorded in 1989. In August SMO received only 1.5 cm of rainfall (0.5 cm at the NWS site) and in November rainfall totaled over 40.6 cm. All instruments performed well during the year.

Precipitation Chemistry

Daily precipitation samples continued to be analyzed for pH and conductivity during the year. These samples were then sent to MLO for further analyses. No problems with the Aerochem wet/dry collector occurred during the year.

Cooperative Programs

The cooperative programs at the observatory changed somewhat during the year. Three programs were discontinued: the air sampling programs of the USGS, the Argonne National Laboratory, and the U.S. Bureau of Mines. Two new programs were added during 1989: the University of Washington and the University of California, Irvine, started programs to study ¹³CH₄/¹²CH₄ and light hydrocarbons, respectively. Similar programs exist at other CMDL observatories.

The most significant cooperative program involvement during the year was the observatory staff's participation in the NASA GLOBE Program through the SEASpan Project of the University of Miami. During the month of November, daily filter collections were made to provide ground measurement support for the program. A new collection system was installed on the Ekto tower from which filters were exposed on a daily basis. The previous filter collections had been made on top of the tower at Matatula Point.

TABLE 2.5. Summary of Measurement Programs at SMO in 1989

Program	Instrument	Sampling Frequency
<i>Gases</i>		
CO ₂	URAS-2T IR analyzer	Continuous
CO ₂ , CH ₄	3-L glass flasks	1 pair wk ⁻¹
	0.5-L glass flasks, through analyzer	1 pair wk ⁻¹
	0.5-L glass flasks, P ³ pump unit	1 pair wk ⁻¹
Surface O ₃	Dasibi ozone meter	Continuous
Total O ₃	Dobson spectrophotometer no. 42	4 day ⁻¹
O ₃ profiles	Balloonborne ECC sonde	2 mo ⁻¹
CFC-11, CFC-12, N ₂ O	300-mL stainless steel flasks	1 pair wk ⁻¹
CFC-11, CFC-12, N ₂ O, CCl ₄ , CH ₃ CCl ₃	HP5890 automated GC	1 sample (2 h) ⁻¹
N ₂ O	Shimadzu automated GC	1 sample (2 h) ⁻¹
<i>Aerosols</i>		
Condensation nuclei	Pollak CNC	1 day ⁻¹
	G.E. CNC	Continuous
Optical properties	Four-wavelength nephelometer	Continuous
<i>Solar Radiation</i>		
Global irradiance	Eppley pyranometers with Q and RG8 filters	Continuous
	Eppley pyranometers with Q filters on tilted mounts	Continuous
Direct irradiance	Eppley pyrheliumeter with Q filter	Continuous
	Eppley pyrheliumeter with Q, OG1, RG2, and RG8 filters	Discrete
Turbidity	Sunphotometers with 380-, 500-, 778-, and 862-nm narrowband filters	Discrete
<i>Meteorology</i>		
Air temperature	Thermistors (2)	Continuous
	Max.-min. thermometers	1 day ⁻¹
Dewpoint temperature	Polished mirror	Continuous
Pressure	Capacitance transducer	Continuous
	Mercurial barometer	1 wk ⁻¹
Wind (speed and direction)	Bendix Aerovane	Continuous
Precipitation	Rain gauge, weighing bucket	Continuous
	Rain gauge, tipping bucket	Continuous
	Rain gauge, plastic bulk	1 day ⁻¹
	Aerochem wet/dry collector	1 day ⁻¹
<i>Precipitation Chemistry</i>		
pH	Fisher model 805 meter	1 day ⁻¹ (CMDL); 1 wk ⁻¹ (NADP)
Conductivity	Beckman model RC-16C meter	1 day ⁻¹ (CMDL); 1 wk ⁻¹ (NADP)
<i>Cooperative Programs</i>		
CO ₂ , ¹³ C, N ₂ O (SIO)	5-L evacuated glass flasks	3 flasks wk ⁻¹
GAGE project: CFC-11, CFC-12, N ₂ O, CH ₃ CCl ₃ , CCl ₄ (OGC)	HP5880 gas chromatograph	1 h ⁻¹
Various trace gases (OGC)	Stainless steel flasks	3 flasks wk ⁻¹ (3 flasks set ⁻¹)
¹³ C, ¹⁸ O, CO ₂ (CSIRO)	5-L glass flasks	1 pair mo ⁻¹
Wet-dry deposition (NADP)	HASL Chemetrics wet-dry collector	1 wk ⁻¹ , wet; discrete, dry
Bulk deposition (EML)	Plastic bucket	Continuous (1 bucket mo ⁻¹)
Hi-vol sampler (EML)	High-volume sampler	Continuous (1 filter wk ⁻¹)
Hi-vol sampler (SEASpan Project)	High-volume sampler	Continuous (1 filter wk ⁻¹)
CO ₂ , CH ₄ , trace gases (NCAR)	Evacuated stainless steel flasks	1 pair wk ⁻¹
¹³ C/ ¹² C ratio (Univ. of Wash.)	30-L pressurized cylinder	2 mo ⁻¹
Light hydrocarbons (UCI)	1-L evacuated stainless steel flasks	3-4 flasks qtr ⁻¹

2.4. SOUTH POLE

E. CROZER

2.4.1. OPERATIONS

CMDL atmospheric monitoring programs at Amundsen-Scott (South Pole) station, Antarctica, are conducted in cooperation with NSF. Amundsen-Scott station is about 150 m from the geographical South Pole at an elevation of about 2.8 km.

Operations at South Pole are conducted on an annual basis from about November 1 to October 31 of each year. The station is accessible by U.S. Navy ski-equipped LC-130 aircraft from about November 1 to February 15. During the rest of the year, the station is inaccessible and no supplies or mail can be delivered with the exception of one mid-winter airdrop in June.

Measurements of atmospheric trace gas constituents are made in the CAF, which is located upwind of the main complex of the Amundsen-Scott station. Because the winds at the South Pole blow from the northeast 98% of the time, the CAF is suitably placed to sample uncontaminated air. The area upwind of the CAF is known as the Clean Air Sector and is off limits to all personnel, vehicles, and aircraft.

Materials were ordered in preparation for refurbishing the CAF during the 1989-1990 summer. The CAF requires electrical rewiring and re-insulation of the roof. Several building inspections were made by electricians in early 1989, and in the course of the inspections it was discovered that one power line coming into the CAF was supplying only 95 V. The voltage was increased to 100 V by bypassing the CAF isolation transformer, which was causing part of the voltage drop. On the whole, very few power outages were experienced during the year. There were several planned outages while the CAF power supply was worked on and only a few unplanned outages of short duration. Most of the CAF equipment has UPS backup power supplies to assure minimal data loss.

During the summer SPO acquired a Micro-VAX computer to replace the PDP-11 in use for many years. The installation of the new computer also included a dedicated VAX terminal at the CAF. The VAX could also be accessed via two personal computers at the CAF. At the present time there is only one line to the CAF, and all PCs and terminals must share this line. Plans call for inclusion of the CAF in the station's Ethernet network, allowing the PCs and terminal to access the VAX independently. The network would also facilitate data transfer from the CAF to the VAX because communications programs would not have to be used.

Heating and cooling inside of the CAF continued to be a problem. During the summer, solar heating, added to interior hot spots generated by instrument clusters, resulted in uneven and elevated temperatures inside the CAF. These occurrences are particularly evident when the sun shines

through the CAF windows on calm days when outside air temperatures are relatively warm. Pulling the interior shades over the CAF windows has minimal effect, as the air behind the shades and inside the three-pane windows heats to over 150°F, transferring heat into the building. During the winter, cold outside temperatures in combination with strong winds, produce cold spots inside the CAF. These cold spots are in areas that are distant from where instrument clusters normally generate enough heat to compensate for the cooling events. Circulation of air throughout the CAF could improve this situation. Installation of reflective film on outside storm windows would most likely reduce the amount of heat conducted through the windows and still allow light into the room. The use of reflective film, along with wall-mounted fans, will be tried during the summer of 1989-1990.

In March there was a fire at the ATS-3 communication satellite ground station in Florida. The station was destroyed and SPO was left without ATS-3 communications for several weeks. The ATS-3 was the only satellite used for SPO communications this season. During this down time, communication with Boulder was maintained by reverting to HF transmissions through McMurdo to the Commercial Refile Center in Georgia, then via telex to Boulder. The University of Miami set up a temporary station to receive and send ATS-3 communications until the main groundstation was rebuilt and activated in September. An unusual number of solar flare events blacked out HF communications several times over the course of the winter and in the austral spring.

2.4.2. PROGRAMS

The CMDL programs at SPO during 1989 were essentially the same as in the previous year; atmospheric measurements included carbon dioxide, surface and total ozone, ozone vertical distribution, halocarbons, meteorology, and solar radiation. In addition, CMDL personnel operated a number of cooperative projects for other institutions. Only CMDL and affiliated programs were conducted at the CAF this year, contrary to past years when several other institutions maintained experiments there with their own personnel. Table 2.6 summarizes the programs at SPO. Further discussion of some of the programs follows:

Carbon Dioxide

The CO₂ analyzer system was thoroughly checked for leaks at the beginning of the summer. Some leaks were found and stopped, and the data quality improved. Flask samples were obtained weekly, with the method of sample collection alternating between use of a portable P³ pump unit and sampling through the CO₂ analyzer apparatus.

Surface Ozone

Surface ozone was measured with a Dasibi ozone meter. No problems were experienced with the Dasibi instrument itself, although the data were not always recorded correctly by the CAMS system.

TABLE 2.6. Summary of Measurement Programs at SPO in 1989

Program	Instrument	Sampling Frequency
<i>Gases</i>		
CO ₂	URAS-2T IR analyzer	Continuous
CO ₂ , CH ₄	0.5-L glass flasks, through analyzer 0-5L glass flasks, P ³ pump unit	1 pair twice mo ⁻¹ 1 pair twice mo ⁻¹
Surface O ₃	Dasibi ozone meter	Continuous
Total O ₃	Dobson spectrophotometer no. 82	3 day ⁻¹
Ozone profiles	Balloonborne ECC sonde	1 wk ⁻¹ , summer, autumn, winter, 1 (3 day) ⁻¹ , spring
CFC-11, CFC-12, N ₂ O, CH ₃ CCl ₃ , CCl ₄	Shimadzu automated mini-2 gas chromatographs 300-mL stainless steel flasks	1 sample (3 h) ⁻¹ 1 pair wk ⁻¹ , summer
CFC-11, CFC-12, N ₂ O	300-mL stainless steel flasks	3 wk ⁻¹ , summer
<i>Aerosols</i>		
Condensation nuclei	Pollack CNC G.E. CNC	2 day ⁻¹ Continuous
Optical properties	Four-wavelength nephelometer	Continuous
Carbon aerosols	Aethalometer	Continuous
<i>Solar and Terrestrial Radiation</i>		
Global irradiance	Eppley pyranometers with Q and RG8 filters	Continuous, summer
Direct irradiance	Eppley pyrheliometer with Q, OG1, RG2, and RG8 filters	Discrete, summer
Turbidity	Sunphotometers with 380-, 500-, 778-, and 862-nm narrowband filters	Discrete, summer
Albedo	Eppley pyranometers with Q and RG8 filters, downward facing	Continuous, summer
<i>Meteorology</i>		
Air temperature	Platinum resistor, 2- and 20-m heights	Continuous
Snow temperature	Platinum resistor, 0.5 cm	Continuous
Pressure	Capacitance transducer Mercurial barometer	Continuous 2 times wk ⁻¹
Wind (speed and direction)	Bendix Aerovane	Continuous
Frost-point temperature	Hygrometer	Continuous
<i>Cooperative Programs</i>		
CO ₂ , ¹³ C, N ₂ O (SIO)	5-L evacuated glass flasks	2 mo ⁻¹ (3 flasks sample ⁻¹)
Total surface particulates (DOE)	High-volume sampler	Continuous (4 filters mo ⁻¹)
Various trace gases (OGC)	Stainless steel flasks	Twice mo ⁻¹ (3 flasks set ⁻¹)
¹⁴ C (NOAA/ARL)	3,000 psi spheres	500 psi day ⁻¹
Snow acidity (NOAA/ARL)	125-mL Nalgene flasks	1 (2 wk) ⁻¹
Interhemispheric ¹³ C/ ¹⁴ C (CSIRO)	5-L glass flasks	1 or 2 flasks mo ⁻¹
CH ₄ , CO ₂ , CO (NCAR)	2.5-L steel flasks	Daily, winter
Ultraviolet radiation (NSF)	UV radiometer, data logger	Periodic
Polar stratospheric clouds (Univ. of Rome)	Optical lidar	Instrument inoperative

Total Ozone

Total ozone measurements were made with Dobson spectrophotometer no. 82. This instrument worked well all year without calibration drift. The only impediment to observations was the weather, especially when winter moon observations had to be made.

Ozone Profiles

ECC ozonesondes were launched once a week for most of the year except during September through November months when launches were made every 3 days to study Antarctica springtime ozone depletion. Winzen 19K

plastic balloons were used for the flights almost exclusively. The balloons were launched from the balloon-inflation tower.

Very few instrument failures were experienced prior to September. September brought on a rash of unexplained radiosonde and ozonesonde failures with no consistent causes. Often sondes were launched on successive days in order to maintain the once every 3-day flight schedule. Despite the age of the radiosonde signal device tracking equipment, no sonde data were lost due to its failure. A long period of bad weather and high winds contributed to the difficulty in launching the sondes during springtime.

Halocarbons and Nitrous Oxide

Two automated gas chromatographs were operated all year. The systems were overhauled during the summer. GC1 continued to function all year with no problems. GC2 ran all year but experienced an unknown problem in July that affected the data. Column bakes and hydrogen purges were tried on GC2 with no improvement. An extra long hydrogen purge was made in September that improved data quality considerably.

Halocarbon air sample flasks were filled during the summer and retrograded to CMDL Boulder. Samples were not collected during the winter.

Aerosols

Although problems were encountered with the Pollak counter all year, measurements were obtained. The G.E. CNC was not working at station opening in 1988. After completely dismantling the instrument it was discovered that the valve shaft was inserted 180° out of phase. When this was corrected, the instrument functioned all year with only minor problems. With the Pollak counter not always working properly, it was difficult to ensure that the G.E. CNC was always giving accurate readings. A new TSI CNC was installed early in the season and operated with no problems. It provided a good CNC record for the year. The nephelometer was on line all year with no problems.

Solar Radiation

This program was continued as in the past. A new albedo rack was installed at the beginning of the summer. The new rack proved to be sturdy and easy for one person to rotate by 180° when intercalibrating with upward-facing pyranometers. A new upward-facing pyranometer was also installed. All instruments operated normally during the summer months. The pyranometers were removed from their mounts and stored during wintertime. There were a few problems with reinstallation at sunrise when it was found that electrical cables had been damaged by the high winds during spring (e.g., the motor on the tracking pyranometer failed). These problems were all corrected by the beginning of October.

Meteorology

As in previous years, meteorological observations included measurements of temperatures at 2 and 20 m, pressure, wind speed and direction, and frost point temperature. Snow surface temperature measurements made in the past at SPO were discontinued at the beginning of the summer.

New temperature probes and cables for the 2- and 20-m measurements were installed during the summer. This proved to be a lengthy operation; calibrations were performed before, during, and after the installations. Calibrating the new probes took several days, using different calibration constants. The 10-m temperature probe failed on day 120 and was inoperative until day 174. The dewpoint hygrometer worked only until the temperature reached -60°C. At lower temperatures the values became negative and not reliable.

Cooperative Programs

The majority of the cooperative programs listed in Table 2.6 were continued from the previous year. The USGS and SUNYA programs were discontinued. Problems were experienced with the alignment of the University of Rome aerosol lidars. Despite the large amount of work done on the lasers, the system was never operable. The NSF UVB radiometer was upgraded with new computers and new programs. It experienced various intermittent problems throughout the year, which were worked on through frequent communications with BSI, the developer of the instrument.

2.5. REFERENCES

- Bodhaine, B.A., and R.M. Rosson (Eds.), *Geophysical Monitoring for Climatic Change, No. 16: Summary Report 1987*, 110 pp., NOAA Air Resources Laboratory, Boulder, CO, 1988.
- Elkins, J.W., and R.M. Rosson (Eds.), *Geophysical Monitoring for Climatic Change, No. 17: Summary Report 1988*, 142 pp., NOAA Air Resources Laboratory, Boulder, CO, 1989.
- Schnell, R.D., and R.M. Rosson (Eds.), *Geophysical Monitoring for Climatic Change, No. 15: Summary Report 1986*, 155 pp., NOAA Air Resources Laboratory, Boulder, CO, 1987.
- Thoning, K.W., P.P. Tans, and W.D. Komhyr, Atmospheric carbon dioxide at Mauna Loa Observatory, 2, Analysis of the NOAA GMCC Data, 1974-1985, *J. Geophys. Res.*, 94(D6), 8549-8565, 1989.

3. Aerosols and Radiation Monitoring Group

B.A. BODHAINE (Editor), J.J. DELUISE, E.G. DUTTON, D.W. NELSON, AND R. STONE

3.1. CONTINUING PROGRAMS

3.1.1. SURFACE AEROSOLS

The aerosol monitoring program at BRW, MLO, SMO, and SPO continued during 1989 as in previous years. CN concentration was measured continuously with a G.E. CN counter and daily calibration points were provided by Pollak CN counters at all stations. TSI (butanol-based) CN counters have been operated at MLO since May 1988 and at SPO since January 1989. TSI CN counters will be installed at BRW and SMO during 1990. After a 1-year overlap of the new TSI CN counter with the existing G.E. CN counter at each station, the G.E. CN counters will be retired. Aerosol scattering extinction coefficient (σ_{sp}) at 450-, 550-, 700-, and 850-nm wavelengths was measured continuously at each station with a four-wavelength nephelometer. Aerosol black carbon concentration was measured continuously using aethalometers at BRW since April 1988 and at SPO since December 1986. An aethalometer will be installed at MLO during 1990.

Figure 3.1 shows 1989 daily geometric means of CN concentration, σ_{sp} , and Ångstrom exponent at the CMDL stations (except at SPO where only CN data were obtained).

Three independent values of Ångstrom exponent were calculated from the four channels of σ_{sp} data using the relation $\alpha = -\Delta\sigma_{sp}/\Delta\lambda$, where α is Ångstrom exponent and λ is wavelength. The interpretation of α in terms of aerosol size distribution was discussed by Bodhaine and DeLuise [1985]. Monthly geometric means of the 1989 aerosol data are listed in Table 3.1. A graphical presentation of the monthly geometric means of the entire data record for the four stations is shown in Figure 3.2.

The BRW data in Figure 3.1 show a σ_{sp} maximum of about $2 \times 10^{-5} \text{ m}^{-1}$ during winter and spring, typical of the well-known Arctic haze. The BRW long-term record in Figure 3.2 clearly shows this annual cycle in σ_{sp} . No 850-nm data for BRW are shown in Table 3.1 because of instrument problems that required deletion of much of the data at that wavelength. The BRW CN record shows a more variable semiannual cycle, having a maximum that usually coincides with the maximum in σ_{sp} and another maximum in late summer or early spring. The secondary maximum in late summer is thought to be caused by local oceanic emissions of DMS gas that is eventually converted to sulfate aerosol [Radke et al., 1990].

The MLO σ_{sp} data in Figure 3.1 are fairly typical; high values occur in April and May and low values in fall and

TABLE 3.1. Monthly Geometric Means During 1989 of CN Concentration (cm^{-3}), and σ_{sp} (m^{-1}) at 450, 550, 700, and 850 nm, for BRW, MLO, and SMO, and of CN Concentration for SPO

	Jan.	Feb.	March	April	May	June	July	Aug.	Sept.	Oct.	Nov.	Dec.
<i>BRW</i>												
CN	304	272	515	340	201	415	834	485	320	272	129	149
σ_{sp} (450)	1.35-5	8.18-6	1.62-5	1.21-5	6.88-6	2.81-6	2.73-6	3.66-6	2.54-6	3.44-6	8.86-6	1.26-5
σ_{sp} (550)	1.25-5	7.54-6	1.40-5	1.02-5	5.61-6	2.21-6	2.40-6	3.32-6	2.49-6	3.12-6	7.84-6	1.10-5
σ_{sp} (700)	8.80-6	5.44-6	8.93-6	6.51-6	3.34-6	1.36-6	1.72-6	2.44-6	2.11-6	2.37-6	5.57-6	7.35-6
<i>MLO</i>												
CN	258	181	181	190	220	249	242	247	230	233	176	235
σ_{sp} (450)	5.98-7	8.50-7	1.81-6	2.74-6	5.17-6	1.84-6	1.76-6	1.07-6	9.20-7	1.52-6	1.14-6	5.90-7
σ_{sp} (550)	4.29-7	6.45-7	1.33-6	2.09-6	4.09-6	1.39-6	1.26-6	7.49-7	6.57-7	1.09-6	8.25-7	4.16-7
σ_{sp} (700)	2.92-7	4.94-7	9.75-7	1.56-6	3.05-6	1.02-6	8.41-7	5.16-7	4.67-7	7.12-7	5.68-7	2.73-7
<i>SMO</i>												
CN	285	241	190		232	230	174	231	222	271	267	201
σ_{sp} (450)	1.98-5	1.95-5	1.76-5		1.96-5	2.09-5	1.52-5	1.64-5	2.12-5	2.01-5	1.61-5	2.00-5
σ_{sp} (550)	1.90-5	1.84-5	1.70-5		1.82-5	2.08-5	1.49-5	1.57-5	2.10-5	1.92-5	1.57-5	1.93-5
σ_{sp} (700)	1.88-5	1.80-5	1.71-5		1.75-5	2.14-5	1.50-5	1.48-5	2.12-5	1.90-5	1.57-5	1.96-5
σ_{sp} (850)	2.00-5	1.89-5	1.82-5		1.82-5	2.31-5	1.69-5	1.52-5	2.27-5	2.00-5	1.78-5	2.12-5
<i>SPO</i>												
CN	186	194	139	29	25	22	18	14	25	66		237

A compact exponential format is used for σ_{sp} such that 1.35-5 = 1.35×10^{-5} .

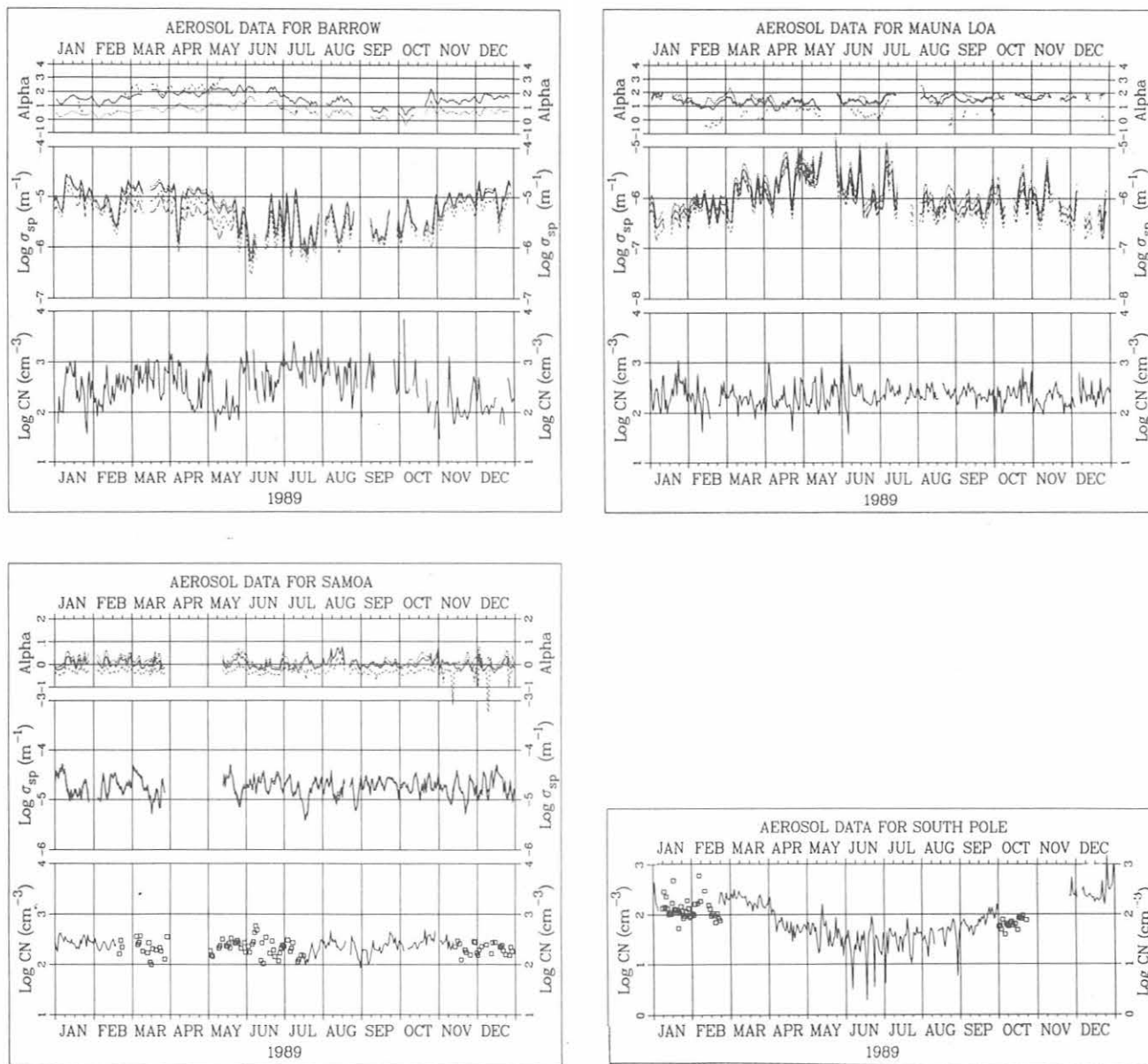


Fig. 3.1. Daily geometric means for 1989 of σ_{sp} , CN data, and Ångström exponents (alpha) at BRW, MLO, and SMO; and of CN data at SPO. Data for MLO are included only for 0000-0800 LST. σ_{sp} data are shown for 450 (dotted curve), 550 (solid curve), 700 (dashed curve), and 850 (long-dashed curve) nm. Ångström exponents were calculated from 450- and 550-nm σ_{sp} data (dotted curve), 550- and 700-nm σ_{sp} data (solid curve), and 700- and 850-nm σ_{sp} data (dashed curve). The CN data represented by squares for SMO and SPO are from the Pollak CN counter.

winter. Large events in April and May, caused by the long-range transport of Asian desert dust in the upper troposphere to the vicinity of Hawaii, dominate the record. As discussed in the previous *Summary Report* [Elkins and Rosson, 1989], σ_{sp} values have been generally higher since the installation of the new nephelometer in 1985 and have not reached the low values expected in winter. A nephelometer-comparison experiment will be performed in 1990 to determine if the new MLO nephelometer is less sensitive than the old one. This should help determine if σ_{sp} has generally increased at MLO. The increasing trend in σ_{sp} at

MLO is obviously caused by higher winter values in the latter part of the record. No 850-nm data for MLO are given in Table 3.1 because of instrument problems that required deletion of much of the data at that wavelength. The MLO CN record shown in Figure 3.1 is fairly typical, giving an annual geometric mean concentration of 218 cm^{-3} , compared with 216 cm^{-3} for the previous year. Note that all MLO aerosol data presented here are in the form of geometric means during 0000-0800 HST (1000-1800 UT) in order to include data for downslope wind conditions only.

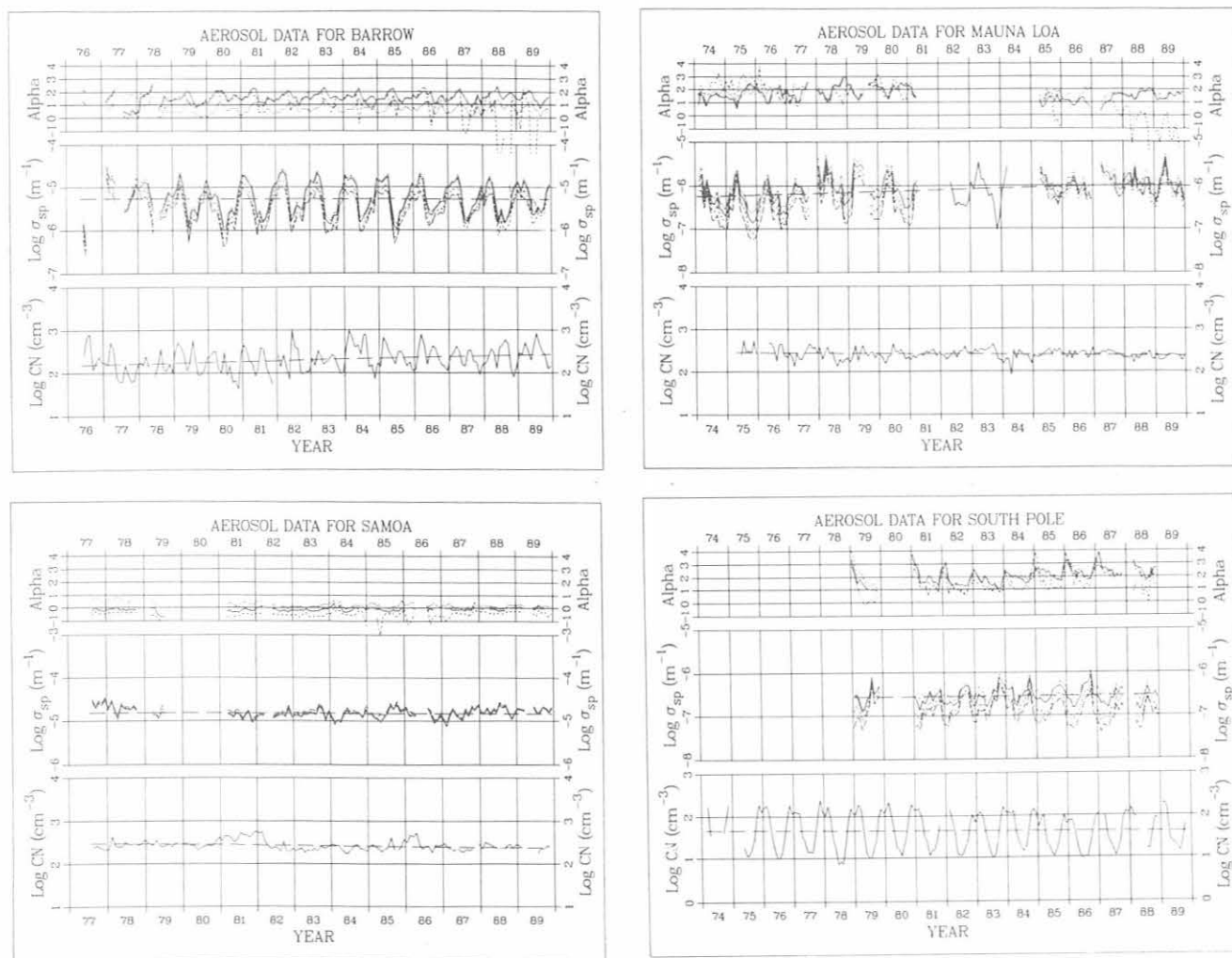


Fig. 3.2. Monthly geometric means of σ_{sp} , CN data, and Angstrom exponents (alpha), at BRW, MLO, SMO, and SPO for the entire record. See the Figure 3.1 legend for plot details. Trend line data are given in Table 3.2.

The SMO σ_{sp} and CN data continued as in previous years with no significant annual cycle or long-term trend. The SMO 1989 annual mean is about $1.80 \times 10^{-5} \text{ m}^{-1}$ for σ_{sp} (550 nm) and about 229 cm^{-3} for CN concentration, representative of the background marine boundary layer in that region. The SMO nephelometer experienced electronic problems in April and May; the automatic CN counter was down from mid-February to mid-June and mid-November through December. The CN record was augmented with Pollak counter observations when available. A detailed analysis of the SMO data record through 1983 was presented by *Bodhaine and DeLuigi* [1985].

The SPO CN data for 1989 from the TSI CN counter are presented in Figure 3.1. These data show a strong annual cycle reaching a maximum of about 200 cm^{-3} in the austral summer and a minimum of about 10 cm^{-3} in the winter, similar to previous years. On the same graph are daily means from the Pollak CN counter. Instrument problems with the SPO nephelometer caused loss of σ_{sp} data for the

entire year. Referring to the long-term data set for SPO shown in Figure 3.2, the σ_{sp} data generally show intermediate values in the austral summer, a minimum in May, and large events, sometimes exceeding 10^{-6} m^{-1} , in late winter. These large aerosol events are caused by the transport of sea salt in the upper troposphere from stormy regions near the Antarctic coast to the interior of the continent. Analyses of the SPO data were presented by *Bodhaine et al.* [1986, 1987].

The least-squares trend lines in Figure 3.2 were calculated using the common logarithms of the monthly means for the entire data record. Trend data are summarized in Table 3.2. Similar trend lines have been calculated and presented in previous Summary Reports.

3.1.2. SOLAR AND THERMAL RADIATION

Introduction

Surface radiation budget, atmospheric transmission, and aerosol remote sensing measurement projects at the four

TABLE 3.2 Least-Squares Trend Analysis of the Common Logarithms of the Data Shown in Figure 3.2*

	Parameter	Slope	Intercept	S.E.	Trend, % yr ⁻¹
BRW	CN	0.0179	0.826	0.285	4.21
	σ_{sp}	-0.00154	-5.14	0.378	-0.35
MLO	CN	-0.00705	2.99	0.121	-1.61
	σ_{sp}	0.0196	-7.70	0.311	6.05
SMO	CN	-0.00807	3.12	0.111	-1.84
	σ_{sp}	-0.00185	-4.67	0.119	-0.43
SPO	CN	-0.00333	1.93	0.431	-0.76
	σ_{sp}	-0.00660	-7.10	0.189	-1.53

*The time axes in Figure 3.2 are in fractional years, with a data point centered at the center of a month; e.g., Jan. 1974 = 74.042; Feb. = 74.125; etc.

CMDL observatories continued through the year with no significant modifications in the measurement systems. Table 3.3 shows the current observatory monitoring projects being overseen by the ARM group. Another ongoing project maintained by the ARM group is the surface radiation budget measurements made at the top of the 300-m BAO tower near Erie, Colorado. Annual and diurnal cycles in the near-surface radiation budget measured at BAO are discussed by Dutton [1990b]. A new surface radiation measurement project was begun on the island of Kwajalein in the Marshall Islands where downwelling solar and thermal infrared irradiances are being monitored. The Kwajalein data were used in an extensive satellite ground-truth comparison during April 1989. The site is also a candidate for long-term participation in the WCRP Baseline Surface Radiation Network.

TABLE 3.3. Current Radiation Measurements at CMDL Observatories

	SWD	SWU	LWD	LWU	RG8D	DIRQ	FWNIP	SPHTM	MISC
BRW	X	X	X	X	X	X	X	X	O
MLO	X	O	O	O	X	X	X	X	X
SMO	X	O	O	O	X	X	X	X	O
SPO	X	X	X	X	X	X	X	X	X

X, measurements made; O, measurements not made; SWD, shortwave downward solar irradiance; SWU, shortwave upward (reflected) solar; LWD, longwave downward (sky emitted); LWU, longwave upward (earth emitted); RG8D, downward solar (RG8 filter, 0.7 to 3.0 μm) irradiance; DIRQ, direct solar; FWNIP, filter wheel normal incidence pyrheliometer (discrete observations, four solar bands); SPHTM, multiwavelength sunphotometer; MISC, miscellaneous—MLO: global diffuse solar, downward solar (OG1 filter, 0.53 to 3.0 μm), 2-channel sunphotometer (water vapor), 3-channel sunphotometer (calibration standard); SPO: RG8 albedo, direct sun (RG8 filter).

Processing and analysis of the data acquired during the year is complete. Results of these and other ARM radiation projects during past and preceding years have been used in numerous studies of surface radiation budget characteristics, light-sensitive atmospheric chemical reactions, satellite algorithm verification, climatic impact of volcanic eruptions, climatic trends and variability, errors in ozone remote sensing, surface optical properties, cloud optical properties, radiative transfer calculation verification, instrument development and improvement, and solar energy assessment and utilization. Data acquired are available in various published reports or directly from the ARM radiation project leader.

Beginning in 1989 a different procedure for assuring the long-term calibration stability of the solar radiation sensors was implemented for the four CMDL sites. The new procedure involves swapping instruments once every 2 years with an instrument recently calibrated at the Boulder Solar Radiation Facility. This procedure replaces the system whereby the instruments' calibrations were monitored on site by a traveling standard. Some on-site visits by traveling standards will continue as a secondary check on the instruments' calibration.

Observatory Activities

The BRW forced-air system used to prevent ice buildup on the pyranometer domes was further refined to improve its efficiency. The mounting mechanism that supports the global radiometers that observe the upwelling irradiances was overhauled; it had sunk into the permafrost and sustained minor damage. The pyrgeometers' mode of operation was changed by removing the temperature compensating battery from both instruments. The battery circuit data were only used for real-time monitoring but tended to interfere with other signals.

The MLO Q global pyranometer was exchanged in May; instrument 12271 replaced 12616. The automated solar tracking dome, which houses continuous recording sunphotometers, operated during the year with only occasional unexplained failures. Data were nevertheless obtained during about 90% of the time, including unattended operation on weekends. The rain sensor that closes the dome in the event of significant precipitation is suspected of occasionally sending spurious signals, causing unwanted dome closures. All other radiation systems operated without problems during the year.

SMO continues to be a severe testing site for radiation instrumentation; weather-tight instruments absorb moisture, spectral filter material provides a culture for various fungus and bacterial growth, and calibration constants drift 3-4 times faster than expected from specifications. Nonetheless, the program is maintained by relatively frequent instrument exchanges and calibration corrections. Quartz pyranometer 12274 replaced instrument 12276 in June. NIP replacement is planned during 1990.

At SPO, upward-facing pyranometer 12271 was replaced by instrument 12272 in January 1988. Pyranometer 12271 demonstrated an extremely steady calibration over the past decade, but the base plate became warped, and leveling it

became impossible. The new albedo rack support system served well during its first year of operation but has proved to be somewhat difficult to rotate to the upward-facing position. The rack is designed to keep the downward facing instruments 2-2.5 m above the surface. Ice forming on the instruments, particularly on the upward-facing pyrgeometers, is checked on nearly a daily basis by the SPO observers, but it still accumulates to an extent that data are lost. Data that can be determined to be degraded by icing are edited from the data base during post processing.

Results

Annual averages of total downward solar irradiances at BRW, MLO, SMO, and SPO for times that the sun is above the horizon, have been calculated and are shown in Figure 3.3. Net solar radiation follows these variations except at BRW where the albedo can be highly variable. Although no significant long-term linear trends exist in the data of Figure 3.3, some features are of considerable interest. The magnitude of the interannual variability over the length of time shown has only rarely been determined at any globally remote site. These variations relate to climatologically significant interannual variations in the Earth's energy budgets. Both the MLO and the SMO records demonstrate rather steady year-to-year values punctuated by occasional large perturbations. Only the dip in 1982 in the MLO record can be partially explained; it is most likely due to the tremendous injection of aerosols into the stratosphere by the El Chichon eruption [Dutton, 1990a]. Clouds can cause the interannual variations but the question of climatological interest then would relate to the cause of cloud variations. An interesting feature of both the BRW and SPO record, especially the SPO record, is the apparent long-term, slowly varying (autocorrelated) nature of the time series. Although the data records are too short to properly assess the statistical

significance of the indicated signals, such variations, if real, could be important in forcing climate change. Although the downward, or even net, solar irradiance at SPO has never been considered a major variable in climatic forcing, the atmospheric phenomena causing the SPO variations could affect a much larger portion of the Antarctic region.

Net solar radiation measured at the top of the BAO 300-m tower has been used to substantiate a new concept for obtaining net solar irradiance at the Earth's surface from satellite measurements, as proposed by *Cess and Vulis* [1989]. The comparison between the BAO net solar irradiance with ERBE top-of-the-atmosphere net solar observations verified the proposed nearly linear relationship between the two quantities during clear-sky conditions [Cess et al., 1990]. The new method provides a technique for determining surface net solar irradiance over most of the globe with higher accuracy than previously achieved while not requiring accurate knowledge of the underlying surface reflectance (albedo). Work is continuing in applying the technique to overcast and partly cloudy skies, with excellent initial success.

For the past 9 years, nominally once a month, a comparison has been made at MLO of direct solar beam irradiance measurements from an active cavity radiometer (ACR) and from an on-line continuous tracking pyrheliometer (NIP). Results are shown in Figure 3.4. Each plotted data point is derived from an average of 12 ACR observations made 15 seconds apart and a simultaneous 3-min average NIP observation. If more than one 3-min comparison was made within a month, all results were averaged to obtain the plotted point for the month. Although several rather large excursions are evident in the record, the long-term stability of the relative calibration of the two instruments is indicated to better than $\pm 0.1\%$ until late 1989. Some of the larger excursions in the record are related

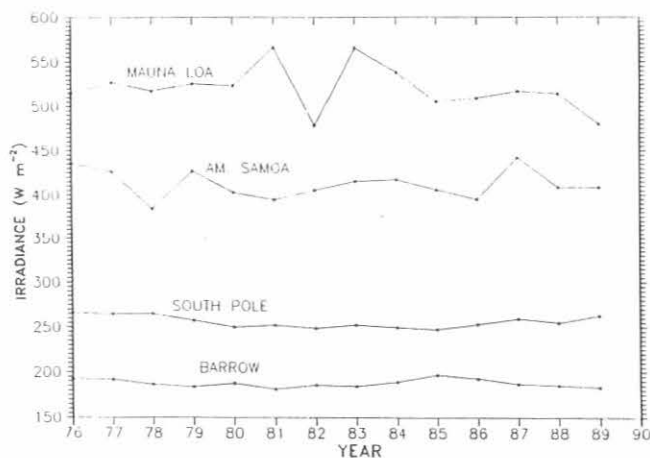


Fig. 3.3. Annual average downward global solar irradiance at the four CMDL observatories. The average is for all hours for which the true center of the sun was above the true horizon (refraction not included) for the entire hour or at either the beginning or end of the hour.

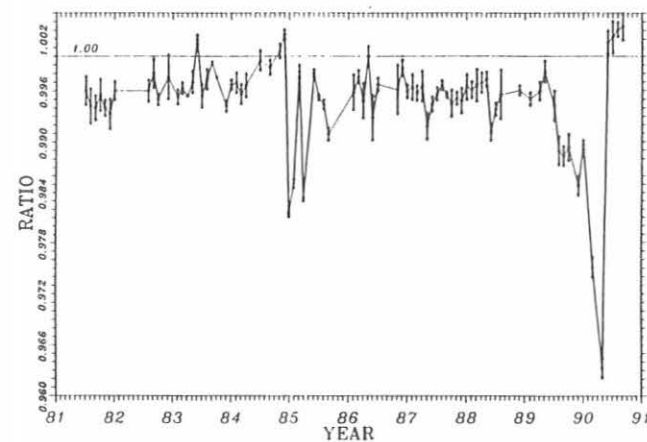


Fig. 3.4. Time series of the ratio of direct solar beam irradiance measured at MLO with the continuous tracking NIP and with the active cavity pyrheliometer. The comparisons were made sporadically; each plotted point represents an average for a given month. Standard deviations associated with the monthly averages are also shown on the plot.

to electrical measurement problems with the ACR. However, the shift at the end of 1989 was due to loss of sensitivity of the tracking NIP, after nearly 20 years of continuous operation. A new tracking NIP, 16657, was put on line in early May, and the ratio returned to near 1.00, as indicated in Figure 3.4.

The relative transmission (commonly called apparent transmission) of the atmosphere over MLO is monitored with a pyrheliometer using a procedure developed by *Ellis and Pueschel* [1971]. The record since 1958 has been shown to be very sensitive to small changes in the absolute atmospheric transmission and reveals the effects of many volcanic eruptions and other aerosol events discussed by *Mendonca et al.* [1978]. The most recent published account of the MLO relative transmission record, its water vapor sensitivity, and its physical interpretation is given by *Dutton et al.* [1985]. The complete record into 1990 is given in Figure 3.5. Note the dramatic effect of the 1982 El Chichon eruption (including effects of smaller eruptions that have occurred since 1982) and the long recovery. The recovery appears to be continuing. Both the 12-mo unweighted mean apparent transmission centered on December 1989, and the individual value for January 1990, are higher than they have been since the time of the El Chichon eruption in 1982. The effects of the El Chichon aerosol on the different components of solar radiation (direct, diffuse, and total) at MLO were given by *Dutton and DeLuisi* [1987].

3.1.3. SOLAR RADIATION FACILITY

Operations 1989

The SRF historical obligations were continued during 1989. These obligations included, but were not limited to, hardware maintenance of NOAA SOLRAD network sensors and solar trackers; support of solar radiation measurement

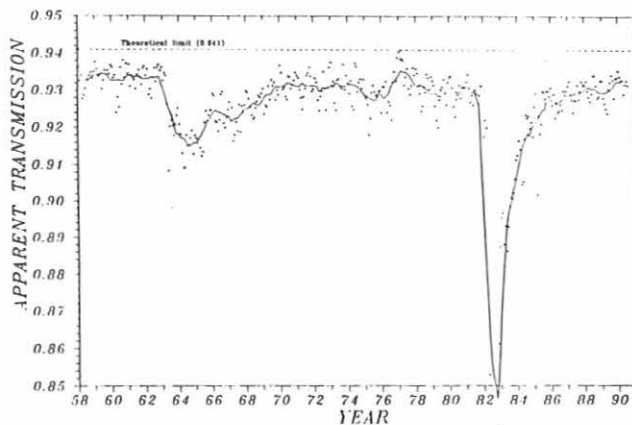


Fig. 3.5. Time series of the monthly means of the MLO apparent atmospheric transmission. The solid curve denotes the 12-mo running mean. The theoretical limit is determined from a LOWTRAN-modeled case with no aerosol and average MLO water vapor and ozone. NOTE: theoretical limit could be exceeded for a very dry and low aerosol case.

programs at the CMDL observatories; installation in Kwajalein Atoll in the Pacific of ground-based solar radiation sensors; logistics support for and instrument calibrations at the BAO site east of Boulder; and instrument calibrations for other ERL laboratories. Thirty-five sites in addition to Boulder are supported with regularly recalibrated sensors and solar tracking equipment. Currently, a mixture of older equatorial mount trackers and the newer computer-controlled altitude/azimuth-style units are in use.

Measurements

The SRF maintained an operational array of sensors on the roof of the ERL building in Boulder. Global solar radiation measurements using pyranometers and direct-beam measurements using pyrheliometers mounted on solar trackers were obtained throughout the year. These data are summarized in Figure 3.6. The SRF has a capacity for collecting data from up to 100 sensors if required. The typical mix of sensors on line consists of a core group of control sensors whose operation is traceable back to the mid-1970's and additional sensors for special studies or calibrations. Plots of the daily totals of hourly averaged global, diffuse, and direct beam radiation are shown in Figure 3.6. The diffuse component was computed as the difference between the measured global irradiance and the vertical component of the direct beam irradiance, measured with a pyranometer and pyrheliometer, respectively.

Special additions to the measurement programs at the SRF during 1989 included installation of a prototype version of a rotating shadowband radiometer. It was installed during June and continues in operation. This sensor will eventually be added to the measurement array at the BAO site, after evaluation of its performance characteristics.

A ground-level set of shortwave radiation monitoring sensors was installed at the BAO site for comparison with the array that has been in place at the 300-m level of the tower. An automatic tracker carrying two pyrheliometers, one with a clear window and the second fitted with an RG-8 cutoff filter, was installed for direct solar beam measurements. A pyrgeometer, a clear-dome pyranometer, and a pyranometer with an RG-8 dome were installed for global measurements.

Standards Activities

The SRF reference absolute cavity radiometer, TMI Mark VI, serial number 67502 (manufactured by Technical Measurements Inc.), was used as a traceable standard for all the calibrations performed during 1989. This unit has a history of comparisons with other similar units dating back to the mid-1970s, and has been compared with the reference cavities in the World Standard Group maintained in Davos, Switzerland, at regular intervals since its purchase in 1975. The most recent comparison to a world standard occurred during April 1989, at a WMO-sponsored comparison in Ensenada, Mexico. In addition to the international comparisons, the SRF reference is compared with other SRF cavities when conditions permit. Yearly comparisons with

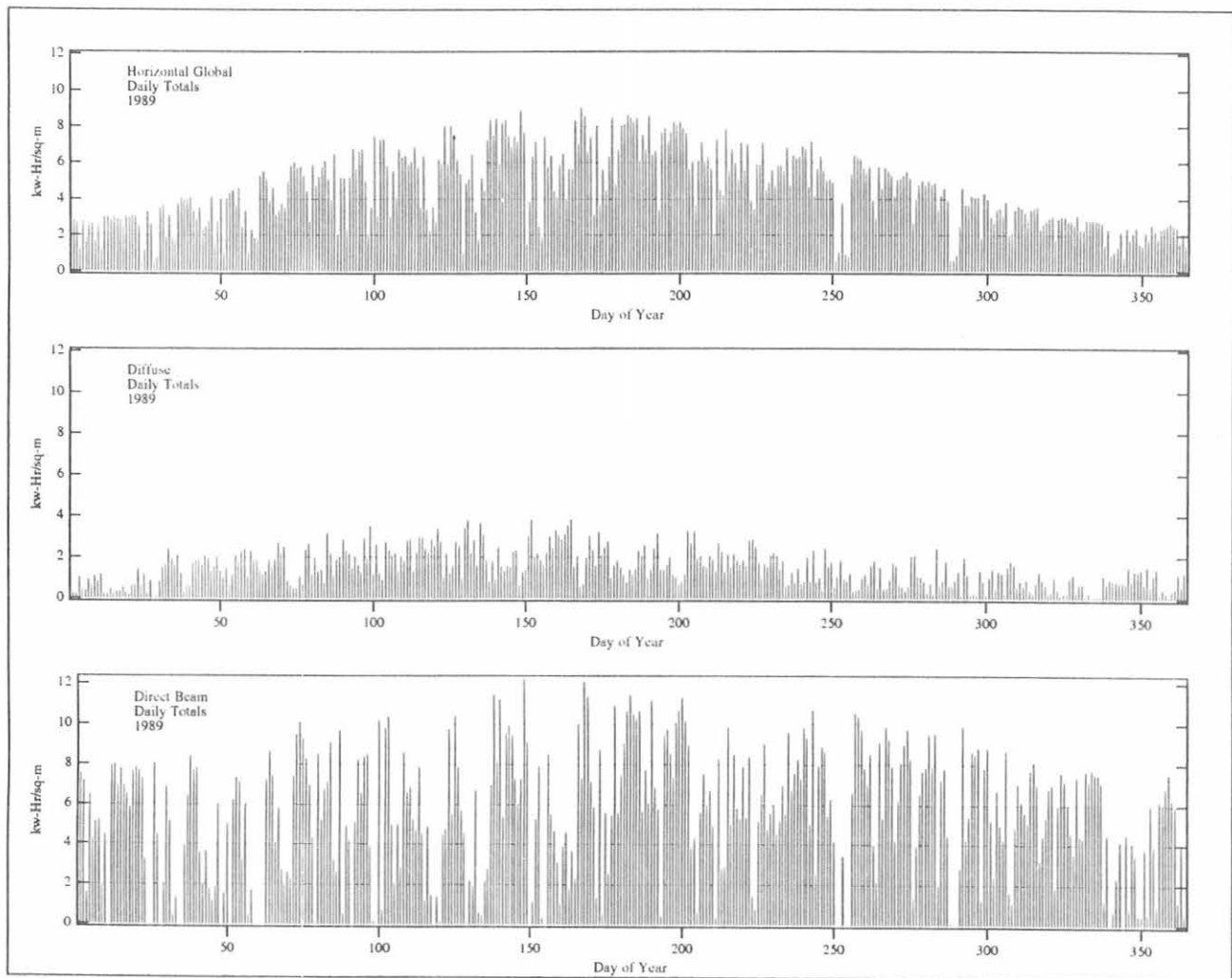


Fig. 3.6. Daily totals of global, diffuse, and direct beam irradiance at the SRF in Boulder during 1989. A pyranometer, a continuously shaded pyranometer, and a pyrhelimeter were used, respectively, to collect the data.

the SERI reference units have been conducted since 1985. Prior to 1985, the unit had participated in seven New River Intercomparisons of Pyrhelimeters (NRIPs).

3.2. SPECIAL PROJECTS

3.2.1. CN COUNTER COMPARISON AT MLO

Introduction

The GMCC aerosol monitoring program at MLO was initiated in 1974 and consists of the continuous measurement of CN concentration and σ_{sp} . The aerosol program was described by *Bodhaine* [1983]; the complete MLO aerosol data record was presented by *Massey et al.* [1987].

CN concentration is an important measurement at a background location such as MLO because it gives the total particle concentration regardless of particle size or

composition. At a background location the particle population will generally be an aged aerosol, the so-called accumulation mode, that has been subjected to natural coagulation, deposition, and cloud processes in the atmosphere. The CN concentration in the background troposphere, far from continents and anthropogenic activities, is generally of the order of hundreds of particles per cubic centimeter. The long-term geometric mean CN concentration at MLO is about 260 cm^{-3} . Thus, a CN counter sensitive in the range $0\text{-}1000 \text{ cm}^{-3}$ is needed.

An advantage of a CN counter is that it responds to particles in the $0.001\text{-}0.1 \text{ }\mu\text{m}$ diameter size range, the so-called nucleation mode, as well as the accumulation mode ($0.1\text{-}1.0 \text{ }\mu\text{m}$ diameter). Therefore, CN data may be used to identify periods of time when a background sampling site is subject to local pollution influences, such as when the local wind flow is from the direction of a nearby biogenic or

combustion source. At MLO, background data are usually acceptable during downslope flow and are contaminated during periods of upslope flow [Mendonca, 1969]. These periods of upslope flow are obvious in the CN record. Occasionally, most often in April-May, desert dust transported from Asian deserts is detected at MLO [Bodhaine et al., 1981; Parrington et al., 1983].

Instrumentation

CN concentration has been measured continuously at MLO since 1974 using a G.E. automatic CN counter [Skala, 1963]. This instrument measures CN concentrations in the range 3-300,000 cm^{-3} with a response time of 2 seconds. A Pollak CN counter [Metnieks and Pollak, 1959] is located at MLO as the on-site standard. Both of these instruments employ the expansion cloud chamber technique and use water as the condensation medium. Daily calibration points obtained with the Pollak counter were used to calibrate the G.E. counter [Bodhaine and Murphy, 1980].

Because of continuing maintenance and calibration problems with the G.E. CN counter, a decision was made in 1988 to install a TSI Inc. model 3760 alcohol-based CN counter at MLO and to phase out use of the G.E. counter. The TSI instrument uses a continuous flow of sample air through a cooling tube to produce a high supersaturation, and uses butyl alcohol as the condensation medium to produce a cloud. As the air stream passes through a focused laser beam, individual cloud droplets are detected, and an electronic pulse for each droplet is provided at the output of the instrument. A critical orifice and external vacuum pump provide a flow rate of 1.4 L min^{-1} . The maximum particle concentration detectable by this instrument is 10,000 cm^{-3} . Coincidence counting errors (two or more particles in the laser beam simultaneously), although correctable, become significant for high concentrations (about 6% at 10,000 cm^{-3}). For ease of data acquisition, a frequency-to-voltage converter was used to provide a linear 0-10 V output scale in which 10 V is equivalent to 10,000 particles cm^{-3} , giving a maximum count rate of 235.8 kHz. An additional logarithmic 0-10 V output, scaled at 2 V decade⁻¹ from 0.1 to 10,000 cm^{-3} , was provided as a chart recorder driver. Because of its single-particle counting capability, the TSI CN counter is sometimes considered an absolute standard.

It was decided to operate both the G.E. and TSI counters during an overlap period on the natural aerosol at MLO. Data could then be compared to determine if a correction factor is needed to maintain continuity for the long-term data set at MLO across this instrument change.

Data Comparison

Hourly mean data for February-March 1989 were used for a comparison of the two automatic CN counters operating at MLO. Figure 3.7 is a direct tracing of a typical upslope wind event recorded for both instruments on a Leeds & Northrup chart recorder with 35-s time resolution on each channel. It is apparent from Figure 3.7 that not only do the general features of the data correspond well, but even the smallest details of aerosol variations are reproduced

faithfully by both instruments. This correspondence strengthens the credibility of both instruments and suggests that these small variations are indeed real.

Unedited hourly mean data, recorded on the MLO data acquisition system during February-March 1989 for both instruments, are shown in Figure 3.8 (left). All data pairs were included regardless of data quality unless the data point for one or both instruments was missing. A linear regression was applied to the logarithms (base 10) of the resulting 1233 data pairs. Although the fit is very good, large numbers of outliers are evident. These outliers were caused primarily by daily checks, calibrations, maintenance, and unknown reasons for both instruments. Rather than editing the data manually, which would require a subjective decision whether or not to accept each hourly data point, we wanted a simple objective method for removing outliers.

The outliers were removed by calculating $\log(\text{G.E./TSI})$ for each data pair and then removing the points above and below 1 standard deviation from the mean of the distribution of the 1233 $\log(\text{G.E./TSI})$ data points. Also, any concentration larger than 1000 cm^{-3} was removed to restrict the comparison to the concentration range of interest for background monitoring at MLO. Figure 3.8 (right) shows the result of a linear regression on the remaining 997 data points after the outliers were removed. Note that the standard error of 0.029 translates to about 6.8%. The predicted values of G.E. CN concentration (calculated from the regression line) at 10, 100, and 1000 nuclei cm^{-3} differ from the TSI CN concentrations by about +10%, +2%, and -5% respectively.

It is possible that the negative bias of the G.E. counter at the higher concentrations could be partially explained by the data acquisition method. Data from both instruments were acquired at the rate of 1 Hz, and hourly arithmetic means were calculated by the data acquisition system. Since the TSI counter has a linear output, its hourly mean is an arithmetic mean. However, since the G.E. counter has a logarithmic output, its hourly mean is a geometric mean.

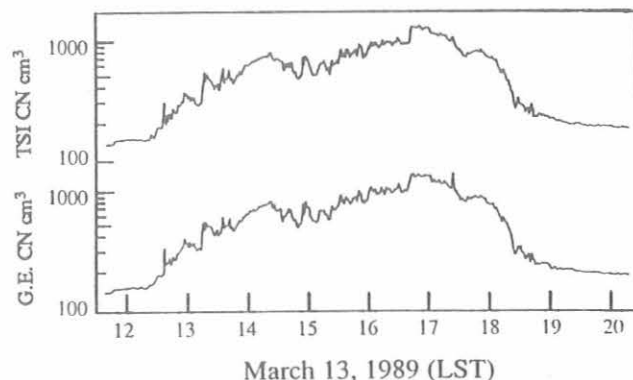


Fig. 3.7. Time series comparison of TSI (top) and G.E. (bottom) CN counter data during an upslope wind event at MLO on March 13, 1989. These data were recorded on a multichannel chart recorder with 35-s time resolution.

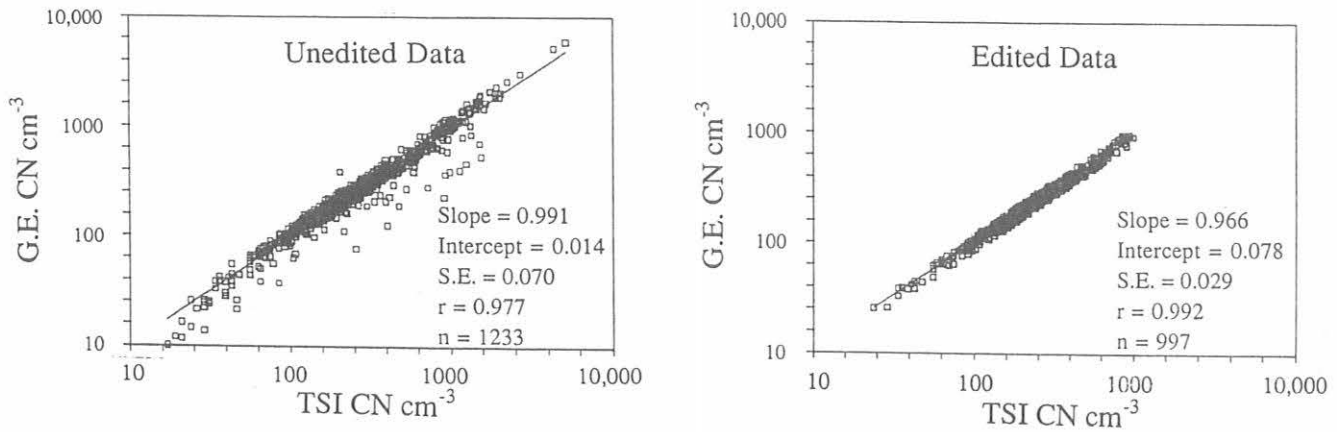


Fig. 3.8. Comparison of TSI and G.E. hourly mean CN concentration at MLO for February-March 1989 for unedited data (left) and data with outliers removed (right). The linear regression was performed on the common logarithms of the data.

Under conditions of high data variability, which commonly occurs at higher concentrations, the geometric mean may be significantly smaller than the arithmetic mean. For example, if the CN concentration increases linearly from 100 to 1000 cm^{-3} , the hourly geometric mean will be on the order of a few percent lower than the arithmetic mean. If the CN concentration increases exponentially, the difference will be about 4%. However, if the concentration varies wildly, the difference can be much greater.

Conclusions

As a result of this study, the credibility of the long-term G.E. CN counter data record at MLO has been substantiated. The calibration of the G.E. counter is established on site by the Pollak counter; therefore, the present study also may be viewed as a comparison between the TSI and Pollak CN counters. Since the TSI counter is a single-particle counting instrument, many researchers in the aerosol field view it as an absolute instrument. This study provides additional verification for the calibration of the Pollak CN counter, particularly at the low concentrations occurring at background locations. Finally, this study shows that the water- and alcohol-based instruments give comparable results.

3.2.2. RADIATIVE AND METEOROLOGICAL EFFECTS OF TRANSIENT WEATHER DISTURBANCES AT THE SOUTH POLE DURING WINTER

Introduction

Theoretical models of the atmosphere's general circulation indicate that high-latitude regions are particularly susceptible to greenhouse warming because of global increases in the concentrations of radiatively active trace gases [e.g., *Schlesinger and Mitchell*, 1985]. Radiative forcing due to clouds, however, potentially far exceeds that due to gaseous greenhouse warming [*Ramanathan et al.*, 1989]. Thus, even small changes in frequency, type, or spatial distribution of clouds may cause significant climate change in polar regions. Analyses of ground-based radiation measurements indicate that anomalous surface warming

occurs in polar regions when clouds are observed [e.g., *Cogley and Henderson-Sellers*, 1984; *Stone et al.*, 1989] and that the heating effects are monotonic with increasing cloud cover and/or cloud optical depth. The distribution of clouds is, in turn, controlled mainly by large-scale dynamical processes. The motivation for the present study is to understand better the processes that force the lower tropospheric radiation, temperature, and wind fields at the South Pole.

Data

SPO provides an ideal laboratory to study the processes that affect the climate of a large region of the Antarctic Plateau. Surface and upper-air meteorological data, sky-cover observations, and measurements of the surface radiation balance components for SPO were assimilated for this study. Two sources of upper-air data were analyzed: daily SPO 0000 UT rawinsonde profiles, and the NMC global, gridded, upper-air data.

Data were stratified according to sky-cover (SC) observations. Only "clear-sky" (SC < 1/10) and "overcast" (SC > 9/10) conditions are analyzed here to contrast the state of a cloudy atmosphere relative to a clear one. Results for the austral winter months of 1986 are presented.

Results and Discussion

Clear-sky conditions at the pole are characterized by a weak, steady katabatic flow of cold air from higher terrain, and a strong, persistent, surface-based temperature inversion. Transient weather disturbances, on the other hand, are characterized by increased cloud cover, surface warming, a shift in wind direction, increased wind speed, and a weakening of the inversion. Surface warming is well correlated with enhancements of downwelling LW radiation which, in turn, correlate with increased sky cover [*Elkins and Rosson*, 1989].

Clouds over the Antarctic Plateau tend to form in the warm layer capping the surface-based inversion [*Schwerdtfeger*, 1984]. As was discussed by *Stone et al.* [1989], surface warming during the austral winter is due, in large part, to positive LW cloud radiative forcing. *Carroll*

[1983] suggested two other possible mechanisms for surface warming at the South Pole: (1) downward mixing of warm upper-level air, and (2) northerly warm-air advection (with north taken to be the Greenwich meridian). Hogan et al. [1982] showed that heat, water vapor, and aerosols are transported poleward at preferred levels in the troposphere when the position of the polar high-pressure ridge, normally centered over the high plateau, shifts to a more northerly position.

It is clear that the surface temperature field at the South Pole responds to complicated, interrelated radiative and dynamical mechanisms that are somehow linked to large-scale circulation patterns. We seek to understand these mechanisms better in the context of climate change.

Net Cloud Radiative Effects. Figure 3.9 is a scatter plot of 2300 and 0000 UT hourly mean values of net surface irradiance stratified according to 0/10 SC and 10/10 SC for the 1986 winter season. The 2300 and 0000 UT time periods were selected to bracket the rawinsonde launch times for subsequent comparisons. Figure 3.9 shows the mean values for all clear (35) and all overcast (20) days observed during the study period. A significant negative value of net irradiance characterizes clear days, and a slightly positive value is observed for overcast conditions. Nearly half the overcast days show net gains exceeding 10 W m^{-2} , which represents a significant convergence of radiant energy at the surface available to warm the snow pack and near-surface air.

Tropospheric Temperatures and Winds. Transport processes are crucial to the formation and spatial distribution of clouds over the Antarctic Plateau. An analysis of the surface and upper level wind fields is therefore essential to gain an understanding of these processes. Figures 3.10 shows surface wind roses for the 35 clear and 20 overcast days. Clear days are characterized by surface flow that is weak and from the easterly quadrant 90% of the time,

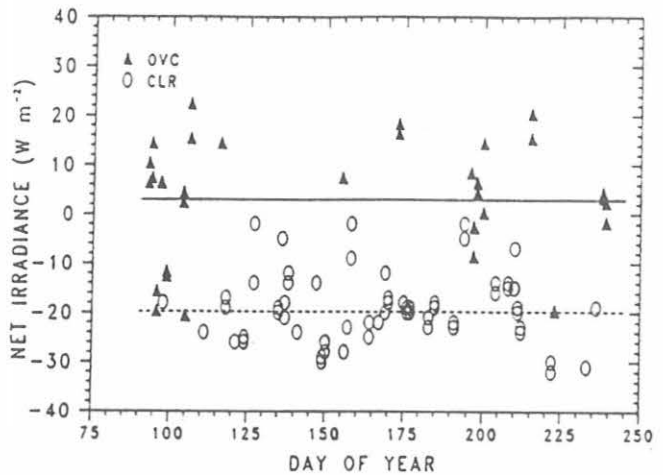


Fig. 3.9. Selected 2300 and 0000 UT hourly mean values of net surface irradiance for April-August 1986. Circles denote clear conditions and filled triangles denote overcast conditions. The dashed and solid lines are the mean values for the subsets of 35 clear and 20 overcast days, respectively.

whereas overcast days are distinctly characterized by much stronger, northerly winds.

Coincident 0000 UT rawinsonde data were used to characterize the temperature and the wind profiles for clear and overcast conditions. Individual soundings were interpolated into prescribed height intervals to enable averaging the desired subsets of data for clear and overcast days. A shallow surface-based layer of large positive temperature gradient is typically overlain by a rather deep quasi-isothermal layer of much warmer air throughout the winter at the South Pole. The boundary between these layers, in most cases, is readily defined by a significant inflection in temperature gradient between two adjacent layers, which is denoted arbitrarily as the top of the inversion.

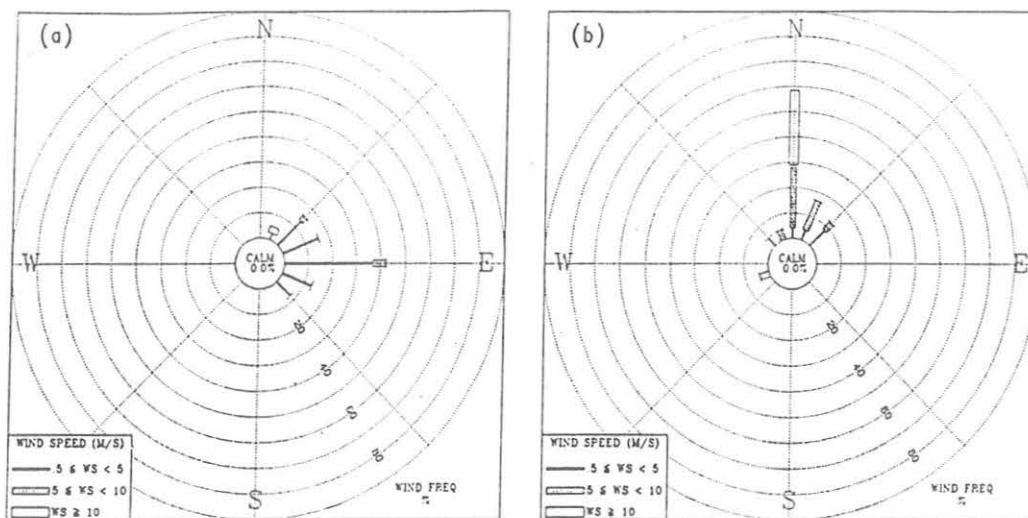


Fig. 3.10. Surface wind roses for (a) 35 clear days, and (b) 20 overcast days, during the austral winter of 1986.

Figure 3.11 is a composite of the resultant mean temperature and wind profiles for the lowest 3165 m of the SPO atmosphere for all the clear and all the overcast days during the winter of 1986. The depth of the inversion under clear and under overcast skies is indicated, as well as wind barbs for selected levels. The mean clear-sky wind profile shows weak northeasterly flow through the entire depth of the lower troposphere. The overcast-sky profile, however, is characterized by much stronger winds increasing and veering with height, indicative of northerly to northwesterly warm-air advection. The increased wind shear observed through the boundary layer suggests that turbulence must also increase. Thus sensible and latent heat can more readily mix downward from the warm layer to the surface. The combination of cloud radiative forcing, warm-air advection, and vertical mixing weakens the surface inversion significantly when transient disturbances reach the South Pole. *Stone and Kahl [1991]* suggest that a change in climate in this region may be detected by quantifying the bulk wind shear in the lower troposphere and the intensity of the inversion. A detectable trend in either or both of these parameters may then be linked to changes in large-scale atmospheric circulation patterns.

Synoptic-Scale Conditions and Trajectories. To understand better the synoptic-scale circulation patterns characterizing clear and overcast conditions at the South Pole, the upper-air NMC global gridded database was used

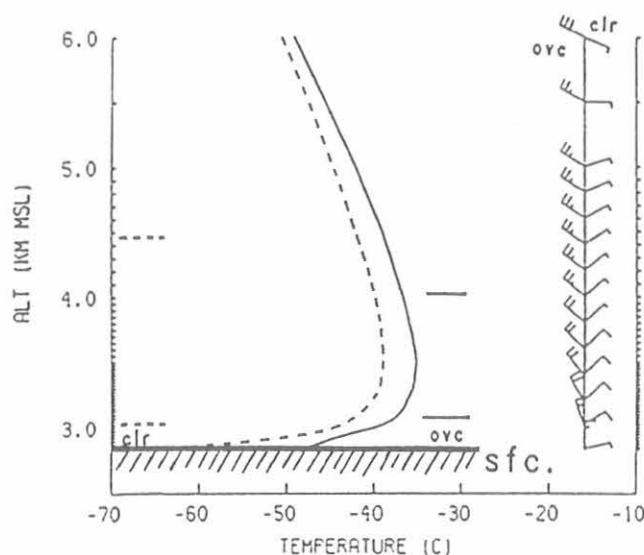


Fig. 3.11. Composite mean temperature profiles (to 6 km altitude) at 0000 UT for 35 clear days (dashed) and 20 overcast days (solid) during the winter of 1986 at the South Pole. Tops of surface inversions are indicated by horizontal dashed and solid lines for the clear and overcast days, respectively. The mean wind profiles for overcast and clear conditions are shown to the right of the temperature profiles. One full barb represents 5 knots. The tic marks on the ordinate axes show the levels to which individual sounding data were interpolated.

to produce mean 500-mbar geopotential height fields for all clear and all overcast days during July and August of 1986. This period best represented the entire winter period, since clear and overcast days were reasonably well distributed. Each field was analyzed for the region poleward of 60°S latitude. The results for the set of (13) clear days and (9) overcast days are presented in Figure 3.12.

The mean clear-day 500-mbar height field (Figure 3.12a) is characterized by a weak, high-pressure ridge oriented northwest-southeast along the axis of the east Antarctic Plateau coupled with a region of weak, low pressure over West Antarctica extending from the Weddell Sea to the Ross Sea. For overcast conditions at the pole (Figure 3.12b) the high-pressure ridge intensifies and shifts to a more northerly position. The low-pressure system deepens in a two-lobe pattern, with one center over the Weddell Sea and another over the Ross Sea. The coupling of the Weddell Sea low and the high-pressure ridge over the plateau produces a sufficient pressure gradient force to break down the normal continental outflow of air caused by subsidence aloft and katabatic flow near the surface. A cyclonic flow results, providing the necessary mechanism to transport warm, marine air and energy poleward from the region of the Weddell Sea.

This conclusion is supported by analyses of isobaric trajectories using the method of *Harris [1982]*. Back trajectories at the 700-mbar level, extending 2.5 days upwind, are presented in Figure 3.12 for all clear and all overcast days during the study period. A katabatic flow from higher on the plateau, initiated by intense regional radiative cooling [e.g., *Parish and Bromwich, 1987*], typifies clear-sky conditions, whereas rapid transport from the northern quadrant is characteristic of overcast conditions. Southwesterly transport has also been documented [*Bodhaine et al., 1986*], and apparently occurs when the gradient between the East Antarctic high-pressure ridge and the Ross Sea low-pressure center is of sufficient magnitude to force marine air poleward over the Transantarctic Mountain Range.

Summary and Conclusions

Analysis of the 1986 South Pole radiation data indicates that positive net cloud radiative forcing occurs during the austral winter when overcast conditions prevail. The resulting convergence of radiant energy in the lower troposphere combined with an increase in the horizontal and vertical flux of sensible and latent heat causes a significant weakening of the surface-based temperature inversion relative to clear-sky conditions. These processes are directly linked regionally to the dynamical state of the lower atmosphere, in that cloudiness and increased advection occur under rather well-defined synoptic conditions. Northerly transport of heat and moisture is favored when the Weddell Sea low-pressure system deepens and the East Antarctic high-pressure ridge intensifies, resulting in a pressure gradient force sufficient to reverse the normal katabatic outflow from the plateau.

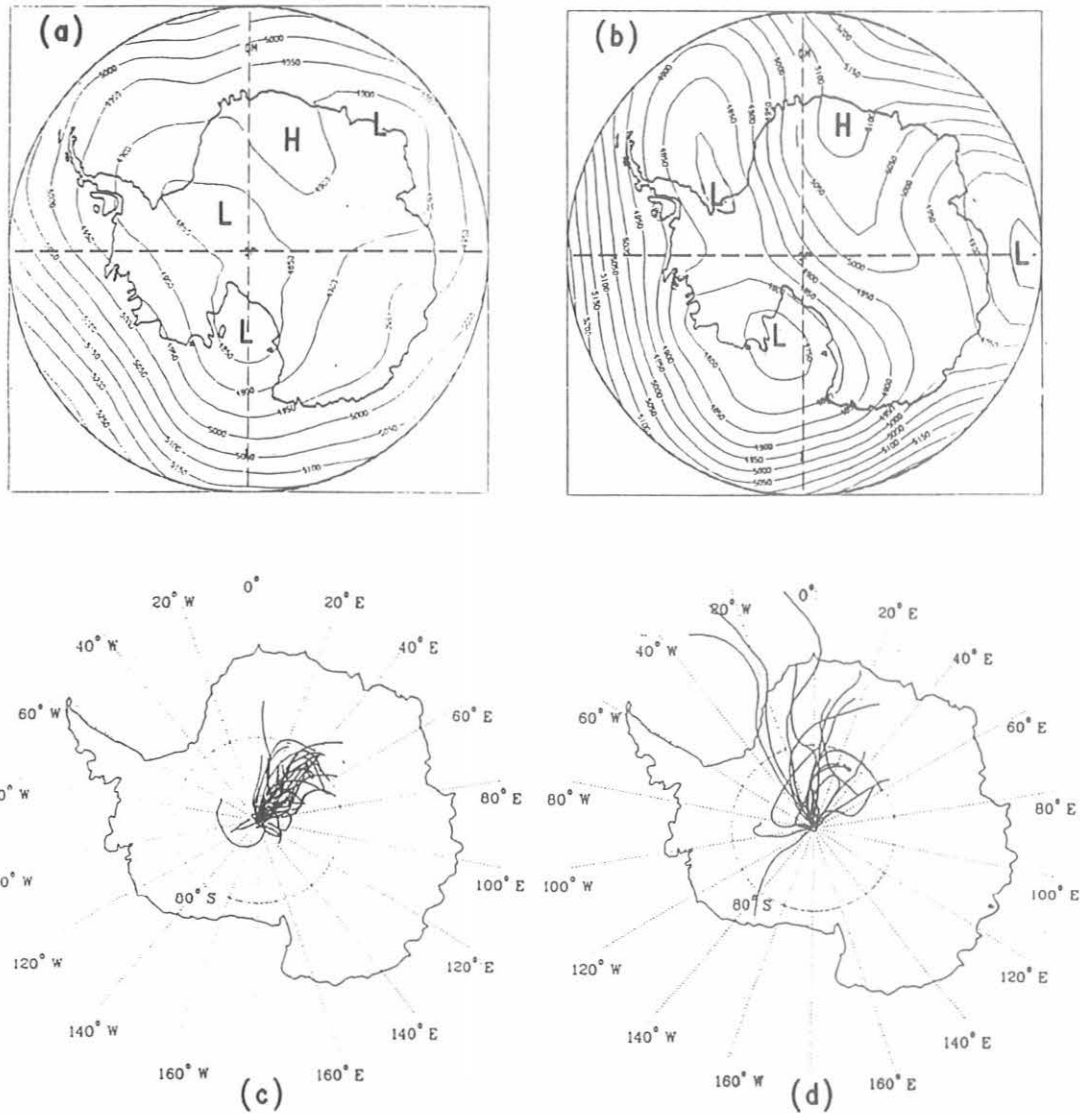


Fig. 3.12. Mean geopotential height fields (in meters) for the 500-mbar pressure surface south of 60° latitude for (a) 13 clear days, and (b) 9 overcast days, during July and August 1986, and 2.5-day 700-mbar back trajectories from the South Pole for (c) all clear days and (d) all overcast days during the winter of 1986.

The inversion intensity and bulk wind shear are suggested as appropriate indices to characterize the South Pole troposphere as it responds to varying regional circulation patterns. As such, these parameters may be useful indicators of climate change.

3.2.3. CONFIRMATION OF GROUND-BASED MEASUREMENTS OF OZONE AND STRATOSPHERIC AEROSOL AND COMPUTATIONS OF UMKEHR PROFILE AEROSOL ERRORS

Introduction

During the early phase of the El Chichon injection of aerosols into the stratosphere, ground-based lidar

measurements provided the bulk of information on stratospheric aerosol profiles. These measurements, together with ozone profiles derived from balloon ozonesonde observations, were used to correct Umkehr ozone profiles that were subsequently examined for trends during the period 1979-1986. (Umkehr observations are adversely affected by stratospheric aerosols.) The lidar observations were point measurements, not necessarily co-located with Umkehr measurements, and although it is generally assumed that stratospheric aerosols rapidly become uniformly spread over the globe, and more so zonally, confirmation of the procedure we used was desirable. Our recent work has concentrated mainly on the application of SAGE II data for (1) validating the zonal

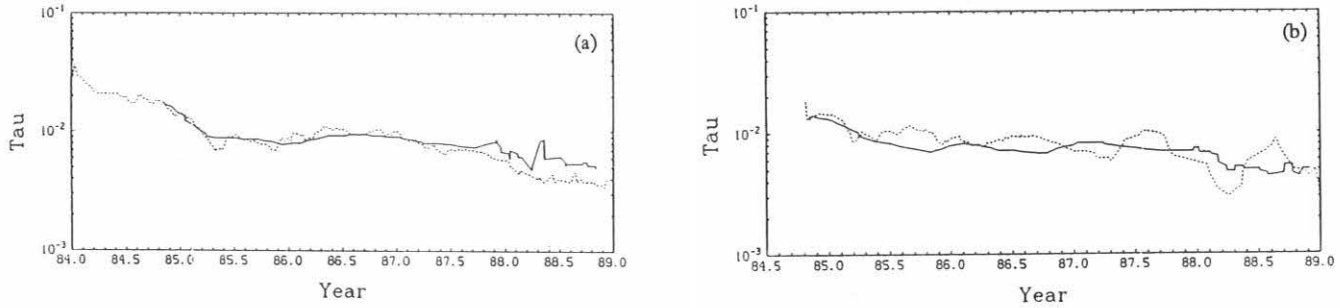


Fig. 3.13. Comparison of aerosol optical thickness (τ) derived from lidar observations (dashed-curve) and SAGE II observations (solid curve), at (a) MLO and (b) Boulder, Colorado.

representativeness of lidar aerosol and balloon ozone profile data for correcting Umkehr observations for aerosol effects, and (2) using SAGE II aerosol and ozone data alone for correcting ozone profiles derived from Umkehr observations made during 1984-1988.

Stratospheric Aerosols

The eruption of El Chichon produced greater than an order of magnitude increase in the equatorial stratospheric aerosol. Because of global spreading of the aerosols, Umkehr observations made in 1982 and later suffered serious errors. The only measurements of stratospheric aerosols available shortly after the eruption were from a network of lidar stations. Measurements from a selected set of northern midlatitude stations in this network were used to correct Umkehr ozone profiles from 1977 to 1986. The assumptions that were customarily invoked to reduce the lidar data introduced uncertainties that could only be assessed when SAGE II data became available. The SAGE II measurements began in 1984, 2 years after the El Chichon eruption. We conducted a preliminary comparison of lidar and SAGE II measurements made at MLO (19.3°N) and Boulder, Colorado (40°N), with SAGE II measurements averaged zonally in 10°-wide latitude bands centered at 20°N and 40°N. The SAGE II data were used to calculate aerosol optical thickness and lidar backscatter ratios ($1 + \text{aerosol}/\text{Rayleigh}$), with aerosol extinction-to-backscatter ratio assumed to be 50.

Figure 3.13 compares aerosol optical thickness derived from MLO lidar and the Boulder lidar data with similar data from SAGE II observations. The 1988 SAGE II data were not edited for cirrus contamination and therefore are noisy.

The comparisons show reasonably good agreement at both latitudes; however, note that there appears to be an annual cycle difference at the Boulder latitude. The difference is attributed to two likely factors. The first stems from use of a standard atmosphere to calculate Rayleigh backscatter. At 40°N the seasonal variation in air density with altitude is strong, while at 20°N the variation is relatively weak. The second results from use of 1.03 as the lidar backscatter minimum found in the troposphere or near the tropopause. It turns out that the Boulder ruby lidar backscatter minimum

frequently appeared to exist (we are not sure that this is real) in the troposphere at 5 km, or higher, above the surface. Also, the SAGE II data show that the tropopause aerosol minimum backscatter varies with season. It is suspected that the 1.03 minimum value may not be completely valid for the lidar normalization. Examination of 1985 and 1986 backscatter ratios calculated from SAGE II data in the vicinity of the tropopause suggests that the normalization procedure could be improved. Table 3.4 presents provisional mean aerosol backscatter data, mean aerosol extinction data, and mean heights of aerosol backscatter minima for 20°N and 40°N, derived from the 2 years of SAGE II observations. Note the large variabilities in the extinction and the backscatter ratios at 40°N compared with those observed at 20°N. The backscatter ratios exhibit an annual cycle (not shown) at 40°N with amplitude ranging from 1.01 to 1.06.

Another useful comparison of aerosol profile features is the altitude of median optical thickness, i.e., the altitude at which one-half the optical depth is above and one-half is below. Figure 3.14 shows comparisons of MLO and Boulder lidar results with SAGE II results. Here again, the 1988 SAGE II data have not been edited for cirrus contamination. Overall, the gross features of these comparisons show good agreement.

TABLE 3.4. Near-Tropopause Mean Minimum Values of Aerosol Extinction and Aerosol Backscatter Ratios, and Mean Altitudes of Aerosol Backscatter Minima at 20°N and 40°N, Derived for SAGE II Observations Made in 1985 and 1986

Latitude, °N	Mean Extinction,* km ⁻¹	Backscatter Minimum Mean Altitude, km	Backscatter Ratio†
20	0.00045 ± 0.00021	14.6 ± 1.2	1.010 ± 0.003
40	0.00126 ± 0.00058	14.3 ± 1.1	1.032 ± 0.015

Indicated variabilities are standard deviations.

*Aerosol extinction to backscatter ratio is 50 ± 5 .

†Lidar backscatter ratio is defined by $(R_B + M_B)/R_B$ where R_B is the Rayleigh backscattering and M_B is Mie scattering.

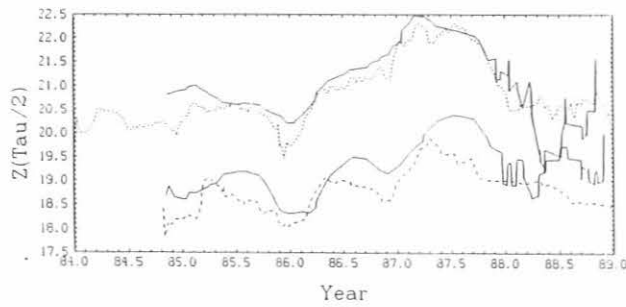


Fig. 3.1.4. Comparison of the altitude of median aerosol optical thickness for lidar observations (dashed curve) and SAGE II observations (solid curve). The upper plot shows MLO data and the lower plot shows Boulder data.

An interesting difference in altitude of 1.5-2.0 km is evident for the measurements made at the two different latitudes. Differences in aerosol profile features are related to differences in atmospheric structure and dynamics at the two latitudes.

Ozone Profiles

Computations of stratospheric aerosol-induced errors in Umkehr ozone profiles are ozone profile dependent. Therefore, it is important to use ozone profiles that are representative of conditions in the regions where stratospheric aerosol information is derived. Before SAGE II ozone data became available, aerosol-induced errors in Umkehr profiles were calculated using monthly ozone profile climatology data to 30 km altitude derived from ozonesonde flights made at MLO and Boulder. An average ozone profile from 30 to 80 km, currently in use for SBUV-2 satellite ozone data processing, is attached to the ozonesonde profile at 30 km.

Table 3.5 compares monthly average SAGE II ozone data (zonal) with ozonesonde and Umkehr data at MLO. These results provide a measure of the zonal representativeness of the ground-based measurements. The second column in Table 3.5 is the bias in the comparison observations in terms of the percentage difference in ozone referenced to the SAGE data. The third column in the table is the root-mean-square difference between the two types of measurements, while the fourth column lists the root-mean-square differences with biases removed. Root-mean-square difference with bias removed is a better measure of the ozone sensing variability of the two types of measurements. In layers 1 and 2 the Umkehr and SAGE II measurements are fraught with difficulties; the Umkehr sensitivity to ozone is minimal, and the SAGE measurements are affected by cirrus. Therefore, these layers are not included in the comparison.

Comparison of Lidar and SAGE II Error Calculations

Calculations of the stratospheric aerosol error to Umkehr ozone profiles were made with the monthly average ozonesonde and lidar data from MLO. Similar calculations were made through the use of the SAGE II data representing

TABLE 3.5 Comparison of Climatological SAGE II Ozone Data at MLO With Climatological Ozonesonde and Umkehr Data at MLO

Umkehr Layer No.	Bias, %	RMS Error, %	RMS Error, (Bias Removed), %
<i>SAGE II and Ozonesonde Data Compared</i>			
6	-5.6	7.2	4.5
5	-2.5	3.2	2.1
4	-5.9	7.7	4.8
3	-8.3	23.9	22.4
<i>SAGE II and Umkehr Data Compared</i>			
9	-6.4	10.3	8.0
8	2.5	6.4	5.9
7	3.1	6.2	5.3
6	-1.3	4.4	4.2
5	4.5	5.5	3.3
4	-3.5	6.8	5.8
3	-6.1	5.7	5.2

a 10°-wide latitude band centered at 20° for MLO. Plots of the results for 1985 are compared in Figure 3.15. The good agreement noted in this comparison suggests that the lidar

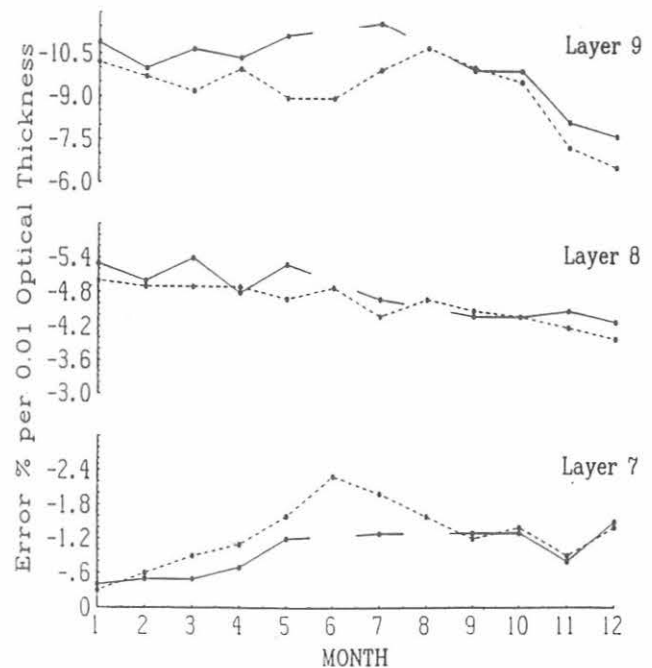


Fig. 3.15. Comparison of calculated stratospheric aerosol-induced errors in Umkehr profile layers 7-9 derived from SAGE II data for 20°N latitude (solid-line curve) and MLO lidar data for 19° latitude (dashed-line curve), obtained in 1985. Layer 9 is at approximately 45 km; layer 8 is at approximately 40 km; and layer 7 is at approximately 35 km. The indicated errors are well within the daily noise level of the Umkehr observations.

measurements used for the aerosol error corrections are reasonably representative of existing conditions.

Conclusion

The availability of SAGE II data has greatly increased the stratospheric aerosol data base for calculating errors to Umkehr ozone profiles. Moreover, whether ground-based lidar or satellite stratospheric aerosol data are used to calculate these errors, the results are consistent. This work served as an independent verification of the use of lidar stratospheric aerosol profile data to correct Umkehr measurements before 1984 when only lidar data were available.

4. REFERENCES

- Bodhaine, B.A., Aerosol measurements at four background sites, *J. Geophys. Res.*, **88**, 10753-10768, 1983.
- Bodhaine, B.A., and J.J. DeLuisi, An aerosol climatology of Samoa, *J. Atmos. Chem.*, **3**, 107-122, 1985.
- Bodhaine, B.A., and M.E. Murphy, Calibration of an automatic condensation nuclei counter at the South Pole, *J. Aerosol Sci.*, **11**, 305-312, 1980.
- Bodhaine, B.A., B.G. Mendonca, J. M. Harris, and J. M. Miller, Seasonal variations in aerosols and atmospheric transmission at Mauna Loa Observatory, *J. Geophys. Res.*, **86**, 7395-7398, 1981.
- Bodhaine, B.A., J.J. DeLuisi, J.M. Harris, P. Houmère, and S. Bauman, Aerosol measurements at the South Pole, *Tellus*, **38B**, 223-235, 1986.
- Bodhaine, B.A., J.J. DeLuisi, J.M. Harris, P. Houmère, and S. Bauman, PIXE analysis of South Pole aerosol, *Nucl. Instr. Meth.*, **B22**, 241-247, 1987.
- Carroll, J.J., Studies of atmospheric energy transfer at the South Pole, *Ant. J. U.S.*, **18**(5), 248-249, 1983.
- Cess, R.D., and I.L. Vulis, Inferring surface solar absorption from broadband satellite measurements, *J. Climate.*, **2**, 974-985, 1989.
- Cess, R.D., E.G. Dutton, J.J. DeLuisi, and F. Jiang, Determining surface solar absorption from broadband satellite measurements for clear skies: Comparison with surface measurements, *J. Climate*, accepted, 1990.
- Cogley, J.G., and A. Henderson-Sellers, Effects of cloudiness on the high-latitude surface radiation budget, *Mon. Weather Rev.*, **112**, 1017-1032, 1984.
- Dutton, E.G., Comments on "Major volcanic eruptions and climate: a critical review," *J. Climate*, **3**, 587-588, 1990a.
- Dutton, E.G., Annual forcing of the surface radiation balance diurnal cycle measured from a high tower near Boulder, CO, *J. Climate*, in press, 1990b.
- Dutton, E.G., and J.J. DeLuisi, Measurements of solar radiation at Mauna Loa observatory, 1978-1985, with emphasis on the effects of the eruption of El Chichon, *NOAA Data Rep. ERL ARL-13*, 35 pp., NOAA Air Resources Laboratory, Boulder, CO, 1987.
- Dutton, E.G., J.J. DeLuisi, and A.P. Austring, Interpretation of Mauna Loa atmospheric transmission relative to aerosols, using photometric precipitable water amounts, *J. Atmos. Chem.*, **3**, 53-68, 1985.
- Elkins, J.W., and R.M. Rosson (Eds.), *Geophysical Monitoring for Climatic Change, No. 17: Summary Report 1988*, 142 pp., NOAA Air Resources Laboratory, Boulder, CO, 1989.
- Ellis, H.T., and R.F. Pueschel, Solar radiation: Absence of air pollution trends at Mauna Loa, *Science*, **172**, 845-846, 1971.
- Harris, J.M., The GMCC atmospheric trajectory program, *NOAA Tech. Memo. ERL ARL-116*, 30 pp., NOAA Air Resources Laboratory, Boulder, CO, 1982.
- Hogan, A., S. Barnard, J. Samson, and W. Winters, The transport of heat, water vapor and particulate material to the South Polar Plateau, *J. Geophys. Res.*, **87**(C6), 4287-4292, 1982.
- Massey, D.M., T.K. Quakenbush, and B.A. Bodhaine, Condensation nuclei and aerosol scattering extinction measurements at Mauna Loa Observatory: 1974-1985, *NOAA Data Rep. ERL ARL-14*, 174 pp., NOAA Air Resources Laboratory, Silver Spring, MD, 1987.
- Mendonca, B.G., Local wind circulation on the slopes of Mauna Loa, *J. Appl. Meteorol.*, **8**, 533-541, 1969.
- Mendonca, B.G., K.J. Hanson, and J.J. DeLuisi, Volcanically related secular trends in atmospheric transmission at Mauna Loa, Hawaii, *Science*, **202**, 513-515, 1978.
- Metnieks, A.L., and L.W. Pollak, Instruction for use of photoelectric condensation nucleus counters, *Geophys. Bull. No. 16*, School of Cosmic Physics, Dublin Institute for Advanced Study, Dublin, Ireland, 1959.
- Parish, T.R., and D.H. Bromwich, The surface wind field over the Antarctic ice sheets, *Nature*, **328**, 51-54, 1987.
- Parrington, J.R., W.H. Zoller, and N.K. Aras, Asian dust: Seasonal transport to the Hawaiian Islands, *Science*, **220**, 195-197, 1983.
- Radke, L.F., C.A. Brock, R.J. Ferek, and D.J. Coffman, Summer-time Arctic hazes, Paper A52B-03 presented at the AGU Fall Annual Meeting, San Francisco, December 3-7, 1990.
- Ramanathan, V., R.D. Cess, E.F. Harrison, P. Minnis, B.R. Barkstrom, E. Ahmad, and D. Hartmann, Cloud-radiative forcing and climate: Results from the Earth Radiation Budget Experiment, *Science*, **243**, 57-63, 1989.
- Schlesinger, M.E., and J.F.B. Mitchell, Model projections of equilibrium climatic response to an increased carbon dioxide concentration, in *Projecting the Climatic Effects of Increasing Carbon Dioxide*, DOE/ER-0237, edited by M.C. MacCracken and F.M. Luther, pp. 81-147, U.S. Dept. of Energy, Carbon Dioxide Research Division, Livermore, CA, 1985.
- Schwerdtfeger, W., *Weather and Climate of the Antarctic*, Elsevier Science, Amsterdam, 1984.
- Skala, G.F., A new instrument for the continuous measurement of condensation nuclei, *Anal. Chem.*, **35**, 702-706, 1963.
- Stone, R.S., and J.D. Kahl, Variations in boundary layer properties associated with clouds and transient weather disturbances at the South Pole during winter, *J. Geophys. Res.*, **96** (D3), 537-5144, 1991.
- Stone, R.S., E.G. Dutton, and J.J. DeLuisi, Surface radiation and temperature variations associated with cloudiness at the South Pole, *Ant. J. U.S.*, **24**, 230-232, 1989.

4. Carbon Cycle Group

P. NOVELLI (Editor), T.J. CONWAY, D.G. KITZIS, P.M. LANG, R. MARTIN, K. MASARIE,
L.P. STEELE, P.P. TANS, K.W. THONING, AND L.S. WATERMAN

4.1. CONTINUING PROGRAMS

4.1.1. CONTINUOUS IN-SITU AND FLASK SAMPLE CARBON DIOXIDE MEASUREMENTS

The concentration of atmospheric CO₂ was measured with continuously operating NDIR analyzers at the four CMDL observatories during 1989 as in previous years. Monthly and annual mean CO₂ concentrations [in the WMO 1985 mole fraction scale (X85)] are given in Table 4.1. These values are provisional, pending final calibrations of station standards. Preliminary selected daily average CO₂ concentrations for 1989 are plotted versus time for the four observatories in Figure 4.1. The CO₂ measurement programs and data for MLO (through 1985) and SMO (through 1987) were analyzed in detail; and the results were published in 1989 [Komhyr *et al.*, 1989; Thoning *et al.*, 1989; Waterman *et al.*, 1989].

The continuous CO₂ measurements made at BRW in 1989 exhibited an increase in the number of hourly-averaged concentrations showing high short-term variability. Figure 4.2 shows unselected (except for instrumental malfunctions) hourly-averaged BRW data for 1987, 1988, and 1989. Higher variability, especially in the months of May, June, July, and August was evident in 1989. In addition, the distribution of standard deviations of the hourly averages showed an increase in the number of hours with large (>0.3 ppm) variability for 1989. These variable concentrations were not always correlated with wind directions from the town of Barrow (except for January and February), but did show some correlation with temperature. Anomalously warm periods showed high variability in CO₂. Continuous CH₄ measurements from BRW showed this same effect.

TABLE 4.1. Provisional Monthly CO₂ Concentrations (ppm, Relative to Dry-Air X85 Mole Fraction Scale) from the 1989 Continuous Analyzer Data

	BRW	MLO	SMO	SPO
Jan.	360.88	352.72	351.29	349.03
Feb.	358.16	353.16	351.62	348.99
March	359.15	353.68	351.38	348.90
April	359.27	355.29	351.40	348.98
May	358.74	355.54	351.66	349.75
June	357.04	355.02	350.73	350.20
July	349.34	353.70	351.04	350.55
Aug.	344.48	351.30	351.07	350.96
Sept.	346.18	349.89	350.62	351.04
Oct.	351.19	350.19	350.21	351.08
Nov.	355.81	351.42	350.63	350.42
Dec.	358.29	352.76	350.60	349.89
Annual	354.88	352.89	351.02	349.98

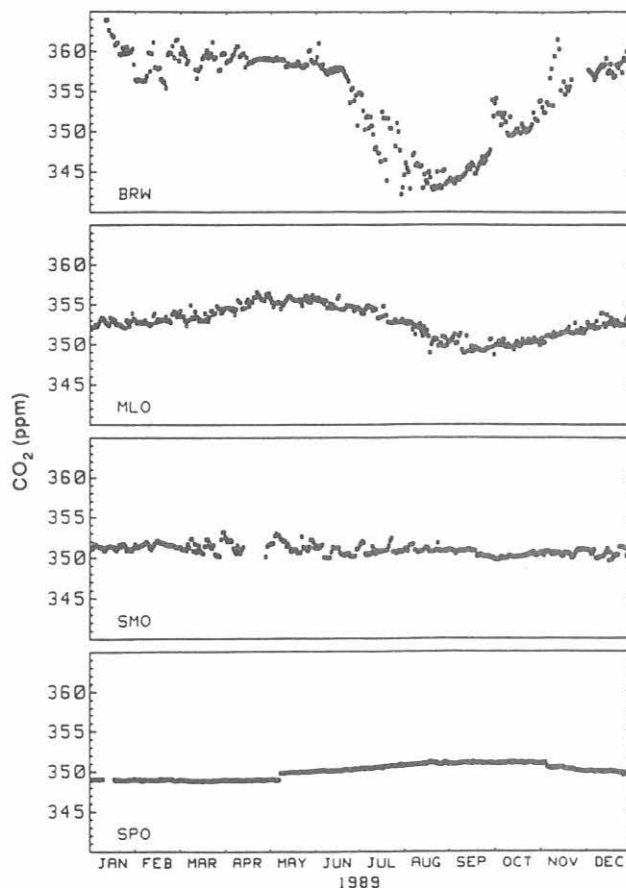


Fig. 4.1. Preliminary selected 1989 daily-average CO₂ concentrations from the in-situ measurements at BRW, MLO, SMO, and SPO.

Because June, July, and August were unusually warm in 1989, this suggests a relationship between CO₂ and CH₄ concentrations and temperature during the summer.

In 1989 the conversion from synthetic-air standards to natural-air CO₂ standards was begun. Natural air standards were prepared using dried ambient air collected at the C1 site on Niwot Ridge (NWR), Colorado. The CO₂ concentrations were adjusted during the tank-filling procedure either by adding a small amount of air with a very high CO₂ concentration or by dilution with air having a very low CO₂ concentration. These cylinders will be used as station standards, station working gases, flask analysis working gases, and test gases. Our goal is to make all CO₂ measurements with respect to natural-air CO₂ reference gases. This should eliminate the possibility of small carrier gas effects, which may vary from one NDIR instrument to another [Griffith, 1982; Bodhaine and Rosson, 1988]. This

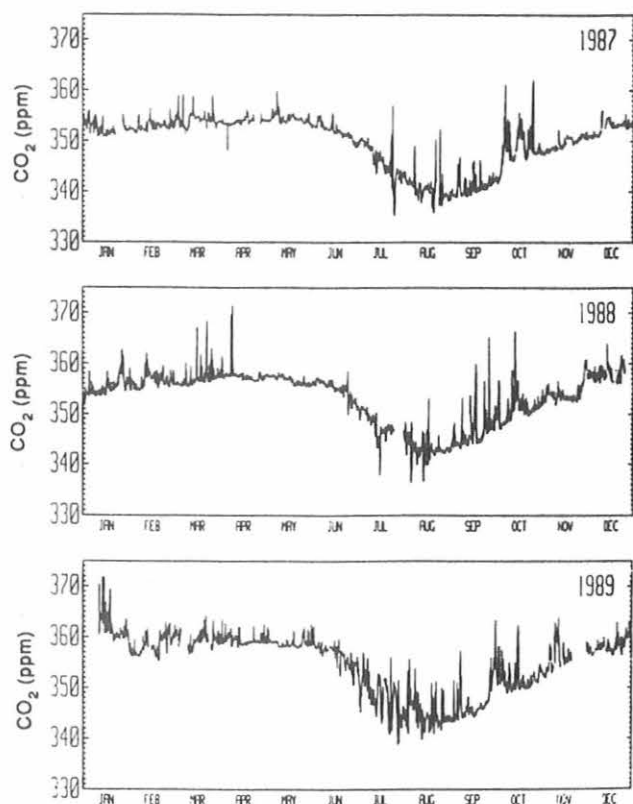


Fig. 4.2. Unselected hourly-average CO₂ concentrations measured at BRW during 1987-1989.

conversion will require filling ~75 cylinders per year at the NWR site.

The measurement of the global distribution of atmospheric CO₂ from flask samples collected at the CMDL cooperative flask sampling network continued. In 1989 the network consisted of 29 sites (Table 4.2); two sampling sites in Bermuda were added to the network in 1989, one on the west coast (BMW) and one on the east coast (BME). Provisional annual mean CO₂ concentrations are also given in Table 4.2. The Pacific air sampling program (called PAC) aboard the container ship *Southland Star* also continued in 1989.

The measurement of atmospheric CO was expanded to several more flask network sites in 1989 (see section 4.3). Because the CO measurements require flasks equipped with Teflon O-ring stopcocks rather than the greased stopcocks used for CO₂, we overlapped sampling in the two types of flasks to ensure that no offsets were introduced into the CO₂ time series. These field comparisons showed no significant offset due to the Teflon O-rings. In fact, they resulted in significantly improved sample quality at several sites. Figure 4.3 shows the percentage of acceptable pair-samples (defined as having a CO₂ pair difference of ≤ 0.5 ppm), according to sample stopcock types, for six sites where overlapped sampling was conducted.

TABLE 4.2. Provisional 1989 Annual Mean CO₂ Concentrations From the Flask Network Sites

Code	Station	CO ₂ , ppbv
ALT	Alert, N.W.T., Canada	355.1
AMS	Amsterdam Island	350.5
ASC	Ascension Island	351.7
AVI	St. Croix, Virgin Islands	353.5
AZR	Terceira Island, Azores	[]
BME	Bermuda (east coast)	[]
BMW	Bermuda (west coast)	[]
BRW	Barrow, Alaska	355.1
CBA	Cold Bay, Alaska	354.4
CGO	Cape Grim, Tasmania	350.3
CHR	Christmas Island	353.3
CMO	Cape Meares, Oregon	354.4
GMI	Guam, Mariana Islands	353.6
HBA	Halley Bay, Antarctica	[]
KEY	Key Biscayne, Florida	354.4
KUM	Cape Kumukahi, Hawaii	352.9
MBC	Mould Bay, Canada	355.6
MID	Midway Island	354.1
MLO	Mauna Loa, Hawaii	352.8
NWR	Niwot Ridge, Colorado	353.1
PSA	Palmer Station, Antarctica	350.9
RPB	Ragged Point, Barbados	352.9
SEY	Mahé Island, Seychelles	352.3
SGI	South Georgia Island	[]
SHM	Shemya Island, Alaska	354.5
SMO	American Samoa	351.7
SPO	South Pole, Antarctica	350.4
STM	Ocean Station M	354.0
SYO	Syowa Station, Antarctica	349.7

Square brackets indicate insufficient data to calculate annual mean.

At Ascension, Cape Kumukahi, SMO, and Guam the percentage of acceptable pairs increased from ~60% for the greased stopcock flasks to better than 80% for the Teflon O-ring stopcocks. The already high percentages of acceptable pairs at BRW and MLO increased only slightly. This suggests that the greased stopcocks produce variable amounts of contamination in the flasks under conditions of intense sunlight, high temperatures, and/or high humidity, leading to poor pair agreement. On the basis of these results, we have discontinued sampling in greased stopcock flasks at these sites. Also, a long-term program has been initiated to convert to use of larger flasks (2.5 L) equipped with Teflon O-ring stopcocks at all sampling sites.

The globally averaged CO₂ growth rate determined from the flask network data reached a peak of ~2.6 ppm yr⁻¹ in late 1987-early 1988 (Figure 4.4). This peak was followed by a minimum of ~1.2 ppm yr⁻¹ in early 1989. The average growth rate for 1988 was ~2.0 ppm yr⁻¹, and for 1989 it was ~1.6 ppm yr⁻¹. As reported earlier [Elkins and Rosson, 1989], the 1987-1988 growth rate variations were consistent with previous El Niño/Southern Oscillation patterns. It appears that the changes in global atmospheric CO₂ concentration are even more complicated and less well understood than we previously believed.

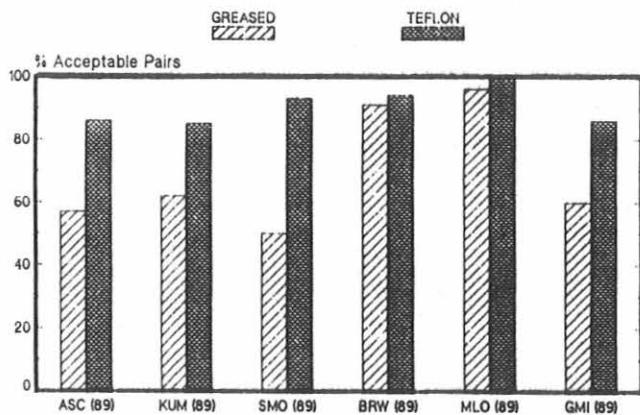


Fig. 4.3. Percentage of flask sample pairs meeting the 0.5 ppm CO₂ pair difference criterion. During 1989 samples were collected at these six sites in standard greased-stopcock flasks and also in flasks equipped with Teflon O-ring stopcocks.

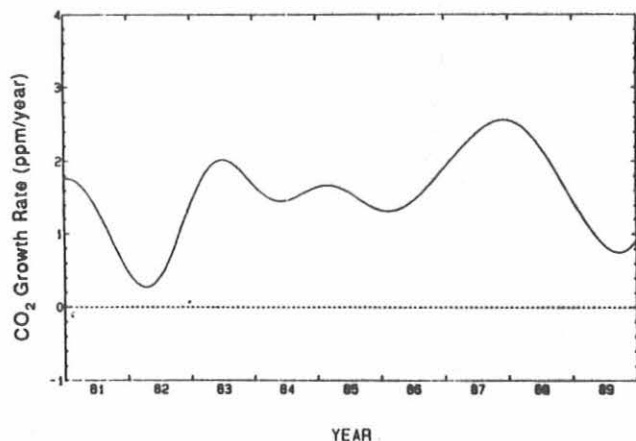


Fig. 4.4. The globally averaged CO₂ growth rate determined from the flask network data for 1981-1989.

Figure 4.5 shows the normalized annual-mean CO₂ latitude gradients determined from the flask network data for 1981-1987, 1988, and 1989. The north pole-to-south pole difference increased from ~2.8 ppm (1981-1987 mean), to ~3.6 ppm in 1988, and then to ~4.6 ppm in 1989. To establish the robustness of this result, we plotted the difference between annual hemispheric means calculated from the flask network data (Figure 4.6). A linear regression analysis reveals that the hemispheric difference is increasing at 0.13 ppm yr⁻¹ ($\sigma = 0.03$ ppm yr⁻¹; $r = 0.84$). Analysis of the in-situ data from the four CMDL observatories yields a similar result. These results suggest that a change is occurring in the relative magnitudes of northern and southern hemisphere CO₂ sources and sinks.

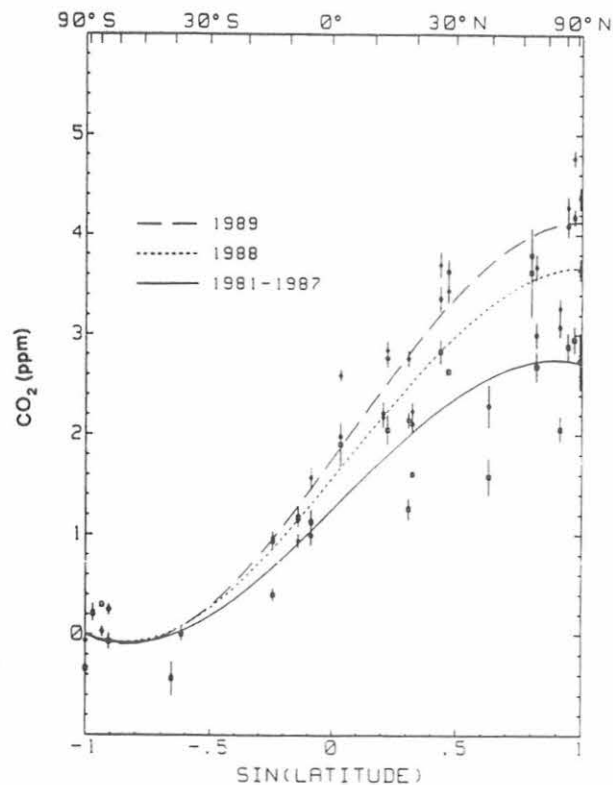


Fig. 4.5. A comparison of the 1988 (x) and 1989 (◊) CO₂ latitude gradients determined from flask network data, with the mean gradient for 1981-1987 (□). The curves are third-degree polynomials fitted to the annual means; the three curves are forced through 0 at the South Pole.

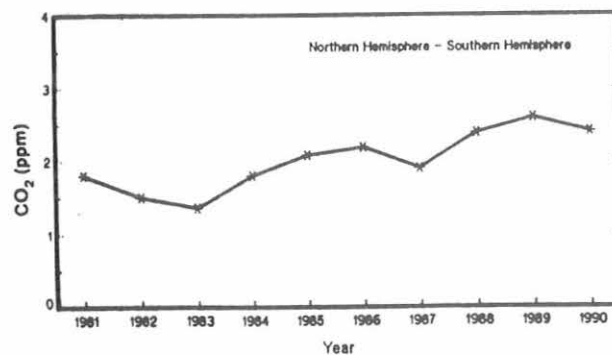


Fig. 4.6. Differences between northern hemisphere and southern hemisphere annual CO₂ averages determined from the flask network data for 1981-1990. A linear regression analysis shows a significant trend in the interhemispheric difference of 0.13 ppm yr⁻¹ ($\sigma = 0.03$ ppm yr⁻¹; $r = 0.84$).

Preliminary results obtained using the two-dimensional model of *Tans et al.* [1989] provide no clear explanation of the observations. In 1988 the model requires a larger northern hemisphere source and in 1989 a larger southern hemisphere sink. Changes in known and estimated fossil fuel CO₂ emissions are too small to account for the observed trend in the latitude gradient. A source/sink imbalance of $\sim 1 \times 10^{15}$ g C yr⁻¹, or $\sim 20\%$ of the annual fossil fuel CO₂ emissions, is needed to produce a 1 ppm increase in the north pole-to-south pole difference. This startling result highlights our incomplete understanding of the global carbon cycle and, therefore, the fundamental uncertainty inherent in all predictions of future atmospheric CO₂ and greenhouse effect scenarios.

4.1.2. FLASK SAMPLE METHANE MEASUREMENTS

During 1989 the determination of the global distribution of atmospheric CH₄ continued. Measurements of the atmospheric CH₄ concentration were made from weekly flask samples collected at 29 sites in the CMDL flask sampling network. Provisional annual mean CH₄ concentrations, calculated from the monthly means for each site in the flask network are shown in Table 4.3. Missing annual mean values indicate that there were insufficient data during 1989 for that particular site. We began collecting flask samples from BME in February and BMW in May 1989. Azores and Seychelles had sampling problems that resulted in large gaps in the data record for 1989. Samples from Halley Bay for the latter part of 1989 have not yet arrived in Boulder. The CH₄ measurement data for the past 6 years are shown in Figure 4.7. (Data from the high altitude sites at NWR and

TABLE 4.3. Provisional 1989 Annual Mean CH₄ Concentrations From the Flask Network Sites

Code	Station	CH ₄ , ppbv
ALT	Alert, N.W.T., Canada	1777.2
AMS	Amsterdam Island	1635.6
ASC	Ascension Island	1647.1
AVI	St. Croix, Virgin Islands	1704.4
AZR	Terceira Island, Azores	[]
BME	Bermuda (east coast)	[]
BMW	Bermuda (west coast)	[]
BRW	Barrow, Alaska	1790.6
CBA	Cold Bay, Alaska	1763.3
CGO	Cape Grim, Tasmania	1635.4
CHR	Christmas Island	1662.9
CMO	Cape Meares, Oregon	1756.0
GMI	Guam, Mariana Islands	1695.7
HBA	Halley Bay, Antarctica	[]
KEY	Key Biscayne, Florida	1721.7
KUM	Cape Kumukahi, Hawaii	1707.1
MBC	Mould Bay, Canada	1779.8
MID	Midway Island	1729.5
MLO	Mauna Loa, Hawaii	1696.8
NWR	Niwot Ridge, Colorado	1725.3
PSA	Palmer Station, Antarctica	1633.9
RPB	Ragged Point, Barbados	1702.5
SEY	Mahé Island, Seychelles	[]
SGI	South Georgia Island	[]
SHM	Shemya Island, Alaska	1770.7
SMO	American Samoa (Matatula Point)	1643.2
SPO	South Pole, Antarctica	1633.8
STM	Ocean Station M	1765.2
SYO	Syowa Station, Antarctica	1634.4

Square brackets indicate insufficient data to calculate annual mean.

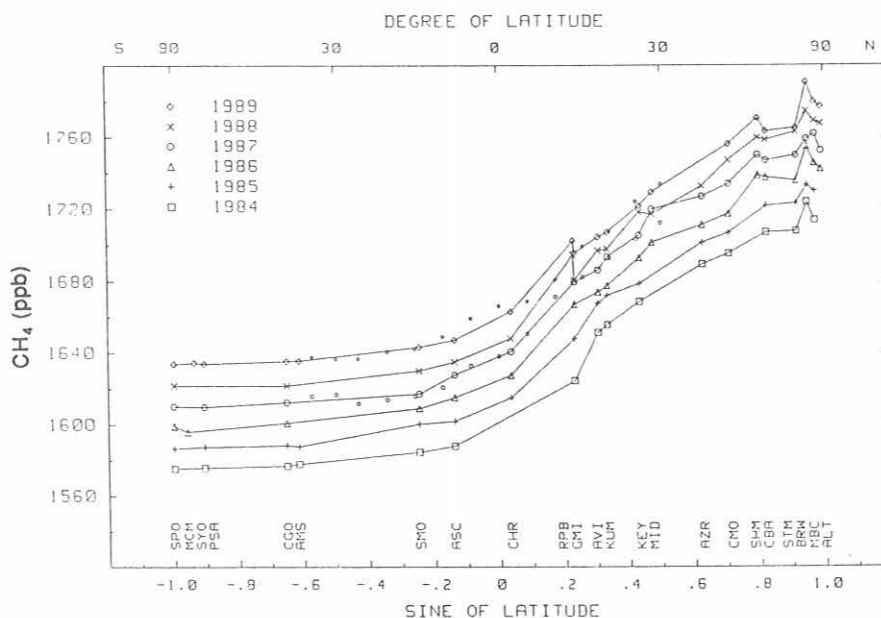


Fig. 4.7. Latitudinal distribution of the annual mean CH₄ concentrations for 1984-1989. Annual means are determined from flask samples. Data from the high-altitude sites MLO and NWR are excluded. The small circles are data from the *Southland Star*.

MLO are not included.) Annual mean CH₄ concentrations in the figure are plotted as a function of sine latitude for the years 1984 to 1989. (Sine latitude was used to better represent relative global surface areas for each latitudinal band.)

Three important points concerning the global distribution of CH₄ in the troposphere are apparent in Figure 4.7. First, there is a strong gradient in the CH₄ concentration between the northern and southern hemispheres, which reflects the greater CH₄ source strength in the north. Second, the atmospheric CH₄ concentration is increasing rapidly, by approximately 0.8% per year. Third, the CH₄ concentration varies little from site to site in the southern hemisphere. The average growth rate for SPO, calculated from 12-month running means, is 11.9 ppbv yr⁻¹.

In addition to weekly samples collected at sites in the flask sampling network, flask samples were collected aboard the container ship *Southland Star*. The flasks were collected at approximately 5° latitude intervals (Table 4.4). Approximately 17 samples were collected at each latitude during the year, at roughly 3-week intervals. The provisional 1989 annual mean CH₄ concentrations are shown in Figure 4.7 as the small circles. Agreement between shipboard and flask site samples was excellent, strongly supporting our view that the global distribution of CH₄ in the marine boundary layer can be reliably evaluated through the flask network.

4.1.3. IN-SITU METHANE MEASUREMENTS AT MLO

CH₄ measurements at MLO continued in 1989. Boulder personnel traveled to MLO and completely overhauled the GC and sampling systems. The internal switching valves of the GC, which can lead to poor-quality data when operating unsatisfactorily, were replaced. This preventative maintenance ensured an uninterrupted stream of data. A new secondary standard, calibrated against the four CMDL primary methane standards, was put into service.

TABLE 4.4. Provisional 1989 Annual Mean CH₄ Concentrations From the *Southland Star* Shipboard Flasks

Latitude	CH ₄ , ppbv
35°S	1637.7
30°S	1636.8
25°S	1636.9
20°S	1640.7
15°S	1642.2
10°S	1649.0
5°S	1659.3
Equator	1666.3
5°N	1668.8
10°N	1681.2
15°N	1699.3
20°N	1707.4
25°N	1724.3
30°N	1733.9

The daily average CH₄ concentrations for 1987-1989 are shown in Figure 4.8. Daily averages were calculated after removing data from periods when the GC was performing unsatisfactorily. The causes for the approximately 40 ppbv variations in CH₄ concentration occurring on the time scale of days to weeks are as yet unclear. A thorough analysis of these variations is in progress. Provisional monthly averages from the in-situ measurements at MLO are shown in Table 4.5. These monthly averages were calculated from the daily average CH₄ concentrations and exclude data edited for instrument performance. During 1989 the CH₄ GC system at MLO was operating satisfactorily for 89% of the time. The in-situ measurements were in good agreement with the CH₄ concentrations determined in flask samples (Figure 4.9).

4.1.4. IN-SITU METHANE MEASUREMENTS AT BRW

In-situ measurements of CH₄ at BRW continued in 1989 with a frequency of 60 measurements per day. Daily averages are shown in Figure 4.10 for the period 1986-1989. During 1989 the CH₄ GC system at BRW was operating

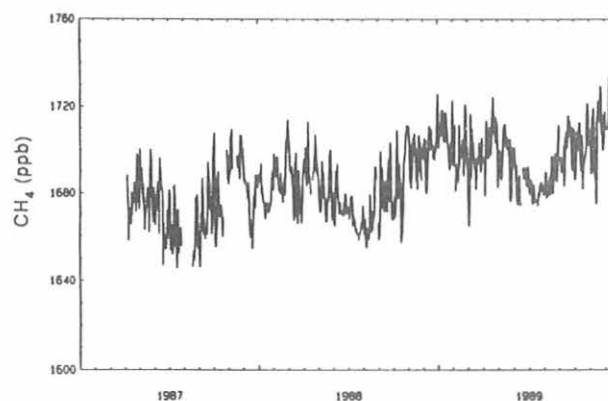


Fig. 4.8. Unselected daily average CH₄ concentrations for MLO for 1987-1989. Gaps in the data are due to instrument malfunctions.

TABLE 4.5. Provisional 1989 In-Situ CH₄ Monthly Means at MLO

Month	CH ₄ , ppbv	Std. Dev., ppbv
Jan.	1706.9	8.39
Feb.	1697.9	10.11
March	1693.8	10.41
April	1705.0	9.60
May	1697.6	10.30
June	1687.6	8.19
July	1681.3	4.42
Aug.	1687.2	7.47
Sept.	1703.2	9.18
Oct.	1701.0	9.16
Nov.	1705.6	13.05
Dec.	1710.0	8.68

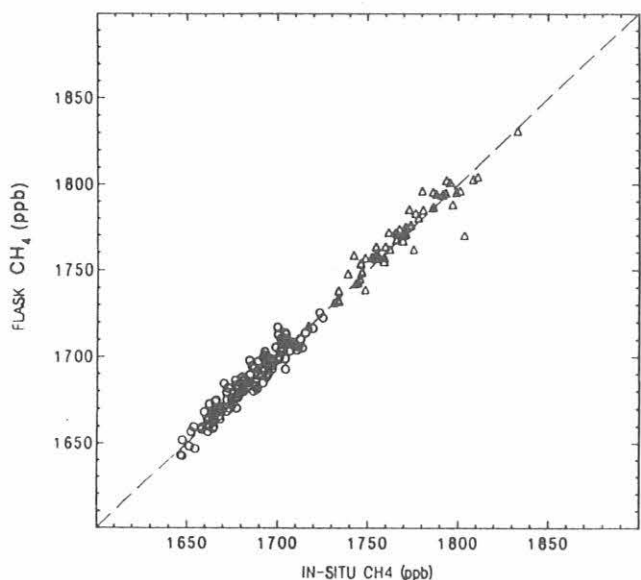


Fig. 4.9. Atmospheric CH₄ concentrations at MLO (o) and BRW (Δ) from flask samples versus the corresponding hourly-average in-situ CH₄ concentration for each site. The comparison period is April 1987 through December 1989. The dashed line represents perfect agreement between the two types of measurements.

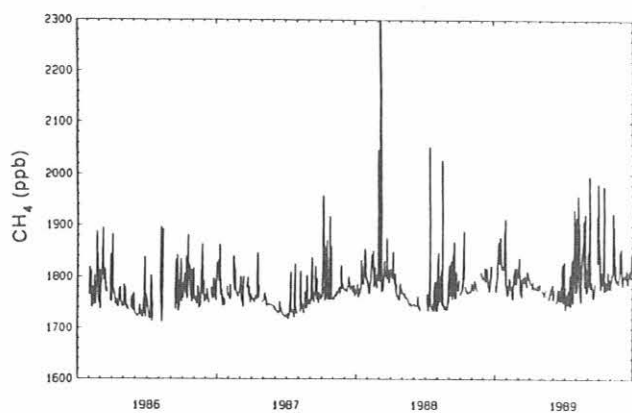


Fig. 4.10. Unselected daily average CH₄ concentrations for BRW for 1986-1989.

satisfactorily 92% of the time. The data presented in Figure 4.10 are unselected for wind speed and direction. The large short-term variations in CH₄ concentrations result from local contamination sources that affect the site during periods when winds blow from specific directions (for example, from the direction of the town). Selected monthly averages (calculated from daily-average CH₄ concentrations) are listed in Table 4.6. These CH₄ values are associated with wind speeds greater than 3 m s⁻¹ and within a sector defined as 20° to 110°. On the basis of CMDL meteorological data from BRW, 1989 was an anomalous year when winds were predominantly from the west during January, February, and March. Agreement between the flask samples collected at BRW and the in-situ measurements was excellent, as shown in Figure 4.9.

TABLE 4.6. Provisional 1989 In-Situ CH₄ Monthly Means at BRW

Month	CH ₄ , ppbv	Std. Dev., ppbv
Jan.	1790.5	*
Feb.	1791.1	10.94
March	1795.6	18.33
April	1780.2	6.05
May	1766.8	6.53
June	1758.1	10.11
July	1777.8	27.79
Aug.	1814.8	54.63
Sept.	1785.7	39.33
Oct.	1787.9	20.96
Nov.	1801.3	27.89
Dec.	1797.7	8.21

*This concentration represents only 1 day of this month. The standard deviation was not calculated.

4.1.5. FLASK SAMPLE CARBON MONOXIDE MEASUREMENTS

In collaboration with the Halocarbons Group, we have established a set of 17 gravimetric reference gas mixtures for use in the measurement of atmospheric CO. The mixing ratios of the gravimetric standards range from 25 to 1003 ppb (parts per billion by mole fraction) (Table 4.7). This concentration range covers that present in the background troposphere (approximately 50 to 250 ppb), and also those levels found in remote locations affected by anthropogenic activities such as biomass burning. The standards are contained in 5.9-L aluminum cylinders with brass fittings. Standards with CO concentrations reflecting those in the atmosphere were prepared from one of three high-concentration "parents." Two parents were prepared gravimetrically from 99.97% CO to have CO concentrations of ~250 ppm, from which a total of 14 lower-concentration standards were prepared. In addition, we prepared three low-concentration standards using a NIST SRM (CO concentration of 9.7 ppm) as the parent. Comparison of standards derived from the gravimetric standards with those derived from the SRM show no statistical difference between the two scales. Therefore, all low-concentration standards were pooled to define a new reference scale for CO (Figure 4.11).

The CO scale defined by the gravimetric standards was used to create a set of six internally consistent secondary standards. These secondary standards, all of natural air, were obtained at NWR and are contained in 29-L aluminum cylinders. The standards range in concentration from approximately 100 to 200 ppb (Table 4.8). Intercomparison of the CO content of the air contained in the 29-L cylinders has shown that these cylinders are stable with respect to CO for at least 2 years. However, we found the CO content of the primary standards to be increasing at rates ranging from 1 to 3 ppb yr⁻¹. Comparison of CO reference scales defined with and without the standards exhibiting CO growth showed no significant difference. Therefore, although the useful

TABLE 4.7. Primary CO Standards

Cylinder ID	Date*	CO Mole Fraction, ppb
FF31482	April 8, 1988	45.22
FF31476	April 8, 1988	110.8
FF31460	April 7, 1989	107.1
FF32804	April 10, 1989	145.1
FF31459	April 10, 1989	199.1
FF31474	April 17, 1989	128.1
FF31475	July 7, 1989	76.59
FF32780	July 6, 1989	344.0
FF31450	July 6, 1989	49.98
FF32792	July 6, 1989	166.0
FF31451	Aug. 2, 1989	25.25
FF32788	Aug. 2, 1989	254.1 [†]
FF32805	Aug. 3, 1989	74.85 [†]
FF32813	Aug. 4, 1989	141.9 [†]
FF32799	Aug. 4, 1989	Blank [‡]
FF31488	Aug. 6, 1989	291.5
FF32819	Oct. 9, 1989	1002.9

*Date of standard preparation.

[†]These standards were prepared using a NIST SRM as the parent. All other standards were prepared from one of two high-concentration CO standards prepared by gravimetric methods in our laboratory.

[‡]The blank was prepared using Ultrapure air as the parent.

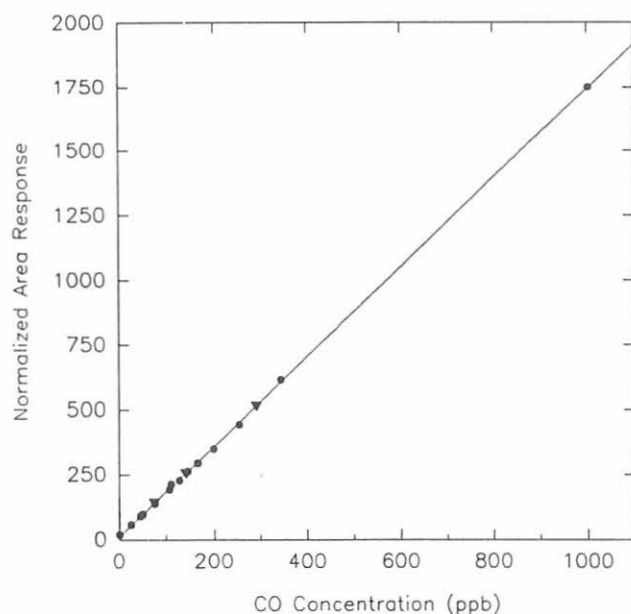


Fig. 4.11. Chromatographic peak area response versus CO concentration for all atmospheric-level gravimetric standards. The solid circles are standards prepared from one of two "parents" by gravimetric methods in our laboratory; the inverted triangles represent standards prepared using a NIST SRM as the parent. Each point represents the mean area response of at least 15 aliquots, normalized to the air contained in a 29-L cylinder, which is believed to be stable with respect to CO over time. The standard error of the mean is contained within the size of the point. The normalization procedure removes small effects due to both short- and long-term detector variations. The solid line represents the linear least squares fit to the data.

TABLE 4.8. Secondary CO Standards*

Cylinder ID	Air [†]	Date [‡]	CO Mole Fraction, ppb [§]
AAL-17262	NWR	Nov. 1987	113.9 ± 1.5
AAL-17268	NWR	Nov. 1987	127.7 ± 2.0
AAL-17269	NWR	Nov. 1987	118.5 ± 0.6
CC68734	NWR	Dec. 1988	159.7 ± 1.5
CC61344	NWR	Dec. 1988	181.5 ± 1.5
CC64035	NWR	Nov. 1989	113.9 ± 1.1

*Concentrations for the secondary standards were calculated using the empirical relationship between area response and CO concentration determined using the gravimetric primary standards.

[†]Air used for the reference gas. NWR indicates that the air was collected by our lab at Niwot Ridge, Colorado.

[‡]Date of the final fill of the cylinder.

[§]CO concentrations are referenced against the NOAA/CMDL gravimetric standards. The quoted uncertainty is one standard deviation.

lifetime of some cylinders may be limited, CO growth has not affected the overall scale defined by the set of standards.

We compared our standards with two certified, NIST-traceable CO standards purchased from Scott-Marrin, Inc. (CO concentrations of these standards were 0.49 ppb and 0.98 ppb). The concentrations assigned these standards by the manufacturer agreed to within 3% with the concentrations that we calculated with reference to our CO scale. We also compared our reference scale with a CO standard maintained at CSIRO, which is tied to the scale developed and distributed by OGC. One cylinder of natural, dried air, having an unknown CO concentration, was calibrated by both laboratories. Results of this intercomparison showed that CO concentrations referenced against the standard scale developed at CMDL are 25% greater than those calculated using the CSIRO standard. This result agreed well with that of *Weeks et al.* [1989], who found that the concentration of a CO standard, when referenced to the OGC scale, was 22% lower than that calculated against a NIST-traceable standard.

The measurement of CO concentrations in flask samples collected at BRW, NWR, and SMO continued in 1989. In addition, we began measuring CO levels at the following CMDL cooperative flask sampling network sites (the date of the first sample is given in parentheses): Ascension Island (02/02); Cape Kumukahi (03/07); MLO (07/07); Guam (09/10); and Christmas Island (25/12). These sites were chosen on the basis of several criteria including latitude, sample transit time between the site and Boulder (sample contamination is associated with long storage time), and scientific value (i.e., samples from Ascension Island, at nearly the same latitude as SMO, provide information on longitudinal variations in CO levels). CO measurements were made only in glass flasks fitted with Teflon O-ring stopcocks. CO was measured at all sites in flasks of 0.5-L volume (except Christmas Island where only 3-L Teflon

O-ring flasks were used); at Cape Kumukahi, BRW, and SMO, CO was also measured in flasks having volume of approximately 3 L.

The record of monthly mean CO concentrations determined in flasks filled at BRW during 1989 is presented in Figure 4.12. The seasonal concentration variations observed at this site are typical of the northern hemisphere: higher concentrations were found in winter, lower concentrations were observed in summer. This seasonal cycle, in large part, reflects variations in hydroxyl radical [e.g., Logan *et al.*, 1981]. As noted in section 4.2, meteorological conditions at BRW were unusual during the winter of 1989 in that winds were predominantly from sectors not considered to transport "background" air to the sampling site. Local contamination may have elevated CO concentrations above background levels; however, local CO sources are not believed to drive the observed seasonal variations. They could, however, affect the magnitude of the seasonal concentration amplitudes. The high CO concentrations observed in January reflect, in part, a period of very high CO concentrations (up to 270 ppb) associated with an Arctic high-pressure system situated over BRW during the middle of the month.

4.2. SPECIAL PROJECTS

4.2.1. AGASP III

On six aircraft flights during AGASP III, 186 air samples were collected throughout the Arctic troposphere and lower stratosphere in glass flasks equipped with Teflon O-ring stopcocks. These flask samples were analyzed for concentrations of CO₂ by NDIR analysis; CH₄ by GC/FID; and CO by a mercuric oxide reduction technique.

The concentrations of the three gases varied significantly both horizontally and vertically. Elevated trace gas concentrations were found in layers with high anthropogenic aerosol concentrations (Arctic haze). The data from flight 306 are shown as an example (Figure 4.13). The concentrations of CO₂, CH₄, and CO were highly correlated during all flights. A linear regression of CH₄ versus CO₂ for pooled data from all flights yielded a correlation coefficient (r^2) of 0.88 with a slope of 13.5 ppb CH₄/ppm CO₂ (n = 186). For CO versus CO₂ a pooled linear regression gave $r^2 = 0.91$ with a slope of 12.4 ppb CO/ppm CO₂ (n = 183). CO₂, CH₄, and CO also exhibited mean vertical gradients with slopes of -0.56 ppm km⁻¹, -6.6 ppb km⁻¹, and -5.79 ppb km⁻¹, respectively.

Since the CO₂ variations observed in the Arctic atmosphere during winter are due to variations in the transport of anthropogenic CO₂ from lower latitudes, these results suggest that the CH₄ and CO data might be similarly interpreted. Using reliable estimates of CO₂ emissions for various source regions, it should be possible to estimate corresponding regional CH₄ and CO sources using the measured CH₄/CO₂ and CO/CO₂ ratios. Such estimates are important in light of the large uncertainties in current estimates of global CH₄ and CO emissions.

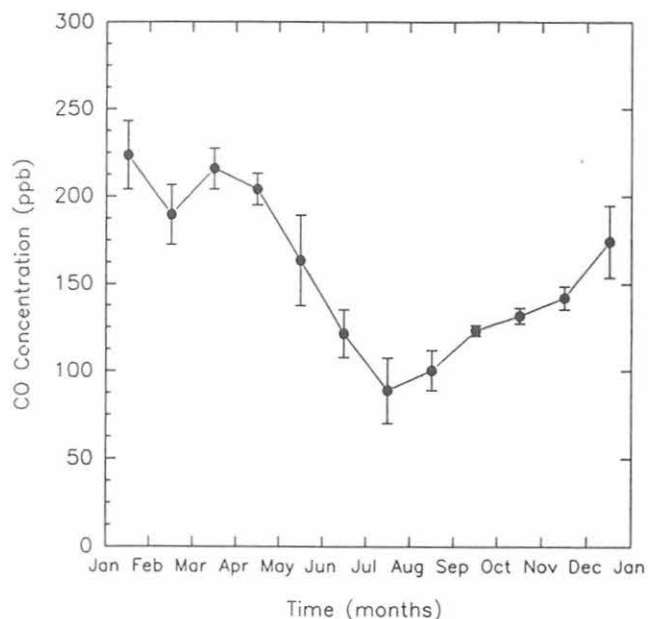


Fig. 4.12. Monthly mean CO concentrations determined in flask samples collected at BRW during 1989. Each point represents the mean of about four weekly samples, with at least two aliquots analyzed from a single sample. Instrument precision on replicate samples was always better than 1%. The error bars represent one standard deviation around the mean.

4.2.2. SHIPBOARD SAMPLING

During January and February, the National Marine Fisheries Service conducted its first expedition to the Antarctic using the NOAA ship *Surveyor*. The primary purpose of the cruise was to provide fisheries data for the U.S. delegation that advises the Convention for the Conservation of Antarctic Marine Living Resources, an agency of the Antarctic Treaty system. The Carbon Cycle Group used this opportunity to make continuous measurements of CO₂ in surface waters of the Scotia Sea area of the southern oceans [Waterman, 1989]. The expedition made stops at Palmer Station, Antarctica, and at Bird Island, South Georgia (remote sampling sites in the flask network).

The shipboard measurement system was fully operational before departure from Punta Arenas, Chile. A nearly complete record of both atmospheric CO₂ concentrations and pCO₂ in the surface ocean was obtained along the entire Leg I track. Preliminary examination of pCO₂ values shows areas of both undersaturation and supersaturation, with sometimes sharp boundaries. These conditions were first observed in the Drake Passage crossing. The total area surveyed represents a small portion of the southern oceans and should not be construed as representative of the whole region.

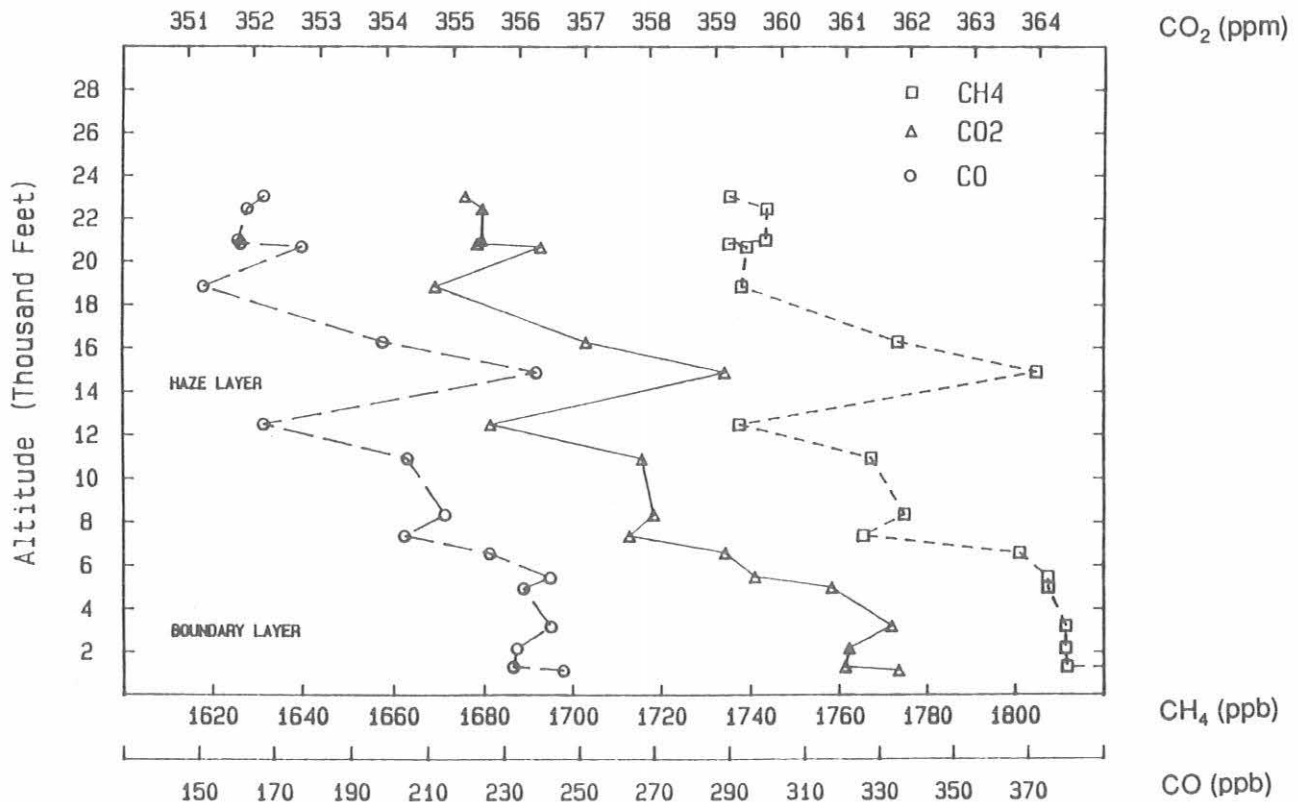


Fig. 4.13. Concentrations of CO₂, CH₄, and CO measured in flask samples collected during flight 306 (March 21, 1989) as part of the AGASP III mission.

4.3. REFERENCES

Bodhaine, B.A., and R.M. Rosson (Eds.), *Geophysical Monitoring for Climatic Change, No. 16: Summary Report 1987*, 110 pp., NOAA Air Resources Laboratory, Boulder, CO, 1988.

Elkins, J.W., and R.M. Rosson (Eds.), *Geophysical Monitoring for Climatic Change, No. 17: Summary Report 1988*, 142 pp., NOAA Air Resources Laboratory, Boulder, CO, 1989.

Griffith, D.W.T., Calculations of carrier gas effects in nondispersive infrared analyzers, I, Theory, *Tellus*, 34, 376-384, 1982.

Komhyr, W.D., T.B. Harris, L.S. Waterman, J.F.S. Chin, and K.W. Thoning, Atmospheric carbon dioxide at Mauna Loa Observatory, 1, NOAA Global Monitoring for Climatic Change measurements with a nondispersive infrared analyzer, 1974-1985, *J. Geophys. Res.*, 94, 8533-8547, 1989.

Logan, J.A., M.J. Prather, S.C. Wofsy, and M.B. McElroy, Tropospheric chemistry: A global perspective, *J. Geophys. Res.*, 86, 7210-7254, 1981.

Tans, P.P., T.J. Conway, and T. Nakazawa, Latitudinal distribution of the sources and sinks of atmospheric carbon dioxide derived from surface observations and an atmospheric transport model, *J. Geophys. Res.*, 94, 5151-5172, 1989.

Thoning, K.W., P.P. Tans, and W.D. Komhyr, Atmospheric carbon dioxide at Mauna Loa Observatory, 2, Analysis of the NOAA GMCC data, 1974-1985, *J. Geophys. Res.*, 94, 8549-8565, 1989.

Waterman, L.S., Monitor air and surface water CO₂ content, Leg 1, in *United States Antarctic Marine Living Resources Program, Cruise Report AMLR 8901*, edited by Roger Hewitt, pp. 9-10, NOAA National Marine Fisheries Service, La Jolla, CA, 1989.

Waterman, L.S., D.W. Nelson, W.D. Komhyr, T.B. Harris, K.W. Thoning, and P.P. Tans, Atmospheric carbon dioxide measurements at Cape Matatula, American Samoa, 1976-1987, *J. Geophys. Res.*, 94, 14817-14829, 1989.

Weeks, I.A., I.E. Galbally, P.J. Fraser, and G. Matthews, Comparison of the carbon monoxide standards used at Cape Grim and Aspendale, in *Baseline 1987*, edited by B.W. Forgan and G.P. Ayers, pp. 21-25, CSIRO, Melbourne, Australia, 1989.

5. Ozone Group

S.J. OLTMANS (Editor), W.D. KOMHYR, R.D. GRASS, R.D. EVANS, G.L. KOENIG, R.K. LEONARD, AND D.H. QUINCY

5.1. CONTINUING PROGRAMS

5.1.1. TOTAL OZONE OBSERVATIONS

Routine total ozone observations were made with Dobson spectrophotometers during 1989 at 16 stations that make up the U.S. total ozone station network (Table 5.1). Of all the stations, five are operated by CMDL personnel, four are operated by NWS, three are domestic cooperative stations, and four are foreign cooperative stations. Ozone measurements at the Tallahassee, Florida, Dobson instrument station,

operated by Florida State University, were terminated November 30, 1989. Plans are being made to transfer the operation of this program to NWS at Tallahassee, Florida. Table 5.2 lists provisional monthly mean total ozone amounts measured at the various stations during 1989.

The mean trend in total ozone over the United States, derived from provisional total ozone amounts measured from 1980 through mid-1990 at Bismarck, Boulder, Caribou, Fresno, Nashville, Tallahassee, and Wallops Island, is -0.34% yr⁻¹. This value compares favorably with the trend of -0.46% yr⁻¹ derived from corrected TOMS satellite data

TABLE 5.1. U.S. Dobson Ozone Spectrophotometer Station Network for 1989

Station	Period of Record	Instrument No.	Agency
Bismarck, ND	Jan. 1, 1963-present	33	NOAA
Caribou, ME	Jan. 1, 1963-present	34	NOAA
Wallops Is., VA	July 1, 1967-present	38	NOAA; NASA
SMO	Dec. 19, 1975-present	42	NOAA
Tallahassee, FL	May 2, 1964-Nov. 30, 1989	58	NOAA; Florida State University
Boulder, CO	Sept. 1, 1966-present	61	NOAA
Poker Flat, AK	March 6, 1984-present	63	NOAA; University of Alaska
Lauder, New Zealand	Jan. 29, 1987-present	72	NOAA; DSIR
MLO	Jan. 2, 1964-present	76	NOAA
Nashville, TN	Jan. 2, 1963-present	79	NOAA
Perth, Australia	July 30, 1984-present	81	NOAA; Australian Bureau Meteorology
SPO	Nov. 17, 1961-present	82	NOAA
Haute Provence, France	Sept. 2, 1983-present	85	NOAA; CNRS
Huancayo, Peru	Feb. 14, 1964-present	87	NOAA; IGP
BRW	June 6, 1986-present	91	NOAA
Fresno, CA	June 22, 1983-present	94	NOAA

TABLE 5.2. Provisional 1989 Monthly Mean Total Ozone Amounts (m-atm-cm)

Station	Jan.	Feb.	March	April	May	June	July	Aug.	Sept.	Oct.	Nov.	Dec.
Bismarck, ND	352	362	364	380	353	347	309	313	303	295	307	342
Caribou, ME	357	366	398	423	365	355	357	335	312	310	320	385
Wallops Is., VA	320	315	341	374	377	333	337	322	205	205	298	310
SMO	263	248	252	256	254	267	265	265	278	271	272	267
Tallahassee, FL	285	296	296	323	323	296	299	294	294	284	272	
Boulder, CO	321	313	329	339	341	335	307	298	289	282	287	317
Poker Flat, AK				374	372	355	323	300	292			
Lauder, New Zealand	290	286	280	271	298	319	340	358	337	370	339	308
MLO	264	277	280	301	309	268	282	277	279	267	253	248
Nashville, TN	297	308	323	352	350	342	319	317	301	296	295	303
Perth, Australia	287	276	278	278	284	295	313	324	334	339	320	301
SPO	286	269		263	245	268	259			161	235	303
Haute Provence, France	327	355	342	395	360	353	330	323	310	287	299	312
Huancayo, Peru	262	262	252	256	254	253	258	259	273	262	264	259
BRW			420	439	376	345	327	311	301			
Fresno, CA	319	319	316	333	338	327	313	311	302	290	274	279

obtained from late 1979 through mid-1990 in a zonal band centered at 40°N latitude (R. Stolarski, NASA Goddard Space Flight Center, private communication, 1991). At MLO and SMO in the equatorial Pacific, ozone decreased during 1976-1987 at rates of $-0.27\% \text{ yr}^{-1}$ and $-0.41\% \text{ yr}^{-1}$, respectively (Figure 5.1). (Prior to 1976, ozone at MLO had been increasing at $0.34\% \text{ yr}^{-1}$.) However, since mid-1988, ozone amounts at these locations have increased. Essentially zero ozone trends are computed at MLO and SMO from 14 years of data ending in August 1990 (Figure 5.1).

Although stratospheric ozone amounts are expected to decline as more and more anthropogenic CFCs reach the stratosphere, the pattern of ozone changes described here suggests that other mechanisms may also be at work to cause the changes. Times of enhanced UV flux associated with the 11-year solar cycle may increase column ozone amount by 0.7-2.0% [Watson *et al.*, 1988]. Recent work [Komhyr *et al.*, 1991] suggests that long-term changes in atmospheric circulation processes resulting from tropical sea surface temperature changes may also lead to approximately decadal trends in ozone.

Figure 5.2 plots mean total ozone amounts measured at South Pole during October 15-31 of 1962-1989. (Mid-October is when Dobson spectrophotometer total ozone observations first become possible each year at South Pole following the polar night.) Note that the 1989 mean value approached that of 1987, which to date has been the record low. The 1988 ozone depletion was considerably less severe; the mean October 15-30 total ozone amount was comparable with values that occurred several times prior to 1978.

5.1.2. DOBSON SPECTROPHOTOMETER CALIBRATIONS

During 1989 CMDL continued its program of upgrading and calibrating Dobson ozone spectrophotometers of the global Dobson instrument network. Instruments calibrated in 1989 are listed in Table 5.3. In March 1989 the Pretoria, South Africa, instrument no. 89 was received in Boulder for recalibration. It was modified with U.S. solid-state electronics, optically aligned, recalibrated, and returned to Pretoria. All calibrations were performed relative to World Standard Dobson spectrophotometer no. 83.

Provisional calibration of the four U. S. Dobson instruments showed them to be out of calibration as follows: no. 63, -0.2% ; no. 65, $+0.5\%$; no. 92, $+1.5\%$; and no. 94, $+1.1\%$. A positive sign indicates that the instrument was measuring ozone values too high. Japanese instrument no. 116 was found to be out of calibration by $+1.05\%$. No calibration check was made on the Pretoria instrument, since it was not operational when it arrived in Boulder, and it had not been used in Pretoria for 16 years.

5.1.3. UMKEHR OBSERVATIONS

Umkehr observations with automated Dobson ozone spectrophotometers were continued during 1989 in Boulder, Colorado (40°N , 105°W); Mauna Loa, Hawaii (20°N ,

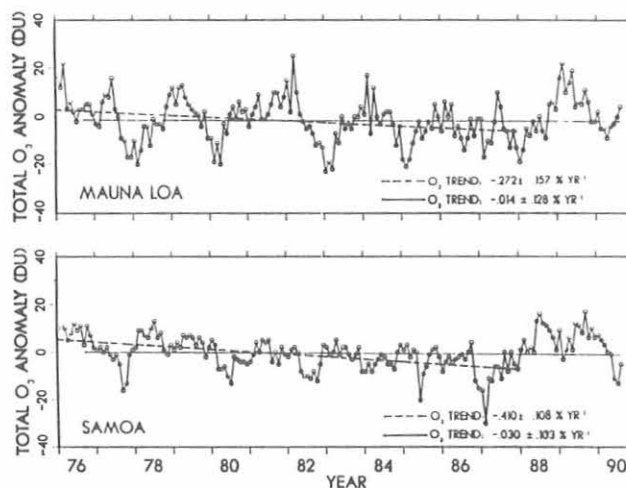


Fig. 5.1. Ozone trends at MLO and SMO for 1976-1987 (dashed lines) and August 1, 1976-August 31, 1990 (solid lines). The trends are least-squares regressions fitted to the ozone monthly anomalies. Indicated uncertainties are 95% confidence limits (t-statistic).

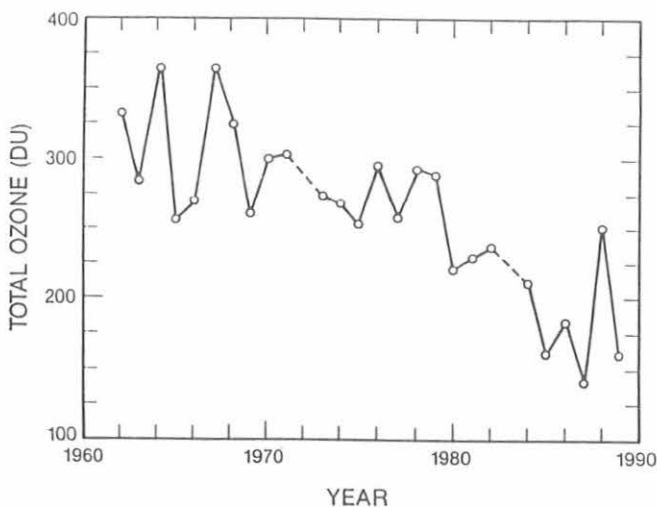


Fig. 5.2. South Pole October 15-31 mean total ozone amounts in Dobson units for 1962-1989.

TABLE 5.3. Dobson Spectrophotometers Calibrated in 1989

Country	Station	Instrument No.
South Africa	Pretoria	89
Japan	Tateno	116
United States	Poker Flat	63
United States	Boulder	65
United States	Barrow	91
United States	Fresno	94

156°W); Haute Provence Observatory, France (44°N, 6°E); Poker Flat, Alaska (65°N, 148°W); Perth, Australia (32°S, 116°E); and Lauder, New Zealand (45°S, 169°E). A total of 1242 ozone profiles were obtained. All provisional data have been archived at the WMO World Ozone Data Centre, Atmospheric Environment Service, Downsview, Canada.

Umkehr observations were also made at Huancayo, Peru, but manually. Operation of the instrument in the automatic mode failed, and because of political turmoil in the country, replacement of electronic parts has not been possible. Communications have become a problem between the observatory and Boulder.

5.1.4. TROPOSPHERIC OZONE

The first year of surface ozone observations from three of the AEROCE sites in the North Atlantic provide a first glimpse of the pattern of ozone behavior in this region. Although only a few months of data have been obtained at Mace Head, Ireland, nearly a year's data have been obtained at Barbados and more than a year's data at Bermuda. Because the AEROCE sites are surrounded by several major continents, it will eventually be possible, using the information from a number of the chemical measurements being made at the sites, to decipher the role of anthropogenic emissions on the ozone distribution in this region.

Several important characteristics of the ozone distribution at Bermuda and Barbados can be seen even in the short available record. At Bermuda there is a prominent seasonal cycle (Figure 5.3) with a spring maximum and late summer minimum. During the spring peak season hourly average mixing ratios occasionally exceeded 75 ppb, and day-to-day fluctuations were large (Figure 5.4). This pattern appears to reflect rather sudden influxes of ozone and then a gradual decay before the appearance of another pulse of high ozone.

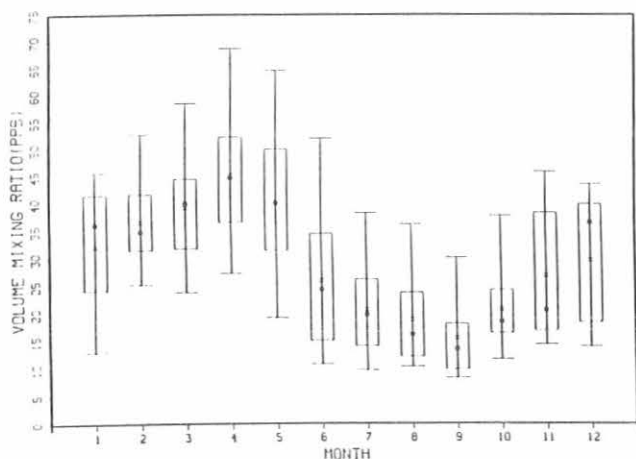


Fig. 5.3. Ozone volume mixing ratio by month at Bermuda for 1989. The x's denote mean values, the dots indicate median values, the boxes represent the middle 50th percentiles, and the bars, the middle 90th percentiles.

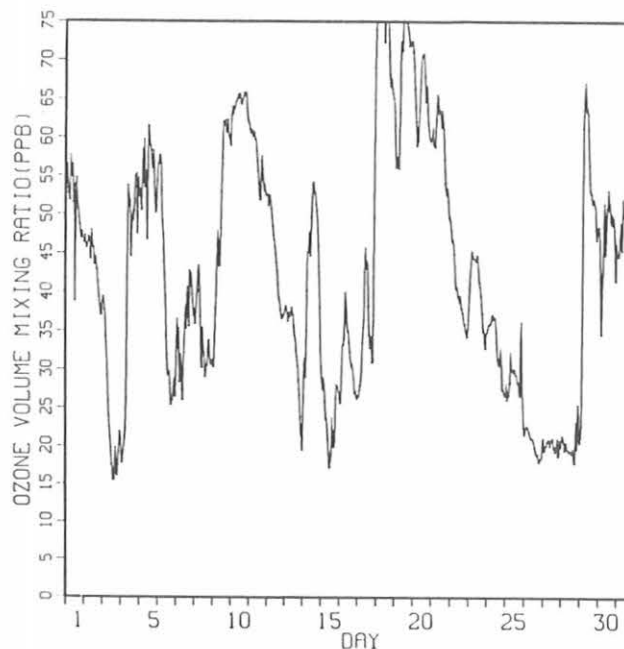


Fig. 5.4. Hourly ozone volume mixing ratios in parts per billion at Bermuda for May 1989.

Such fluctuations are on a time scale similar to synoptic-scale meteorological disturbances. During the summer, however, the pulses of ozone are smaller and less frequent and there is a general overall decline in the ozone concentration. This reflects the dominating influence of the Bermuda high-pressure system that prevents weather systems from the north and west from reaching Bermuda. Under the influence of high pressure, it appears that ozone is gradually destroyed as hydroxyl increases and nitrogen oxides remain low.

A diurnal cycle is evident at Barbados (Figure 5.5) with maximum concentrations in the morning and minima in the afternoon. This pattern is very similar to that at SMO (14°S), which is the same distance south of the equator as Barbados (14°N) is north of the equator. This "reverse" diurnal cycle appears to be typical of the tropical marine lower atmosphere [Oltmans, 1981; Johnson *et al.*, 1990] where odd nitrogen ($\text{NO}_x = \text{NO} + \text{NO}_2$) concentrations are low.

As at Bermuda, the seasonal surface ozone variation at Barbados is also prominent (Figure 5.6), with the ozone peaking early in the year. Again the pattern is very similar to that at SMO, but the maximum at Barbados is in January and at SMO in July. The minima occur also 6 months apart. The amplitude of the seasonal cycle at the two sites is nearly identical. Barbados, however, has an annual mean ozone concentration that is 7.5 ppb (~50%) higher than the SMO annual mean. This is in keeping with the overall pattern of higher tropospheric ozone concentrations in the northern hemisphere.

Surface ozone monthly means for the four CMDL sites with longer observational records are shown in Figure 5.7.

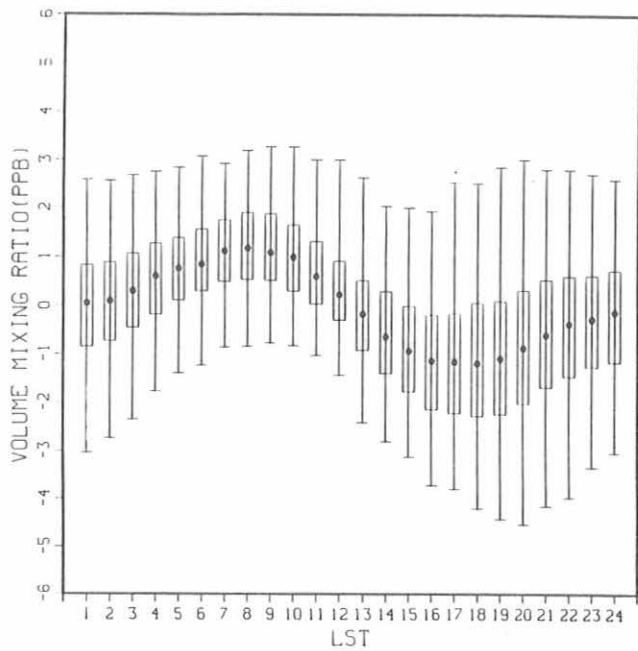


Fig. 5.5. Average ozone volume mixing ratio deviations from daily means for each hour of the day at Barbados, derived from nearly one year's observations. Symbols are as in Fig. 5.3.

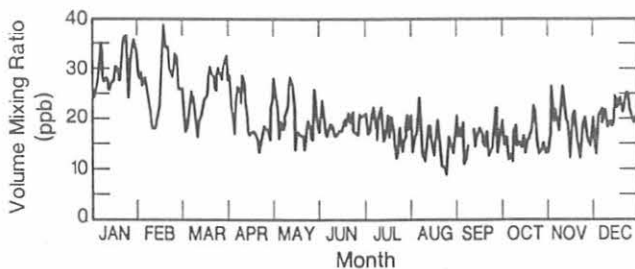


Fig. 5.6. Daily surface ozone volume mixing ratios in parts per billion at Barbados for 1989.

Superimposed on the plots are linear-least-squares ozone trend lines derived from fits to plots of surface ozone monthly anomalies. At MLO the last 6 years of average concentrations have markedly slowed the long-term surface ozone growth rate. The positive ozone trend of nearly 1% yr⁻¹ at BRW is the result mainly of large increases in ozone with time during summer and autumn months, as discussed in last year's report [Elkins and Rosson, 1989]. At SMO the strong temporal decrease in surface ozone that has occurred during summer months has been offset by modest ozone increases during the remainder of the year. At SPO the marginally significant overall decrease in surface ozone is a result of the strong decrease during summer months, a time of the seasonal minimum in tropospheric ozone.

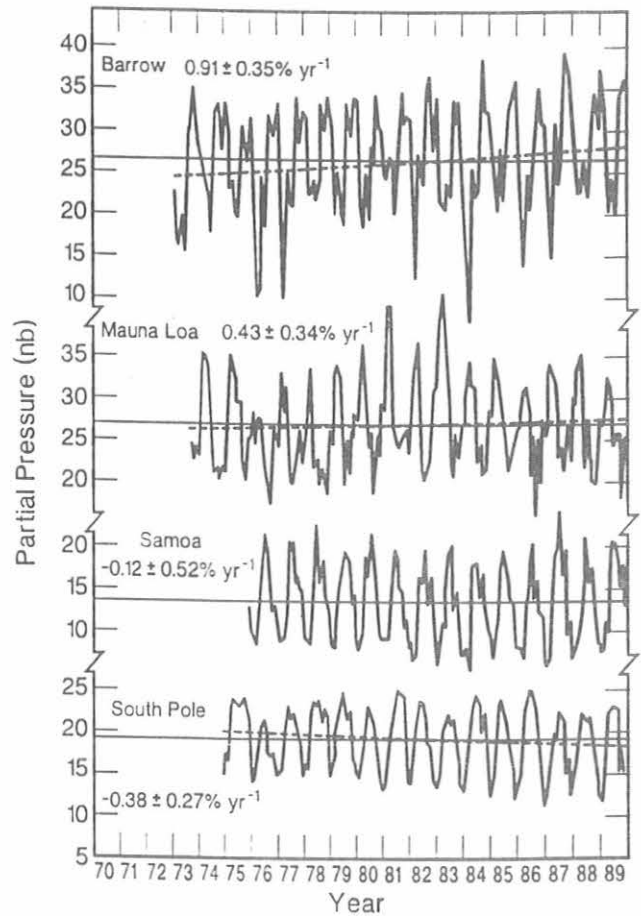


Fig. 5.7. Monthly mean surface ozone partial pressures at BRW, MLO, SMO, and SPO. Trend lines (dashed) are linear-least-squares fits to monthly ozone anomalies. Solid lines represent the mean ozone partial pressures for the periods of record. Uncertainties in the indicated trend estimates are 95% confidence limits.

5.1.5. OZONESONDE OBSERVATIONS

Weekly measurements of atmospheric ozone vertical distribution with ECC ozonesondes were continued at Hilo, Hawaii. Ozone soundings were also made at Boulder, Colorado, and SMO, but at irregular intervals, yielding about 20 profiles at each site. ECC ozonesondes were also flown at SPO [Komhyr et al., 1990a].

The 1989 observations at SPO were a continuation of a program that began in 1986 to study Antarctic springtime ozone depletion. A total of 60 balloon ozonesonde soundings were made. The instruments were flown once per week, except during the months of September-November when frequency was increased to 2-3 soundings per week.

Figure 5.8 compares ozone profile data for August 20 or 21, 1987-1989, with that for October 9 or 10, 1987-1989. The August profiles, having total ozone amounts of 263-272 DU, and shown in Figure 5.8 only for the region of the

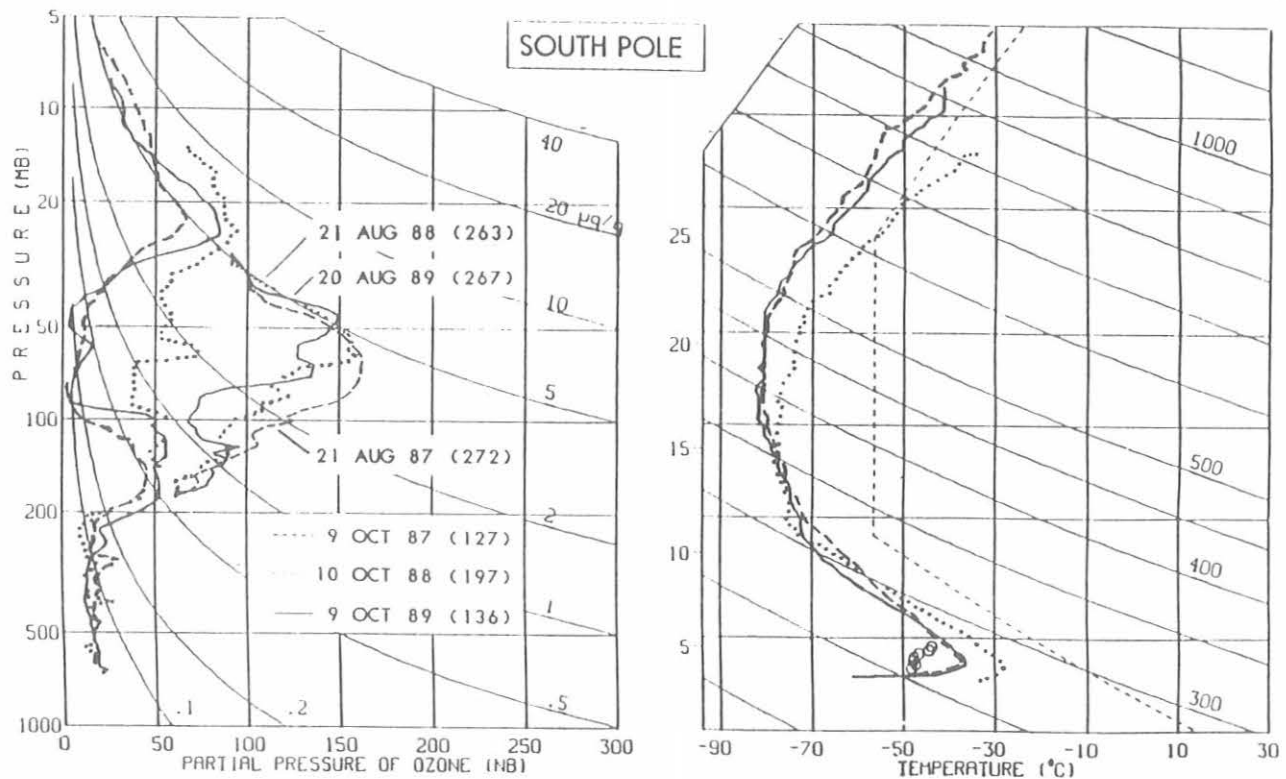


Fig. 5.8. South Pole ozone and air temperature profiles, at times (~October 9) in 1987-1989, of Antarctic springtime maximum ozone destruction. The August profiles, shown for comparison, indicate the amount of ozone present in the region of the normal stratospheric ozone maximum prior to onset each year of the ozone depletion process.

Antarctic stratospheric ozone maximum, represent the ozone distributions at SPO at 190-30 mb prior to onset each year of the Antarctic springtime ozone depletion phenomenon. Stratospheric ozone depletion at South Pole generally begins in late August or early September and reaches a maximum October 9-10, at which time the minimum total ozone amount for the year is observed.

Note from Figure 5.8 that the degree of ozone depletion in October 1989 approached that in October 1987—a year of record depletion. Almost total destruction of ozone occurred in the 100-50 mb region. Minimum observed total ozone amounts were 127 and 136 DU on October 9 in 1987 and 1989, respectively. In contrast, ozone depletion in 1988 was considerably less severe, the October 10 total ozone value being 197 DU. Breakdown of the Antarctic circumpolar vortex and ozone recovery began early in December in 1987, about 2 weeks earlier in 1989, but early in November in 1988.

5.1.6. VALIDATION OF SATELLITE INSTRUMENT OZONE DATA

CMDL maintains and operates World Standard Dobson spectrophotometer no. 83, which was designated in 1980 by the WMO as the primary standard Dobson spectrophotometer

for the world. The instrument was established as a standard for total ozone measurements in the United States in 1962. Long-term total ozone measurement precision of the instrument has been maintained throughout the years to $\pm 0.5\%$ [Komhyr et al., 1989]. Since the mid 1970's, the instrument has been used extensively to calibrate Dobson ozone spectrophotometers of the global Dobson instrument network.

Total ozone data, obtained with instrument no. 83 at MLO since 1979 while calibrating the instrument, have been used to validate TOMS and SBUV satellite instrument ozone data obtained aboard the Nimbus 7 satellite [McPeters and Komhyr, 1991]. Results are shown in Figure 5.9 where the TOMS and SBUV ozone data are compared with data from instrument no. 83 as well as from 39 select Dobson stations of the global Dobson station network. Note that relative to instrument no. 83, the TOMS instrument calibration has drifted 7% in 10 years. The cause has been degradation of a diffuser plate aboard the Nimbus satellite that is periodically viewed by the TOMS and SBUV instruments.

5.1.7. STRATOSPHERIC WATER VAPOR

A continuing program of approximately monthly balloon frost-point hygrometer soundings at Boulder since 1981 has

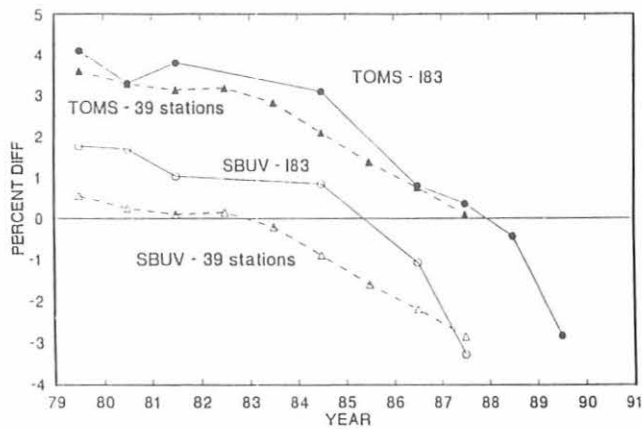


Fig. 5.9. Calibration drifts of TOMS and SBUV satellite ozone instruments relative to the calibration levels of World Standard Dobson instrument no. 83 (I83) and of 39 select Dobson instruments of the global Dobson instrument network. Results were derived from total ozone observations made during satellite and ground-based instrument comparisons. The version 5 algorithm was used in processing the satellite data.

delineated several important features of the seasonal and long-term behavior of upper tropospheric and stratospheric water vapor [Bodhaine and Rosson, 1988; Elkins and Rosson, 1989]. Based on data from 1981-89, average water vapor volume mixing ratios at selected atmospheric pressures between 250 and 17 mb are shown in Table 5.4. Note the rapid drop in water vapor across the tropopause, the minimum near 80 mb, and the gradual increase in mixing ratio with altitude in the stratosphere.

Since the launch of the SAGE II satellite sensor in 1984, a number of balloonborne, frost-point hygrometers have been flown to provide correlative stratospheric water vapor profiles for satellite measurement validation. As part of this effort, balloon measurements have been made in Boulder, Colorado; Laramie, Wyoming; Fairbanks, Alaska; and Pago Pago, American Samoa. An example of correlative measurement profiles is shown in Figure 5.10. The

TABLE 5.4. Stratospheric Water Vapor Mean Volume Mixing Ratio for 1981-1989 at Boulder, Colorado

Pressure, mb	Approximate Altitude, km	Mean H ₂ O-Vapor Mixing Ratio, ppmv	Mixing Ratio Std. Dev., ppmv	Number of Obs.
250	10.5	68.27	52.53	82
120	15.0	3.97	1.35	83
80	17.5	3.61	0.44	83
50	20.5	4.01	0.32	80
40	22.0	4.14	0.29	78
25	25.0	4.27	0.30	72
17	27.5	4.35	0.33	33

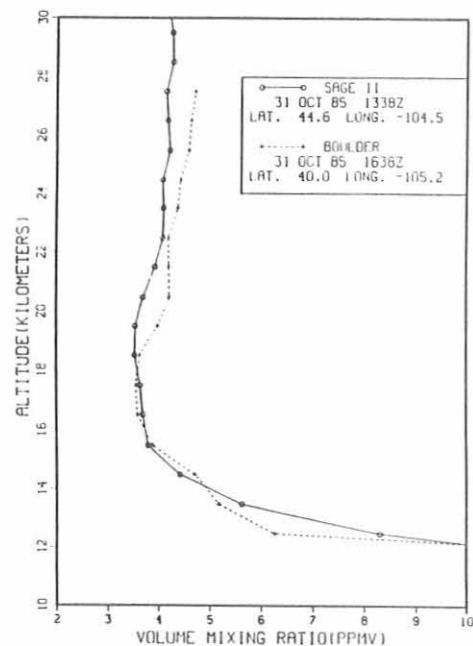


Fig. 5.10. Stratospheric water vapor mixing ratio profiles derived from SAGE II satellite observations (solid line) and from balloonborne, frost-point hygrometer soundings at Boulder (dashed line).

satellite-obtained profile is a preliminary one; final corrections for interference from aerosols and ozone will be applied later. The overall agreement, however, appears to be very good. The difference in the layer 19-28 km may result from a partially unaccounted for interference by ozone in the satellite profile retrieval algorithm.

In January 1989 an experiment was conducted at Alert, Northwest Territories, Canada, to investigate the formation and properties of polar stratospheric clouds (PSCs) during the Arctic night [Rosen et al., 1989]. The presence and optical characteristics of the PSCs were measured using a balloonborne sensor that measures the optical backscatter at two wavelengths from a xenon flash lamp triggered every 7 seconds. The sonde is especially sensitive to large particles that may be present in PSCs. Water vapor, backscatter ratio, ozone, and temperature were measured during the balloon soundings; their profiles are shown in Figure 5.11. The high backscatter ratios shown for the red channel (950 nm) of the backscatter sonde below 200 mb (Figure 5.11b) are associated with tropospheric ice clouds. The water vapor mixing ratios in this region (Figure 5.11a) show saturated or even possibly supersaturated conditions. The enhanced backscatter in the region 100-25 mb is the signature of PSCs. Water vapor mixing ratios in that region are high (6-10 ppmv) but not saturated. Thus these are not water ice crystals but nitric acid trihydrate (HNO₃ · 3H₂O) particles that form at temperatures above the frostpoint of water. Depending on the mixing ratios of water and HNO₃, the nitric acid trihydrate clouds form at temperatures colder than

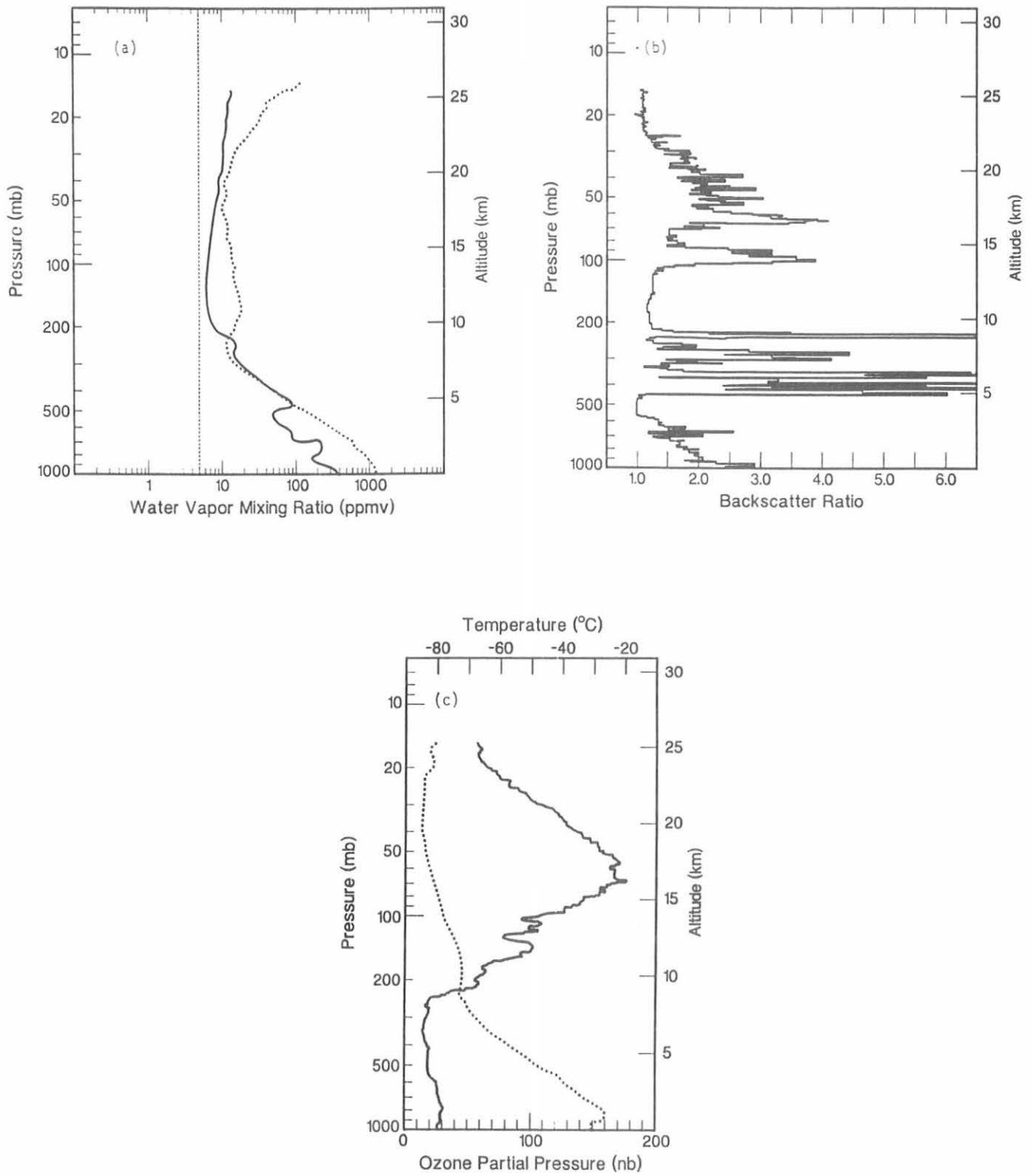


Fig. 5.11. Vertical profiles from Alert, Northwest Territories, Canada, on January 21, 1989, for (a) water vapor volume mixing ratio (solid line) and saturation mixing ratio (dotted line); (b) backscatter ratio from the PSC sonde; and (c) ozone partial pressure (solid line) and temperature (dotted line).

about -78°C . As can be seen in Figure 5.11c, temperatures reach this low value near the 100-mb level. If temperatures drop below water saturation ($\sim -80^{\circ}\text{C}$ at 100 mb and $\sim -84^{\circ}\text{C}$ at 30 mb), then water ice crystals will form. These larger particles will fall out of the stratosphere, removing both water vapor and HNO_3 . At the time of these measurements no significant dehydration is noted. On January 21 it is still dark at Alert (82°N) and over much of the Arctic. Since sunlight is required for chlorine that has been released by heterogeneous reactions on PSCs to catalytically destroy ozone, destruction should not yet have begun. Figure 5.11c shows that this is indeed the case. Ozone profiles obtained later in February do suggest that ozone was destroyed [Evans, 1990]. A similar set of measurements is planned for 1990.

5.2. SPECIAL PROJECTS

5.2.1. STRATOSPHERIC OZONE INTERCOMPARISON CAMPAIGN

A NASA-sponsored campaign was conducted at the JPL Table Mountain Facility in California July 19 to August 2, 1989, to intercompare the performance of several kinds of instruments measuring stratospheric ozone. Participating scientific groups and instruments were NOAA/CMDL and NASA/Wallops Island, with ECC ozonesondes; JPL and NASA/GSFC, with lidars; and Millitec Corporation, with a microwave instrument. Additionally, participants from NOAA/CMDL and from AES made total ozone and Umkehr observations with Dobson and Brewer spectrophotometers, respectively. Overall, results of the ozone measurement comparisons were highly satisfactory [Komhyr *et al.*, 1990b].

Mean results of 10 sets of comparison measurements are shown in Figure 5.12a. "Blind" data are plotted in the figure; they were obtained during the campaign prior to availability of the data for general examination. Only 2 of 10 ECC ozonesondes reached an altitude of 39 km; most of the rest of the instruments reached altitudes of 34-36 km. Figure 5.12b indicates that the ECC ozonesondes, the two lidars, and the microwave instrument measured ozone amounts between about 20 and 36 km altitude that agreed to $\pm 5\%$. In the region of 36-39 km, ECC ozonesondes measured 10% less ozone than did the JPL lidar and the microwave instrument, and about 6% less ozone than did the NASA/GSFC lidar.

Seven sets of quasi-simultaneous ozonesonde and conventional Umkehr observations were obtained during the campaign. Total ozone amounts used in processing the raw Umkehr data by the standard inversion method, applicable to observations on C wavelengths, were expressed

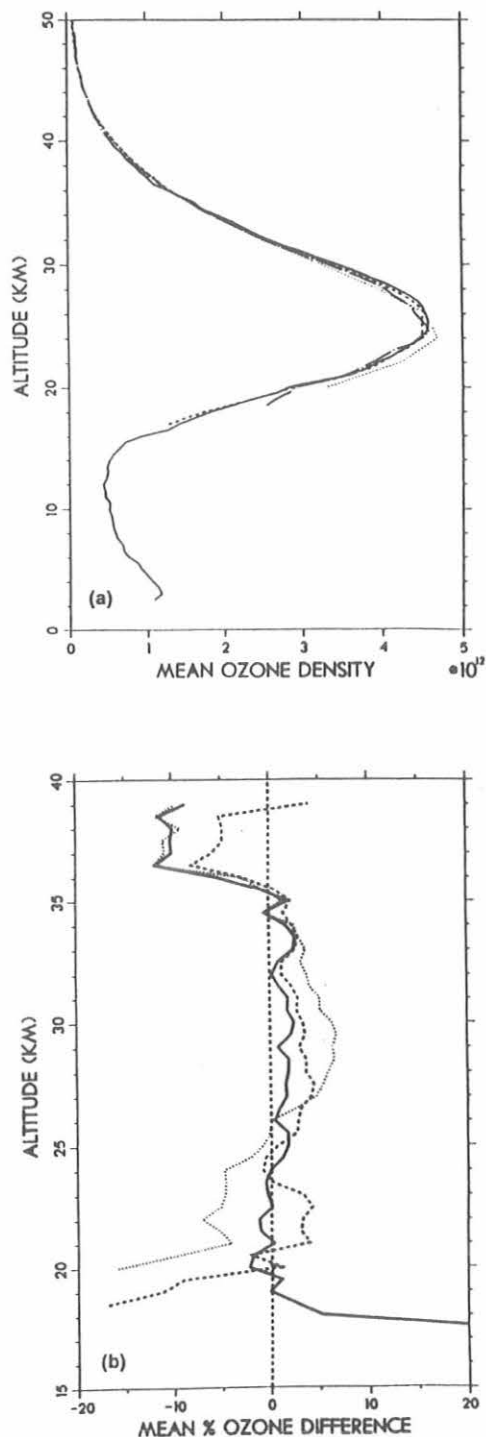


Fig. 5.12. (a) ECC ozonesonde (—), JPL lidar (---), GSFC lidar (· · · ·) and Millitec Corporation microwave (— · —) mean ozone number densities obtained from 10 sets of observations at Table Mountain; and (b) mean ozone differences in percent: ECC ozonesonde minus JPL lidar (—), minus GSFC lidar (---), and minus Millitec Corporation microwave (— · —).

in the *Bass and Paur* [1985] ozone absorption coefficient scale. Averaged data, with the sonde data reduced to Umkehr ozone layers, are plotted in Figure 5.13. Because the balloon ascents reached varying maximum altitudes, there were seven comparisons in Umkehr layers 1 to 5, six in layer 6, and two in layer 7.

Tropospheric differences are large as expected, since the Umkehr technique is not very sensitive to ozone in this region. The Umkehr method also generally underestimates ozone in the region of ozone maximum. In Umkehr layers 6 and 7, above the ozone maximum, the Umkehr and balloon soundings give results that agree to $\pm 5\%$.

5.2.2. OZONESONDE OBSERVATIONS AT MIRNY, ANTARCTICA

Measurements of the vertical distribution of atmospheric ozone were made at Mirny (66.33°S, 93.00°E, elevation 40 m), Antarctica, during 1989 to study the ozone decrease

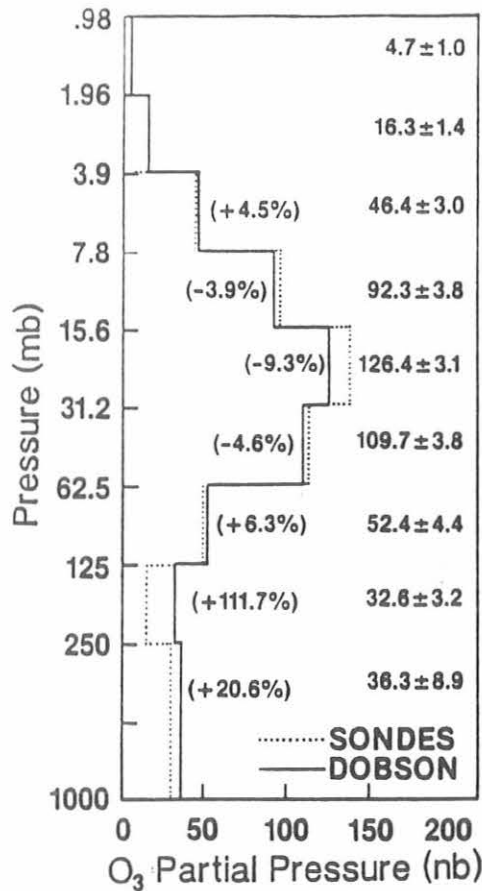


Fig. 5.13. Averaged data from seven pairs of ECC ozonesonde and Dobson instrument Umkehr observations obtained quasi-simultaneously during July 23-30, 1989. Indicated ozone partial pressures (nb) with standard deviations apply to the Dobson Umkehr data. Values in parentheses are mean percent differences in layer ozone for the sonde and Dobson instrument Umkehr.

indicated in Antarctica in recent years by Dobson spectrophotometer and satellite total observations [*Komhyr et al.*, 1990c]. The project was a joint U.S.-U.S.S.R. effort conducted under the auspices of the US-USSR Bilateral Agreement on Environmental Protection--Working Group VIII. Most of the observations (20 of 24) were made during late winter and spring (August-November). Whereas the polar vortex (and, hence, the region of the Antarctic springtime ozone depletion) was displaced roughly to the west-northwest of South Pole in 1988, i.e., away from Mirny, it was situated approximately symmetrically about the Pole in 1989. As a result, stratospheric temperatures over Mirny during the latter part of August and in September 1989 were cold enough between 12 and 23 km altitude to sustain polar stratospheric clouds and, hence, partial ozone destruction by heterogeneous photochemical processes. Maximum ozone depletion at Mirny was observed in the ECC ozonesonde sounding of October 15 (Figure 5.14). Ozone amounts increased substantially above about 70 mb over Mirny following mid-October, but reduced ozone amounts persisted in the lower stratosphere through November.

5.2.3. OZONESONDE OBSERVATIONS AT BRW

During the early 1989 Airborne Arctic Stratospheric Expedition conducted in the eastern Arctic to study

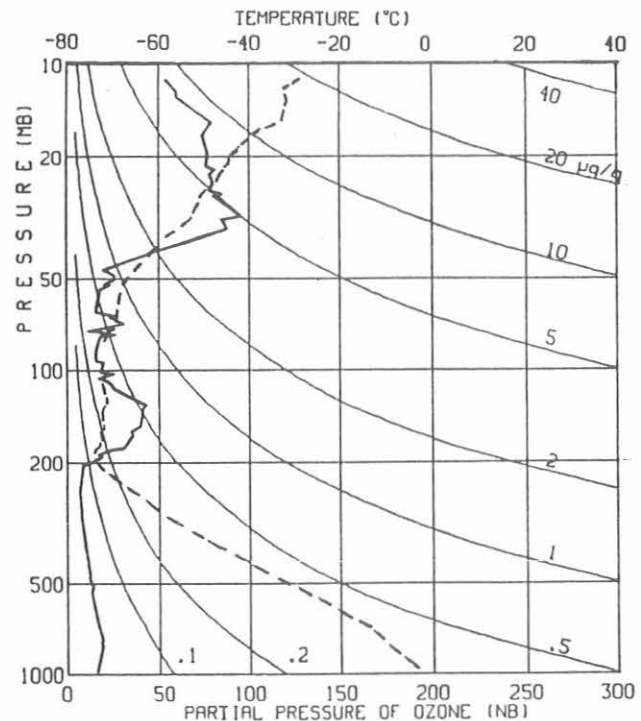


Fig. 5.14. Ozonesonde (solid line) and air temperature (dashed line) data, showing maximum ozone depletion on October 15, 1989.

possible wintertime stratospheric ozone destruction such as that which occurs in springtime in Antarctica, ECC ozonesondes were flown by CMDL personnel at BRW in an attempt to detect possible similar ozone destruction in the western Arctic. A total of 33 ozone soundings were made, spanning the time interval of January 16-April 19.

No unequivocal evidence appeared in the ozone profiles of ozone destruction similar to that which occurs in Antarctica in the presence of PSCs. Stratospheric temperatures were never colder than -70°C and were often as warm as -50°C . Thus even nitric acid trihydrate PSCs, which form at warmer temperatures (approximately -78°) than do pure ice crystal clouds, were not present in the stratosphere over BRW. Neither was there evidence in the ozone profiles of stratospheric transport of partially depleted ozone from the eastern Arctic to the BRW area.

The BRW ozone profiles could be categorized into two basic classes: those that occurred January 25-30, February 22-March 8, and March 17-24, having characteristics of polar air masses with ozone tropopause pressure altitudes of 350-450 mb and total ozone of 450-540 DU; and all others

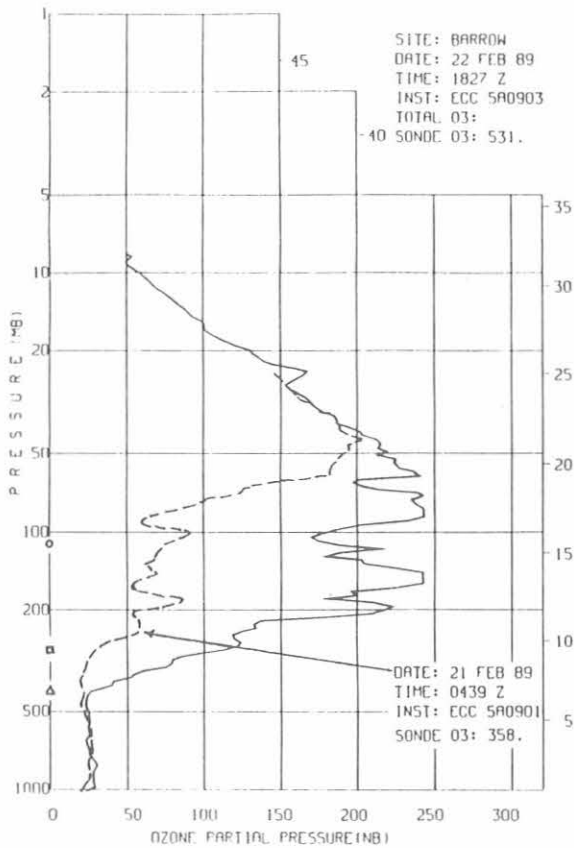


Fig. 5.15. ECC ozonesonde profiles obtained at BRW February 21 and 22, showing an increase in total ozone of 48% in 1.5 days time. The symbols circle, box, and triangle on the ordinate axis of the plot denote approximate pressure altitudes of the tropical, mid-latitude, and polar tropopause, respectively.

(except one) having characteristics of mid-latitude air masses with ozone tropopause pressure altitudes of 200-300 mb and total ozone of 350-400 DU. One ozone profile, that of February 6 with total ozone of 307 DU, exhibited an ozone tropopause near 100 mb, characteristic of ozone profiles in tropical regions.

Figure 5.15 is a plot of BRW ozone profiles of February 21 and 22 obtained 1.5 days apart. Note the large increase in ozone (48%) during the interval. The ozone profile of February 21 exhibits features of both tropical and mid-latitude air masses, whereas that of February 22 typifies polar air mass ozone profiles.

5.3. REFERENCES

- Bass, A.M., and R.J. Paur, The ultra-violet cross-sections of ozone, I, the measurements, in *Atmospheric Ozone, Proceedings of the Quadrennial Ozone Symposium*, Halkidiki, Greece, pp. 606-1610, D. Reidel, Hingham, MA, 1985.
- Bodhaine, B.H., and R.M. Rosson (Eds.), *Geophysical Monitoring for Climatic Change, No. 16: Summary Report 1987*, 110 pp., NOAA Environmental Research Laboratories, Boulder, CO, 1988.
- Elkins, J.W., and R.M. Rosson (Eds.) *Geophysical Monitoring for Climatic Change No. 17, Summary Report 1988*, 142 pp., NOAA Environmental Research Laboratories, Boulder, CO, 1989.
- Evans, W.J.F., Ozone depletion in the Arctic vortex at Alert during February 1989, *Geophys. Res. Lett.*, 17, 167-170, 1990.
- Johnson, J.E., R.H. Gammon, J. Larsen, T.S. Bates, S.J. Oltmans, and J.C. Farmer, Ozone in the marine boundary layer over the Pacific and Indian Oceans: Latitudinal gradients and diurnal cycles, *J. Geophys. Res.*, 95, 11,847-11,856, 1990.
- Komhyr, W.D., R.D. Grass, and R.K. Leonard, Dobson spectrophotometer 83: A standard for total ozone measurements, 1962-1987, *J. Geophys. Res.*, 94(D7), 9847-9861, 1989.
- Komhyr, W.D., E.A. Crozer, J.A. Lathrop, and M.A. Winey, ECC ozonesonde observations at South Pole, Antarctica during 1989, *NOAA Data Report ERL CMDL-5*, 247 pp., NOAA Environmental Research Laboratories, Boulder, CO, 1990a.
- Komhyr, W.D., J.A. Lathrop, and D.P. Opperman, ECC ozonesonde and Dobson Umkehr observations during STOIC 1989, *Digest of Topical Meeting on Remote Sensing of the Atmosphere, 1990, Vol. 4*, pp. 441-444, Optical Society of America, Washington, DC, 1990b.
- Komhyr, W.D., J.A. Lathrop, V.N. Arbutova, V.U. Khattalov, V.I. Pilipenko, and V. V. Rudakov, ECC ozonesonde observations at Mirny, Antarctica, during 1989, *NOAA Data Report ERL CMDL-4*, 84 pp., NOAA Environmental Research Laboratories, Boulder, CO, 1990c.
- Komhyr, W.D., S.J. Oltmans, R.D. Grass, and R.K. Leonard, Possible influence of long-term sea surface temperature anomalies in the tropical Pacific on global ozone, *Can. J. Phys.*, in press, 1991.
- McPeters, R.D., and W.D. Komhyr, Long-term changes in SBUV/TOMS relative to World Primary Standard Dobson spectrophotometer 83, *J. Geophys. Res.*, 61(D2), 2987-2993, 1991.
- Oltmans, S.J., Surface ozone measurements in clean air, *J. Geophys. Res.*, 86(C2), 1174-1180, 1981.
- Rosen, J.M., S.J. Oltmans, and W.F. Evans, Balloonborne observations of PSCs, frost point, ozone, and nitric acid in the North Pole vortex, *Geophys. Res. Lett.*, 16, 791-794, 1989.
- Watson, R.T., M.J. Prather, and M.J. Kurylo, Present state of knowledge of the upper atmosphere 1988: An assessment report, *NASA Reference Publication 1208*, 200 pp., NASA Office of Space Science and Applications, Washington, DC, 1988.

6. Acquisition and Data Management

G. HERBERT (Editor), J. HARRIS, M. BIENULIS, AND J. MCCUTCHEON

6.1. CONTINUING PROGRAMS

6.1.1. STATION CLIMATOLOGY

The CMDL station climatology is derived from surface weather observations of wind direction, wind speed, station pressure, air and dewpoint temperature, and precipitation amount. The 13-year station climatologies are an important record for the interpretation of measured values of aerosols, trace gases, and climatic change. The sensors currently in use were selected not only for high accuracy but also for ruggedness, to minimize failures in the extreme conditions of the polar regions (Table 6.1). Since the last reporting of the complement of instrumentation at the stations [Nickerson, 1986], the dewpoint hygrometer has been changed to correspond to the hygrometer used by the NWS. To the extent that it is practical, WMO siting standards are followed.

Barrow

Descriptions of the BRW station and its climate are given in previous *GMCC Summary Reports* [e.g., DeLuisi, 1981]. Wind roses of hourly average resultant wind direction and speed are presented in 16 direction classes and 4 speed classes (Figure 6.1). The distribution of wind by direction for the 1989 wind rose shows a higher percentage of winds from the southwest quadrant (31%) compared with the 12-year climatology (19%). The "clean-air sector," the northeast-southeast quadrant, showed a decreased percentage of winds (55%) compared with the 12-year climatology (60%). The anomalous southwest winds were primarily recorded during the months of January-March. The year's peak gust of 43 m s⁻¹ on February 25, was the highest wind speed ever recorded at the station.

The average temperature for 1989 (Table 6.2) was 2.4°C warmer than the climatological average of -12.7°C. The year's minimum temperature of -47°C occurred on January 26, and the maximum of 21°C on August 10, which ties the all-time high. January was 7°C colder than normal, and the average pressure for the month was 3 hPa lower than normal. On January 30 the pressure reached 1057 hPa, matching the old high-pressure record. The high-pressure ridge over Alaska persisted into March, advecting Pacific maritime air northward and causing unseasonably warm temperatures. February 1989 was the warmest February on record with a -13°C average, which is 13°C above normal. Monthly mean temperatures were above normal for 9 months in 1989.

Mauna Loa

In this report the climatology of MLO is regarded as consisting of two distinct regimes (Table 6.3) because the bimodal distribution of the wind direction changes generally consistently with the time of day. The day (upslope) period (0600-1800 LST) and the night (downslope) period (1800-0600 LST) define the two regimes. The 12-year day and night wind roses illustrate the two distinct wind patterns (Figure 6.2).

Day regime. The 12-year day wind rose (Figure 6.2) indicates that light wind speeds in the northwest-northeast sector were observed nearly 50% of the time. This represents the upslope flow attributed to the daytime heating of Mauna Loa. The 1989 day wind rose (Figure 6.3) compares well with the 12-year rose except for strong west-southwesterlies representative of storm-related winds through the 12-year period. The day wind roses are more

TABLE 6.1. CMDL Meteorological Sensor Deployment

Sensor	BRW		MLO		SMO		SPO	
	Serial No.	Elevation, m						
Primary anemometer	576	16.7	931	8.5	782	13.7	585	12.2
Secondary wind Aerovane*			883	38.5				
Pressure transducer†	2366	9	225	3397	752	30	8	2841
Mercurial barometer	641	9	278	3397	961	30		
Air temperature A‡	8801	2.5	8807	1.7	8807	9	703	2.2
Air temperature B§	8802	15.3	8809	37.8	8808	2.3	701	23.2
Air temperature C‡	8	3.1	46	2.0	2	9.0	835	2.2
Dewpoint temperature hygrometer**	8	3.1	46	2.0	1	9.0	3720	2.2

*Aerovane, Bendix, Inc., model no. 141, Baltimore, MD.

† Pressure transducer, Rosemount, Inc., model no. 1201F1b, Minneapolis, MN. Heights of all pressure sensors are given with respect to MSL.

‡Linearized thermistors, Yellow Springs Inst. Co., model no. 44212, Yellow Springs, OH.

§Thermometer, positioned at the top of the local sampling tower to facilitate an estimation of boundary layer stability.

**Hygrothermometer, Technical Services Laboratory model no. 1063, Fort Walton Beach, FL.

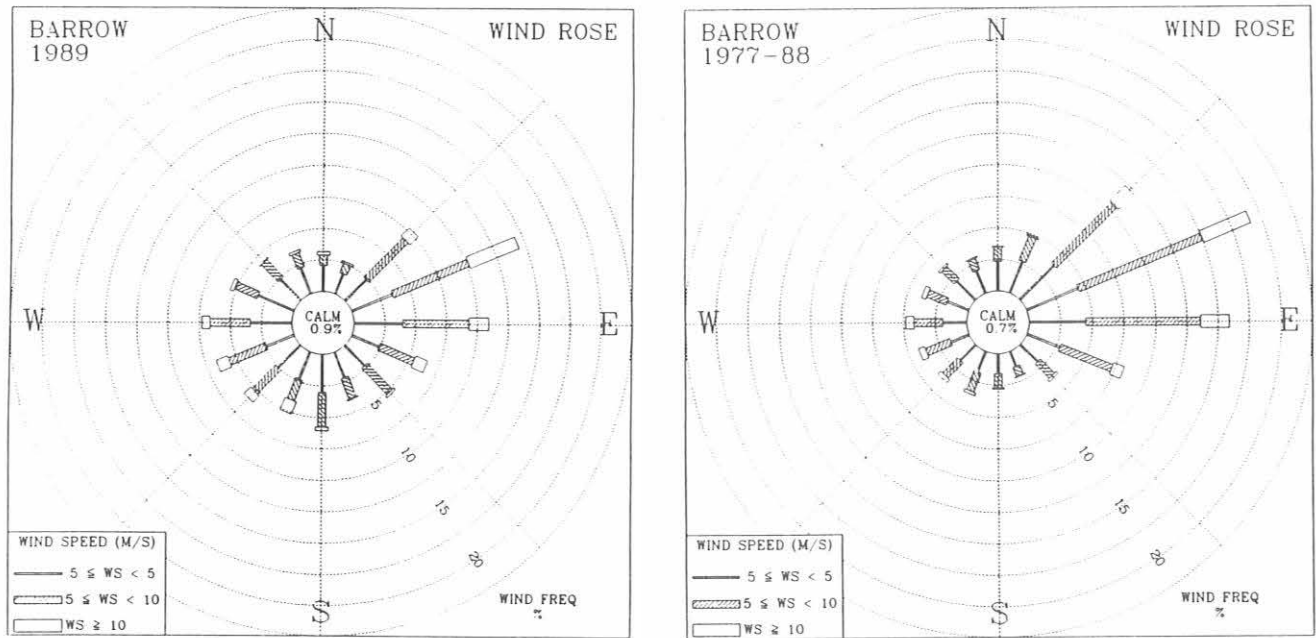


Fig. 6.1. Wind roses of surface winds for BRW for 1989 (left) and 1977-1988 (right). The distributions of the resultant wind direction and speed are in units of percent occurrence for the year and 12-year period, respectively. Wind speed is displayed as a function of direction in three speed classes.

TABLE 6.2. BRW 1989 Monthly Climate Summary

	Jan.	Feb.	March	April	May	June	July	Aug.	Sept.	Oct.	Nov.	Dec.	1989
Prevailing wind direction	W	SSW	NW	ENE	E	E	E	E	ENE	ENE	ENE	ENE	ENE
Average wind speed (m s ⁻¹)	5.7	8.6	5.7	6.4	4.9	4.7	5.6	6.1	6.6	7.1	6.1	8.1	6.3
Maximum wind speed* (m s ⁻¹)	14	33	17	14	13	15	17	16	14	19	17	19	33
Direction of max. wind* (deg.)	114	232	105	249	80	346	239	272	77	79	72	71	232
Average station pressure (hPa)	1011.3	1019.4	1022.8	1017.0	1018.3	1013.8	1009.9	1008.3	1011.9	1011.1	1017.4	1019.7	1015.0
Maximum pressure* (hPa)	1057	1055	1044	1033	1034	1025	1024	1021	1027	1044	1034	1038	1057
Minimum pressure* (hPa)	986	981	1005	998	1002	996	996	999	996	981	1008	1003	981
Average air temperature (°C)	-31.6	-13.0	-22.4	-14.4	-8.2	1.3	6.4	7.6	1.7	-7.3	-23.5	-22.7	-10.3
Maximum temperature* (°C)	-3	-2	-1	2	3	14	18	21	15	3	-12	-12	21
Minimum temperature* (°C)	-47	-36	-40	-29	-24	-4	-1	0	-3	-25	-32	-41	-47
Average dewpoint temperature (°C)	-35.6	-14.9	-26.0	-17.0	-10.1	-0.9	6.2	3.8	-3.2	-13.8	-28.3	-25.5	-14.8
Maximum dewpoint temperature* (°C)	-6	-2	-2	0	1	2	13	13	8	2	-18	-13	13
Minimum dewpoint temperature* (°C)	-53	-41	-45	-33	-27	-8	-3	-4	-8	-30	-36	-45	-53
Precipitation (mm)	0	27	0	2	0	8	61	25	19	1	0	0	144

Instrument heights: wind, 16.7 m; pressure, 9 m (MSL); air and dewpoint temperature, 2.5 m. Wind and temperature instruments are on a tower 25 m northeast of the main building.

*Maximum and minimum values are hourly averages.

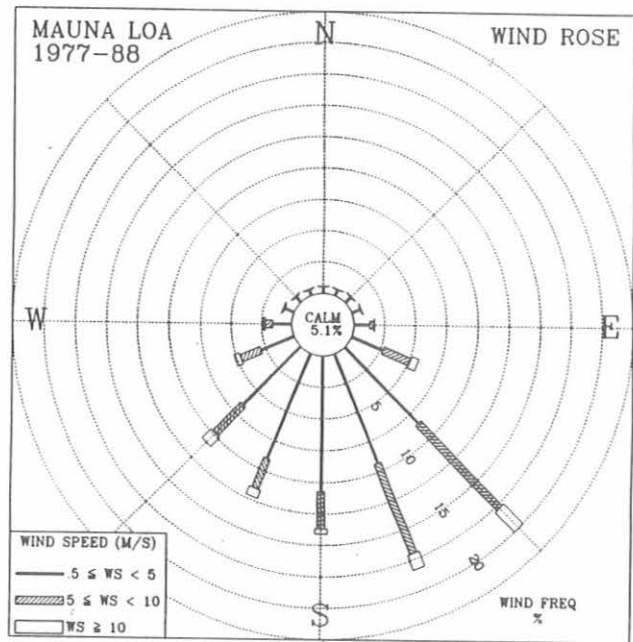
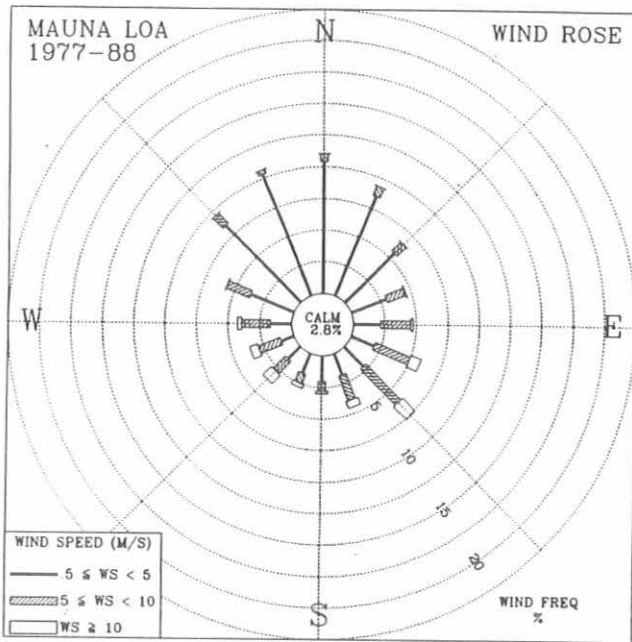


Fig. 6.2. Wind roses of the surface winds for MLO for 1977-1988 day (left) and night (right). The distributions of resultant wind direction and speed are given in units of percent occurrence for the 12-year period. Wind speed is displayed as a function of direction in three speed classes.

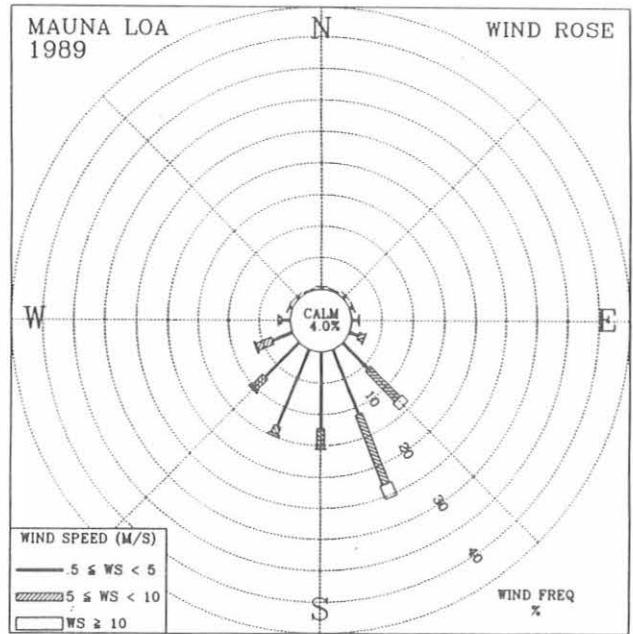
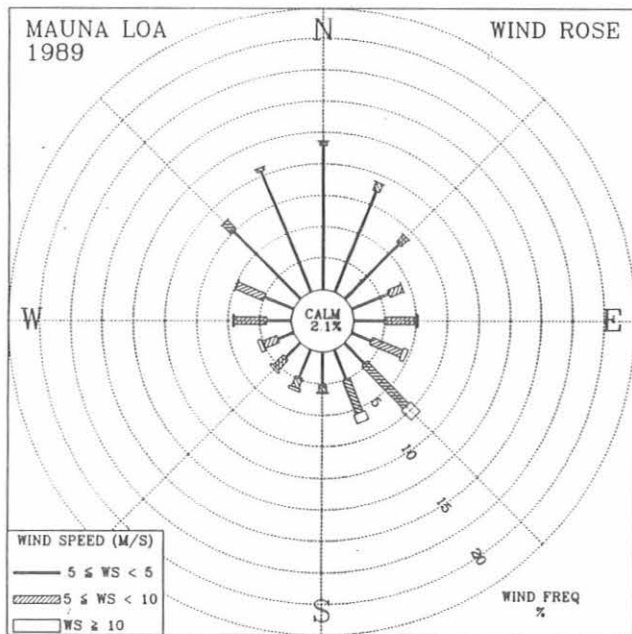


Fig. 6.3. Wind roses of the surface winds for MLO for 1989 day (left) and night (right). The distributions of the resultant wind direction and speed are given in units of percent occurrence for the year. Wind speed is displayed as a function of direction in three speed classes. Note the scale change in the night plot for 1989.

TABLE 6.3. MLO 1989 Monthly Climate Summary

	Jan.	Feb.	March	April	May	June	July	Aug.	Sept.	Oct.	Nov.	Dec.	1989
<i>Day</i>													
Prevailing wind direction	SE	SE	SE	N	NNW	NE	SE	NNE	N	N	NW	W	N
Average wind speed (m s ⁻¹)	5.4	4.5	5.7	3.5	4.0	3.9	5.3	3.8	3.5	3.3	4.2	4.7	4.3
Maximum wind speed* (m s ⁻¹)	12	15	14	11	12	12	15	9	9	11	14	12	15
Direction of max. wind* (deg.)	151	160	129	159	249	164	163	158	156	146	131	283	160
Average station pressure (hPa)	678.6	678.1	679.4	678.1	680.4	681.4	681.8	681.2	680.2	680.5	680.1	678.9	679.9
Maximum pressure* (hPa)	682	682	684	681	683	685	684	683	682	684	685	684	685
Minimum pressure* (hPa)	675	674	673	674	676	679	679	679	679	678	677	671	671
Average air temperature (°C)	4.4	4.8	7.1	5.3	7.4	10.6	10.4	10.8	10.9	8.7	9.1	7.4	8.1
Maximum temperature* (°C)	10	11	15	12	13	18	16	18	18	15	15	15	18
Minimum temperature* (°C)	-4	-3	-1	-1	1	2	2	3	2	3	1	-3	-4
Average dewpoint temperature (°C)	-4.2	-3.5	-4.2	-0.6	-2.0	-4.3	-2.3	-3.2	-4.3	1.5	-9.7	-11.1	-3.9
Precipitation (mm)	47	46	30	115	75	30	70	17	13	23	1	19	486
<i>Night</i>													
Prevailing wind direction	SSE	SSE	SE	SSW	SSE	SSE	SSE	SSE	SSE	S	SSE	WSW	SSE
Average wind speed (m s ⁻¹)	5.8	5.1	5.8	3.4	4.1	4.4	5.8	3.6	3.8	2.8	4.2	4.8	4.5
Maximum wind speed* (m s ⁻¹)	13	13	20	12	9	12	19	12	11	10	13	11	20
Direction of max. wind* (deg.)	157	227	230	157	238	166	149	159	159	160	131	279	230
Average station pressure (hPa)	678.7	678.2	679.3	678.0	680.4	681.2	681.6	681.0	680.1	680.6	680.1	679.0	679.9
Maximum pressure* (hPa)	682	682	683	681	683	685	684	683	682	683	684	684	685
Minimum pressure* (hPa)	675	673	672	674	676	679	679	679	678	678	677	672	672
Average air temperature (°C)	1.2	1.6	3.0	2.2	3.4	6.0	5.8	6.3	6.4	5.3	5.2	3.4	4.2
Maximum temperature* (°C)	6	6	8	7	9	13	12	13	13	9	9	9	13
Minimum temperature* (°C)	-4	-3	-1	-1	-1	1	1	2	3	2	1	-3	-4
Average dewpoint temperature (°C)	-7.3	-6.6	-6.9	-5.5	-5.7	-9.9	-5.8	-10.6	-12.2	-1.7	-14.6	-14.8	-8.5
Precipitation (mm)	19	27	13	20	8	1	30	2	0	20	0	12	153

Instrument heights: wind, 8.5 m; pressure, 3397 m (MSL); air and dewpoint temperature, 2.0 m. Wind and temperature instruments are on a tower 15 m southwest of the main building.

*Maximum and minimum values are hourly averages.

uniformly distributed than the night wind roses, possibly because of the occurrence of variable wind directions during the transition periods of dawn and dusk, most of which are included in this regime.

Night regime. The 12-year night wind rose (Figure 6.2) shows that 75% of all winds observed were from the southwest-southeast downslope wind sector. The 1989 wind rose (Figure 6.3) shows a higher percentage of south-

southeasterly winds than does the 12-year rose. These anomalous winds are most prevalent in the January-March period. Storm-related winds ($WS \geq 10 \text{ m s}^{-1}$) are evident in the 12-year night wind rose, but are considerably reduced in the 1989 night wind rose.

The 1989 average day-night temperature difference is 3.9°C , and the average dewpoint depression for 1989 is 12.4°C (Table 6.3). The year's maximum temperature of 18.1°C occurred on June 21 and the minimum of -4°C occurred on January 5. The lowest pressure in 1989 of 671 hPa occurred December 12. The year's peak gust of 29 m s^{-1} from the southwest was recorded on March 2. The precipitation total for 1989 of 639 mm is 120% of the normal yearly precipitation. During January-May, 400 mm of precipitation was measured, which was 63% of the annual amounts. In April the highest precipitation amount of 135 mm was measured. August-December recorded only 107 mm (17%); November recorded only a trace. The MLO precipitation pattern for 1989 may be correlated with the La Niña event of 1988.

Samoa

A comparison of SMO's 1989 wind rose with that for the 12-year period shows a higher percentage (13%) of north-northwest winds in 1989 (Figure 6.4). Winds were predominantly from the south-southeast sector (53%) in 1989, which agrees with the 12-year wind climatology (56%). The anomalous northerly winds occurred primarily in January and February. The peak gust in 1989 of 29 m s^{-1} on January 7 set a new January record.

The average temperature for 1989 of 26.6°C is consistent with the 12-year average of 27°C , although January and February were a degree colder than normal (Table 6.4). The average pressure for 1989 of 1001.5 is 0.5 hPa higher than the 12-year average of 1001.0 hPa. High pressure values were evident during January-March, a time period of anomalously northerly winds.

The precipitation total for 1989 was 2535 mm. This is 375 mm above the normal yearly amount. Anomalous amounts were measured at the beginning of 1989 and in November, which measured a record 422 mm. The SMO dry season (June-September) was present again in 1989. The most rain measured in a 24-h period occurred on December 13 when 149 mm was reported. The anomalous precipitation, high pressure, and northerly winds for the first 3 months of 1989 can be correlated with the La Niña event of 1988. Previous periods of below-normal sea surface temperatures in the eastern tropical Pacific have demonstrated anomalous precipitation patterns in many areas of the globe [Arkin, 1989].

South Pole

The distribution of the surface wind direction in 1989 is nearly identical to that of the 12-year pattern (Figure 6.5) with winds predominantly from the northeast sector (80%). A slightly higher percentage of winds from the east-southeast direction can be seen in the 1989 wind rose compared with the 12-year wind rose. The irregular east-southeast wind

directions were primarily observed in April. Strong winds from the Antarctic plateau were measured during the winter period. The strongest of these winds measured 18 m s^{-1} on August 24, and set a new August wind speed record.

The 1989 temperature and pressure averages are consistent with the 12-year record, although April, May, and June were anomalous (Table 6.5). The average pressure for May of 668.3 hPa is 10 hPa below the May normal, and temperatures averaged 4°C colder than normal during the period. The strong winds in August broke the inversion, mixing down warm air from aloft, and causing the average surface temperature for August to be 2.5°C warmer than normal. The maximum pressure for 1989 of 706 hPa on August 28 was 1 hPa short of tying the all time high pressure record.

6.1.2. DATA MANAGEMENT

During 1989 the performance of the CAMS surpassed that of previous years, having an overall downtime of less than 1%. Table 6.6 gives the CAMS operations summary according to block type for 1989. The longest downtimes occurred for the CO₂ CAMS at BRW and SPO. These systems were offline for 1-2 weeks while the CO₂ analyzer and the flow equipment were overhauled.

Every observatory experienced power outages from time to time that caused brief losses of data. At MLO the CAMS system memory board, a tape controller, and a power supply were replaced. Most of the data lost at SMO was due to operator error during personnel changeovers, as well as tape and tape drive problems. Most notable among the latter was the problem of capstans that had dried, hardened, and cracked, leading to errors in writing and reading the tapes. These were replaced and the problems disappeared. BRW had a few problems related to worn out tapes.

In an attempt to minimize the effects of two other CAMS problems that can cause loss of data, A&DM personnel devised a monthly hardware test with the object of locating the problems before data are lost. The two problems are clock failure when CAMS operations are interrupted, and periodic random access memory failure. A clock failure can happen if the clock's power circuit is not activated or if the battery is worn out; the results are spurious dates and times being recorded. The hardware test involves unplugging each box at the beginning of each month when data tapes are changed. After 1 minute, the operator plugs the box in again, checks the clock, and reads the front panel message and the calibration constants. If the clock or the memory is not able to recover from the deliberate power outage, the problem can be fixed during the hardware test and data loss should be reduced.

During 1989, a CAMS status report was developed that provides information on the number of missing blocks according to station, box, and tape number, and the overall percentage of data acquisition by station for the month. Comments are added to the report form to document hardware problems, and the form is distributed to the CMDL Director's office and the observatories once a month.

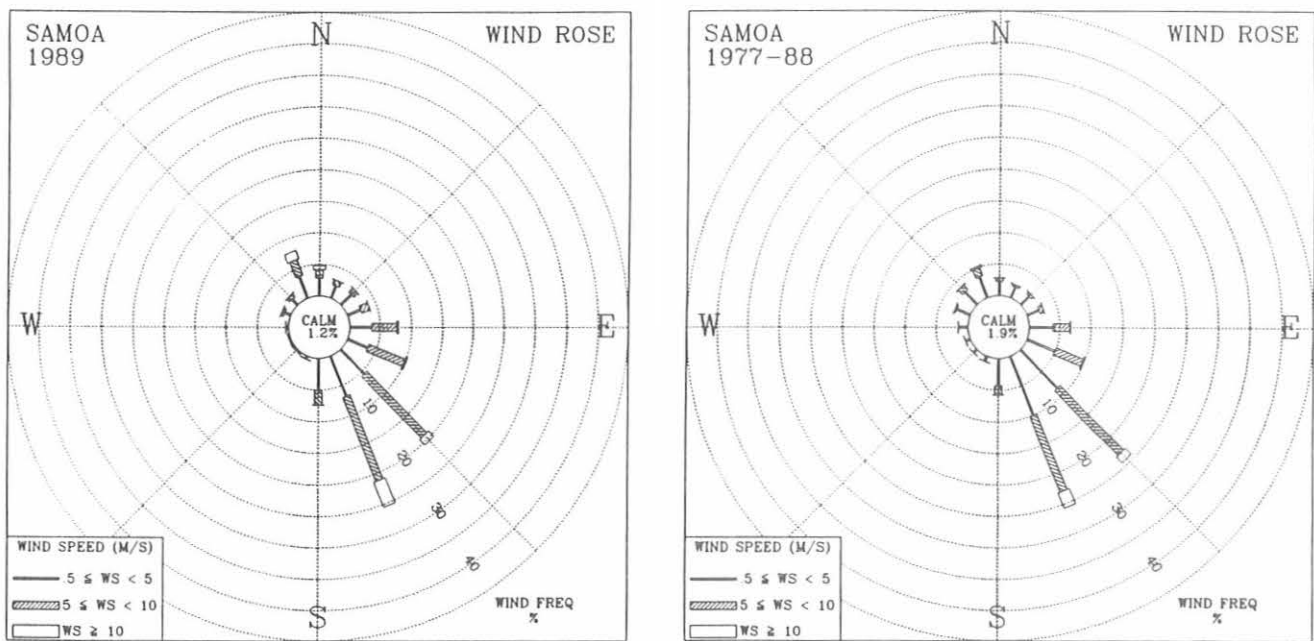


Fig. 6.4. Wind roses of the surface wind for SMO for 1989 (left) and 1977-1988 (right). The distributions of the resultant wind direction and speed are in units of percent occurrence for the year and 12-year period, respectively. Wind speed is displayed as a function of direction in three speed classes.

TABLE 6.4. SMO 1989 Monthly Climate Summary

	Jan.	Feb.	March	April	May	June	July	Aug.	Sept.	Oct.	Nov.	Dec.	1989
Prevailing wind direction	NNW	NNW	SE	SE	SSE	SSE	SSE	SSE	SE	SE	SE	SSE	SSE
Average wind speed (m s ⁻¹)	5.9	5.8	5.0	5.3	4.8	7.7	6.2	5.8	7.9	5.9	5.2	4.5	5.8
Maximum wind speed* (m s ⁻¹)	17	15	12	12	10	14	13	12	13	13	13	12	17
Direction of max. wind* (deg.)	342	92	1	160	53	124	160	159	156	155	94	141	342
Average station pressure (hPa)	999.3	1000.4	1001.4	1000.5	1002.1	1003.6	1003.2	1003.4	1003.5	1001.9	999.6	999.2	1001.5
Maximum pressure* (hPa)	1004	1004	1005	1004	1005	1006	1007	1008	1006	1006	1004	1005	1008
Minimum pressure* (hPa)	994	997	998	997	999	999	1000	1000	999	998	996	990	990
Average air temperature (°C)	26.6	26.7	27.2	27.3	26.8	26.5	25.8	26.0	26.5	26.7	26.6	26.8	26.6
Maximum temperature* (°C)	31	30	31	32	31	29	31	30	29	31	31	32	32
Minimum temperature* (°C)	22	22	22	23	23	22	23	24	23	23	22	23	22
Precipitation (mm)	312	298	236	250	130	87	171	14	21	249	422	345	2535

Instrument heights: wind, 13.7 m; pressure, 30 m (MSL); air temperature, 9 m. Wind and temperature instruments are on Lauagae Ridge, 110 m northeast of the main building. Pressure sensors are in the main building.

*Maximum and minimum values are hourly averages.

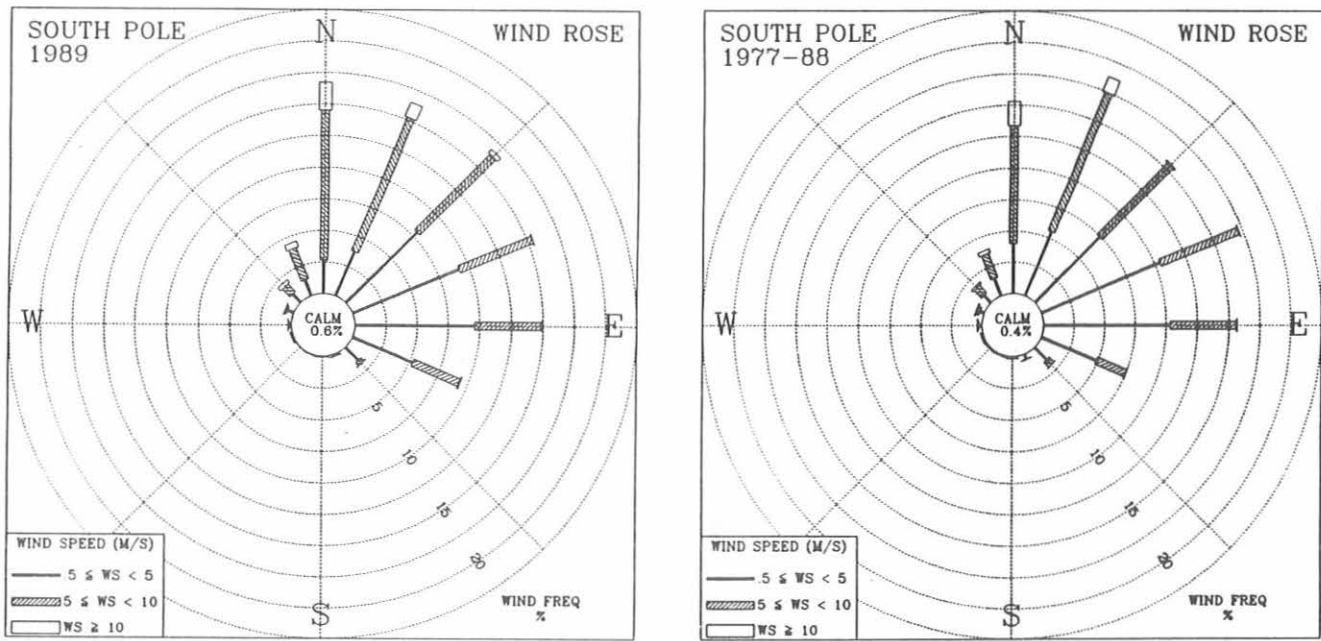


Fig. 6.5. Wind roses of the surface wind for SPO for 1989 (left) and 1977-1988 (right). The distributions of the resultant wind direction and speed are in units of percent occurrence for the year and 12-year period, respectively. Wind speed is displayed as a function of direction in three speed classes.

TABLE 6.5. SPO 1989 Monthly Climate Summary

	Jan.	Feb.	March	April	May	June	July	Aug.	Sept.	Oct.	Nov.	Dec.	1989
Prevailing wind direction	E	ENE	NE	ESE	E	E	NNE	NE	NE	E	N	NNE	NE
Average wind speed (m s ⁻¹)	3.3	4.6	5.8	5.8	5.9	5.7	6.9	7.1	7.3	5.2	5.1	5.7	5.7
Maximum wind speed* (m s ⁻¹)	8	10	12	12	14	12	15	17	13	10	10	12	17
Direction of max. wind* (deg.)	10	321	7	116	35	10	343	308	22	36	18	357	308
Average station pressure (hPa)	688.0	681.8	682.1	680.2	668.3	671.7	673.9	679.4	676.8	674.5	682.9	689.9	679.1
Maximum pressure* (hPa)	694	692	699	703	680	682	689	706	693	689	696	696	706
Minimum pressure* (hPa)	681	668	674	661	653	663	651	659	653	657	669	681	651
Average air temperature (°C)	-28.0	-40.4	-53.6	-60.5	-62.0	-61.9	-58.5	-56.5	-58.1	-53.1	-37.5	-25.0	-49.6
Maximum temperature* (°C)	-20	-27	-39	-37	-39	-45	-38	-37	-41	-35	-26	-20	-20
Minimum temperature* (°C)	-38	-54	-67	-74	-75	-78	-78	-75	-74	-66	-48	-32	-78

Instrument heights: wind, 12.2 m; pressure 2841 m (MSL); air temperature, 2.2 m. The anemometer and thermometer are on a tower 100 m grid east-southeast of CAF. Pressure measurements are made inside CAF.

*Maximum and minimum values are hourly averages.

TABLE 6.6. CMDL CAMS Operations Summary, 1989

Block Type	Description	Expected No. of Blocks 1989*	Blocks Recorded and [Blocks Missing]			
			BRW	MLO	SMO	SPO
A	Hourly aerosol data	2190	2164 [26]	217 [19]	2159 [31]	2171 [19]
B	Secondary aerosol data	Variable	2140	2158	24	1623
H	Daily aerosol data	365	362 [4]	363 [2]	360 [5]	363 [2]
S	Hourly solar radiation data	8760	8659 [103]	8681 [79]	8637 [123]	8686 [74]
T	Daily solar radiation data	365	343 [4]†	157 [2]†	184 [0]†	57 [3]†
C	Hourly CO ₂ data	Variable	8006 [170]	8339 [9]	8325 [90]	8183 [169]
D	Daily CO ₂ data	365	356 [4]	363 [0]	361 [4]	358 [7]
E	Hourly CO ₂ calibration data	Variable	410	371	341	393
F	CO ₂ calibration report	52	53	53	48	53
M	Hourly meteorological data	4380	4357 [23]	4362 [20]	4346 [36]	4376 [5]
O	Daily surface ozone data	365	365 [0]	364 [1]	362 [3]	365 [0]
W	Daily meteorological data	365	365 [0]	364 [1]	362 [3]	365 [0]
I	Meteorological calibration	365	363 [2]	364 [1]	362 [3]	365 [0]
N	Surface ozone calibration	52	53	61	62	33

*Discrepancies between the expected number of blocks and blocks recorded + blocks missing are due to clock problems or autorestarts.

†T block added to data suite during 1989.

6.2. SPECIAL PROJECT: ATMOSPHERIC TRAJECTORIES

CMDL isobaric trajectory calculations have been documented by *Harris* [1982], and isentropic trajectories have been described in *Harris and Bodhaine* [1983] and validated by *Herbert et al.* [1989]. In addition, most *Summary Reports* contain an article describing the latest developments in and studies using atmospheric trajectories.

Input available for the trajectory calculations consists of 13 years of gridded meteorological data from NMC. A shorter but comparable data set from ECMWF is also available for 1980-1989. The latter data set is used in comparison studies and for trajectories computed using three-dimensions, which were developed this year because ECMWF provides vertical wind speeds at each mandatory pressure level. The three-dimensional trajectories track the winds according to the u, v, and w fields so that an estimate of the vertical motion in the atmosphere can be provided along with the usual horizontal trajectory estimate. Some three-dimensional trajectories were produced for AGASP II case studies. They compared favorably with those produced by a University of Washington model.

The following includes most of the organizations for which atmospheric trajectories were produced during 1989: Institute of Marine Geology, Italy; National Research Center for Marine Environmental Forecasts, P.R.C.; University College Galway, Ireland; Center for Atmospheric Science, Mexico; Institute of Natural Science, Korea; Institute for Atmospheric Physics, Yugoslavia; Academy of Atmospheric Physics, U.S.S.R.; University of Las Palmas, Spain; Atmospheric Environment Service, Canada; Idaho National Engineering Laboratory; Lawrence Berkeley Laboratory; NCAR; USGS; University of Colorado; University of Alabama; AOML; PMEL; and ARL. CMDL staff responded to more than 60 requests for trajectories from within the

Laboratory as well as from other government agencies, universities, and research organizations. Whenever possible, trajectories are provided for collaborative studies whose theme reflects CMDL's mission.

A study was completed in 1989 [*Harris and Kahl*, 1990] that used cluster analysis of trajectories to describe the principle flow regimes affecting MLO. Eight years (1981-1988) of 10-day MLO back trajectories on the 500- and 700-hPa surfaces were analyzed. Cluster analysis is a multivariate technique that groups cases based on their similarity. A method was chosen that minimizes the within-group variances, with the result of grouping trajectories that describe similar wind flow patterns. These patterns could then each be represented with a cluster mean or average trajectory for the cluster, thereby summarizing many trajectories with only a few distinct flow patterns.

The analysis was performed for both levels for each year to examine the year-to-year variability. Then trajectories were clustered by month to describe the seasonal variations in MLO's flow regime. Figure 6.6 shows six cluster means for typical years at both levels: (a) 1984, 700 hPa, and (b) 1983, 500 hPa. Clusters for other years appear in *Harris and Kahl* [1990]. In Figure 6.7, 700-hPa clusters obtained for three months, (a) August, (b) October, and (c) December, show the transition from the summer easterly tradewind regime to the winter flow dominated by westerly winds.

This trajectory climatology disclosed the following features of MLO's flow patterns:

- (1) The gross features of atmospheric transport to MLO are similar from year to year.
- (2) Easterly transport occurs 38-54% of the time at 700 hPa. It is most frequent in summer but is present during all months. Easterly winds are not as pronounced at 500 hPa.
- (3) Strong westerly transport from Asia or beyond is frequent at both levels. This pattern is strongest at 500 hPa

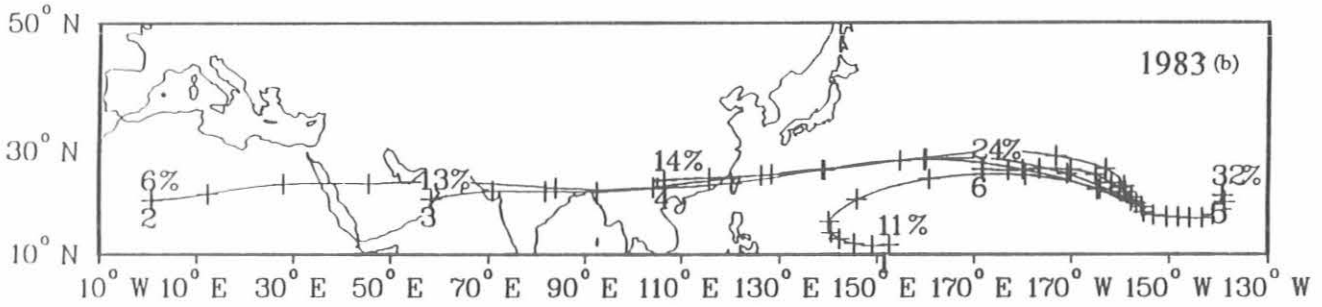
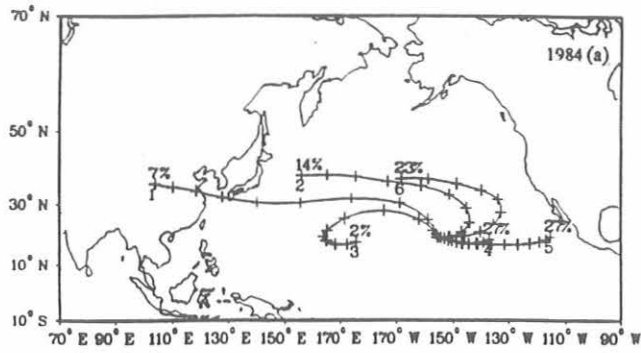


Fig. 6.6. Atmospheric transport regimes for MLO, depicted by cluster-mean trajectories at (a) 700 hPa, 1984, and (b) 500 hPa, 1983. Plus signs indicate 1-day upwind intervals. The numbers 10 days upwind of MLO show the percentage of complete trajectories occurring in the cluster (top number) and arbitrary cluster number used for identification (bottom number).

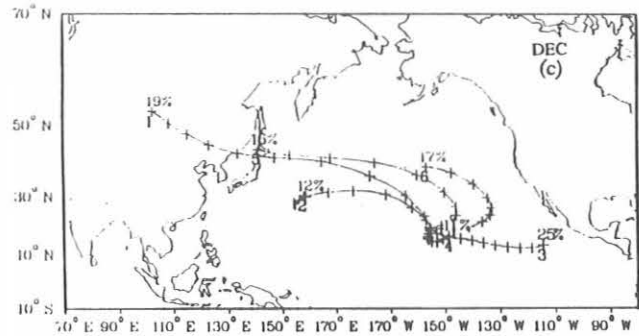
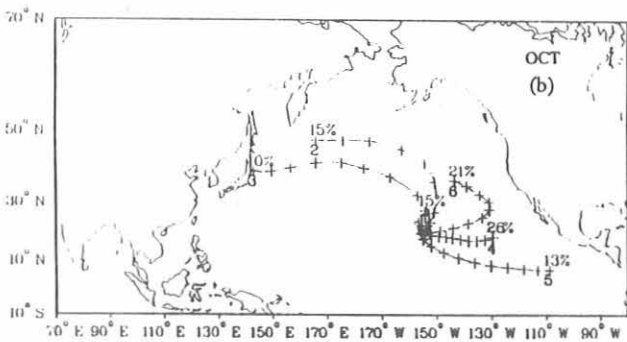
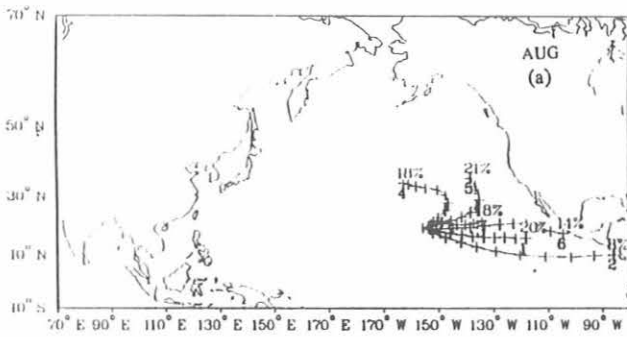


Fig. 6.7. Atmospheric transport regimes for MLO, by month, depicted by cluster-mean back trajectories at 700 hPa for the period 1981-1988: (a) August, (b) October, and (c) December. Symbols are as in Figure 6.6.

because of the influence of the subtropical jet stream; the longest trajectories occur from October through May.

(4) Both levels exhibit westerly flow patterns that curve anticyclonically to approach MLO from the north and northeast. This pattern is most pronounced at 700 hPa.

(5) The flow climatology indicates an annual progression from westerly transport during winter to easterly transport during summer and a transition corresponding to the migration of the North Pacific anticyclone.

(6) The greatest directional shear between the 500- and 700-hPa levels occurs during winter and the least during July, August, and September.

6.3. REFERENCES

Arkin, P.A., *Seasonal Climate Summary*, Vol. 2, 737 pp., NOAA/NWS Climate Analysis Center, National Meteorological Center, Washington, DC, 1989.

DeLuisi, J.J. (Ed.), *Geophysical Monitoring for Climatic Change, No. 9: Summary Report 1980*, 163 pp., NOAA Environmental Research Laboratories, Boulder, CO, 1981.

Harris, J.M., The GMCC atmospheric trajectory program, *NOAA Tech. Memo. ERL ARL-116*, 30 pp., NOAA Environmental Research Laboratories, Boulder, CO, 1982.

Harris J.M., and B.A., Bodhaine (Eds.), *Geophysical Monitoring for Climatic Change, No.11: Summary Report 1982*, pp. 67-75, NOAA Environmental Research Laboratories, Boulder, CO, 1983.

Harris, J.M., and J.D. Kahl, A descriptive atmospheric transport climatology for the Mauna Loa Observatory using clustered trajectories, *J. Geophys. Res.*, 95(D9), 13651-13667, 1990.

Herbert, G.A., J.M. Harris, and B.A. Bodhaine, Atmospheric transport during AGASP II: The Alaskan flights (2-10 April 1986), *Atmos. Environ.*, 23, 2521-2536, 1989.

Nickerson, E.C. (Ed.), *Geophysical Monitoring for Climatic Change, No. 13: Summary Report 1984*, 111 pp., NOAA Environmental Research Laboratories, Boulder, CO, 1986.

7. Air Quality Group

J. BOATMAN (Editor), L. GUNTER, M. LURIA, J. RAY, H. SIEVERING, B. WATKINS, AND C. VAN VALIN

7.1. CONTINUING PROGRAMS

7.1.1. INTRODUCTION

Research objectives of the AQG are: (1) to improve understanding of the acidic deposition phenomenon; (2) to determine the amount and fate of various trace species that are advected eastward from North America; (3) to provide an observational data base to validate the acid deposition models; and (4) to gain a better understanding of the concentration of acid-causing agents within clouds. Emphasis during 1989 was on a new, related activity funded by the U.S. Army Atmosphere Research Group, namely, characterization of natural aerosol background in clean continental air. The work was conducted aboard the NOAA King Air research aircraft (Figure 7.1). Table 7.1 summarizes the research flights made by the King Air in support of our activities during 1989.

7.1.2. ATMOSPHERIC LIDAR VALIDATION EXPERIMENT

ALIVE was part of a coordinated multi-institution study of aerosol optical properties over a remote continental

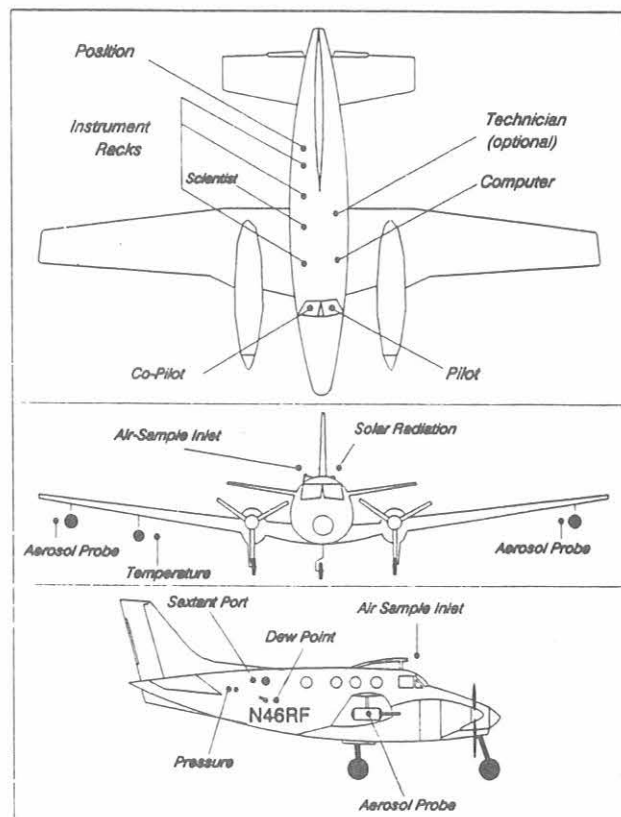


Fig. 7.1. The NOAA King Air C-90, configured for research.

TABLE 7.1. NOAA King Air Research Flights
During 1989

Date	Start, MST	End, MST
<i>ALIVE-1</i>		
Feb. 7	0823	1018
Feb. 8 (flight 1)	0745	0938
Feb. 8 (flight 2)	1520	1705
Feb. 8 (flight 3)	2107	2255
Feb. 9	1510	1700
Feb. 10 (flight 1)	0708	0901
Feb. 10 (flight 2)	1512	1703
<i>ALIVE-2</i>		
July 10 (flight 1)	0817	0946
July 10 (flight 2)	1330	1518
July 11 (flight 1)	0703	0900
July 11 (flight 2)	1241	1622
July 12 (flight 1)	0639	0913
July 12 (flight 2)	1830	2106
July 13	1735	2002
July 14	0237	0502
<i>ALIVE-3</i>		
Dec. 11	0815	1024
Dec. 11	1503	1725
Dec. 12	0804	1107
Dec. 12	1440	1718
Dec. 13	0804	1035
Dec. 13	1408	1612
Dec. 14	0751	1026
Dec. 14	1524	1724
Dec. 15	0751	1225
<i>J. Elkins Research</i>		
Feb. 24 (flight 1)	0903	1220
Feb. 24 (flight 2)	1444	1632

region. Measurements were made of meteorological variables, condensation nuclei, and aerosol optical scattering and absorption, using the NOAA King Air C-90 research aircraft (46RF) equipped with navigational, meteorological, and aerosol instrumentation. Flights occurred over south-central New Mexico in coordination with ground-based lidar measurements. The present data set allows for a calculation of the tropospheric column optical extinction and an assessment of the contribution of absorption to this extinction.

A goal of the project was to develop an understanding of the effect of hydration on the optical properties of internally mixed particles containing both scattering and absorbing material. This will allow more accurate predictions of in-situ aerosol optical properties, based on known source strengths, source emission characteristics, and transport pathways to the location in question.

The discussion here is restricted primarily to the results from two typical flights in the 16-flight series: one winter flight (February 8, 1989) and one summer flight (July 11, 1989).

Figure 7.2 shows data from the winter flight, plotted as a function of pressure and altitude. Figure 7.2a depicts air and dewpoint temperatures; Figure 7.2b shows aerosol backscatter from the three-wavelength integrating nephelometer; Figure 7.2c displays the aerosol black carbon content; and Figure 7.2d gives the condensation nucleus concentration. This series of flights was the first use of the aethalometer aboard the NOAA King Air for absorption measurements, and sampling rate problems reduced its sensitivity. Consequently, it was necessary to average the black carbon data for the flights of the winter series. Figure 7.2c depicts average black carbon concentrations in the boundary layer and in the free troposphere for the three flights on February 8 and presents similar data for two flights on February 10.

Figure 7.3 shows data for the same variables, but during the summer flight. The aethalometer sensitivity was improved by this time. Therefore, Figure 7.3c displays average black carbon concentrations, representing aerosol accumulations over periods of a few minutes. The horizontal bars in Figure 7.3c depict the range of aethalometer readings for each averaging period.

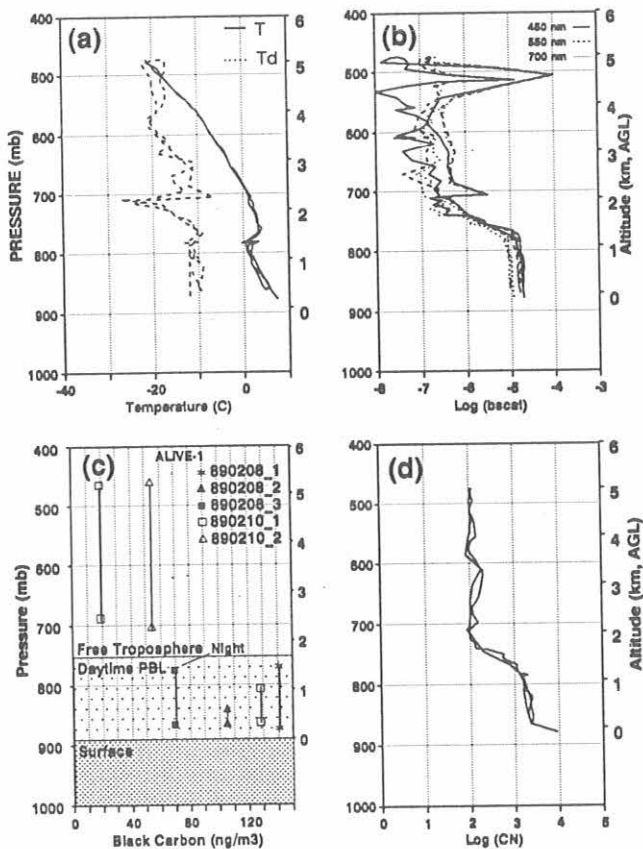


Fig. 7.2. Profiles of (a) air and dewpoint temperatures, (b) aerosol backscatter (m^{-1}), (c) aerosol black carbon content, and (d) condensation nucleus concentrations (cm^{-3}), from measurements on February 8, 1989. The black carbon data include measurements on February 10, 1989.

The data in Figures 7.2 and 7.3 indicate substantial differences between the vertical profiles in winter and summer. All flights were limited in altitude by local air traffic control, so profiles are available only from ground level (1.2 km above mean sea level; 886 mb) to a maximum altitude of about 4.5 km AGL (520 mb).

Data from the wintertime flight show clear evidence of a polluted boundary layer extending from the surface to approximately 750 mb, overlain by clean air. The temperature and dewpoint data show an inversion extending from 780 to 760, where the relative humidity is fairly high.

The optical scattering in the boundary and inversion layers is high in winter, $(1-5) \times 10^{-5} \text{ m}^{-1}$, and the condensation nucleus counts are also high, about 1000 cm^{-3} . Above about 750 mb the aircraft entered a layer of drier air with a normal temperature lapse rate. Within this layer the optical scattering diminished greatly with increasing altitude to about 10^{-7} m^{-1} at about 700 mb, and the condensation nucleus counts declined by a factor of 10 to about 100 cm^{-3} . Above 700 mb, humidity increased again; dewpoint temperatures approached air temperatures at 500 mb. Optical scattering near 500 mb showed occasional excursions that may indicate the presence of hygroscopically grown cloud nuclei. The aerosol black carbon data, representing the measurement averages, show higher concentrations of

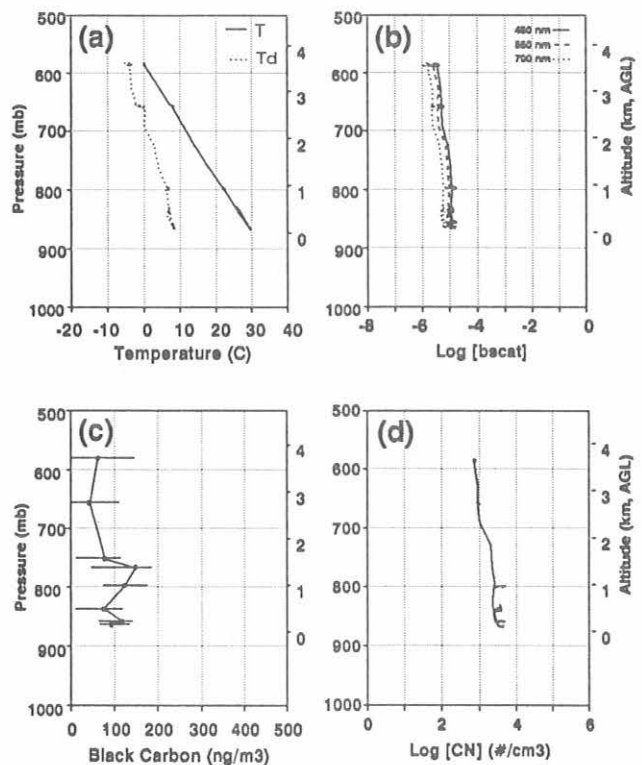


Fig. 7.3. Profiles of (a) air and dewpoint temperatures, (b) aerosol backscatter (m^{-1}), (c) aerosol black carbon content, and (d) condensation nucleus concentrations (cm^{-3}), from measurements on July 11, 1989.

70-150 ng m⁻³ in the boundary layer, diminishing to 30-50 ng m⁻³ in the cleaner layer aloft.

In contrast, the summertime data presented in Figure 7.3 show that the aircraft was at all times within a deep, mixed boundary layer of polluted air. The psychrometric plot (Figure 7.3a) shows a normal temperature lapse rate, and the air being dry at all levels. The optical scattering shows large values, about 10⁻⁵ m⁻¹, and very little vertical structure. Similarly the condensation nucleus counts decline by a factor of only 2 from ground level to the flight ceiling. In Figures 7.3a, 7.3b, and 7.3d an inflection is seen at 660-680 mb, suggesting a slight change in air mass characteristics at that altitude. The aerosol black carbon data show moderately large concentrations at all altitudes, with a mean of approximately 100 ng m⁻³ but slightly lower values at the higher levels. However, none of these data show a sharp boundary between a polluted lower layer and cleaner air aloft, and so the actual vertical extent of the polluted air mass that was sampled is unknown.

In summary, the wintertime soundings showed a distinct boundary layer of polluted air of approximately 1-km depth, overlain by clean air. The summertime results showed that the aircraft was at all times within a deep, well-mixed layer that extended from the surface to above the operational ceiling. In both cases, we measured relatively high values of optical scattering and absorption, leading to column optical depths of around 0.03 for the lowest 5 km segment of the troposphere. Absorption typically accounted for 5-10% of the total extinction, which was itself of similar magnitude to that measured at other remote locations in the southwest United States that are impacted by the long-range transport of pollutants. It is concluded that the entire region is probably suffused with anthropogenic emissions from both nearby and distant sources and that distribution and transport are dominated by the prevailing meteorology.

7.2. SPECIAL PROJECT: SULFUR MONITORING AT MLO

The longest continuous atmospheric CO₂ record is from measurements performed at MLO [*Pales and Keeling*, 1965; *Komhyr et al.*, 1989, and references therein]. The location of the observatory is nearly perfect for global background atmospheric measurements because of its remoteness from anthropogenic activity, its elevation of 3400 m ASL, and the lack of vegetation in the immediate area. But the ongoing volcanic activity on the island and its atmospheric release of large quantities of CO₂ and SO₂ [*Casadevall et al.*, 1987] was found to disturb the CO₂ record under certain meteorological conditions [*Miller and Chin*, 1978].

The major continuous source of sulfur is the Puu O'o vent on the east rift zone of Mauna Loa at an elevation of 500 m ASL. Current estimates indicate an emission rate of 1000-2000 tons SO₂ day⁻¹, and an average value of 1200 tons day⁻¹ (T. Gerlach, USGS, private communication). The other continuous source is the Kilauea crater, which is between Puu O'o and the summit of Mauna Loa, at an elevation of 1000 m ASL. The emission rate from Kilauea is estimated at 300 tons SO₂ day⁻¹ [*Casadevall et al.*, 1987]. There are also smaller sources, but their total contribution is well within the

estimated uncertainty of the two major ones. In spite of the known high SO₂ emission, there have been no published reports on atmospheric SO₂ concentrations in Hawaii. *Gill et al.* [1989] measured particulate sulfur concentrations along the west coast of the island and found them to be well below the U.S. national air quality standards, but 10-20 times greater than expected for a remote marine area.

Little information is available on global background concentrations of SO₂ in the marine boundary layer (BL) and the free troposphere (FT) at MLO. *Maroulis et al.* [1980] reported average SO₂ concentrations, based on aircraft measurements, of 0.089 ± 0.069 and 0.122 ± 0.085 ppbv for the BL and FT, respectively, in the Northern Hemisphere, and 0.057 ± 0.018 and 0.09 ± 0.021 ppbv for the BL and FT in the Southern Hemisphere. *Herrmann and Jaeschke* [1984] reported an average SO₂ concentration of 209 ng m⁻³ (approximately 0.08 ppbv) over the Atlantic Ocean at various sites. *Berresheim* [1987] measured average concentrations as low as 0.011 ppbv over the sub-Antarctic and Antarctic ocean area. In a series of studies near Bermuda [*Luria et al.*, 1987, 1989], SO₂ concentrations were below the detection limit of 0.1 ppbv, with a few brief exceptions. In a more recent study near Bermuda [*Luria et al.*, 1990], using a more sensitive technique, 0.06 ± 0.035 and 0.065 ± 0.04 ppbv were reported as average concentrations for the BL and FT respectively. In the latter study, comparable values of 0.050 ± 0.040 pptv for both the BL and FT were observed using the filter pack technique [*Boatman et al.*, 1990].

AQG began a sulfur monitoring project at MLO in 1988. The study was set up to test the following hypotheses:

- (1) Atmospheric sulfur is a surrogate for volcanic contamination at MLO.
- (2) The background atmospheric sulfur concentration in the FT can be successfully measured at MLO.

A CSI real-time total sulfur gas monitor was installed at MLO in March 1988, and a TECO real-time SO₂ gas monitor was installed in November 1988. The CSI device measures all sulfur gases, has a detection limit of 1 ppbv for 1-min samples, and has a response time of 10 seconds. The TECO device measures only SO₂, has a detection limit of 0.1 ppbv for 1-min samples, and a response time of 1 minute. The two instruments are described by *Boatman et al.* [1988].

Data obtained in 1989 indicate that most of the time, SO₂ concentrations at MLO are as low as those observed in other remote locations. Occasionally, high nighttime SO₂ events were observed. Because they occurred in association with abnormally high CO₂ concentrations, the source is believed to be volcanic, with emissions near the MLO summit. Highest SO₂ levels, up to 1000 times background levels, were observed at times concurrent with daytime upslope winds having a predominant wind direction of northerly to northeasterly. Major sources of the SO₂ were most likely the Puu O'o vent on the east rift zone of Mauna Loa, and the Kilauea crater. An annual cycle (high wintertime, low summertime values) in SO₂ was also observed and is tentatively attributed in part to the seasonal variations in SO₂ to SO₄²⁻ conversion rate.

7.3. REFERENCES

- Berresheim, H., Biogenic sulfur emission from the sub-Antarctic and Antarctic oceans, *J. Geophys. Res.*, *92*, 13245-13262, 1987.
- Boatman, J.F., M. Luria, C.C. Van Valin, and D.L. Wellman, Continuous atmospheric measurements aboard an aircraft: A comparison between the flame photometric and the pulsed fluorescence methods, *Atmos. Environ.*, *22*, 1949-1956, 1988.
- Boatman, J.F., W.C. Keene, M. Luria, J.D. Ray, C.A. Barwell, K. Gorzelska, M. Fennel, D.R. Hastie, A.A.P. Pszenny, and D. Whelpdale, An intercomparison of the chemical and meteorological data generated from aircraft and shipboard sampling during GCE/CASE/WATOX, NOAA Tech. Memo. ERL ARL-186, 26 pp., NOAA Air Resources Laboratory, Silver Spring, MD, 1990.
- Casadevall, T.J., J.B. Stokes, L.P. Greenland, L.L. Malinconico, J.R. Casadevall, and B.T. Furukawa, SO₂ and CO₂ emission rates at Kilauea Volcano, 1979-1984, in *Volcanism in Hawaii*, edited by R.W. Decker and T.L. Wright, U.S. Geological Survey Professional Paper 1350, pp. 771-780, USGS, Washington, DC, 1987.
- Gill, T.E., T.H. Tanda, T.A. Cahill, D. Taylor, and H. Matsuura, Air quality on Hawaii Island during a Kilauea eruption, paper presented at the 82nd Annual Meeting of the Air and Waste Management Association, Anaheim, CA, June 1989.
- Herrmann, J., and W. Jaescke, Measurements of H₂S and SO₂ over the Atlantic Ocean, *J. Atmos. Chem.*, *1*, 111-123, 1984.
- Komhyr, W.D., T.B. Harris, L.S. Waterman, J.F.S. Chin, and K.W. Thoning, Atmospheric carbon dioxide at Mauna Loa Observatory: NOAA/GMCC measurements with a nondispersive infrared analyzer, 1974-1985, *J. Geophys. Res.*, *94*, 11429-11436, 1989.
- Luria, M., C.C. Van Valin, J.F. Boatman, D.L. Wellman, and R.F. Pueschel, Sulfur dioxide flux measurements over the western Atlantic Ocean, *Atmos. Environ.*, *21*, 1631-1636, 1987.
- Luria, M., C.C. Van Valin, J.N. Galloway, W.C. Keen, D.L. Wellman, H. Sievering, and J.F. Boatman, The relationship between dimethylsulfide and particulate sulfate in the mid-Atlantic Ocean atmosphere, *Atmos. Environ.*, *23*, 139-147, 1989.
- Luria, M., C.C. Van Valin, R.L. Gunter, W.C. Keene, D.L. Wellman, J.N. Galloway, H. Sievering, and J.F. Boatman, Measurements of low concentration of sulfur dioxide over the western Atlantic Ocean during CASE/WATOX, *Global Biogeochem. Cycles*, submitted, 1990.
- Maroulis, P.J., A.L. Torres, A.B. Goldberg, and A.R. Bandy, Atmospheric SO₂ measurements on project GAMTAG, *J. Geophys. Res.*, *85*, 7545-7549, 1980.
- Miller, J.M., and J.F.S. Chin, Short term disturbances in the carbon dioxide recorded at Mauna Loa Observatory, *Geophys. Res. Lett.*, *5*, 669-671, 1978.
- Pales, J.C., and C.D. Keeling, The concentration of carbon dioxide in Hawaii, *J. Geophys. Res.*, *70*, 6053-6076, 1965.

8. Nitrous Oxide and Halocarbons Group

T.M. THOMPSON (Editor), J.W. ELKINS, J.H. BUTLER, B.D. HALL, K.B. EGAN, C.M. BRUNSON,
J. SCZECZOWSKI, AND T.H. SWANSON

8.1. CONTINUING PROGRAMS

8.1.1. FLASK SAMPLES

The flask air-sampling program continued at BRW, NWR, MLO, SMO, SPO, and ALT as usual throughout the year, with only two minor changes. Larger 1-L flask pairs were pressurized monthly beginning in March at BRW, NWR, MLO, and SMO to meet the larger sample requirements of the LEAPS project. In November, personnel at SPO began using a higher pressure pump (3 atm) to fill flask pairs during their summer sampling period. All CMDL stations will convert to this higher pressure pump in early 1990 to provide sufficient sample amounts for both the LEAPS and flask projects.

The automated flask analysis system was completed according to the original design. However, extensive tests showed some problem areas and the need for redesign. The redesign was completed, and implementation and tests will continue into 1990.

Two calibration gas tanks, T3088 and 62631, were intercompared with standards maintained by the OGIST in Beaverton, Oregon. This work was done in late April.

Preliminary monthly mean N₂O, CFC-11, and CFC-12 concentrations measured at BRW, NWR, MLO, SMO, and SPO during 1989 are listed in Table 8.1. Figure 8.1 shows monthly mean N₂O data for these stations for 1977-1989. The annual N₂O increase is approximately 0.2% at all the sites. BRW data exhibit a weak annual cycle. This cycle is more apparent in the continuous GC record.

CFC-12 and CFC-11 monthly mean concentrations are plotted in Figures 8.2 and 8.3. For the 1977-1984 period, the annual increase for each is less than it is for the 1985-1989 period. It appears that the source strength of these two halocarbons is increasing. The ratio of CFC-12 to CFC-11 concentrations has shown no significant change during the 13-year period, and therefore usage of the two gases is increasing proportionately.

N₂O, CFC-11, and CFC-12 data for ALT continued to be erratic; results from flask pairs did not match well. Actual flask pair averages are shown in Figure 8.4. BRW and ALT data compare favorably on average.

8.1.2. RITS CONTINUOUS GAS CHROMATOGRAPH SYSTEMS AT CMDL BASELINE STATIONS

In-situ sampling of air continued at BRW, MLO, and SMO. Eight analyses were made each day for N₂O, CFC-12, CFC-11, CFC-113, methyl chloroform (1, 1, 1-trichloroethane), and carbon tetrachloride. At SPO, these gases were sampled and analyzed 12 times per day [Elkins *et al.*, 1988].

In January 1989 processing of the chromatographic data began for both peak area and peak height. Concentrations based on peak height are sometimes more precise, yielding less scatter in the data. Small peaks such as those of methyl chloroform and carbon tetrachloride are prone to precision problems, especially if other substances are not chromatographically resolved from them. Processing programs were written to retrieve pre-1989 chromatograms and determine peak heights. A SMO peak-height data base

TABLE 8.1. Monthly Mean Concentrations in 1989 of N₂O (ppb by mole fraction in dry air), CFC-12 (ppt), and CFC-11 (ppt) From Air Samples Collected in Flask Pairs at BRW, NWR, MLO, SMO, and SPO

1989	N ₂ O					CFC-12					CFC-11				
	BRW	NWR	MLO	SMO	SPO	BRW	NWR	MLO	SMO	SPO	BRW	NWR	MLO	SMO	SPO
Jan.	308.5	308.8	308.1	305.9	307.1	459.5	453.6	453.7	437.4	427.4	274.6	269.6	266.6	260.4	
Feb.	309.7	311.5	309.1	309.0		460.0	455.8	447.4	440.5		276.7	270.9	264.3	257.1	
March	307.8	308.4	308.6	307.9		460.8	447.0	450.9	435.0		278.3	267.7	265.6	258.9	
April	309.2	309.4	309.7	306.5		461.6	455.3	454.1	437.8		278.5	270.8	269.6	258.4	
May	309.4	310.6	308.8	306.5		463.1	459.1	452.8	440.6		276.6	271.1	268.8	258.7	
June	308.7	311.6	309.4	308.5		459.8	461.4	461.9	432.2		275.6	272.4	270.2	254.2	
July	310.9	309.8	308.4	306.6		468.1	475.4	453.8	443.1		279.1	285.7	268.4	258.9	
Aug.	309.3	311.5	309.3	309.2		464.1	468.3	458.4	442.3		274.9	277.1	271.3	263.3	
Sept.	309.0	310.0	309.7	308.2		467.1	467.5	460.6	445.2		277.6	279.6	273.7	262.1	
Oct.	308.4	310.6	309.7	306.9		471.0	464.2	464.1	448.4		283.5	275.9	273.8	263.5	
Nov.	310.4	309.6	308.4	307.8		477.1	470.8	467.2	448.1		290.0	280.7	272.2	263.8	
Dec.	309.4	309.4	309.5	308.0	308.2	478.1	468.1	459.7	451.6	445.7	288.2	276.7	276.3	266.2	259.8

These data are provisional, pending final calibration.

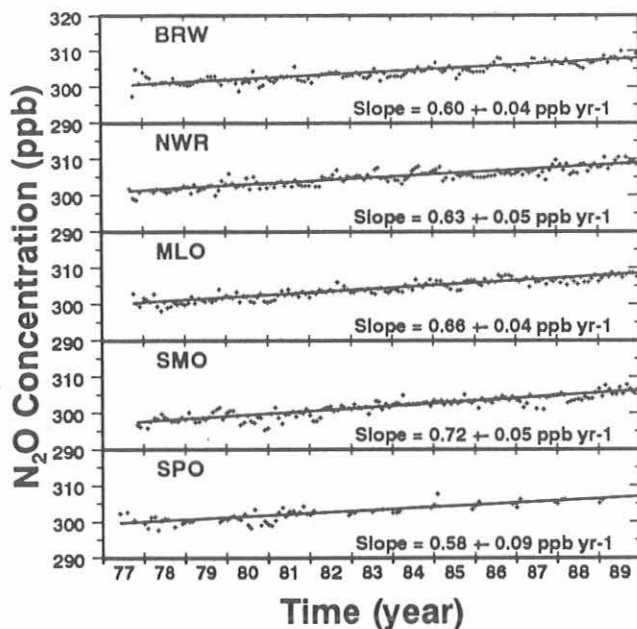


Fig. 8.1. Monthly mean concentrations of N_2O (CO_2 and H_2O corrected) from the CMDL flask air sample network. The trends and 95% confidence intervals are also shown.

was created using these programs. Other station peak-height data will be similarly obtained in 1990.

In April the BRW system was modified so that all three columns could be backflushed. MLO and SMO systems were previously modified in 1988. Precision has been improved because of this change.

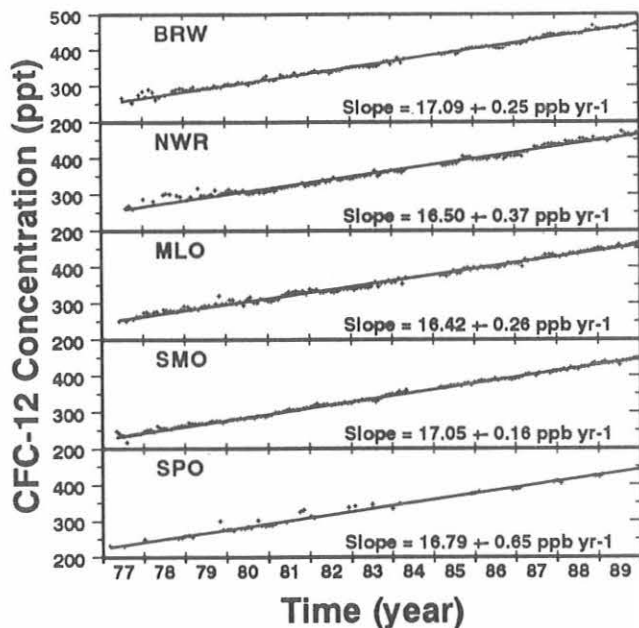


Fig. 8.2. Monthly mean dry concentrations of CFC-12 from the CMDL flask air sample network. The trends and 95% confidence intervals are also shown.

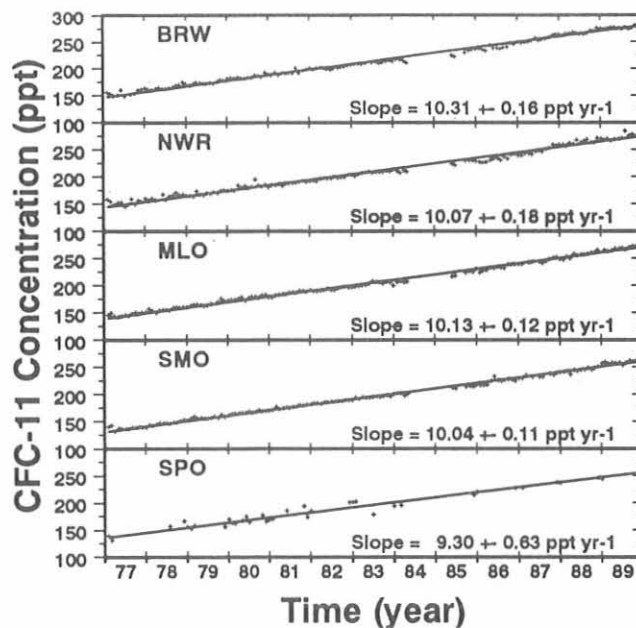


Fig. 8.3. Monthly mean dry concentrations of CFC-11 from the CMDL flask air sample network. The trends and 95% confidence intervals are also shown.

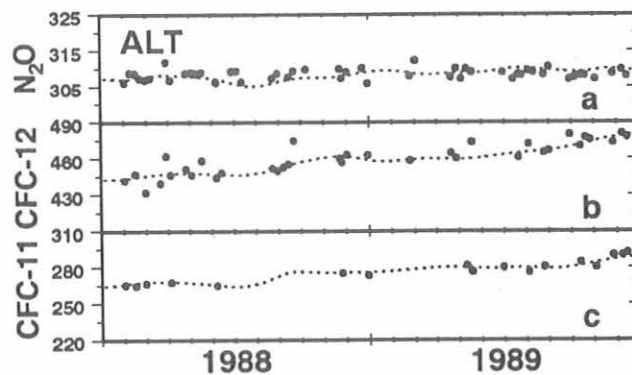


Fig. 8.4. Flask sample concentrations for (a) N_2O , (b) CFC-12, and (c) CFC-11 at Alert observatory, Canada. The dashed lines are spline fits to corresponding BRW flask sample data, for comparison.

In June a new operations manager was hired to oversee the operation of the equipment at the field sites, provide support when equipment or software failures occur, and supply expendables like carrier gas, paper, and disks.

Version 4.2 of the software was completed and tested. This revision changes the way gas is sampled at the field sites. Previously the order of analyses was (1) calibration gas 1, (2) calibration gas 2, and (3) outside air. Now the order is (1) calibration gas 1, (2) outside air sample 1, (3) calibration gas 2, and (4) outside air sample 2. This increases the number of times air is sampled from once every

3 hours to once every 2 hours for hourly analyses. Another change incorporated in the software is storing data using two floppy disk drives instead of a single floppy drive and an emulated disk in RAM.

Both software changes also required hardware changes. In October, an eight-port stream selection valve replaced the old six-port valve at BRW. A dual high-density (1.5 Mbyte) floppy drive was installed. These same hardware and software changes will be made at the other sites in early 1990.

A new RITS GC system, incorporating the new software and hardware, was set up and tested in Boulder. This equipment will be moved to NWR in early 1990 to complete the in-situ measurement program. All flask sites except ALT will then have GC's.

Because of increased data processing needs, an HP340 workstation was purchased with a 330-Mbyte hard disk. This is the first acquisition toward the move to a group computer network.

The 2.5-year record of daily average N_2O concentrations from the in-situ GC's at BRW, MLO, and SMO is shown in Figure 8.5. The annual cycle at BRW has a February maximum and an August-September minimum similar to the periods of the maximum and minimum observed in CO_2 concentrations at BRW. Data for SMO in 1988 appear to be cyclic, but the cycle is not repeated. Because N_2O has a seasonal cycle and is growing at a small rate, it is difficult to establish an annual growth rate with only 2 years of data. The calculated growth rate of atmospheric N_2O concentration for 1988-1989 at BRW is about 0.6 ppb yr^{-1} . However, the MLO record for N_2O shows little growth because of the short record period and larger experimental error in the 1987 data.

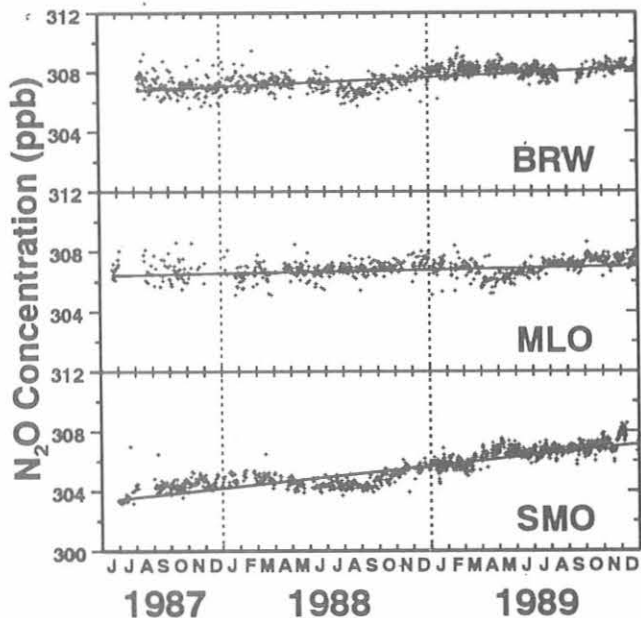


Fig. 8.5. N_2O daily mean concentrations at BRW, MLO, and SMO obtained from the in-situ RITS GC's. The trends were generated using least squares regression analysis.

The growth rate at SMO during 1988-1989 is about 1 ppb yr^{-1} . This value is higher than at other stations and may be the result of calibration gas problems associated with calibration gas tank changes in 1988.

Daily mean CFC-12 concentrations derived from the gas chromatograph measurements are shown in Figure 8.6. The annual increase is about 19 ppt yr^{-1} during 1988-1989 for all three stations. This result confirms observations from flask data during the past few years.

Carbon tetrachloride concentration at our sampling sites appears to have been steady during the past 2 years, in the range of 100-110 ppt. As an example, SMO data are shown in Figure 8.7.

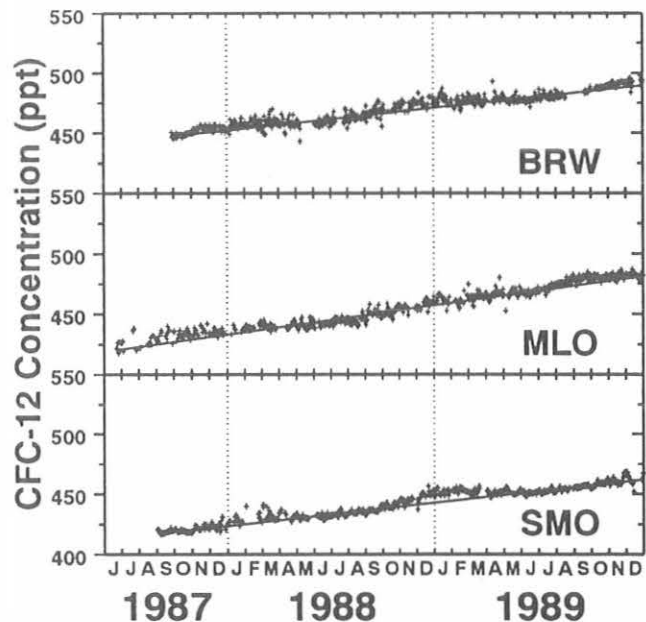


Fig. 8.6. CFC-12 daily mean concentrations at BRW, MLO, and SMO obtained from the in-situ RITS GC's.

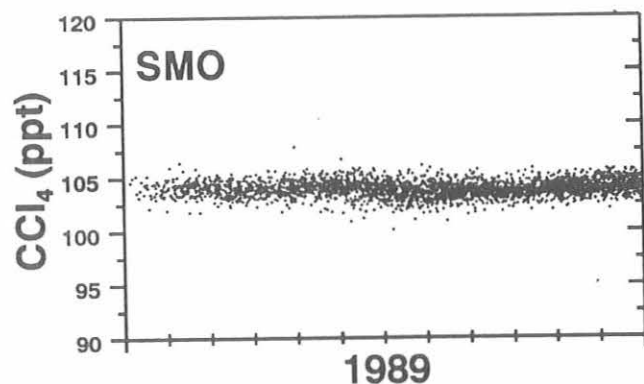


Fig. 8.7. SMO CCl_4 concentrations from the in-situ RITS GC. The air was sampled every 3 hours.

Quantization of methyl chloroform still remains a problem because of an unknown contaminant in some of our calibration gases.

8.1.3. LOW ELECTRON ATTACHMENT POTENTIAL SPECIES

Although formal flask sampling for LEAPS gases began in March, a number of changes were made throughout the year in the sampling and analysis of LEAPS gases. By November, one of the main problems limiting these measurements was resolved when the old flask pump at SPO was replaced with a new sampling pump capable of filling flasks to a gauge pressure of 3 atm. The same type of pump will be installed at the other CMDL stations early in 1990. Contamination tests have shown the pumps to be clean and not a source of CFC-113, a commonly used cleaning agent. Analytical columns were changed as the GC was optimized for the various measurements. Initially, gases were separated with a 0.53 mm \times 50 m methyl-silicone column, which was changed in August to a 0.53 mm \times 25 m Poraplot Q column, and was ultimately replaced by a 0.32 mm \times 10 m Poraplot Q column. The Chrompack cryotrap was modified extensively to allow for the direct measurement of samples from flasks and to improve overall sensitivity of the measurements.

Insufficient data are available to calculate atmospheric trends of the LEAPS gases from flask air samples collected at the CMDL stations. However, flask samples collected from over the Pacific Ocean during the RITS-89 cruise (January-April) on the NOAA ship *Discoverer* were analyzed for H-1301, H-1211, and CFC-113, as were five 8-L flask air samples remaining from the SAGA II cruise (May-July 1987) in the West Pacific and East Indian Oceans. Growth rates for these gases (Table 8.2) were estimated both by considering the differences between 1987 and 1989 measurements and by evaluating the latitudinal gradients (Figure 8.8). These estimates are only preliminary; they are based on small data sets, representing only two "snapshots" in time. Also, the northern hemispheric CFC-113 values from the 1989 cruise were affected by urban contamination

TABLE 8.2. Estimated Annual Growth Rates for LEAPS Gases, Calculated from RITS-89 and SAGA II (1987) Data

Gas	Method 1	Method 2
H-1301	25.7%	23.6%
H-1211	4.4%	10.8%
CFC-113	10.1%	

Data are shown in Figure 8.8. Method 1 involves direct calculations of the average difference between samples collected between 30°S and 40°N on both cruises. Method 2 involves calculations based on the measured latitudinal gradient, a relative production of 20:1 for the two hemispheres, and an assumed interhemispheric exchange time of 1 year [see *Butler et al.*, 1989].

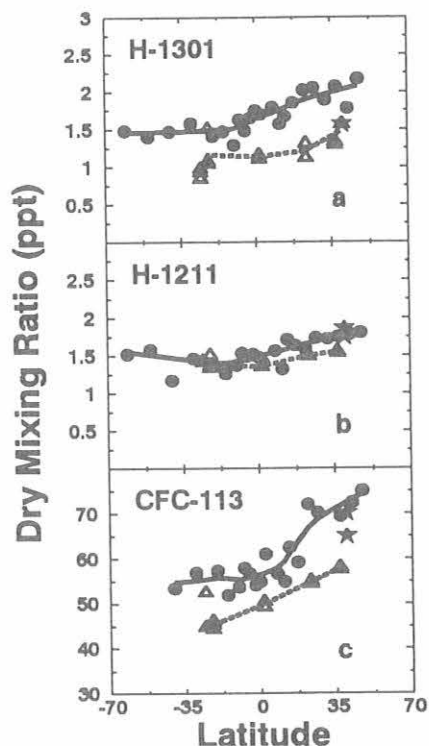


Fig. 8.8. Dry mixing ratios versus latitude in degrees for (a) H-1301, (b) H-1211, and (c) CFC-113, measured in flask air samples collected during SAGA II in 1987 (triangles) and the RITS cruise of 1989 (circles), and in air from a cylinder filled at NWR in 1988 (stars). Estimated growth rates are given in Table 8.2.

as the ship proceeded along the California coast during a period of strong offshore winds. The growth rates for H-1301 calculated by either method agreed well, but there is a discrepancy in results for H-1211. This discrepancy should be resolved when more data from our stations become available.

Sample concentrations of the LEAPS gases to date have been determined by response ratio to CFC-12 compared with the same ratio for a cylinder of NWR air (Scott cylinder SRL-K-009288, Aculife-5-treated steel, filled November 1988 at NWR). However, a detailed evaluation of the response curves for gravimetrically prepared standards shows that the response of the halons, and to a lesser extent CFC-113 and CFC-12, is nonlinear (Figure 8.9). Consequently, the LEAPS GC will be modified further in 1990 to allow measurement of exact sample volume so that nonlinearities in the response can be evaluated. This will lead not only to more accurate results but also much better precision.

8.1.4. GRAVIMETRIC STANDARDS

A principal goal for 1989 was the development of independent calibration scales for all RITS gases. CFC-113,

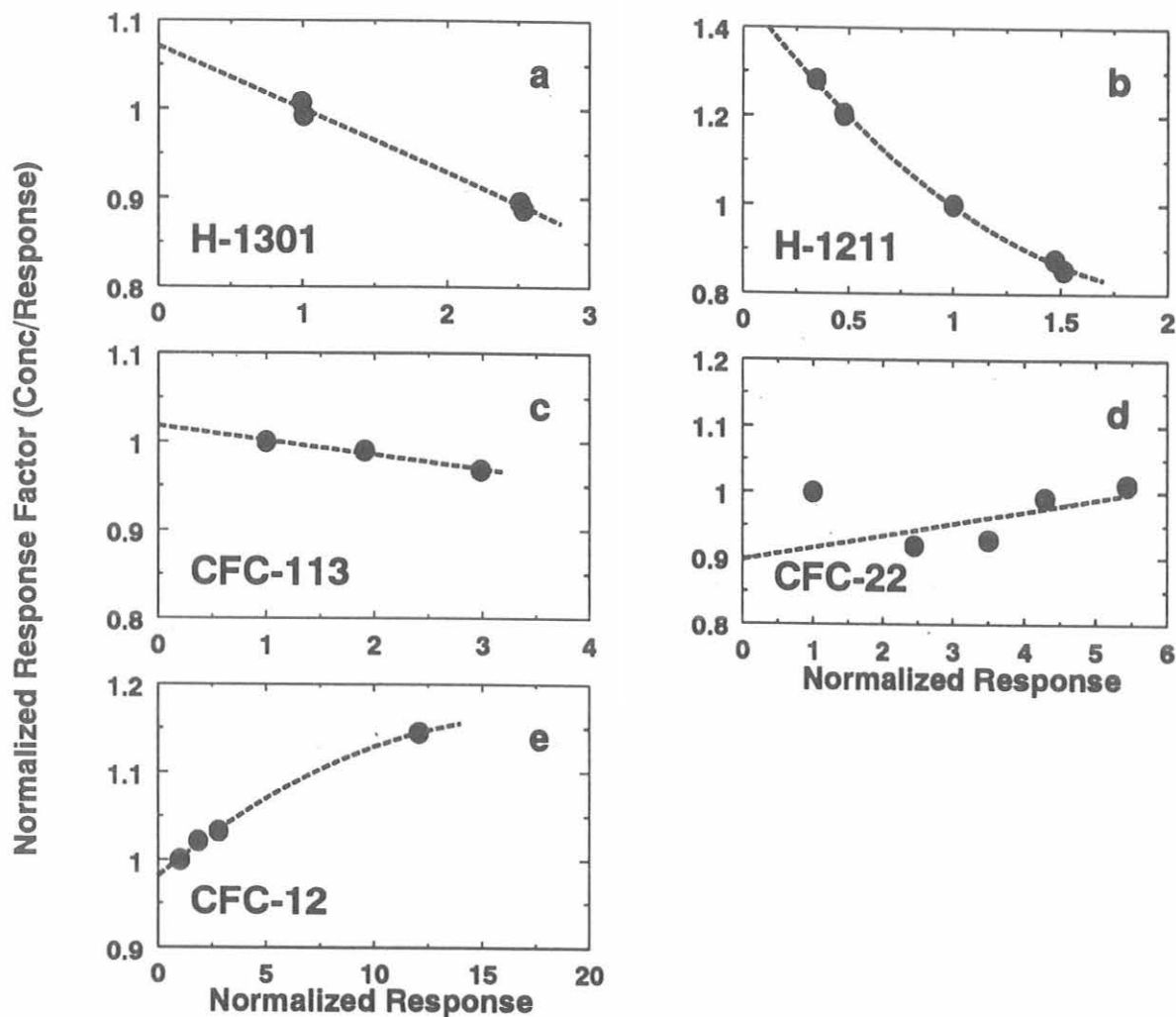


Fig. 8.9. Response curves for (a) H-1301, (b) H-1211, (c), CFC-113, (d) CFC-22, and (e) CFC-12. The data show that nonlinearities in the detector response should be considered in measuring these gas concentrations. (Although CFC-12 is not a LEAPS gas, it is used to estimate sample volume for the LEAPS measurements.) A horizontal plot for the response factor is indicative of a true linear response of the detector to the compound being analyzed.

CH_3CCl_3 , and CCl_4 have proved to be the most difficult to quantify. Several measures were taken to improve our ability to prepare accurate standards at the part per trillion level. Aluminum transfer tubes were Aculife-treated to minimize adsorption and surface reactions during the transfer step for CH_3CCl_3 and CCl_4 . Specially cleaned valves containing as little CFC-113 as possible were purchased and tested.

The gravimetric standards prepared in 1989 are shown in Table 8.3. The CFC-113 standards were prepared in both Aculife-treated aluminum cylinders and 33-L stainless steel cans to investigate possible valve contamination, and a calibration curve (Figure 8.10) was prepared. No valve bias was observed within experimental error. CMDL participated in an intercomparison in which flask air was analyzed for CFC-113. Our result was 36% higher than

that of OGIST (Table 8.4).

Another goal for 1989 was to replace calibration standards at the CMDL observatories and to obtain standards for use during cruises and in the laboratory. This was accomplished by filling several Aculife-treated aluminum tanks and 33-L stainless steel cans with NWR air. These working standards were carefully calibrated using our gravimetric standards. Two each of the new working standards were installed at BRW, MLO, and SMO observatories. These new standards should eliminate CFC-113 contamination problems and help resolve minor discrepancies in results obtained among stations.

Standards support for various other projects continued as in the past. As indicated in Table 8.3, standards were prepared for the LEAPS project, special RITS projects, and the CMDL Carbon Cycle Group.

TABLE 8.3. CMDL Gravimetric Standards Prepared in 1989

Set	Compounds in Cylinder	No. of Cylinders	Range	Project
1	CFC-11, CFC-113, CH ₃ CCl ₃ , CCl ₄	2	ppb, ppt	NOAA/RITS
2	N ₂ O	2	ppb	NOAA/RITS
3	N ₂ O, CO ₂	4	ppb	NOAA/RITS
4	N ₂ O, CO ₂	7	ppm	NOAA/RITS
5	CFC-113, CFC-11	6	ppb, ppt	NOAA/RITS
6	H-1301	2	ppm, ppb	NOAA/LEAPS
7	H-1211	1	ppt	NOAA/LEAPS
8	CFC-22	2	ppm, ppb	NOAA/LEAPS
9	CO	8	ppm, ppb	NOAA/CC

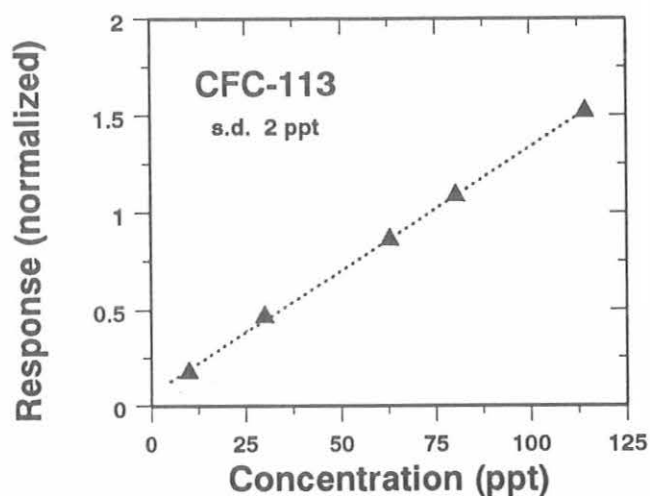


Fig. 8.10. The normalized calibration curve for CFC-113. It is linear in the 10-120 ppt range and has a residual standard deviation of about 2 ppt.

TABLE 8.4. Comparison of Concentration Scales for CFC-113 from CMDL and OGIST

	CFC-113, ppt	Standard Deviation, ppt
NOAA	69.9	1.9
OGIST	51.0	0.6

8.2. SPECIAL PROJECTS

8.2.1. RITS *DISCOVERER* CRUISE

Atmospheric and surface water N₂O, CFC-11, CFC-113, methyl chloroform, and CCl₄ were measured aboard the

NOAA research ship *Discoverer* on the RITS-89 cruise from February to April 1989. Dissolved N₂O at depth was also measured. The cruise track extended south from 47°N to 60°S along 110°W and then returned northward along 140°W (Figure 8.11). The purpose of the cruise was (1) to measure the interhemispheric gradient of these trace gases in the atmosphere, (2) to quantify the ocean's effect on these trace gases in the surface waters, (3) to measure the biological rate for production of dissolved N₂O, and (4) to compare these measurements to those from CMDL observatories. Surface waters near the equator were found to have N₂O supersaturations as high as 140%. Results from this cruise indicate that previous estimates for the global production of N₂O may have underestimated the strength of the ocean source, which could be as high as 30% of the total natural source.

8.2.2. FT-IR SPECTROMETER ARCHIVE PROJECT

Working in collaboration with scientists at NOAA/NSO, CMDL scientists from the CC and NOAA Groups restarted FT-IR spectrometric observations in January 1989 at Kitt Peak, Arizona (30°N, 112°W), which had been terminated in 1985. The purpose of resuming the observations was to compare trace gas concentrations derived from the FT-IR spectrometer observations with values determined from flask air samples collected at the nearest CMDL site, NWR (40°N, 105°W). The sun is tracked at Kitt Peak by a solar telescope, and its beam is directed into an FT-IR spectrometer. Trace gases present in the atmosphere absorb incoming solar IR radiation. Concentrations of trace gases can be determined by measuring integrated areas of absorption lines and comparing these measured values to published line-strength data. *Wallace and Livingston* [1990a, b] have reanalyzed CO₂, CH₄, N₂O, and CO spectra obtained at Kitt Peak during 1979-1985 using the diatomic lines of oxygen as an internal standard to yield average atmospheric concentration values for these gases.

Spectroscopic CO₂ measurements made at Kitt Peak during 1978-1989 yield a mean growth rate of 0.49% per year

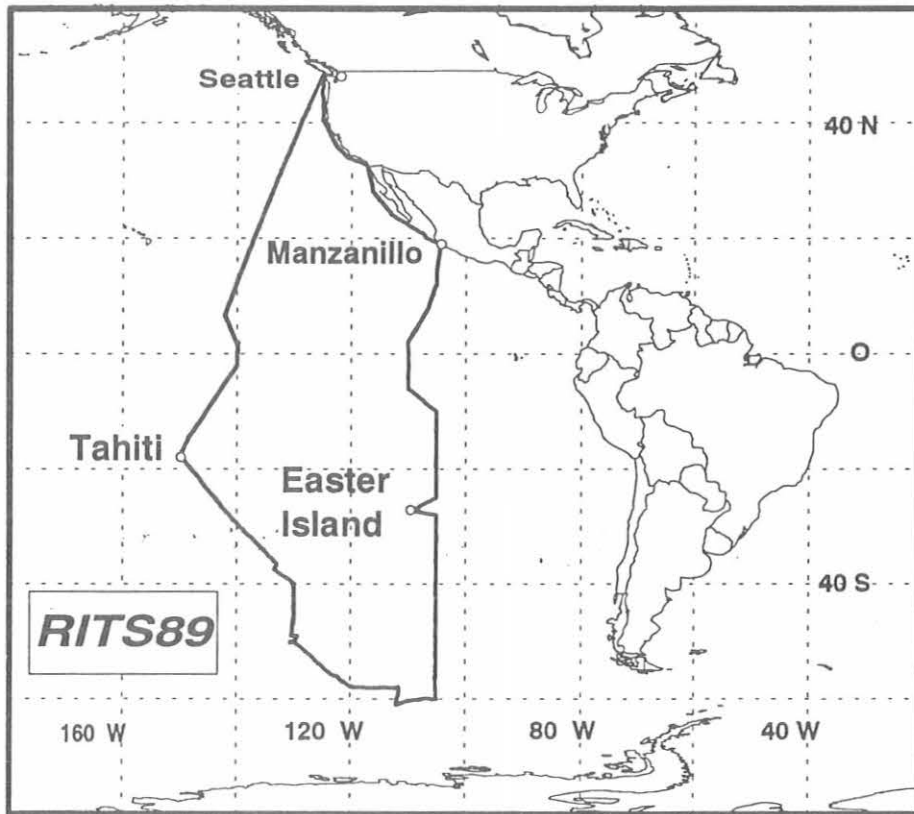


Fig. 8.11. Cruise track of the RITS expedition in the eastern Pacific Ocean.

whereas NWR flask air-sample data yield a mean CO_2 growth rate of 0.48% (Figure 8.12a). There is a difference of ~ 10 ppm between the scales of the two measurement techniques, perhaps due to errors associated with the absolute line strengths or to differences in the features of the vertical profiles of O_2 and CO_2 . A similar comparison of CH_4 concentrations also shows a bias in the measurements

(~ 60 ppb), as well as a difference in growth rates that is not statistically significant. Data from Kitt Peak yield a growth rate of 1.01% per year compared with 0.76% per year for the NWR data (Figure 8.12b). Although the NWR CH_4 flask record began in 1983, air in cylinders was collected at NWR between 1977 and 1979, and was recently analyzed for CH_4 . Including these new data and assuming a linear growth for

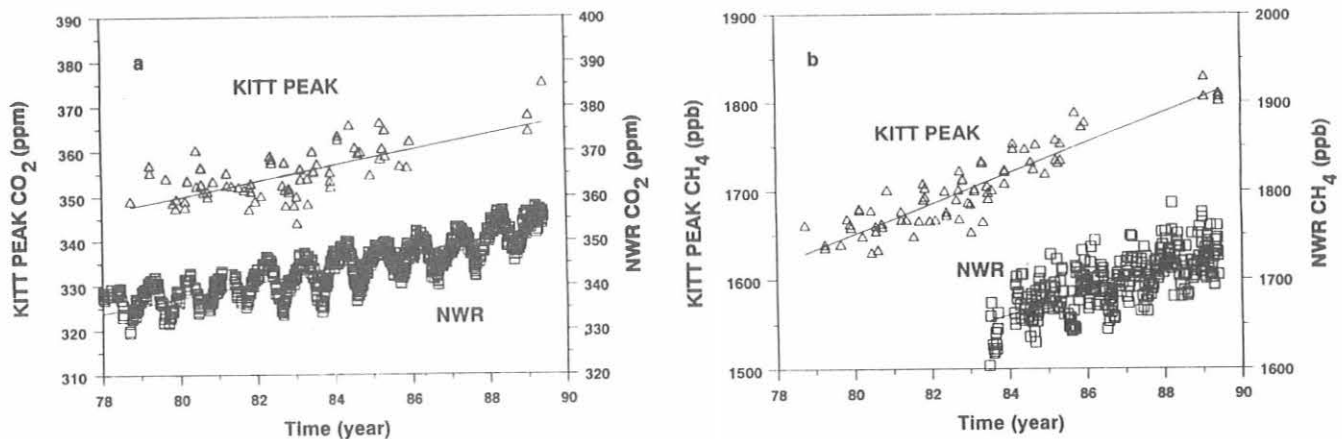


Fig. 8.12. Comparisons of CMDL flask sample data from NWR (squares) with NSO data derived from IR spectra measured at Kitt Peak, Arizona (triangles) (a) CO_2 and (b) CH_4 .

the complete NWR record gives a calculated growth rate of ~1% per year, in good agreement with the spectrometric record.

In early 1991 a CMDL FT-IR spectrometer will be moved to the fifth floor of the building in Boulder. Operation of the spectrometer and archiving of spectra will begin in the summer of 1991 to complement observations made at Kitt Peak.

8.2.3. AIRBORNE GAS CHROMATOGRAPH

Testing of a Shimadzu Mini-2 gas chromatograph continued aboard the NOAA King Air research aircraft. Tylan mass flow controllers were used to maintain a steady carrier gas flow rate. In February N_2O was measured in coal-fired power plant plumes near Miami, Florida. N_2O was also measured in the Pawnee Power Plant plume near Brush, Colorado (Figure 8.13) on July 28. Although data obtained during the flight were not as precise as station data, we did not detect parts per million levels of N_2O in the plumes, and it was therefore concluded that combustion is a minor source of atmospheric N_2O . During the flight in the Pawnee Power Plant plume, air samples were collected in 500 mL airbags for subsequent analyses. Before the flight, the stability of N_2O in the airbags was examined over the course of 24 hours. The airbags proved to be a reliable and inexpensive method of collecting air samples for quick N_2O analysis. Flue gas samples were also collected at the power plant.

High variability in the N_2O in-situ flight data was attributed to changes in the ECD cell pressure. Because the ECD sensitivity increases with decreasing atmospheric pressure, an absolute backpressure regulator was subse-

quently installed on the ECD outlet to maintain a constant cell pressure. Two flights were then made over eastern Colorado on September 7 and 8 during which CFC-11 was measured with the in-situ GC, and flask air samples were collected. With use of both the backpressure regulator and Tylan mass flow controllers, on-board CFC-11 measurements improved; results agreed with flask sample CFC-11 concentrations as well as with the CFC-11 value obtained at our sampling site at NWR (Figure 8.14).

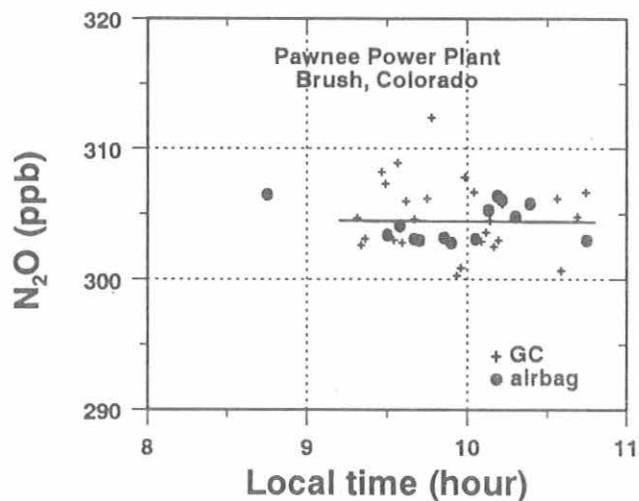


Fig. 8.13. Concentrations of N_2O in the plume at the Pawnee Power Plant, Brush, Colorado, on July 28, 1989, derived from in-situ GC (pluses) and airbag sample (circles) measurements aboard the NOAA King-Air aircraft.

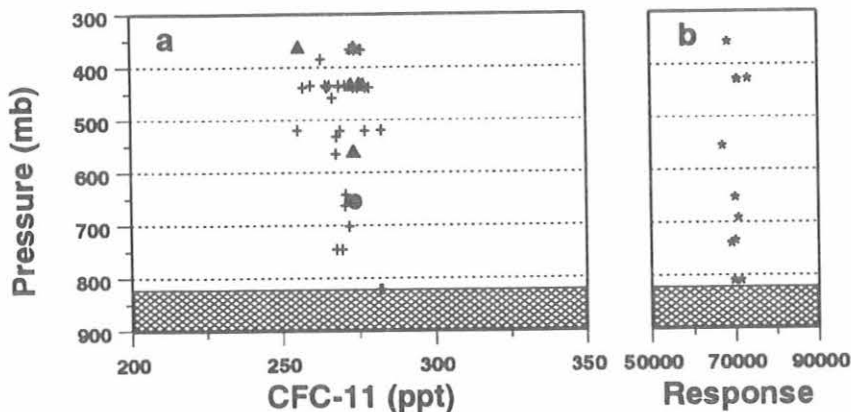


Fig. 8.14. CFC-11 concentrations measured over central Colorado September 8 and 9, 1989, aboard the NOAA King-Air aircraft. (a) Aircraft CFC-11 data obtained from in-situ GC measurements (pluses) and from flask air samples (triangles) are compared with NWR flask sample data (circle). (b) The relative response (peak height) of the in-situ GC while a gas standard was analyzed during the flight. The relative standard deviation for measuring CFC-11 in the standard during the flight was better than 3.0%.

8.3. REFERENCES

- Butler, J.H., J.W. Elkins, T.M. Thompson, and K.B. Egan, Tropospheric and dissolved N_2O of the west Pacific and east Indian Oceans during the El Niño-Southern Oscillation event of 1987, *J. Geophys. Res.*, 94(D12), 14,865-14,877, 1989.
- Elkins, J.W., T.M. Thompson, B.D. Hall, K.B. Egan, and J.H. Butler, NOAA/GMCC halocarbons and nitrous oxide measurements at the South Pole, *Ant. J. U. S.*, 23, 176-177, 1988.
- Wallace, L., and W. Livingston, Spectroscopic observations of atmospheric trace gases over Kitt Peak, 1, Carbon dioxide and methane from 1979 to 1985, *J. Geophys. Res.*, 95(D7), 9823-9827, 1990a.
- Wallace, L., and W. Livingston, Spectroscopic observations at atmospheric trace gases over Kitt Peak, 2, Nitrous oxide and carbon monoxide from 1979 to 1985, *J. Geophys. Res.*, 95(D10), 16,383-16,390, 1990b.

9. Director's Office

9.1. A JOINT U.S./U.S.S.R. EXPERIMENT FOR THE STUDY OF DESERT DUST AND ITS IMPACT ON LOCAL METEOROLOGICAL CONDITIONS AND CLIMATE

DALE A. GILLETTE

9.1.1. INTRODUCTION

A joint U.S./U.S.S.R. expedition to study the causes and effects of desert dust on the environment was carried out in Tadjikistan, S.S.R., in September 1989. The expedition was conducted under the auspices of the bilateral U.S./U.S.S.R. Working Group VIII (Influence of Environmental Changes on Climate). Nine American scientists and one French scientist were led administratively by NOAA; 28 Soviet scientists were led by Academician George Golitsyn. Table 9.1 lists the U.S. participants, their institutions, and research topics. Equipment setup began at the individual sites on September 5, and measurements began on September 6 and continued until September 27, 1989.

9.1.2. PURPOSE

The purpose of the expedition was to measure desert dust production, to determine chemical and physical properties of the dust, and to assess the effects of the dust on meteorological conditions and climate. Characterization of physical properties of the dust focused on optical and radiative properties, while the chemical composition study focused on finding a possible interaction of the alkaline component of the dust with acidic components of gaseous and particulate air pollution in the city of Dushanbe. The experiment was designed to attempt to provide a mass balance of dust production, transport, and deposition in a watershed feeding the Aral Sea (the Kafirnigan River Valley in Tadjikistan south of Dushanbe; see Figure 9.1). Thus the experiment was a complete assessment of dust production by a desert and the climatic and environmental consequences of that dust.

9.1.3. ACTIVITIES

The Kafirnigan River Valley is located within several deserts of Central Asia. The probability of rainfall in the Shaartuz region of southwestern Tadjikistan near the Amu Darya River is less than 1 day during June 1-September 1. Experiments concerned with aerodynamic, soil, optical, and chemical characteristics of the source region were conducted at site 1 (see Figure 9.1). This site is near the center of a local dust source area observed by officials of the village of Shaartuz. Micrometeorological measurements made at site 1 provided information on vertical fluxes of suspended dust. Special attention was paid to the aerodynamic partitioning of momentum between the abrading surface and nonerodible vegetation and the effect of the cryptogamic crusts observed in these desert soils. Specialists concerned with the effects of cryptogamic

TABLE 9.1 U. S. Investigators and Analyses to be Done

Investigator	Data Reduction/Analysis
D. Gillette (NOAA)	Transport modeling, momentum partitioning, dust size distributions, vertical mass flux, saltation flux, threshold velocities
J. DeLuisi (NOAA)	Optical depth, single scattering albedo, asymmetry parameter, aerosol mass in atmospheric column
B. Bodhaine (NOAA)	Time series of nephelometer
D. MacKinnon (USGS)	Optical/radiative parameterization, remote sensing, mass flux of aerosol transport
J. Dobrowolski (Utah St. Univ.)	Cryptogamic soil crusting, soil properties/deposition
E. Patterson (Georgia Tech.)	Single scattering albedo, asymmetry parameter, size distribution of dust
J. Winchester (Florida St. Univ.)	PIXE analysis of streakers, statistical analysis of PIXE data
B. Musick (Univ. of New Mex.)	Vegetative/aerodynamic properties
L. Gomes (Univ. of Paris)	Size/composition of aerosols
P. Stockton (Univ. of Colo.)	Threshold velocity of dust

crusts and desert vegetation and geology carefully surveyed the area and sampled soil, vegetation, and cryptogamic crusts. Dust samples were collected to determine chemical composition and size distribution. Visibility, mass concentration, and solar photometer measurements, including optical thickness determinations, provided data for use in optical calculations, including optical thickness determinations. It is commonly believed that source regions in Afghanistan are responsible for producing much of the dust transported up the Kafirnigan River Valley (hence the name for the dust-bearing wind, Afghanetz). One goal of the experiment was to find the strongest source of dust.

Frequency mapping of dust storms showed that 10 to 30 dust storms are to be expected annually in southern Tadjikistan just north of the Amu Darya River in the Kafirnigan River Valley. The peak season for the storms is summer so one would expect dust storms to occur in early September, the time of the binational experiment. Dominant summer winds blow directly up the river valley (from the south). We focused on conditions in the Kafirnigan River Valley, from the Amu Darya River (Afghanistan border) to Dushanbe. As seen in Figure 9.1, the

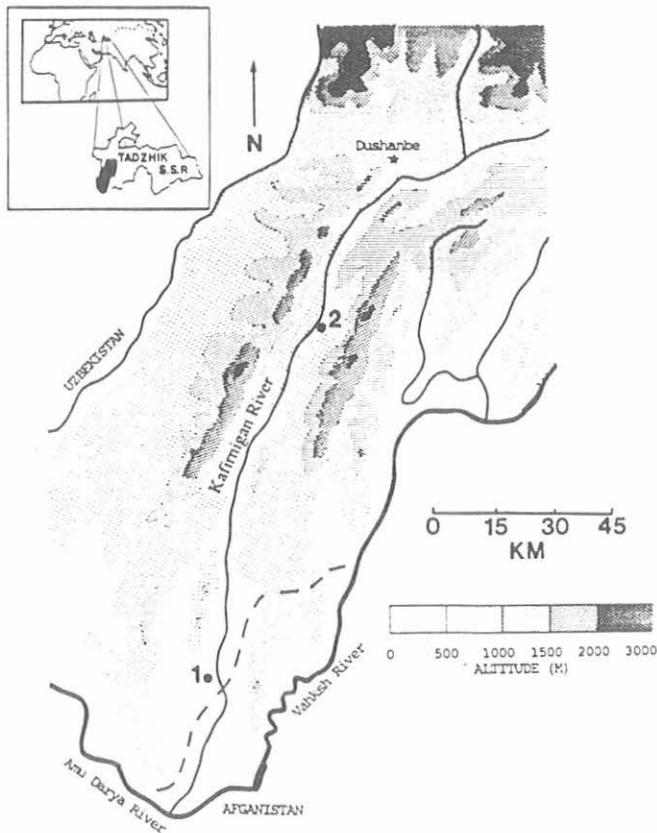


Fig 9.1. The experiment sites in the Kafirgigan River Valley. Site 1 is Shaartuz; site 2 is Isenbai.

river valley narrows from approximately 25 km in width at the Amu Darya to about 5 km near Dushanbe. The desert area at site 1 is in the most southerly part of the valley, an area of about 700 km². Micrometeorological measurements made near the center of this source area will be generalized to the entire desert area of the river valley from Amu Darya to Dushanbe. By using meteorological data provided by the Tadjik Hydrometeorological Service, we specified parameters for a dust flux model to estimate dust fluxes to Dushanbe.

To evaluate dust transport model estimates described above, we calculated dust flux estimates at a downwind location in the river valley. At this location, designated as site 2 in Figure 9.1, detailed measurements of optical properties along with solar photometry measurements were made to determine the total atmospheric column mass loading of aerosol being transported up the valley. Site 2 is at the village of Isenbai, within 70 km of Dushanbe in that part of the Kafirgigan River Valley that is only about 15 km wide. There is no local dust production or local sources of urban pollution near this site. Average wind speed measured at site 2 provided a transport velocity to calculate mass flux for computations of the total mass concentration cross section of desert dust being transported up the Kafirgigan Valley to Dushanbe. Measured optical and physical properties of the dust were used to calculate total atmospheric column dust masses from the solar photometer measurements. Other physical and optical properties measured were single scattering

albedo, asymmetry parameter, size distribution, and real and imaginary index of refraction. An integrating nephelometer was used to measure aerosol scattering extinction directly. Continuous measurements were made with the integrating nephelometer to establish a time series of aerosol data for the entire experimental time period. Filtration samples and automated "streaker" samples were obtained from aerosols during dust storm transport up the river valley. These samples were used for optical studies and chemical composition determinations.

NOAA AVHRR satellite data were obtained for the experimental region and the time of the experiment. The ground-based optical, radiative, and aerosol mass flux data were used to interpret the remotely sensed satellite images before and during dust storms.

Our third experiment site in the Kafirgigan Valley was at the Tadjik Physical Technical Institute in Dushanbe. The instrument used there was the "streaker" aerosol sampler designed to sample automatically and continuously during the experimental period. From data obtained, a continuous time series will be established for the aerosol composition for Dushanbe. Experimental evidence is being sought for the absorption of sulfur by the alkaline desert aerosol. The source of the sulfur would be urban air pollution produced at Dushanbe. The sulfur would be present as CaSO₄, converted from SO₂ by reaction with CaCO₃ in the desert aerosol. Additional sampling by two other streakers at sites 1 and 2 was used to establish relationships of sulfur and the desert aerosol.

9.1.4. SUMMARY

The Kafirgigan Valley Desert Dust Experiment was scientifically divided into five problem areas to encompass the work of the combined team of investigators. When taken together, these five areas give an integrated scientific picture of the causes and consequences of desert dust. The first concerned specification of the source area of the dust. Biological, physical, and chemical investigations were included in this specification. The second involved the specification of the dust movement: flux of dust from the source area, flux of dust to the surface, and transport of dust by the wind (source/sink/transport). The third, which was extremely important, was the physical and optical description of the dust. It includes one of the principal reasons for performing the experiment: to assess the climatic consequences of desert dust. The fourth dealt with the description of the chemistry of the dust, namely, its transformation and interaction with other aerosols and gases, especially those having pollution origin. The fifth concerned determining the large-scale structure of the dust storms sampled and synthesis of the system in models.

Dust storms were experienced on September 16 and 20, 1989. The first dust storm was smaller in magnitude than the second. The storm of September 20 had winds of more than 20 m s⁻¹ at desert site 1 and more than 7 m s⁻¹ at valley site 2; site 1 was a source of dust for 58 minutes. The experiment was successful in providing data for all five problem areas. Analysis of the data is now under way, and a meeting concerned with the first results of the binational experiment will take place in Nalchik, U.S.S.R., in September 1990.

9.2. ANNUAL OZONE CYCLE AND DECADE TREND AT SOUTH POLE

R.C. SCHNELL, S.C. LIU (*Aeronomy Laboratory*), S.J. OLTMANS,
R.S. STONE, D.J. HOFMANN,
W.T. STURGES, E.G. DUTTON,
M. TRAINER (*Aeronomy Laboratory*), AND J.M. HARRIS

9.2.1. INTRODUCTION

Surface ozone at South Pole, Antarctica, displays a distinct summer minimum having a significant downward trend, over the period 1976 to 1990. We suggest that the trend in summer ozone minima is caused by enhanced photochemical destruction of ozone in the lower troposphere due to the increased penetration of UV radiation associated with the stratospheric ozone hole. In addition, the trend in surface ozone is highly correlated with increased cloudiness over the same period, suggesting an influence of atmospheric dynamics.

9.2.2. SEASONAL OZONE VARIATIONS AT SOUTH POLE

The long-term surface ozone record at SPO was studied to determine annual and long-term patterns. Figure 9.2a shows the CMDL hourly average ozone data from SPO (2.8 km MSL), averaged weekly for 1981-1987. Figure 9.2b shows the corresponding mean daily solar radiation measured at the surface at SPO, and modeled for South Pole, McMurdo (77.9°S), and the Antarctic Circle. As the sun rises in late September, ozone begins a period of decline and greater variability, which continues until austral sunset. At that time, ozone begins a steady recovery, peaking in July and August. This negative correlation between surface ozone concentration and solar radiation suggests that tropospheric ozone is being photochemically destroyed seasonally in the Antarctic as it is in the Arctic [Oltmans *et al.*, 1989].

At SPO, decline in ozone begins around the middle of September, but significant solar radiation levels needed to initiate the classic low NO_x ozone destruction reaction are not reached at the pole until mid-October. Ample solar radiation amounts are, however, seen at the Antarctic Circle by early September, suggesting that the springtime ozone depletion observed at SPO has its origin at lower latitudes and is subsequently transported to the pole. Isobaric back trajectories on the 500-mb surface were examined for September-December 1987. During each month, numerous trajectories indicated long-range transport from north of 75°S within 2.5 days. Moreover, transport from north of 65°S in 2.5 days was not uncommon.

Evidence of effective meridional flow to SPO can also be seen in a representative austral summer ozone depletion event measured at SPO and the coincident air temperature time series, presented in Figure 9.3. A 1986 ozone depletion event beginning on day 339 and ending on day 344 is correlated with the intrusion of a warm air mass. This ozone depletion event was associated with much warmer air temperatures, overcast skies, and elevated sea salt concentrations, suggesting the presence of marine air transported inland from a coastal region.

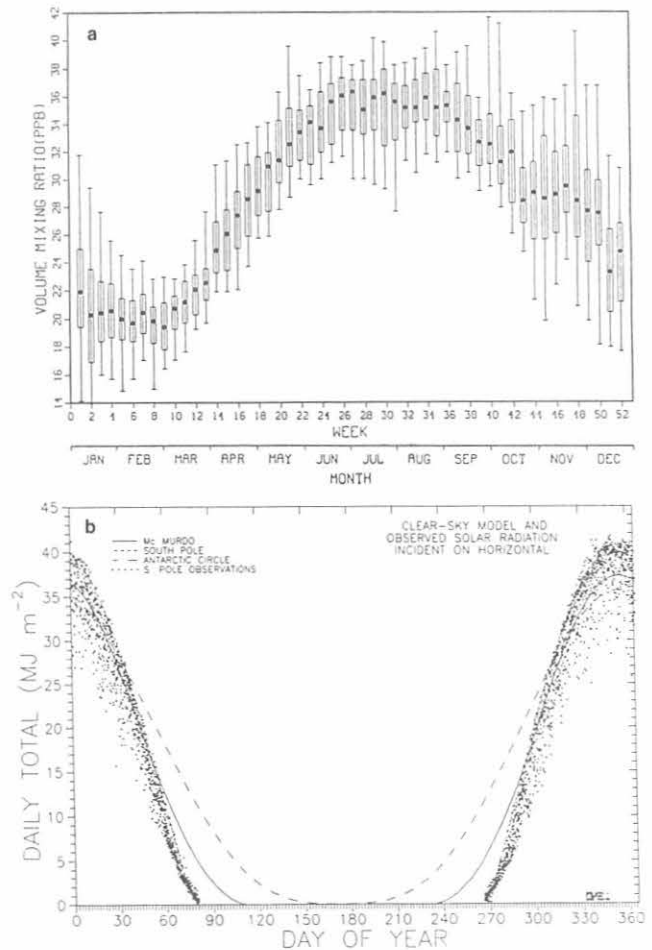


Fig. 9.2.(a) Box and whisker plots showing the seasonal mean surface ozone cycle and variability at South Pole for January 1981 to December 1987. The median (dot), the upper and lower quartiles (ends of the boxes), and upper and lower fifth percentiles (ends of the whiskers) of weekly average ozone values are shown. (b) Observed daily mean global solar radiation at South Pole (dots) and modeled clear-sky solar radiation at McMurdo, at the latitude of the Antarctic Circle, and at the South Pole.

Such marine air intrusion events have been shown to occur regularly at South Pole [Bodhaine *et al.*, 1986]. These events at SPO are consistent with the notion that the seasonal depletion of ozone first occurs in the lower troposphere at lower latitudes and that ozone-depleted air is subsequently transported inland.

9.2.3. LONG-TERM DECREASING OZONE TREND AT SOUTH POLE

The SPO ozone record from 1975 to 1989 (Figure 9.4) shows a statistically significant downward trend in the near-surface ozone concentration for the austral summer months (December, January, February, and March). The decrease is about 17% over the 14-year period, or a rate of about 0.32 ppbv annually when fitted linearly. No statistically significant trend can be found for other seasons. However, a closer examination of these data suggests that a tendency toward a small ozone decrease is first

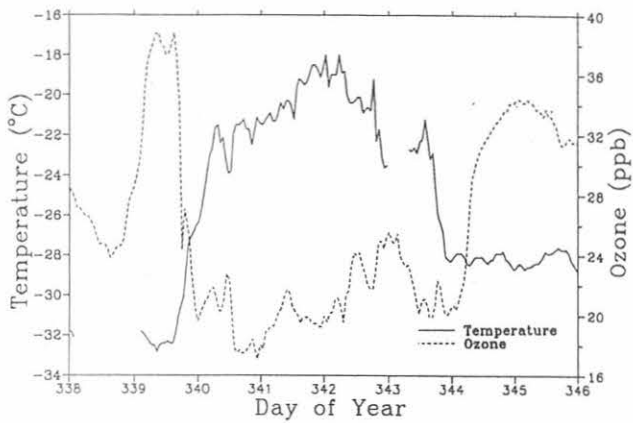


Fig. 9.3. South Pole surface ozone concentrations and the near-surface air temperature record, for December 4-11, 1986 (austral summer).

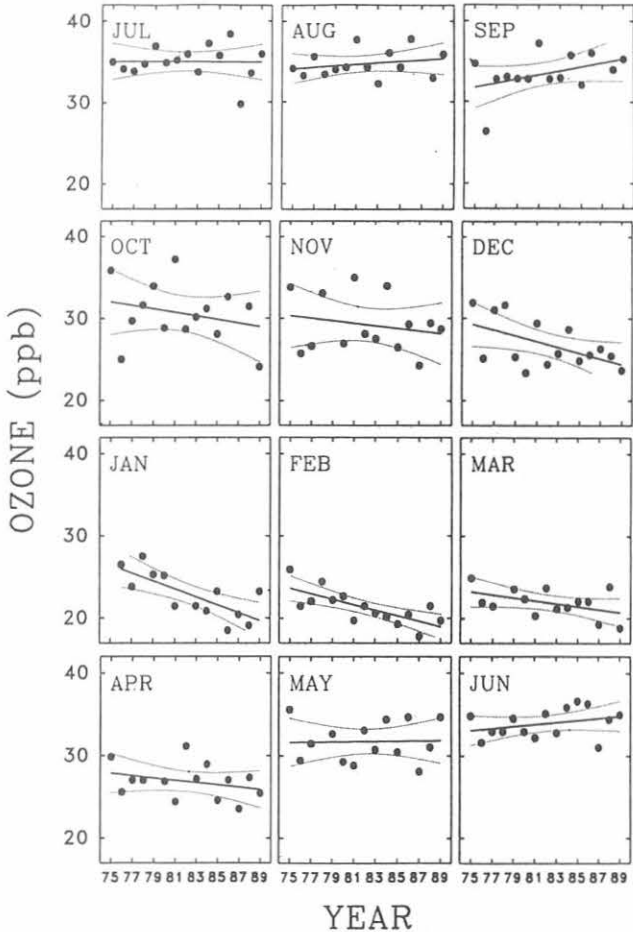


Fig. 9.4. Mean surface ozone mixing ratios by month for 1975-1989. The solid line is a linear least-squares fit to the data for each month. The dotted lines are 95% confidence intervals for the trend lines. The December, January, February, and March trends are significant at the 95% level.

detected in October, reaches a maximum decreasing rate during January, and completely disappears by May. The seasonal pattern (Figure 9.2a), with the surface ozone minimum during the austral summer, is similar to the seasonal pattern in the long-term trend that shows the largest decreases occurring during the summer months. This suggests that photochemical processes are important both in the seasonal cycle and in the long term.

The downward trend in the mean January-February solar irradiance is well correlated with a downward trend in surface ozone concentrations measured at the pole, as shown in Figure 9.5. The observed sky cover for South Pole from 1957 to 1990 is shown in the insert (Figure 9.5). A trend to increased cloudiness in the last decade of the record is apparent. The data in Figure 9.5 suggest that ozone-depleted air transported from lower latitudes contributes significantly to the surface ozone loss during the late austral summer months at South Pole. However, an examination of the solar irradiance data by month shows that the significant downward trend in solar irradiance exists only in January and February, whereas the decrease of surface ozone appears to start as early as October and lasts until the end of April (Figure 9.4). Thus, although the transport mechanism may contribute significantly to the observed downward trend in tropospheric ozone during January and February, it appears it is not the major contributor during other months.

9.2.4. SUMMARY AND CONCLUSIONS

An austral summer surface ozone minimum with a significant long-term decreasing trend ($1.13\% \text{ yr}^{-1}$ during 1976 to 1990) has been documented at SPO. The seasonal variation is most likely

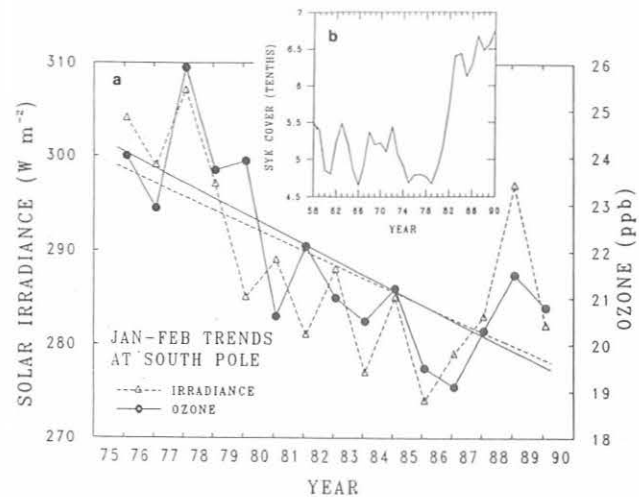


Fig. 9.5(a) Mean January-February surface ozone concentrations and linear trend line for 1976-1990 (connected dots and solid line referenced to right scale) compared with the mean January-February solar irradiance (measurements initiated in 1976) flux measured at the South Pole (triangles referenced to left scale). The trend in solar irradiance for the 14-year period is represented by the dashed line, which is anticorrelated with observed cloudiness at the South Pole. (b) The long-term record of South Pole sky cover (since 1957) for January-February. A 15% lowess smoothing function was applied to the monthly averages of multiple (up to 24) observations.

associated with increased photochemical ozone destruction due to the annual increase in solar radiation at that time, the transport of ozone-depleted air from lower latitudes accounting for the early springtime onset of the reduction.

The decreasing trend in summer surface ozone at SPO since 1979 is very likely the result of enhanced photochemical destruction of ozone in the lower troposphere due to increased penetration of UV radiation associated with the stratospheric ozone hole. The solar irradiance at South Pole, which is inversely proportional to the cloudiness caused by inflow of marine air to South Pole, also shows a significant downward trend for January and February over the same period. This trend correlates very well with the downward trend in ozone concentrations.

9.3. WINTERTIME BLACK CARBON AEROSOL MEASUREMENTS OVER THE SOUTHWESTERN UNITED STATES, DECEMBER 1989

PATRICK J. SHERIDAN, RUSSELL C. SCHNELL,
AND JOE F. BOATMAN

9.3.1. INTRODUCTION

This experiment is the third in a series designed to characterize the aerosol over the high desert of south-central New Mexico and to document aerosol variability as a function of season, atmospheric flow patterns, and altitude of collection. The two previous aircraft-based aerosol sampling missions were conducted in May and July 1989. The field experiment documented in this paper will be referred to as ALIVE-3 (the third Atmospheric Lidar Validation Experiment).

Sampling procedures were similar to those used in the previous experiments. Unlike in the earlier studies, however, high concentrations of carbonaceous particles were observed in many ALIVE-3 cascade impactor samples. This paper describes cascade impactor aerosol carbon measurements collected during the ALIVE-3 flights and concurrent bulk aerosol black C measurements. Our attempts to correlate the bulk and individual-particle aerosol C data are discussed.

9.3.2. EXPERIMENTAL METHODS

Aerosol samples were collected by aircraft over New Mexico during December 11-15, 1989. The research platform for this study was the NOAA King Air aircraft operated by the Air Resources Laboratory. As in the earlier programs, care was taken in this program to limit the lengths and bending of tubing upstream of our aerosol samplers so that particle losses would be kept to a minimum. No evidence was found (e.g., the total absence of very large or very small particles, or obvious particulate contamination) that would lead one to believe that sampling was biased in some way relative to the previous experiments.

Cascade impactor aerosol samples were collected at predetermined altitudes in the sampling area. For each flight, one low-altitude aerosol sample (within the PBL) and one high-altitude sample (above the PBL) were collected. The

samplers were five-stage PIXE Corporation cascade impactors. Particles were collected directly onto thin (10-20 nm thick) Formvar films supported by Ni TEM grids. The grids were commercially prepared in clean-room facilities and were checked for possible contamination before use.

An AEM was employed to obtain information on individual particle chemistry and morphology and on the aerosol size distribution [Sheridan, 1989a]. An ultrathin window x-ray spectrometer interfaced with the microscope permitted the detection of x-rays more energetic (i.e., from heavier elements) than those of Be. Thus, the interesting light elements C and O (and occasionally N) were directly observable in discrete particles. High-resolution photomicrographs were taken of individual particles and particulate deposits on films from all analyzed stages.

Characterization of the fine fraction of the aerosol collected during ALIVE-3 was performed by AEM of particles on the stage 1 (0.25- μm aerodynamic cutoff diameter) films. Preliminary characterization for each sample included counting and classifying all particles within a finite area (a rectangle on the viewing screen of the electron microscope) on a film portion directly under the impactor jet. Analysis of this central aerosol deposit continued until at least 300 particles were counted and resulted in the determination of approximate relative loadings on the films, which, since collected volumes were similar for all samples, reflect relative particle concentrations in the atmosphere.

Aerosol black C measurements were made continuously and in real time onboard the King Air aircraft over a wide range of altitudes. An aethalometer was used to collect the aerosol and to convert aerosol extinction to black C concentrations [Hansen, 1991]. Vertical profiles of aerosol black C concentration were then constructed over the study area.

9.3.3. RESULTS AND DISCUSSION

The results of the individual-particle analysis portion of this study are based on fine-particle (stage 1) data, which we know from previous work contains most of the aerosol C information [Sheridan, 1986]. The majority of supermicrometer particles collected on coarse-fraction impactor stages resembled various types of soil dust, a finding that is consistent with previous aerosol studies in this region [Sheridan, 1989a, b]. Recent studies show that the soil component is responsible for only a small fraction of the total optical extinction in the visible and near-infrared spectral regions [Hansen, 1991].

The composition of the fine aerosol was quite variable during the experiment. The stage 1 aerosol samples collected during ALIVE-3 have been classified as one of three major types. Aerosol class 1 consisted primarily of fine, solid $(\text{NH}_4)_2\text{SO}_4$ particles. In this class of aerosol sample, >80% (sometimes as high as 95%) of the total number of analyzed particles were solid (i.e., neutralized) sulfates.

The second major type of aerosol (aerosol class 2) contained a significant number fraction (15-51%) of small, spherical C-rich (SC) particles externally mixed with the sulfates. These C-rich spheres ranged between ~0.05 and ~1.0 μm in diameter, and had a median size of about 0.2 μm . This type of aerosol

was observed most frequently in low-altitude samples collected during the last half of the experiment (December 13-15). Scientists aboard the aircraft visually confirmed the El Paso urban plume in the research area at this time [Gunter *et al.*, 1991]. The compositions of the aerosol samples collected on these days suggest increased wintertime combustion activities in the El Paso area as likely aerosol sources. This macroclass of aerosol was not observed in our two previous (late spring and summer) ALIVE electron microscope aerosol studies, where generally ~1% or less of the stage 1 particles were found to be C-rich with an obvious combustion (i.e., spherical) morphology.

The third type of aerosol (aerosol class 3) consisted of a large number fraction (near 50%) of nonspherical C-rich (NSC) particles. Particles of this type were observed in the previous ALIVE aerosol studies, but again in much smaller numbers. These particles were classified as "non-combustion C" in past reports [Sheridan, 1989a, b], but may actually be combustion-derived black C resulting from a source with a lower combustion temperature and/or a different fuel mix than that of spherical combustion C particles. Concurrent aethalometer measurements suggest that this might indeed be the case [Gunter *et al.*, 1991]. The various morphologies of C-rich particles collected during the ALIVE-3 flights are shown in Figure 9.6

Sixteen of the eighteen fine aerosol samples collected during ALIVE-3 fit into one of the three general categories described above. The two anomalous samples had moderate fractions of C-rich particles (23% of all analyzed particles in both samples were SC and/or NSC), but not large enough fractions of either discrete type to fit the definition of the "significant SC" or "significant NSC" aerosol classes.

Other major particle types that were less frequently observed in the fine aerosols included liquid (acidic) sulfate, soil dust, composite sulfate/crustal, composite carbonaceous/crustal, Na/Cl-rich, K/Cl-rich, and rounded-to-spherical Fe-, Ti-, Fe/Ti- and Zn-rich particles. These types of particles collectively constituted <10% of the fine aerosol particles on all stage 1 films.

The individual particle aerosol data were compared with concurrent aethalometer data to determine if trends in the bulk aerosol black C concentrations are observable through microanalysis of the aerosol. Table 9.2 shows the fractions of SC and NSC particles, along with the sum of these values representing a total C (TC) fraction. Concurrent black C aethalometer measurements for the December flights were taken from the King Air vertical profiles [Gunter *et al.*, 1991] and are listed next to the microanalysis data. It was initially assumed that if a high correlation between the bulk and individual-particle data existed, it would be most obvious when comparing the aethalometer and SC (i.e., combustion) particle data. However, a quick inspection of the electron microscope data shows that NSC data relate much better to aethalometer measurements for the first two samples than do the SC data.

It is also apparent that aethalometer measurements are inherently dependent not only on aerosol composition but also on aerosol mass (or filter loading). A load factor (LF), directly proportional to the particulate loading on each grid, was calculated by counting all particles within a finite area on the most heavily loaded portion of the stage 1 films. Multiplying the fraction of NSC, SC, and TC particles by this LF creates dimensionless parameters (columns 8-10) that reflect both aerosol composition and mass. We expected these parameters,

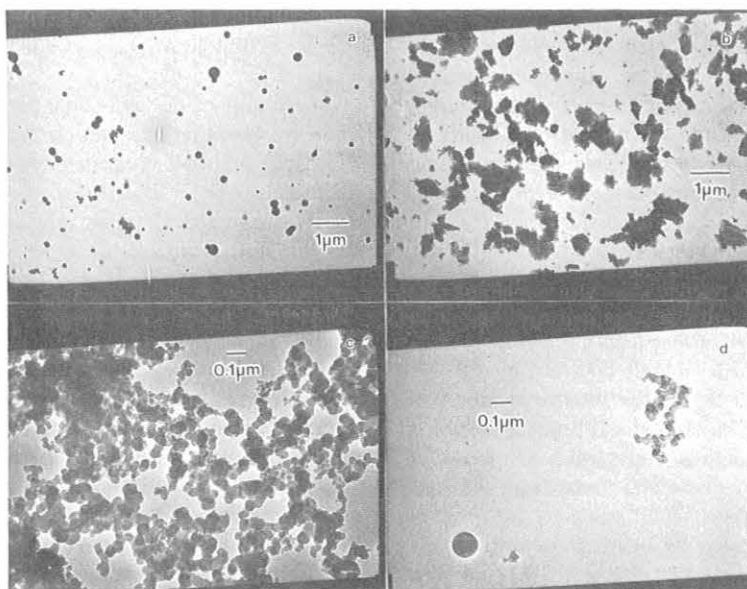


Fig. 9.6. Different morphologies of carbonaceous particles collected during the ALIVE-3 flights. (a) Small C-rich spheres observed in abundance in low-altitude samples during December 13-15. (b) Heavy loadings of nonspherical C-rich particles found in samples 1 and 2. (c) A carbonaceous chain aggregate particle. These larger combustion-derived particles were infrequently observed in most samples. (d) High-magnification field of view of the two types of combustion-morphology black C particles.

TABLE 9.2. Carbonaceous Fine-Particle Fractions and Load Factor Data From the Final Stage of the ALIVE-3 Cascade Impactor Samples, and Concurrent Aethalometer Black C Measurements for Comparison

Sample No.	Sampling Level	Aethalometer Black C, ng m ⁻³	NSC	SC	TC	LF	WNSC	WSC	WTC
1	L	210	0.49	0.02	0.51	7	3.43	0.14	3.57
2	H	245	0.54	0.03	0.57	17	9.18	0.51	9.69
3	L	115	0.07	0.07	0.14	4	0.28	0.28	0.64
4	H	65	0.12	0.03	0.15	6	0.72	0.18	0.90
5	L	ND	0.02	0.02	0.04	5	0.10	0.10	0.20
6	H	ND	0.19	0.04	0.23	8	1.52	0.32	1.84
7	L	150	0.11	0.04	0.15	5	0.55	0.20	0.75
8	H	100	0.09	0.05	0.14	5	0.45	0.25	0.70
9	L	90	0.04	0.05	0.09	5	0.20	0.25	0.45
10	H	60	0.07	0.17	0.24	4	0.28	0.68	0.96
11	L	238	0.06	0.23	0.29	6	0.36	1.38	1.74
12	H	105	0.13	0.10	0.23	5	0.65	0.50	1.15
13	L	75	0.05	0.19	0.24	4	0.20	0.76	0.96
14	H	50	0.06	0.04	0.10	4	0.24	0.16	0.40
15	L	275	0.14	0.51	0.65	6	0.84	3.06	3.90
16	H	45	0.04	0.19	0.23	3	0.12	0.57	0.69
17	L	195	0.05	0.39	0.44	6	0.30	2.34	2.64
18	H	75	0.03	0.15	0.18	5	0.15	0.75	0.90

NSC = nonspherical C-rich particles; SC = spherical C-rich particles; TC = total carbon fraction; LF = load factor; WNSC = weighted NSC; WSC = weighted SC; WTC = weighted TC; L = samples collected at ~6500 ft ASL; H = samples collected at ~9500 ft ASL; ND = no data.

especially the weighted SC (WSC, column 9) and weighted TC (WTC, column 10), to correlate best with bulk aerosol black C measurements.

A linear least-squares fit was performed for each microanalytical parameter against the aethalometer data. The correlations for the 16 aethalometer measurements (a malfunction on December 12 resulted in no concurrent aethalometer data for two of the samples) and the appropriate electron microscope data are presented in Table 9.3. For the first three correlations, which compare the aethalometer data with the fractions of NSC, SC, and TC particles on stage 1 films, the data show a strong correlation between TC and the bulk aerosol black C measurements ($r_{TC} = 0.83$). The fact that the TC versus aethalometer correlation is so much stronger than the SC versus aethalometer correlation is surprising, since SC (thought to be combustion C) is presumably what the aethalometer measures. The TC versus aethalometer data comparison, however, is bolstered by the relationships in samples 1 and 2. These heavy deposits of NSC particles probably contained significant amounts of nonspherical black C, which the aethalometer detected. If samples 1 and 2 are ignored, the correlation coefficients for TC versus aethalometer and SC versus aethalometer change to 0.76 and 0.71, respectively.

The correlation between LF and the aethalometer data in Table 9.3 is not so strong, but suggests that aerosol loading alone on filters plays some role in aerosol extinction measurements. This contention is further supported by the comparisons between aethalometer data and the dimensionless parameters WNSC, WSC, and WTC. Incorporation of the LF into these parameters improves the correlation between the aethalometer

TABLE 9.3. Comparison of Electron Microscope Individual-Particle Data with Concurrent Aethalometer Black C Measurements

Comparison	Correlation (r)
Aethalometer versus NSC	0.55
Aethalometer versus SC	0.43
Aethalometer versus TC	0.83
Aethalometer versus LF	0.59
Aethalometer versus WNSC	0.51
Aethalometer versus WSC	0.58
Aethalometer versus WTC	0.71

Correlation coefficients result from linear least-squares fits of the data.

measurements and SC from $r_{SC} = 0.43$ to $r_{WSC} = 0.58$. The correlation between TC and aethalometer data is weakened by factoring in the LF ($r_{TC} = 0.83$; $r_{WTC} = 0.71$), but this is primarily due to the extremely heavy loading of C-rich particles in sample 2 that is not supported by a correspondingly large black C measurement.

Overall, the correlations between the individual-particle and bulk aerosol data are impressive, and show that at least the heavy episodes of black C aerosol detected by the aethalometer are observable using microanalytical techniques. Much of the variation between the data sets occurred during episodes of lower black C concentrations, which are not as easily detected

using electron microscopy as are the high-concentration samples. Weaker correlation coefficients might be expected, considering the facts that (1) the cascade impactor samples were collected for ~10-min periods while the aircraft flew through horizontal inhomogeneities in the aerosol over a sampling area of several hundred square kilometers, and (2) the two sampling inlets were of similar, but not identical, size and shape and probably passed different fractions of the aerosol to the internal aerosol collectors. Correlation coefficients in the 0.6-0.8 range are noteworthy for the comparison of these very different types of measurements. Other studies [e.g., Sheridan, 1986] have concluded that direct comparisons of simultaneously-collected bulk aerosol and individual-particle data often show much worse correlations ($r < 0.5$) than were found in the present study.

At least two explanations are possible for the TC parameter comparing better with aethalometer data than did the SC (soot) parameter. Either the aethalometer is sensitive to optical extinction by aerosol other than black C, or the irregular C-rich aerosol collected primarily in samples 1 and 2 was composed significantly of black C. The morphologies of these particles are not what we normally expect for sooty C, but perhaps a lower-temperature combustion process that produces a large fraction of nonspherical soot was the source. Whatever the source of these particles was, it is clear that the aethalometer gave a strong signal for black C aerosol at this time. This is the first time to our knowledge that direct comparisons of this type for black C aerosol have been made; answers to some of the questions generated here will undoubtedly require further study.

Acknowledgments. We thank Dennis Garvey and the U.S. Army Atmospheric Sciences Laboratory (White Sands Missile Range) for the funding of much of this work. We also acknowledge members of the NOAA Air Quality Group, especially Dennis Wellman, Lauren Gunter, and Stan Wilkison for assistance in aircraft installation and sample collection.

9.4. REFERENCES

- Bodhaine, B.A., J.J. DeLuisi, and J.M. Harris, Aerosol measurements at the South Pole, *Tellus*, 38B, 223-235, 1986.
- Gunter, L., J.F. Boatman, M. Luria, J. Ray, H. Sievering, B. Watkins, and C. Van Valin, Report to U.S. Army Atmospheric Sciences Laboratory on ALIVE-3 flight operations, in preparation, NOAA ARL Air Quality Group, Boulder, CO, 1991.
- Hansen, A.D.A., Report to U.S. Army Atmospheric Sciences Laboratory on aethalometer black carbon measurements during ALIVE-3, in preparation, Lawrence Berkeley Laboratories, Berkeley, CA, 1991.
- Oltmans, S.J., R.C. Schnell, P.J. Sheridan, R.E. Peterson, S.-M. Li, J.W. Winchester, P.P. Tans, W.T. Sturges, J.D. Kahl, and L.A. Barrie, Seasonal surface ozone and filterable bromine relationships in the high Arctic, *Atmos. Environ.*, 23, 2431-2441, 1989.
- Sheridan, P.J., The use of analytical electron microscopy for the individual particle analysis of the Arctic haze aerosol, Ph.D. dissertation, University of Maryland, College Park, December 1986.
- Sheridan, P.J., Analytical electron microscope analysis of aerosol sampled over White Sands Missile Range, New Mexico, May 3-4, 1989, Final Report to the U.S. Army Atmospheric Sciences Laboratory, Cooperative Institute for Research in Environmental Sciences, Boulder, CO, 25 pp., 1989a
- Sheridan, P.J., Analytical electron microscope analysis of aerosol sampled over White Sands Missile Range, New Mexico, July 10-14, 1989, Final Report to the U.S. Army Atmospheric Sciences Laboratory, Cooperative Institute for Research in Environmental Sciences, Boulder, CO, 30 pp., 1989b.

10. Cooperative Programs

Precipitation Chemistry

R.S. ARTZ

NOAA, Air Resources Laboratory, Silver Spring, Maryland 20910

1. INTRODUCTION

Precipitation chemistry measurements continued generally unchanged at the four CMDL stations and at twelve regional stations. Several changes were instituted in two regional programs as a result of the completion of an additional statistical intercomparison, and work continues in restructuring the CMDL program.

2. CMDL BASELINE MEASUREMENTS

CMDL bimonthly chemistry measurements of snow samples continued normally at both BRW and SPO. At SMO, collection continued using the Aerochem Metrics sampler. Analysis results from the 1989 CMDL samples are not yet available.

Sampling on the Island of Hawaii continued only at MLO; Hilo and 22 Mile Site collections were suspended pending the outcome of quality assurance tests using the funnel and bottle collectors. (Previous comparison of CMDL MLO data with University of Virginia Aerochem Metrics data indicated problems of acidification resulting from the use of the funnel and bottle collectors.) MLO CMDL data for 1989 are not available for additional comparisons.

3. NADP REGIONAL BASELINE MEASUREMENTS

NADP [1990] measurements continued normally at MLO, SMO, and 12 regional stations. As a result of a second statistical intercomparison conducted for stations in Mississippi, the Meridian station was closed. A replacement station was found for the Salem, Illinois, station closed in December 1988, just outside of the nearby town of Omega. Current plans are to include the NADP station in Puerto Rico as part of the NOAA precipitation chemistry network, beginning in FY 1990 or early in FY 1991.

4. NADP MLO AND SMO 1989 PRECIPITATION CHEMISTRY DATA

As noted in previous years, precipitation at MLO is mainly a very dilute solution of sulfuric acid and little else for most samples. Figure 1 shows that although the vast majority of samples have SO_4^{2-} and H^+ concentrations of approximately $20 \mu\text{eq L}^{-1}$ or less, concentrations in excess of $60 \mu\text{eq L}^{-1}$ are occasionally observed in weekly samples. Also note from Figure 1 that SO_4^{2-} concentrations tend to exceed H^+ concentrations, a condition not typically observed in continental North American precipitation. A more careful

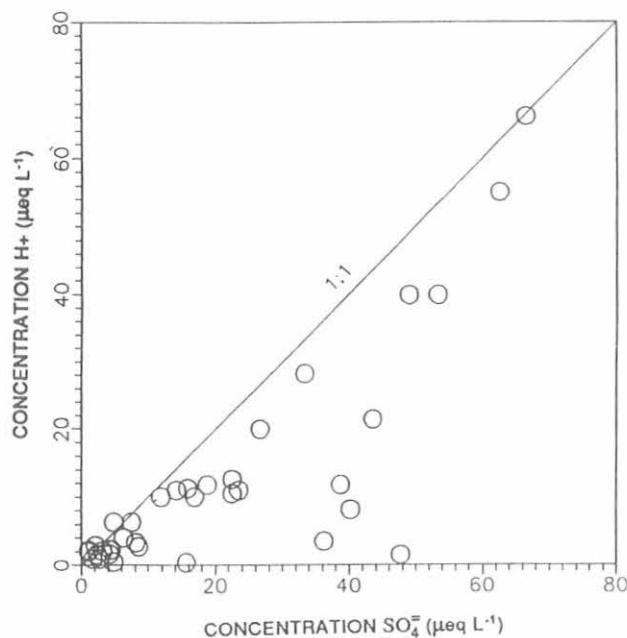


Fig. 1. NADP concentrations of hydrogen ion versus sulfate at MLO, 1989. Note that sulfate concentrations are typically larger than laboratory hydrogen ion concentrations.

study of this condition indicates that cation to anion balances are always close to unity (or as in Figure 2, cation minus values are near zero) when SO_4^{2-} concentrations are low. Conversely, ion balances may be very poor when SO_4^{2-} values are large, suggesting that unmeasured cations frequently exist in samples having high SO_4^{2-} .

Figure 3 shows that the marine influence on MLO precipitation is typically very small. Na^+ and Cl^- concentrations are in most cases less than $5 \mu\text{eq L}^{-1}$ and the excess (non-seasalt) Cl^- concentrations (calculated using Na^+ concentration) are always less than approximately $3 \mu\text{eq L}^{-1}$. Of note in Figure 3, however, are the three samples with relatively high concentrations of Na^+ , which result in an overcorrection of seasalt Cl^- . This indicates that the samples may have been contaminated with additional Na^+ , or more likely, that a small terrestrial source of Na^+ also exists. Sample number 31 appears to be from an event that was substantially influenced by marine source regions.

Figure 4 compares NADP laboratory and field H^+ concentrations for SMO, 1989. Note that in all cases (except for one outlier, not shown) the H^+ values are no higher than approximately $18 \mu\text{eq L}^{-1}$. Also note that with rare

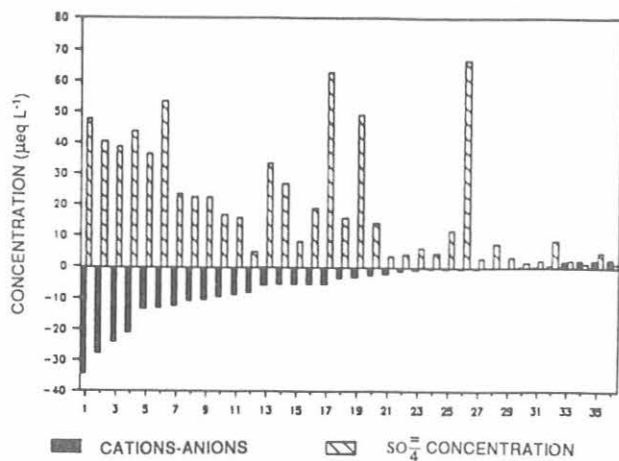


Fig. 2. NADP sulfate concentrations and cation minus anion values at MLO, 1989. The ion differences are nearly zero when sulfate concentrations are low, but high sulfate concentrations typically occur during weeks when ion differences are negative. Negative ion differences may indicate the existence of unmeasured cations.

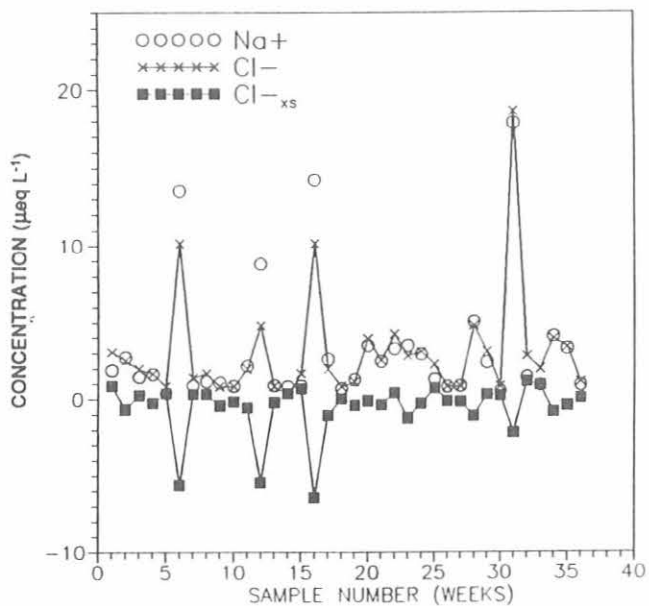


Fig. 3. NADP concentrations of sodium, chloride, and excess (non-seasalt) chloride at MLO, 1989.

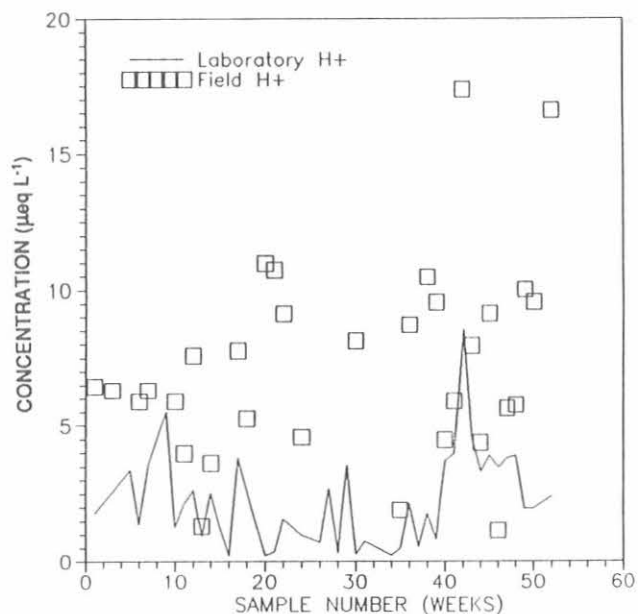


Fig. 4. NADP laboratory and field hydrogen ion concentrations at SMO, 1989. Differences may be due to the disappearance of the organic acids over time or the effects of contamination from the bucket lid O-ring.

exception, the laboratory values are lower than the field values. This is common in precipitation chemistry samples, indicating the disappearance of the organic acids over time and possibly the effects of some contamination from the bucket lid O-ring. Other data from SMO indicate that the extremely low background values routinely observed in weekly samples are essentially unchanged from past years.

5. REFERENCE

National Atmospheric Deposition Program, *NADP/NTN Annual Data Summary, Precipitation Chemistry in the United States, 1989*, Natural Resource Ecology Laboratory, Colorado State University, Fort Collins, 1990.

Continuous Aerosol Monitoring with the Epiphaniometer at MLO

U. BALTENSPERGER,¹ H.W. GAEGGELER, AND D.T. JOST

Paul Scherrer Institute, CH-5232 Villigen PSI, Switzerland

In December 1989, an epiphaniometer was installed at MLO. This instrument was developed recently [Gäggeler *et al.*, 1989] and has the ability for continuous aerosol monitoring even at very low aerosol concentrations [Baltensperger *et al.*, 1990].

The system is described in detail by Gäggeler *et al.* [1989]. A schematic diagram is shown in Figure 1. Aerosols are pumped through a chamber containing radioactive lead isotopes (²¹¹Pb). These single lead atoms are produced at a constant rate by the decay of a short-lived radon isotope (²¹⁹Rn) emanating from a long-lived actinium source (²²⁷Ac). ²¹¹Pb atoms attached to aerosol particles are transported through a capillary that acts as a diffusion barrier for non-attached lead atoms. At the end of the capillary, the aerosol particles and with them the attached lead atoms, are deposited on a filter. The resulting activity on the filter is measured continuously by a surface barrier detector by means of the α -decay of the bismuth isotope ²¹¹Bi, the daughter of ²¹¹Pb. Because of the relatively short half-life of ²¹¹Pb, aerosols can

be continuously monitored by the epiphaniometer, without changing or transporting the filter.

Calibration experiments with artificial aerosols showed that the attachment coefficient of the ²¹¹Pb atoms can be described by the Fuchs theory of coagulation [Fuchs, 1964; Seinfeld, 1986]. Since the device delivers a signal that is proportional to the "Fuchs surface" of the aerosol particles [Gäggeler *et al.*, 1989] it was called epiphaniometer (Greek epiphania = surface of a body). According to Fuchs, at small aerodynamic diameters ($d < 100$ nm, free molecular regime) the epiphaniometer signal is proportional to d^2 . At large aerodynamic diameters (> 3 μm , hydrodynamic regime) the signal is proportional to d . In the intermediate regime, the obtained signal is proportional to d^x , with x varying between 1 and 2, depending on particle diameter. Therefore, for a polydisperse aerosol, the obtained signal is proportional to the integral of the differential products $dN \cdot dS$, with N = particle concentration and S = "Fuchs surface" = $\pi \cdot d^x$. Thus, the size distribution of an aerosol has to be known in order to calculate

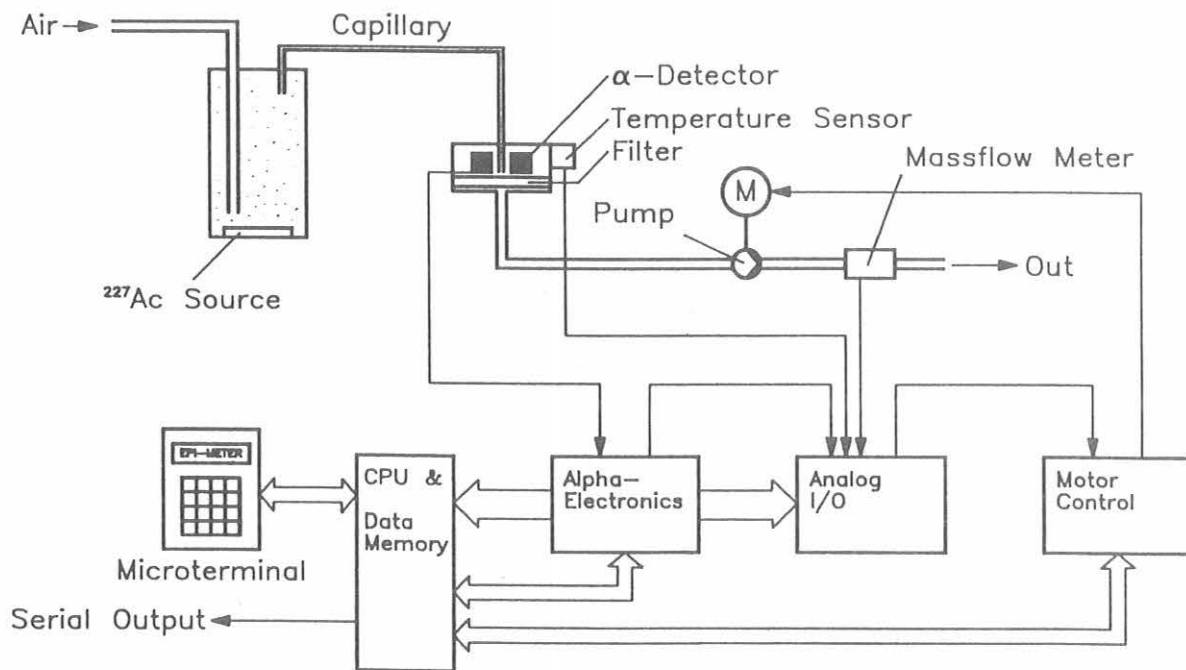


Fig. 1. Schematic diagram of the epiphaniometer.

¹Present address: Department of Chemical Engineering, California Institute of Technology, Pasadena, California 91125.

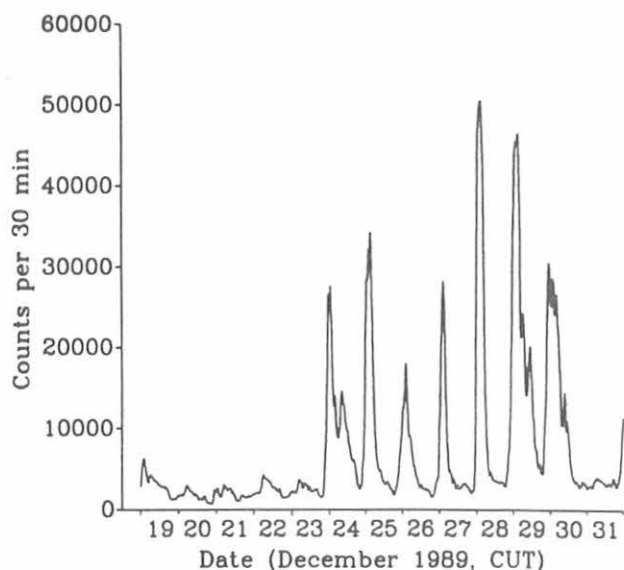


Fig. 2. First epiphaniometer data from MLO for December 1989.

the geometrical surface or the volume concentration. Despite this limitation, the epiphaniometer is well suited for aerosol monitoring. Its excellent sensitivity allows for measurements also at very low concentrations found, for example, at high-alpine sites. Because of the low flow rate of 1 L min^{-1} ,

the device consumes only 8 W, including counting and data processing. It is therefore suitable for battery operation, and it has been used together with a solar panel for continuous aerosol measurements in the Swiss Alps at heights up to 4450 m ASL [Baltensperger *et al.*, 1990].

Figure 2 shows the first epiphaniometer data from MLO for December 1989. With the chosen time resolution of 30 min the lowest values found for this period are 2 orders of magnitude above the detection limit. Preliminary comparisons show very good agreement with CNC and nephelometer data. On several days the usual pattern of diurnal variation caused by up-slope winds can be seen.

Acknowledgment. We thank E. Robinson and A. Yoshinaga for their cooperation and surveillance of the epiphaniometer. Parts of this work were supported by the Swiss National Science Foundation.

REFERENCES

- Baltensperger, U., H.W. Gäggeler, D.T. Jost, M. Emmenegger, and W. Nägeli, Continuous background aerosol monitoring with the epiphaniometer, *Atmos. Environ.*, 24A, in press, 1990.
- Fuchs, N.A., *Mechanics of Aerosols*, Pergamon, New York, 1964.
- Gäggeler, H.W., U. Baltensperger, M. Emmenegger, D.T. Jost, A. Schmidt-Ott, P. Haller, and M. Hofmann, The epiphaniometer, a new device for continuous aerosol monitoring, *J. Aerosol Sci.*, 20, 557-564, 1989.
- Seinfeld, J.H., *Atmospheric Chemistry and Physics of Air Pollution*, John Wiley, New York, 1986.

Antarctic Ultraviolet Spectroradiometer Monitoring Program

CHARLES R. BOOTH, TIM LUCAS, JONATHAN YEH, AND DAVID NEUSCHULER

Biospherical Instruments Inc., San Diego, California 92117

1. INTRODUCTION

The establishment of a monitoring network for UV radiation has been a critical part of the U.S. Antarctic Program. Its purpose is to evaluate the consequences of stratospheric ozone depletion on the health and productivity of Antarctic organisms and personnel. Monitoring network sites are listed in Table 1. This network has collected data showing strong correlations between ozone depletion and elevated levels of short-wavelength UV irradiance.

2. METHODOLOGY

The spectroradiometer system, manufactured by Biospherical Instruments, is designed for permanent mounting in a staffed facility and for continuous operation. The system is automatic, needing attention only for data transfer and periodic inspection. The instrument has wavelength and intensity calibration lamps for automatic calibrations at programmed intervals. An IBM-compatible computer is used to control the system and log the data.

The double monochromator is the heart of the system which is configured with 167- μm input/output slits and a 250 μm intermediate slit. The throughput is $f/3.5$, and the focal length is 0.1 m. The holographic grating is blazed for 1200 grooves mm^{-1} at 250 nm. It can resolve spectral features that are approximately 0.5 nm wide. The wavelength of interest is selected by changing the angle of the two tandem diffraction gratings relative to the input, output, and intermediate slits. The gratings are remotely turned with a computer-controlled stepping motor. The photomultiplier tube is a 28-mm-diameter 11-stage device with a bialkali cathode and a quartz window. Temperatures of the monochromator and photomultiplier are carefully controlled. Automatically actuated calibration sources (tungsten lamp and mercury discharge lamps) perform several calibration checks

each day. The system is periodically calibrated using an optical standard traceable to NIST.

3. RESULTS

The amount of short wavelength UV radiation incident on the earth is governed by several factors, the most important being solar zenith angle, cloud cover, and atmospheric ozone concentration. Although 1988 and 1989 both showed considerable depletion of the ozone layer over Antarctica, the geographical distribution of the ozone "hole" as a function of time was different. A dramatic effect of the ozone depletion is seen in Figure 1. Here we compare spectral scans recorded at McMurdo at the same time on October 20 in 1988 and 1989. In 1988, the TOMS satellite (A. Krueger, NASA Goddard Spaceflight Center, Greenbelt, Maryland, private communication, 1989) reported total column ozone concentration of 386 DU, a relatively high level; 1 year later the concentration was 161 DU, showing considerable ozone depletion.

Most of the concern over ozone depletion has arisen because of the prediction that this would have significant biological impact. The spectral expression of this impact is commonly called the dose weighting or action spectra weighting. Figure 2 shows the product of the irradiance spectra shown in Figure 1 and the DNA damage action spectra determined by *Setlow* [1974]. This dosage increases dramatically at wavelengths shorter than about 310 nm. The total dosage that an organism with this spectral susceptibility would receive is the integral of the area under the curves shown in Figure 2. The integrated doses from Figure 2, along with other spectral integrals and integrated biological doses, are given in Table 2. The effect of the enhanced UVB, reaching several thousand percent below 303 nm, is dramatic. It is interesting to note, also, that the effect of UVB, when defined as being 290-315 nm, is nearly twice that compared with the more popularly defined UVB of 290-320 nm.

TABLE 1. UV Monitoring Sites

Site	Longitude, deg.	Latitude, deg.	Established	Location
McMurdo	166.40E	77.51S	March 1988	Arrival heights
Palmer	64.03W	64.46S	May 1988	Clean air building
South Pole	0	90.00S	February 1988	Clear air building
Ushuaia, Argentina	68.00 W	54.59S	November 1988	CADIC*
Barrow, Alaska	156.78W	71.30N	Fall 1990	
La Jolla, California	117.3W	32.13N	1991	

*CADIC: Centro Austral de Investigaciones Cientificas, Argentina

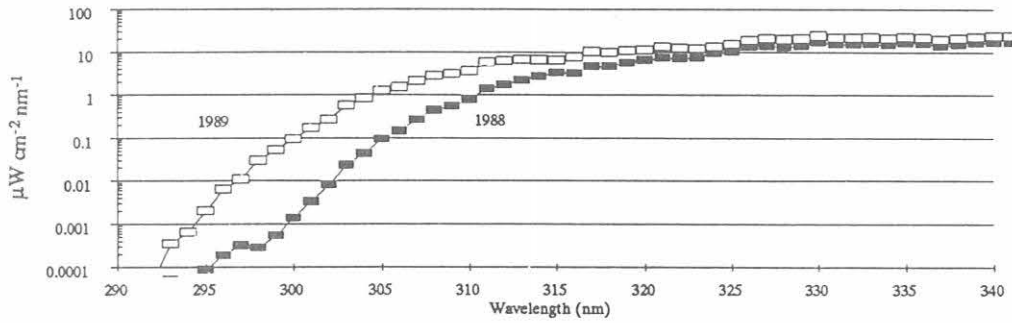


Fig. 1. Log plot of irradiance ($\mu\text{W cm}^{-2} \text{nm}^{-1}$) recorded at 0100 UT on October 20, in 1988 (solid boxes) and 1989 (hollow boxes). TOMS-reported total column ozone was 386 DU (Dobson Units) in 1988 and 161 DU in 1989.

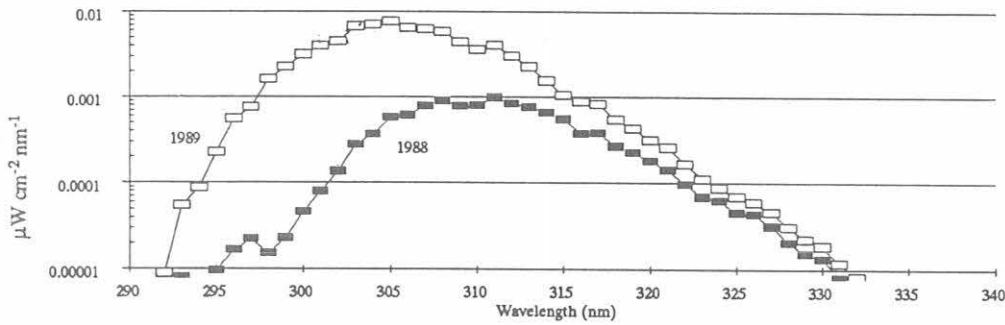


Fig. 2. Log plot of dose weighted irradiance ($\mu\text{W cm}^{-2} \text{nm}^{-1}$) recorded at 0100 UT on October 20, in 1988 (solid boxes) and 1989 (hollow boxes). Setlow's DNA action spectrum [Setlow, 1974] weighting was used.

TABLE 2. Comparisons of 24-h Averaged High Resolution Spectral Irradiance Recorded During October 20 in 1988 and 1989, and of Computed Biological Doses

	1988	1989	% Difference
<i>Irradiance, $\mu\text{W cm}^{-2}$</i>			
UVB (290-315 nm)	3.53	14.74	+317%
UVB (290-320 nm)	11.61	31.77	+174%
298-303 nm	0.006	0.213	+343%
UVA (320-400 nm)	602	786	+31%
Visible (400-600 nm)	2892	3811	+32%
<i>Biological Dose, $\mu\text{W cm}^{-2}$</i>			
Skin [Diffey, 1987]	0.84	2.56	+206%
DNA [Setlow, 1974]	0.003	0.023	+638%
Fish [Hunter, 1979]	0.02	0.074	+267%

TOMS ozone concentrations were 386 DU in 1988 and 161 DU in 1989, a difference of -58%.

Even with ozone highly depleted, the low sun angle at McMurdo on October 20 does not allow significant measurements of irradiance to be made below 290 nm.

For wavelengths shorter than 290 nm in the UVB portion of the spectrum, the effects of atmospheric ozone concentration on irradiance levels predominate the effects of cloud density. Figure 3 examines the period approaching October 20, 1989, as recorded by the spectroradiometer at McMurdo. During this period the total column ozone ranged from a maximum of 255 DU to a minimum of 161 DU, nearly a record low for McMurdo. The mid-UV irradiance (shown at 350 nm in Figure 4) varied only slightly during this period, possibly due to varying cloud densities; the shorter UV irradiance (at 300 nm Figure 3) is much more variable, and shows a strong correlation with ozone concentrations reported by the TOMS satellite. The high-frequency variability exhibited at fringe areas of the ozone hole presents challenges in assessing the effects of ozone depletion on living organisms. It also suggests that a profound biological impact might occur if a stationary region of ozone depletion were to occur over a region of high biological activity.

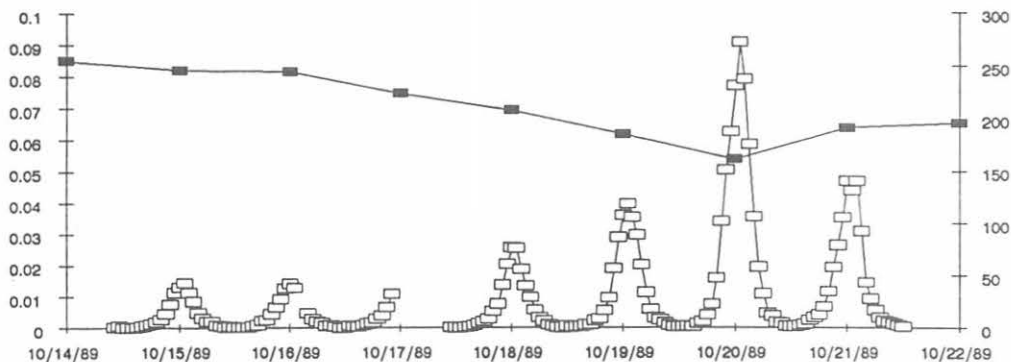


Fig. 3. Time series of irradiance and total ozone recorded at McMurdo station during passage over the station of an ozone-depleted region. The downtrending line with the solid boxes is the total column ozone (DU, right scale) reported by the TOMS satellite. The hollow boxes denote the irradiance ($\mu\text{W cm}^{-2} \text{nm}^{-1}$, left scale) at 300 nm. Solar zenith angle during the time of the measurements ranged from 66° to 92° .

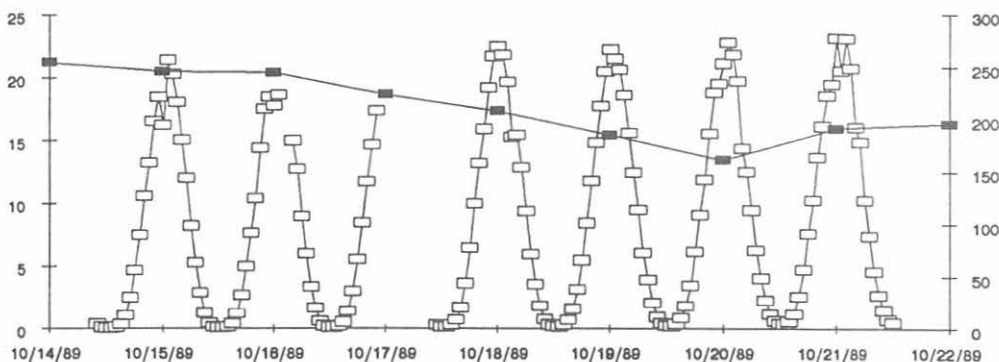


Fig. 4. Time series of mid-UV (350 nm) irradiance and total ozone recorded at McMurdo during passage over the station of an ozone-depleted region. The downtrending line with the solid boxes is the total column ozone (DU, right scale) reported by the TOMS satellite. The hollow boxes denote the irradiance ($\mu\text{W cm}^{-2} \text{nm}^{-1}$, left scale). Solar zenith angle during the time of the measurements ranged from 66° to 92° .

4. SUMMARY

The establishment of a monitoring network for UV radiation has been a critical part of the U.S. Antarctic Program. Its purpose is to evaluate the consequences of stratospheric ozone depletion on the health and productivity of Antarctic organisms and personnel. This monitoring network supports scientific researchers in Antarctica, and has provided independent confirmation of the role of the ozone layer in moderating UV solar irradiance.

Acknowledgment. This research and monitoring activity was funded by contract A9H074 to Biospherical Instruments from ITT Antarctic Services, Inc., and AOT-000010 from Antarctic Support Associates under direction of NSF, Division of Polar Programs. Data from the NSF

UV Spectroradiometer Network is available to all qualified researchers. NSF grantees have priority access to these data. For more information, contact Dr. Polly Penhale, Division of Polar Programs, National Science Foundation, 1800 G St. N.W., Washington, D.C. 20550.

5. REFERENCES

- Diffey, B L., A comparison of dosimeters used for solar ultraviolet radiometry, *Photochem. Photobiol.*, 46, 55-60, 1987.
- Hunter, J. H., J. H. Taylor, and H. G. Moser, The effect of ultraviolet irradiation on eggs and larvae of the northern anchovy, *Engraulis mordax*, and the pacific mackerel, *Scomber japonicus*, during the embryonic stage, *Photochem. Photobiol.*, 29, 325-338, 1979.
- Setlow, R. B., The wavelengths in sunlight effective in producing skin cancer: A theoretical analysis, *Proc. Nat. Acad. Sci. U.S.A.*, 71(9), 3363-3366, 1974.

Chemical Resolution of Fine Aerosol Mass at MLO: The Role of Organic Matter

T. A. CAHILL, L. K. WILKINSON, AND R. A. ELDRED

University of California, Davis, Crocker Nuclear Laboratory, Air Quality Group, Davis, California 95616

1. INTRODUCTION

On March 2, 1988, the U.S. remote-area fine particulate network (IMPROVE) [Eldred *et al.*, 1989] initiated routine monitoring of fine ($D_p < 2.5 \mu\text{m}$) particulate matter at MLO. The IMPROVE protocols allow for a complete resolution of fine mass into its components for the purpose of predicting the effects of aerosols on the scattering and absorption of light and the implications for visibility and the atmospheric radiation balance. Another IMPROVE station was initiated at about the same time at the Hawaii Volcanoes National Park (HAVO).

The protocols for MLO call for a continuous sample of approximately 3 days duration (MALO1) and a clean-air (downslope only) sample over the same 3-day period selected by the Maryland System (MALO2) (Zoller *et al.*, personal communication). Size segregation is accomplished through a nominally $2.5\text{-}\mu\text{m}$ cyclone (modified by altitude), and samples are collected on 25-mm stretched Teflon filters. Samples are mailed weekly to Davis, California, where analyses are done for (1) mass (gravimetric); (2) elemental content, Na to U (PIXE); (3) hydrogen (PESA); and (4) H, Be, B, C, N, O, and Na (FAST) [Cahill *et al.*, 1984]. With the availability of organic matter from the hydrogen content of the filters by means of PESA, we can now attempt a resolution of fine mass into all its chemical components.

2. RECONSTRUCTION OF FINE MASS

Figure 1 shows a comparison between the reconstruction of fine mass (sum of chemical species) to the fine mass measured by weighing the filters for the period March 1-November 30, 1989. The sample chosen was for downslope winds only (MALO2) March 1-November 30, 1989, but a similar result is available for the averaged sample (MALO1). The value of r^2 (0.96) and the intercept (1 ng m^{-3}) show that all measurements are precise and that systematic offset is negligible. The slope (0.84) shows that 84% of the weighted mass is recovered by this reconstruction. There are several possible reasons why this value is less than 100%. Most chemical species are measured in a vacuum, so volatiles such as water are driven from the sample. Further, the exact chemical state of the sulfur is uncertain. We normally assume ammonium sulfate at other remote U.S. sites, but that is not at all certain at MLO. Since across the United States we normally recover 93% of the gravimetric mass by this procedure, we suspect that the sulfates include a component of sulfuric acid and/or ammonium bisulfate, which would tend to raise the reconstructed mass above 90%. Finally, some components such as chlorides and nitrates are not incorporated into the reconstruction mass.

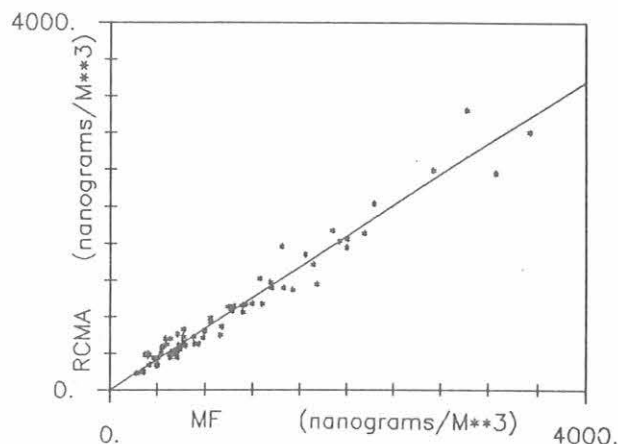


Fig. 1. Reconstructed fine mass (RCMA) versus measured fine mass (MF) for MLO, March 1-November 30, 1989, in downslope winds (MALO2). The slope is 0.84; $r^2 = 0.96$.

3. COMPARISON OF DATA FROM MLO AND HAVO

Further information may be gained by comparing the MLO data with similar data from the HAVO IMPROVE site near the Visitor Center, at an elevation of 1.25 km MSL (Table 1). At this site, nitrates and chlorides are also measured, and reconstructed mass closely matches weighted mass. If we assume that nitrates fall off from HAVO to MLO in proportion to the sulfates, and assume that chlorides in smoke from agricultural burning fall off in the same ratio, MLO reconstructed mass closely approximates the gravimetric mass also. However, this agreement cannot be taken too seriously because of uncertainties in the carbon soot conversion and the extrapolations.

Nevertheless, the comparison data are quite revealing in many areas. The importance of organic matter in downslope winds (MALO2) is somewhat surprising, considering the presumed strong organic-matter sources in Hawaiian vegetation, agricultural burning, and petroleum use. Yet, this does not appear to be the case for fine aerosols. We do not believe this is a measurement error, since the IMPROVE protocols call for two independent measurements of organic matter, one by combustion from quartz filters, and one by hydrogen from Teflon filters. The excellent agreement obtained for over 1300 samples by two different techniques (and two different laboratories) makes us confident that no major error exists in the MALO2 data [Cahill *et al.*, 1990].

4. COMPARISON OF AVERAGE TO DOWNSLOPE WIND SAMPLES AT MLO

To understand the relatively elevated organic matter present in the downslope-wind (MALO2) samples, we can

TABLE 1. Comparison of Aerosols

Parameter Measured	HAVO, ng m ⁻³	MLO	
		MALO1 (Average), ng m ⁻³	MALO2 (Downwind Only), ng m ⁻³
<i>Coarse Aerosols (D_p < 10 μm)</i>			
Mass	14,501	NA	NA
<i>Fine Aerosols (D_p < 2.5 μm)</i>			
Mass (gravimetric)	1825	1107	893
<i>Major Species</i>			
Sulfates [as (NH ₄) ₂ SO ₄]	870	629	430
Chlorides*	312	130 (E1)	99 (E1)
Organic matter (H)	129	86	149
Nitrates (as NH ₄ NO ₃)	98	71 (E2)	48 (E2)
Soils	93	105	82
Soot carbon (?)†	190	165	99
	<u>1692</u>	<u>1186</u>	<u>907</u>
<i>Tracer Species</i>			
Nonsoil potassium (smoke)	9.1	3.8	2.9
Vanadium	0.6	0.2	0.4‡
Nickel	0.4	0.1	0.2
Copper	0.6	0.2	0.4
Zinc	1.7	0.6	0.6
Arsenic	0.2‡	<0.1	<0.1
Selenium	0.3‡	<0.1	<0.1
Bromine	0.8	0.3	0.4
Lead	1.0	0.4	0.5

E1 = Extrapolated based on nonsoil potassium, since sea-level source.

E2 = Extrapolated based on sulfates.

*As NaCl—496 ng m⁻³.

†Conversion from optical absorption to soot carbon mass estimated—no local calibration.

‡Less than 30% of values above minimum detectable limit.

examine the other major components, namely, sulfur (sulfates) and organic matter, shown in Figures 2 and 3. Although the patterns are clearly uncorrelated, more information can be gained by examining sulfur in average (MALO1) and downslope-wind samples, shown in Figure 4. Sulfur in the average samples is always greater than or equal to sulfur in the downslope-wind samples, very much like gravimetric mass. This is not the case for organic matter (Figure 5), which shows both poor correlation between MALO1 and MALO2 samples, and numerous times when organics in downslope winds were higher than averaged values, in agreement with data in Table 1. Thus, it is not surprising that organic matter and sulfur are essentially uncorrelated (Figure 6), having $r^2 = 0.17$.

What does correlate with organic matter in downslope wind samples? The two components that correlate best are both tracers of smoke: optical absorption, expressed as soot carbon (Figure 7), and nonsoil potassium, which is typically 5 to 8% of smoke mass (Figure 8). Thus, the conclusion

must be that most of the organic matter is due to smoke, despite the fact that it occurs in downslope winds. The evidence of sulfur, however, hints that the smoke organics are not Hawaiian, or they too would follow the pattern of Figure 4. Further support for this hypothesis is provided by the observation that organic matter peaks during periods of dust transport from Asian sources [Cahill *et al.*, 1989].

There exists, however, an organic component not associated with smoke, as shown by the nonzero intercept of both graphs. From 50 ng m⁻³ (absorption intercept) to 100 ng m⁻³ (nonsoil potassium intercept) of the organic matter is not smoke related, the non-smoke-related organic matter being as large as 270 ng m³ on some days.

5. CONCLUSION

In conclusion, a reasonable reconstruction of fine gravimetric mass has been made at MLO for both daily average conditions and downslope-wind conditions. Fine

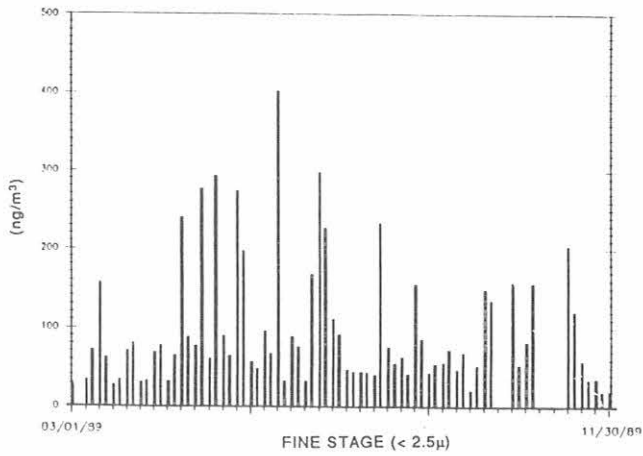


Fig. 2. Fine particulate sulfur at MLO in downslope winds (MALO2). Some data are missing, October 1989.

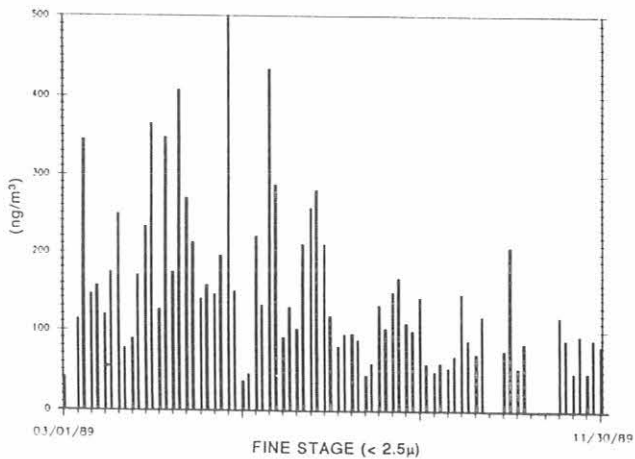


Fig. 3. Fine particulate organic mass from hydrogen at MLO in downslope winds (MALO2). Some data are missing, October 1989.

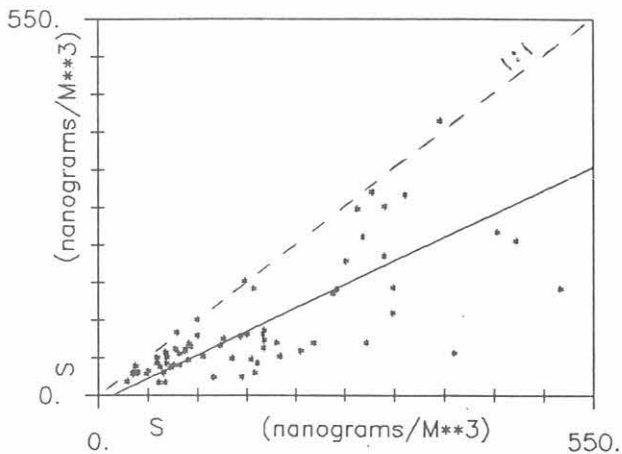


Fig. 4. Fine particulate sulfur, MALO1 (x-axis), versus MALO2 (y-axis), March 1-November 30, 1989. The averaged values (MALO1) are always greater than or equal to values in downslope winds (MALO2) as indicated by the dashed line in the figure.

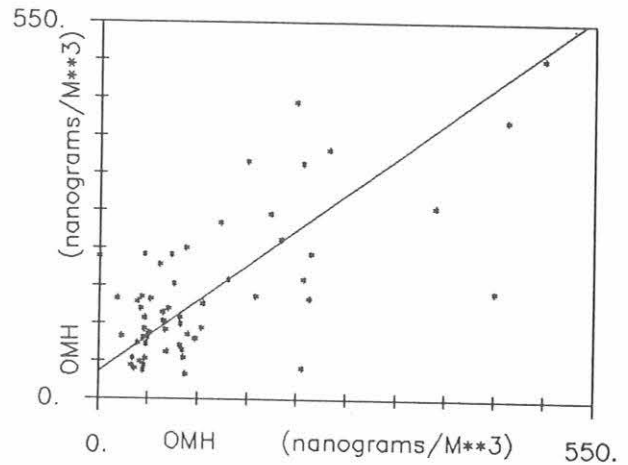


Fig. 5. Fine particulate organic matter, MALO1 (x-axis), versus MALO2 (y-axis), March 1-November 30, 1989. Compare with Figure 4.

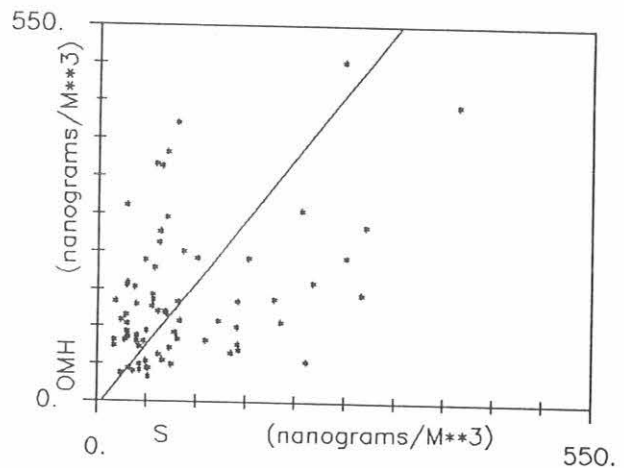


Fig. 6. Fine particulate sulfur versus organic matter at MALO2, March 1-November 30, 1989. Note the lack of correlation; $r^2 = 0.17$.

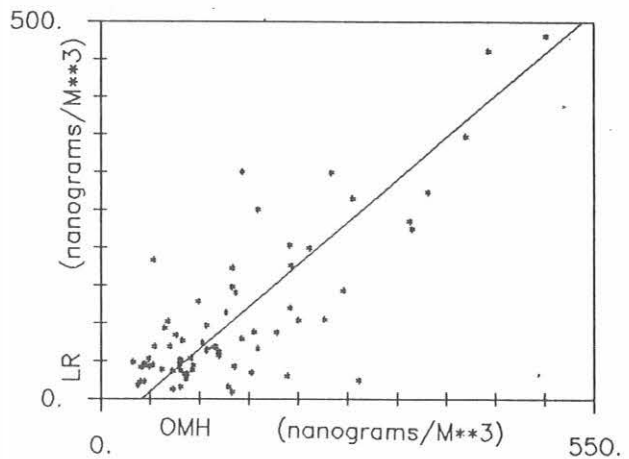


Fig. 7. Optical absorption (LR) versus fine particulate organic matter (OMH) at MALO2, March 1-November 30, 1989. The correlation $r^2 = 0.64$; the slope is 1.02.

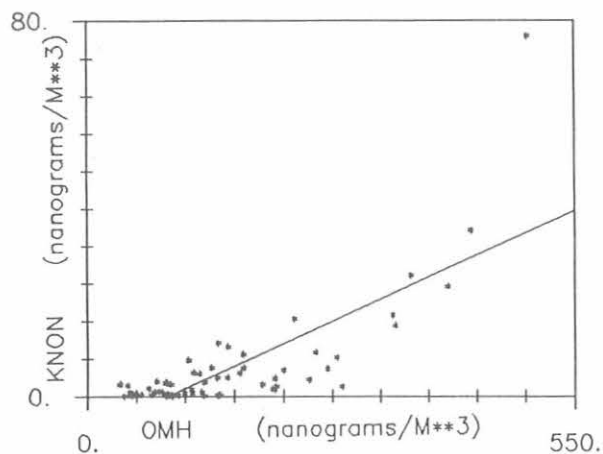


Fig. 8. Excess fine potassium (KNON), a smoke tracer, versus organic matter (OMH) at MALO2, March 1-November 30, 1989. The correlation $r^2 = 0.60$.

aerosol mass at MLO at 3.47 km averages about 60% of that at the HAVO Visitor Center at 1.25 km, while the downslope component averages about 50% of that of the HAVO site. One might expect much lower values at MLO, but this is not

the case. Even more surprising is that organic matter is greater in MLO downslope winds than at HAVO. We have tentatively separated the organic matter into a smoke-related component (~60% of organic mass) and a non-smoke-related component (~40% of organic mass). With the availability of a full year's data, further studies are planned to examine the two components relative to meteorological conditions, with the goal of confirming the Asian source of organic matter.

6. REFERENCES

- Cahill, T.A., R.A. Eldred, D. Shadoan, P.J. Feeney, B.H. Kusko, and T. Matsuda, Complete elemental analysis of aerosols: PIXE, FAST, LIPM, and mass, *Nucl. Instrum. Meth.*, B3, 291-295, 1984.
- Cahill, T.A., L.K. Wilkinson, P. Beveridge, and T. Tanada, Fine particulate matter at Mauna Loa Observatory March 1988 to February 1989, in *Geophysical Monitoring for Climatic Change, No. 17: Summary Report 1988*, edited by J.W. Elkins and R.M. Rosson, pp. 82-84, NOAA Air Resources Laboratory, Boulder, CO, 1989.
- Cahill, T.A., R.A. Eldred, L.K. Wilkinson, and B.P. Perley, Spatial and temporal trends of fine particles at remote U.S. sites, Paper 90-66.4 presented at the 83rd Annual Meeting and Exhibition, Air and Waste Management Association, Pittsburgh, PA, June 24-29, 1990.
- Eldred, R.A., T.A. Cahill, L.K. Wilkinson, P.J. Feeney, and W. Malm, Particulate characterization at remote sites across the U.S.: First-year results of the NPS/IMPROVE Network, *Proceedings of Annual Meeting, Air and Waste Management Association*, Anaheim, CA, paper 89-151.3, 1989.

Artificial Windshielding of Precipitation Gauges in the Arctic

GEORGE P. CLAGETT

Soil Conservation Service, Anchorage, Alaska 99501

1. INTRODUCTION

Precipitation gauges can provide good measurements of the water equivalent of snow precipitation, provided the gauge is protected or shielded from wind effects. Unfortunately, there are no standards for collecting snow precipitation. Gauges located in exposed and windy areas may be totally unshielded, partially shielded by one or more buildings, or equipped with one of several types of artificial shields. The various shielding options in common use, therefore, produce a wide range of gauge catch efficiency. Also, the various studies of artificial shields in the United States and Canada have produced a wide range of results. This must be, in part, due to the wide range of weather conditions under which the various studies have been conducted. A lingering problem is applying the results to the local conditions of Alaska's tundra regions.

2. METHODS

A study of the windshield alternatives, under the unique conditions of Alaska's Arctic coastal region, was set up at the CMDL facility at BRW during September 1989. Snowfall catches from four newly installed precipitation storage gauges were compared with that from an existing storage gauge protected by a Wyoming shield [Hanson, 1988]. Two of the new gauges were shielded—one with a Nipher shield [Goodison *et al.*, 1983] and the other with an Alter shield [Alter, 1937]—and two were unshielded. One of the unshielded gauges was serviced on an event basis, the same as the three shielded gauges. The other unshielded gauge was treated as if it were a remote gauge, allowing rime to build up and dissipate naturally to see what effects rime had on the overall catch. The four newly installed gauges are 20.3 cm in diameter \times 100 cm tall, mounted with the orifice 2 m above the normal ground surface. The existing Wyoming-shielded gauge is 30.5 cm in diameter \times 2 m tall, and is equipped with a Leupold-Stevens water-level recorder.

3. RESULTS

Provisional results from the 1989-1990 winter season indicate that the Wyoming-shielded gauge provided slightly more than 6.0 cm of snowfall water-equivalent catch. The Nipher-shielded gauge caught 3.9 cm of water-equivalent precipitation, or only 64% of that of the Wyoming-shield gauge. The Alter-shielded gauge caught 2.9 cm, or slightly less than half that caught by the the Wyoming-shielded gauge. The unshielded but serviced gauge caught only 1.7 cm of water-equivalent snowfall which was less than 28% of that of the Wyoming-shielded gauge. The unshielded and non-serviced gauge caught the least amount of snowfall, only 1.1 cm water equivalent, or 17% of the snowfall caught by the Wyoming-shielded gauge.

These results are generally what was expected with one exception: the Nipher-shielded gauge was expected to catch as much snow as did the Wyoming-shielded gauge. The results otherwise confirm that the unshielded and Alter-shielded gauges do not catch adequate amounts of precipitation at exposed and windy locations during snowfall events.

Acknowledgment. Appreciation is expressed to D. Endres, Station Chief, BRW, who serviced the precipitation gauges and collected the snow samples.

4. REFERENCES

- Alter, G.C., Shield storage precipitation gauges, *Mon. Weather Rev.*, 65, 262-265, 1937.
- Goodison, B.E., V.R. Turner, and J.E. Metcalfe, A nipher-type shield for recording precipitation gauges, *Proceedings, 5th Symposium on Meteorological Observations and Instrumentation*, Toronto, Ontario, Canada, pp. 2-126, American Meteorological Society, Boston, 1983.
- Hanson, C.L., Precipitation measured by gages protected by the Wyoming shield and the dual-gauge system, *Proceedings, 56th Western Snow Conference*, Kalispell, Montana, pp. 174-177, Colorado State University, Fort Collins, 1988.

UVB Monitoring Data from Rockville, Maryland

DAVID L. CORRELL, CARL CLARK, RUSSELL GOODRICH, AND DOUGLASS HAYES

Smithsonian Environmental Research Center, P.O. Box 28, Edgewater, Maryland 21037

Our laboratory has been continuously monitoring surface irradiance in a series of eight 5-nm band passes in the UVB at various locations on the Earth's surface with high-precision, accurately calibrated, interference-filter spectral radiometers. Significant data sets have been collected at BRW (71°N); Rockville and Edgewater, Maryland (39°N); Tallahassee, Florida (30°N); MLO (19°N); Republic of Panama (9°N); and SPO (90°S). Long-term data sets are now being edited and analyzed for publication and archiving; these sets include data from 1976 to the present at Rockville and from August 1984 to the present at MLO.

Data editing includes checking for file consistency; screening for data processing and file maintenance errors by testing for unreasonable ratios between channels, times of sunrise and sunset, and effects of cloud cover; and correcting for calibration changes, malfunctioning equipment, and altered equipment design.

Rockville data from 1976 through 1989 have now been edited and are archived on 9-track computer tapes. These data are available in archived format on floppy discs with a de-archiving manual and software, for \$100. Extensive analyses of these data are in progress, and a few highlights are reported here. Requests for data and additional information should be directed to David L. Correll, Director, at the above address.

A new-generation, 18-channel, interference-filter spectral radiometer is nearly ready for field operation. In the UVB it will have 2-nm band pass filters. This instrument features not only better spectral resolution and modern electronics, but also improved PC-based data acquisition and microprocessor-controlled choices of set gains over 3 orders of magnitude for different channels in the same operational instrument. Both the present radiometers and the radiometers under development operate as cosine light collectors to measure global irradiance. We are currently surveying possible additional station sites in order to attain an optimal range of latitudes for future data collection.

Dobson spectrophotometer ozone data from Wallops Island, Virginia (Figure 1), were used to drive the Green model [Rundel, 1986; Green, 1983; Green et al., 1980; Schipnick and Green, 1982] for calculations of predicted UVB flux incident on Earth at 39°N latitude under clear-sky conditions and at a fixed solar secant. These predictions were then compared with actual data from Rockville under those conditions (Figures 2-4). In these comparisons we used the effective center wavelength for the appropriate spectra radiometer channel. These effective center wavelengths were obtained by convoluting the appropriate interference filter and blocking filter transmission curves, detector spectral response curves, and calibration lamp and global irradiance spectral curves. In Figure 2, 305-nm monitoring data at a morning solar secant of 2.5 for clear-sky

days are compared with Green model predictions. The results are generally close. In Figures 3 and 4, monitoring data for 305 and 320 nm, respectively, at morning secants of 1.5 under clear-sky conditions are compared with Green model predictions. For 305-nm data, the comparisons are close, although a secular variation is evident in the observational data for which we currently have no satisfactory explanation. For the 320-nm data, the model predictions are consistently about 10-20% higher than the monitoring data. This is probably due to the effects of atmospheric gases such as SO₂, and to aerosols, whose effects are not included in the model calculations. Certainly the changes in global irradiance we are reporting are not due to significant changes in UVB radiation incident on the earth's atmosphere [Lean, 1989].

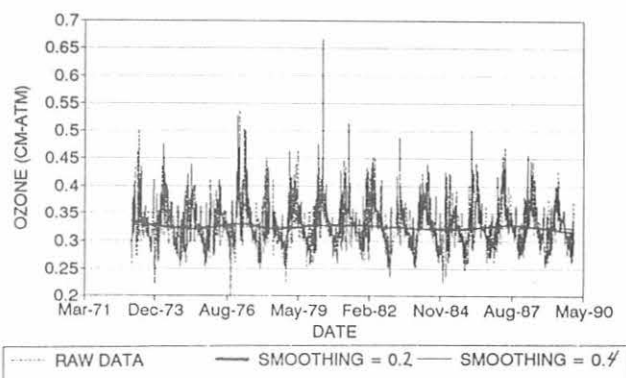


Fig. 1. Dobson spectrophotometer ozone data from the Wallops Island station, used as inputs to the Green model.

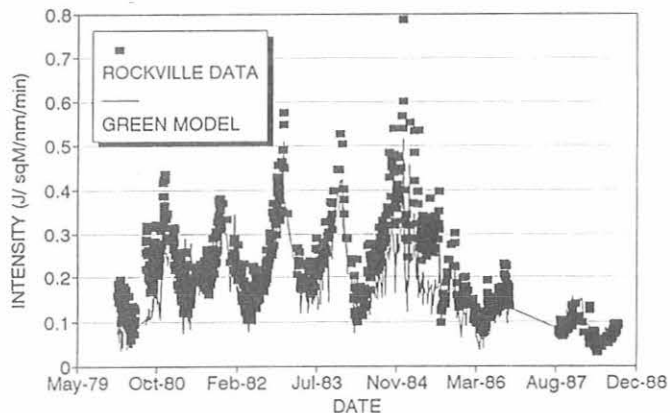


Fig. 2. Comparison of Green model predictions with Rockville, Maryland (30°N), UVB fluxes at 305 nm on clear days at a solar secant of 2.5.

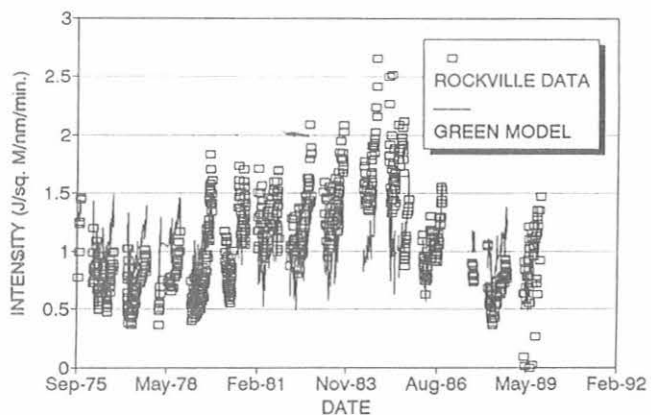


Fig. 3. Comparison of Green model predictions with Rockville, Maryland (39°N), UVB fluxes at 305 nm on clear days at a solar secant of 1.5.

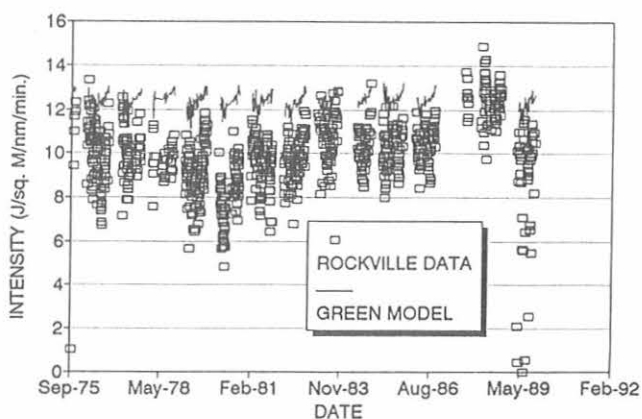


Fig. 4. Comparison of Green model predictions with Rockville, Maryland (39°N), UVB fluxes at 320 nm on clear days at a solar secant of 1.5.

REFERENCES

Green, A.E.S., The penetration of ultraviolet radiation to the ground, *Physiol. Plant*, *58*, 351-359, 1983.
 Green, A.E.S., KR. Cross, and L.A. Smith, Improved analytic characterization of ultraviolet skylight, *Photochem. Photobiol.*, *31*, 59-65, 1980.
 Lean, J., Contribution of ultraviolet irradiance variations to

changes in the sun's total irradiance, *Science*, *244*, 197-200, 1989.
 Rundel, R., Subroutine for Schippnick and Green model, in *Stratospheric Ozone Reduction, Solar Ultraviolet Radiation and Plant Life*, edited by R.C. Worrest and M.M. Caldwell, pp. 361-364, Springer-Verlag, Berlin, 1986.
 Schippnick, P.F., and A.E.S. Green, Analytical characterization of spectral actinic flux and spectral irradiance in the middle Ultraviolet, *Photochem. Photobiol.*, *35*, 89-101, 1982.

Roberston-Berger UVB Meter

GERALD F. COTTON

NOAA, Air Resources Laboratory, Silver Spring, Maryland 20910

1. INTRODUCTION

MLO has served as one of the original 10 monitoring sites for the Robertson-Berger (R-B) sunburning meter network since its inception in 1974. An additional 35 sites, including 11 non-U.S. sites, distributed unevenly worldwide, have operated with varying lengths of record. The period of record of the individual R-B observing sites is given in Table 1. Until June 1989, the Skin and Cancer Hospital of Temple

University has maintained the network, principally with contract support from the NIH, DOT, and EPA, and with extensive field support by NOAA's ERL and NWS. Because the Skin and Cancer Hospital closed this year, the operation of the network is being reviewed to determine whether measurements should be continued to overlap with measurements by more sophisticated instrumentation. The National Cancer Institute of NIH retains the data archive along with ancillary meteorological information.

TABLE 1. Robertson-Berger Meter Network Period of Record and Number of Complete Years of Data Through 1987

Station	Period of Record	Years of Data
<i>U.S. Stations</i>		
1. Albuquerque, NM	Jan. 1974-Present	12
2. Atlanta/Emory, GA	Oct. 1977-Sept. 1987	7
3. Bismarck, ND	Jan. 1974-Feb. 1987	11
4. Burlington, VT	Oct. 1985-Present	2
5. Concord, NH	Oct. 1985-Present	2
6. Des Moines, IA	Jan. 1974-Dec. 1987	9
7. Detroit, MI	Sept. 1977-Present	10
8. El Paso, TX	Jan. 1974-Present	13
9. Ft. Worth, TX	Jan. 1974-Present	14
10. Gainesville, FL	Jan. 1975-Aug. 1980	2
11. Honeybrook, PA	Jan. 1975-July 1985	10
12. La Jolla, CA	May 1979-Mar. 1983	3
13. Lihue, HI	Feb. 1987-Present	0
14. Mauna Loa, HI	Jan. 1974-Present	12
15. Miami, FL	May 1986-Present	0
16. Minneapolis, MN	Jan. 1974-Present	13
17. New Orleans, LA	Nov. 1977-Present	4
18. Oakland/Redwood City, CA	Jan. 1974-Present	12
19. Philadelphia, PA	Jan. 1974-Present	14
20. Pt. Barrow, AK	Oct. 1978-Present	8
21. Rockville, MD	Sept. 1978-July 1985	5
22. Salt Lake City, UT	Oct. 1977-Present	9
23. Seattle, WA	Oct. 1977-Present	9
24. Tallahassee, FL	Jan. 1974-May 1986	12
25. Tucson, AZ	Jan. 1980-Present	6
<i>Non-U.S. Stations</i>		
1. Brisbane, Australia	Oct. 1974-April 1981	7
2. Melbourne, Australia	Dec. 1974-Nov. 1986	11
3. Hamburg, Germany	Feb. 1976-June 1983	5
4. Hamilton, New Zealand	May 1980-Present	3
5. Invercargill, New Zealand	Sept. 1981-Oct. 1985	2
6. Barro Colorado, Panama	Nov. 1978-Present	3
7. Belsk, Poland	May 1975-Present	11
8. Warsaw, Poland	June 1975-Sept. 1976	1
9. Nörrköping, Sweden	Oct. 1982-Present	4
10. Basel, Switzerland	Mar. 1980-Present	7
11. Davos, Switzerland	Jan. 1975-Present	13

2. INSTRUMENTATION AND DATA

The R-B meter was selected in the early 1970's as a UV-monitoring instrument at the surface for the Climatic Impact Assessment Program [CIAP, 1975] sponsored by the DOT in reaction to concerns about possible climate impacts by the projected supersonic air transportation fleet. The instrument, described by Berger [1976], detects radiation in the UVB wavelength band, 295-330 nm. The meter response declines logarithmically such that the response at 330 nm is 1/100th that at 295-300 nm. Although the performance of the R-B meter has always been controversial, especially with respect to the wide UVB bandwidth and more recently with possible long-term instability (calibration drift) [Scotto *et al.*, 1988], it has proved to be a rugged, reliable instrument in the field. The Temple University staff maintained individual instrument calibrations, which were performed annually through mid-1989 except for an unfunded period from mid-1983 to mid-1985. There were several comparisons of the R-B meter with more sophisticated instruments, obtaining side-by-side measurements over varying time periods [Mo *et al.*, 1975; Machta *et al.*, 1976; Barton, 1983; and Paltridge and Barton, 1978]. In addition, DeLuisi and Harris [1983] performed an important, though limited, study of the meter behavior, providing estimates of the radiant energy of the somewhat arbitrary R-B sunburn units of measurement under certain conditions. Finally, there have been efforts to modify the meter sensor in order to more nearly match the erythema (McKinlay-Diffey action spectrum) response function. Berger [1989] prepared two "thin phosphor" instruments that were operated for approximately 1 year each at McMurdo and Temple University. Data from these instruments are unavailable at this writing. The published results of the CSIRO Australian network (1975-1981) include both types of instrumentation [Barton, 1983; Paltridge and Barton, 1978].

The data from the R-B observing sites are retained as half-hourly sunburn units, which are archived with daily and monthly sunburn-unit totals and with observed daily and monthly Dobson spectrophotometer total ozone values, percent sunshine, total cloudiness, and broadband solar radiation amounts, where these are available. These data may be obtained from Joseph Scotto, National Cancer Institute, NIH, Public Health Service, Bethesda, MD 20892.

3. REFERENCES

- Barton, I.J., The Australian UV-B monitoring network, *Technical Paper No. 46*, 12 pp., CSIRO, Division of Atmospheric Physics, Melbourne, Australia, 1983.
- Berger, D., The sunburning ultraviolet meter: Design and performance, *Photochem. Photobiol.*, 24, 587, 1976.
- Berger, D., Product Brochure, Solar Light Co., Philadelphia, Pennsylvania, 1989.
- CIAP (Climate Impact Assessment Program), Impacts of climatic change on the biosphere, *CIAP Monograph 5, Final Report, DOT-TST-75-55*, Department of Transportation, Washington, DC, 1975.
- DeLuisi, J., and J. Harris, A determination of the absolute radiant energy of a Robertson-Berger Meter sunburn unit, *Atmos Environ.*, 17(4), 751-538, 1983.
- Machta, L., G. Cotton, W. Hass, and W. Komhyr, Erythema ultraviolet solar radiation and environmental factors, *Proc. of the Fourth Conference on the Climatic Impact Assessment Program, DOT-TSC-OST-75-38*, pp. 405-411, National Technical Information Service, Springfield, VA, 1976.
- Mo, T., A.T. Chai, and A.E.S. Green, An absolute calibration of the sunburn meter, *CIAP Monograph 5, Appendix L*, Department of Transportation, Washington, DC, 1975.
- Paltridge, G.W., and I.J. Barton, Erythema ultraviolet radiation distribution over Australia: Calculation, detailed results, and input data, *Technical Paper No. 33*, 48 pp., CSIRO, Division of Atmospheric Physics, Melbourne, Australia, 1978.
- Scotto, J., G. Cotton, F. Urbach, D. Berger, and T. Fears, Biologically effective ultraviolet radiation: Surface measurements in the United States, 1974-1985, *Science*, 239, 762-764, 1988.

The CSIRO Latitudinal Gradient Study: Methane Data from Air Samples Collected at CMDL Baseline Observatories and at Cape Grim, Tasmania

PAUL FRASER, PAUL STEELE, ROGER FRANCEY, AND GRAEME PEARMAN

CSIRO, Division of Atmospheric Research, Aspendale, Victoria, Australia 3195

1. INTRODUCTION

In 1983 the CSIRO Division of Atmospheric Research, with the logistical support of NOAA/CMDL, commenced flask sampling of air at the four CMDL baseline atmospheric observatories. The principal purpose of this sampling program is to measure the isotopic composition (^{13}C and ^{18}O) of atmospheric CO_2 , and to assess seasonal and geographic variations in these species [Francey *et al.*, 1989]. In addition to the isotopic analyses of CO_2 , the 5-L flask samples are also analyzed at CSIRO for CH_4 , CO , and CO_2 , by the method of gas chromatography, using a flame ionization detector [Fraser, 1984; Fraser *et al.*, 1986; P. J. Fraser *et al.*, Methane in the southern troposphere: Observations and analysis, in preparation, 1990]. In this report we present the CSIRO CH_4 data from the 5-L flask samples, together with the CSIRO record of atmospheric CH_4 measured at Cape Grim, Tasmania, for 1984-1988. We compare these data with the CH_4 mixing ratios obtained by the CMDL program through flask sampling at the same five sites [Steele *et al.*, 1987; Lang *et al.*, 1990a, b].

2. DATA

The CSIRO monthly mean CH_4 data from the CMDL observatory sites and from Cape Grim are given in Tables 1-5. These CSIRO data are shown in Figure 1, with monthly average data obtained by CMDL at the same sites from air samples collected in 0.5-L glass flasks [Steele *et al.*, 1987; Lang *et al.*, 1990a, b]. The CSIRO data are referenced to a calibration scale that was derived from several calibrated natural air standards supplied by OGIST (formerly OGC) [Rasmussen and Khalil, 1981; Fraser *et al.*, 1986]. In a similar fashion, the CMDL data are referenced to a calibration scale based on two tanks of calibrated natural air purchased from OGIST in 1983-1984 [Lang *et al.*, 1990a].

3. DISCUSSION

Inspection of Figure 1 reveals a striking level of agreement between the two data sets. For each month at each site we calculated, when possible, the ratio of the CMDL value to the CSIRO value. The average values of these ratios for each site are shown in Table 6. At all sites these average ratios are not significantly different from unity (Table 6). There are noticeable differences between the two programs for specific months at BRW, MLO, and SMO. Almost certainly these are due to the lower sampling frequency in the CSIRO program; a representative monthly mean mixing ratio is not always captured.

TABLE 1. Monthly Mean CH_4 Data (ppbv) From 5-L Glass Flask Samples Collected at BRW During 1984-1988 and Analyzed at CSIRO

Month	1984	1985	1986	1987	1988
Jan.		1725	1749	1766	1786
Feb.	1742				
March	1718	1743		1796	
April		1738	1778	1753	
May	1703	1727	1744	1751	1752
June	1702	1708	1730		1738
July				1739	1755
Aug.	1706	1722	1711	1728	1736
Sept.	1705	1745			
Oct.	1715		1775		1777
Nov.	1725			1774	1811
Dec.	1760	1767		1779	
Annual Mean	1720	1734	1748	1761	1765

The average number of flasks filled per month is two.

TABLE 2. Monthly Mean CH_4 Data (ppbv) From 5-L Glass Flask Samples Collected at MLO During 1984-1988 and Analyzed at CSIRO

Month	1984	1985	1986	1987	1988
Jan		1649	1671	1670	
Feb.	1658	1642		1676	1687
March	1630	1664		1658	1696
April	1639	1653	1672	1669	
May	1617	1659	1650		1674
June	1627	1651	1637	1680	1676
July	1618	1647		1667	1675
Aug.	1622	1628	1663	1651	1689
Sept.	1652	1631	1632	1653	1692
Oct.	1640	1672	1691	1697	1668
Nov.	1636	1665	1663	1679	
Dec.	1638	1662	1669	1661	1725
Annual Mean	1634	1652	1661	1669	1687

The average number of flasks filled per month is two.

The results shown in Table 6 indicate that, in an average sense, there is very good agreement between the CMDL and CSIRO measurements of atmospheric CH_4 . It is notable that the two sites at which the standard deviation of the average ratio of the monthly mean concentrations is lowest (Cape Grim and South Pole) are those sites where we expect the

TABLE 3. Monthly Mean CH₄ Data (ppbv) From 5-L Glass Flask Samples Collected at SMO During 1984-1988 and Analyzed at CSIRO

Month	1984	1985	1986	1987	1988
Jan.		1571	1612	1619	1607
Feb.					1634
March	1563	1586		1619	1618
April	1572	1591	1598	1607	1628
May	1578	1591	1611	1604	1638
June	1575	1593		1613	1629
July	1586	1601	1616	1626	1638
Aug.	1587	1591	1614	1625	1637
Sept.	1586	1599	1610	1631	1635
Oct.	1588	1604	1608	1627	1636
Nov.		1594	1604		
Dec.	1590	1602	1602	1620	1650
Annual Mean	1581	1593	1608	1619	1632

The average number of flasks filled per month is one.

TABLE 4. Monthly Mean Methane Data (ppbv) From 5-L Glass Flask Samples Collected at SPO During 1984-1988 and Analyzed at CSIRO

Month	1984	1985	1986	1987	1988
Jan.		1570	1581	1599	
Feb.	1551	1568		1596	1607
March	1551	1569	1584	1596	1606
April	1555	1574	1582	1600	1605
May	1565	1583	1589	1606	1612
June	1573	1591	1600	1615	1619
July	1581	1594	1606	1619	1627
Aug.	1586	1603	1611	1626	1635
Sept.		1602	1616	1629	1635
Oct.	1587	1602		1627	1639
Nov.	1586	1596	1611	1628	1635
Dec.	1578	1587	1607	1613	
Annual Mean	1571	1587	1599	1613	1622

The average number of flasks filled per month is one.

lowest short-term variability in atmospheric CH₄ concentrations, because they are the most distant from the known CH₄ sources (largely concentrated in the northern hemisphere). These findings suggest that the overall level of agreement between the CH₄ calibration scales in these two programs is better than about 3 ppbv. For a more precise definition of the relationship between these calibration scales, we need to carry out a regular exchange of appropriate standard gases. This has now commenced.

TABLE 5. Monthly Mean CH₄ Data (ppbv) From Glass and Stainless Steel Flask Samples Collected at Cape Grim, Tasmania, During 1984-1988 and Analyzed at CSIRO

Month	1984	1985	1986	1987	1988
Jan.	1561	1569	1583	1598	1615
Feb.	1557	1565	1580	1593	1606
March	1556	1569	1583	1597	1606
April	1565	1574	1588	1604	1612
May	1572	1582	1599	1612	1620
June	1579	1586	1601	1615	1626
July	1585	1594	1610	1626	1634
Aug.	1593	1602	1614	1628	1638
Sept.	1591	1603	1616	1628	1642
Oct.	1587	1602	1616	1630	1642
Nov.	1584	1597	1612	1626	1634
Dec.	1580	1588	1606	1619	1628
Annual Mean	1574	1586	1601	1615	1625

The average number of flasks filled per month is 20-25

TABLE 6. Average of the Monthly Mean CH₄ Concentration Ratios (CMDL/CSIRO) Observed at the Five Sites for 1984-1988

Station	Ratio	No. Months
BRW	1.000 (0.007)	39
MLO	1.000 (0.008)	51
SMO	1.000 (0.006)	50
Cape Grim	1.000 (0.002)	57
SPO	1.000 (0.003)	54

The number in parentheses is one standard deviation of the mean. The last column refers to the number of months in which a monthly value was obtained from both programs.

Other important elements to consider in the comparison of the CSIRO and CMDL CH₄ data sets are the differences between the two programs in both flask types and sampling methods. The latter has been the subject of an ongoing cooperative study at Cape Grim since 1984. The first results of this study have been reported by *Steele et al.* [1989] and *Conway et al.* [1990], and indicate clearly that there are no significant differences in the CH₄ concentrations obtained when air samples are collected by the different sampling methods. To address the issue of different flask types, a very detailed comparison of the CSIRO and CMDL flask records at Cape Grim is now being undertaken.

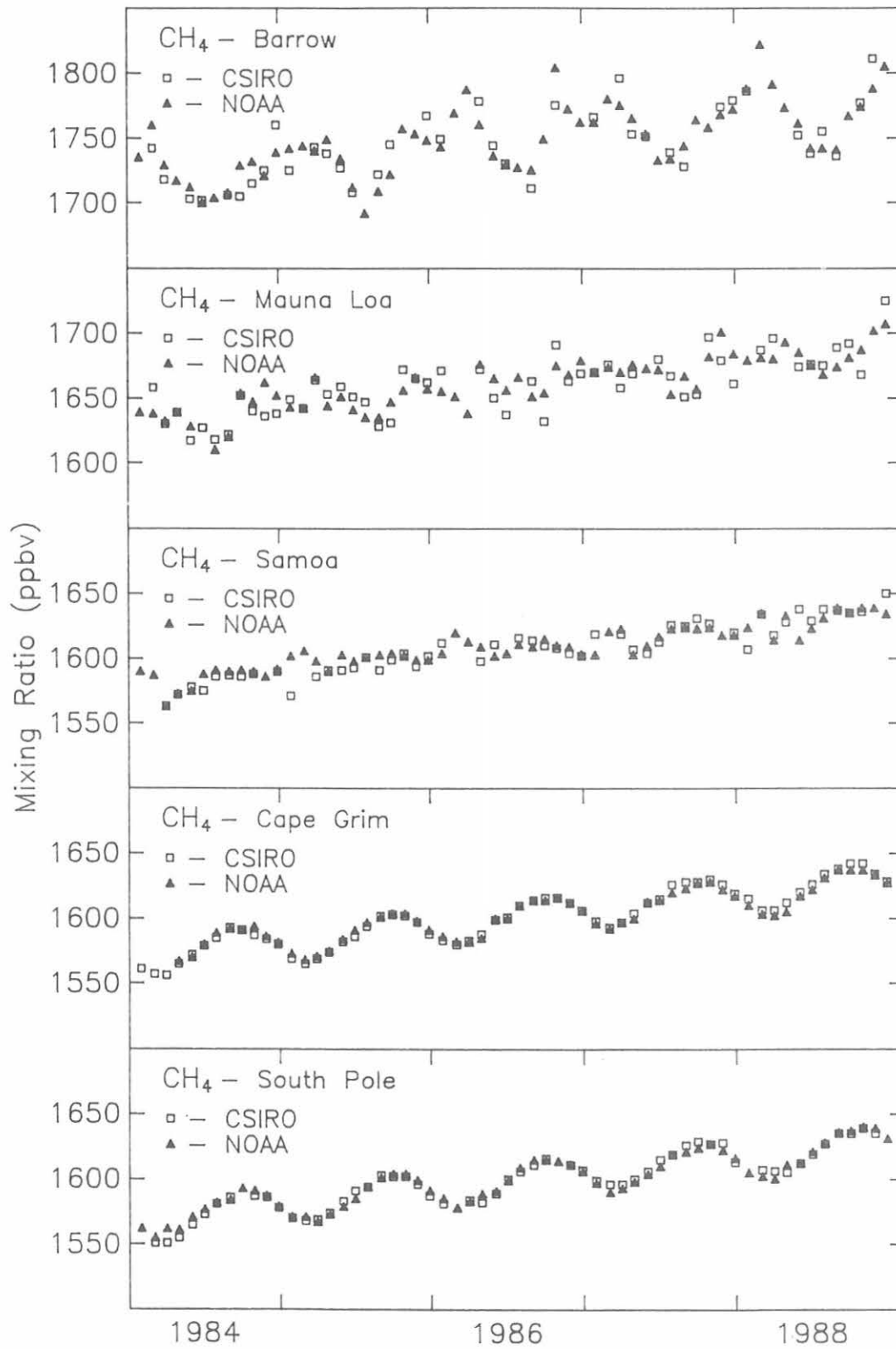


Fig. 1. Monthly mean CH_4 mixing ratios (ppbv) from air samples collected in 5-L glass flasks at the four CMDL baseline observatories and in glass and stainless steel flasks at Cape Grim, Tasmania, all analyzed at CSIRO (open squares). The monthly mean data at these five same sites from the CMDL program are also shown (filled triangles).

4. REFERENCES

- Conway, T.J., L.P. Steele, P.M. Lang, and L.S. Waterman, NOAA/GMCC carbon dioxide and methane measurements at Cape Grim, in *Baseline Atmospheric Program (Australia) 1988*, edited by S. Wilson and G.P. Ayers, CSIRO, Melbourne, Australia, in press, 1990.
- Francey, R.J., P.J. Fraser, and G.I. Pearman, The CSIRO latitudinal gradient study of CO₂ isotopes, in *Geophysical Monitoring for Climatic Change, No 17: Summary Report 1988*, edited by J.W. Elkins and R.M. Rosson, pp. 91-93, NOAA Air Resources Laboratory, Boulder, CO, 1989.
- Fraser, P.J., Atmospheric methane and carbon monoxide observations at Cape Grim, Tasmania, in *Baseline Atmospheric Program (Australia) 1981-1982*, edited by R.J. Francey, Canberra Publishing and Printing Co., pp. 25-36, Canberra, Australia, 1984.
- Fraser, P.J., P. Hyson, R.A. Rasmussen, A.J. Crawford, and M.A.K. Khalil, 1986, Methane, carbon monoxide and methylchloroform in the southern hemisphere, *J. Atmos. Chem.*, 4, 3-42, 1986.
- Lang, P.M., L.P. Steele, R.C. Martin, and K.A. Masarie, Atmospheric methane data for the period 1983-1985 from the NOAA/GMCC global cooperative flask sampling network, *NOAA Tech. Memo. ERL CMDL-1*, 90 pp., NOAA Environmental Research Laboratories, Boulder, CO, 1990a.
- Lang, P.M., L.P. Steele, and R.C. Martin, Atmospheric methane data for the period 1986-1988 from the CMDL global cooperative flask sampling network, *NOAA Tech. Memo. ERL CMDL*, 108 pp., NOAA Environmental Research Laboratories, Boulder, CO, in press, 1990b.
- Rasmussen, R.A., and M.A.K. Khalil, Atmospheric methane (CH₄): Trends and seasonal cycles, *J. Geophys. Res.*, 86, 9826-9832, 1981.
- Steele, L.P., P.J. Fraser, R.A. Rasmussen, M.A.K. Khalil, T.J. Conway, A.J. Crawford, R.H. Gammon, K.A. Masarie, and K.W. Thoning, The global distribution of methane in the troposphere, *J. Atmos. Chem.* 5, 125-171, 1987.
- Steele, L.P., T.J. Conway, L.S. Waterman, and P.M. Lang, The NOAA/GMCC measurements of CH₄ and CO₂ from flask air samples at Cape Grim, in *Baseline Atmospheric Program (Australia) 1987*, edited by B.W. Forgan and G.P. Ayers, pp. 48-50, CSIRO, Melbourne, Australia, 1989.

Secular Variation in the Carbon-13 Content of Atmospheric Carbon Dioxide

I. FRIEDMAN, J. GLEASON, AND A. WARDEN

U.S. Geological Survey, Denver, Colorado 90225

1. INTRODUCTION

Measurements were made of the $\delta^{13}\text{C}$ of atmospheric CO_2 , separated cryogenically from samples of air collected from early 1981 to early 1989 at MLO, BRW, SMO, and SPO.

2. EXPERIMENTAL PROCEDURES

The efficiency of the CO_2 separation and purification was checked by filling our stainless steel 10-L flasks with air from a single high-pressure cylinder. A series of 16 air samples was processed over a period of 4 months in 1980-1981, yielding an average $\delta^{13}\text{C}$ value of -8.081‰ with a standard deviation of 0.034‰ . A similar experiment was carried out over a period of 2 weeks in 1989 when six replicate samples from another high-pressure cylinder that was filled at the same time as the first cylinder gave an average $\delta^{13}\text{C}$ value of -8.140‰ with a standard deviation of 0.002‰ . The difference of 0.06‰ between the two sets of determinations carried out 8 years apart is not considered significant in view of the long storage time and the fact that the air in each flask might have initially been slightly different.

3. CORRECTION FOR N_2O

During the cryogenic separation of CO_2 from air, N_2O , present in air at about 0.3 ppm, is separated together with the CO_2 . Because N_2O has the same isotopic masses as CO_2 , it interferes with mass spectrometric analysis of the CO_2 , and a correction must be applied to the final $\delta^{13}\text{C}$ results [Craig and Keeling, 1963]. Although the theoretical correction is about $+0.32\text{‰}$, in practice the correction depends upon the relative efficiency of ionization of the two gases in the

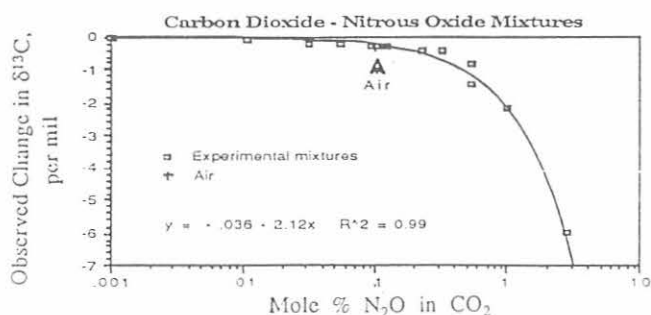


Fig. 1. The observed change in $\delta^{13}\text{C}$ (per mil) as N_2O is added to CO_2 . The proportion of N_2O is given in mole percent.

particular mass spectrometer used for the analysis. For example, Mook *et al.* [1983] found that their instrument required a correction of about $+0.18 \pm 0.06\text{‰}$. This value was obtained by Mook *et al.* by passing CO_2 over copper metal at 700°C . We could not detect a change in $\delta^{13}\text{C}$ greater than 0.01‰ upon repeated passage of our atmospheric CO_2 over copper metal at 700°C which should remove the N_2O by reducing it to nitrogen.

To determine the efficiency of ionization of N_2O for our mass spectrometer, we made a series of mixtures of tank N_2O and pure CO_2 prepared by the reaction of 100% phosphoric acid with our standard limestone. The data shown in Figure 1 indicate that the efficiency of ionization of N_2O in our instrument is equal to that of CO_2 . Accordingly, all the $\delta^{13}\text{C}$ data reported in this paper have been corrected by adding 0.32‰ to the analytical values.

4. RESULTS

4.1. COMPARISON WITH RESULTS OF PREVIOUS INVESTIGATORS

There was an overlap in sample collection between Mook *et al.* [1983] and our group at MLO during 1981 and at SPO during the latter one-half of 1981. Figure 2 is a plot of both

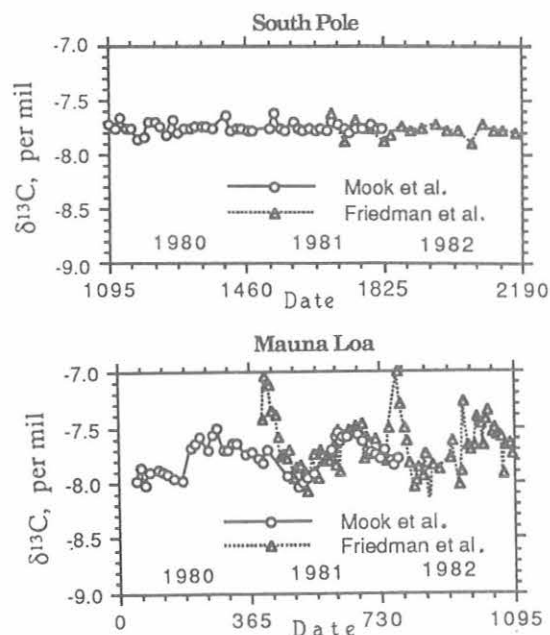


Fig. 2. $\delta^{13}\text{C}$ values from Mook *et al.* [1983] and from the current analysis, for samples collected at SPO and MLO.

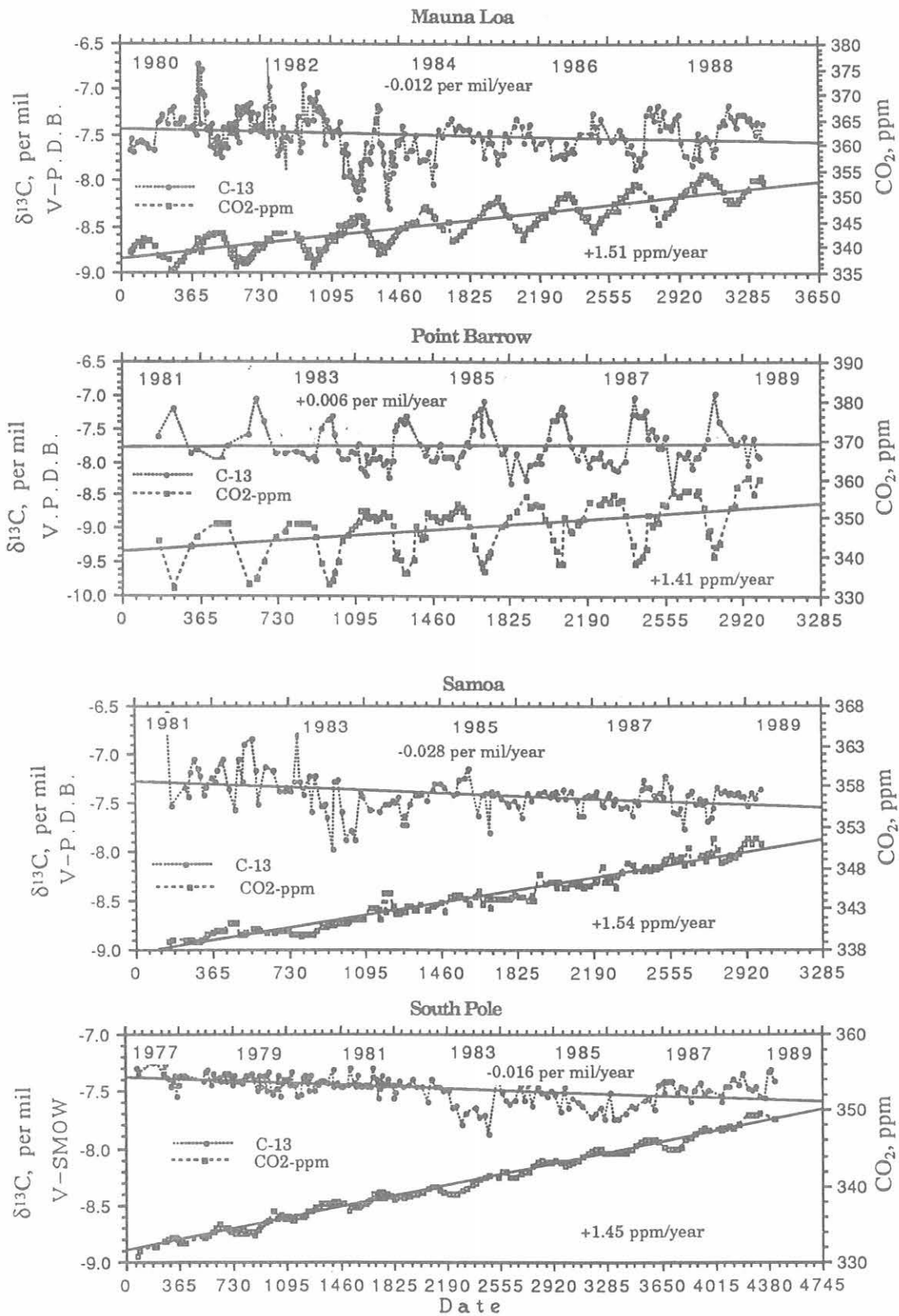


Fig. 3. $\delta^{13}\text{C}$ (per mil) and CO_2 concentration (ppm). Data from Mook *et al.* [1983] for SPO and MLO are included in the plots. All sample analyses were made relative to the Vienna PDB air standard. CO_2 concentration data are from CMDL and from Mook *et al.* [1983].

sets of data for the two collection sites. Our data deviate from those of *Mook et al.* during two periods at MLO. We have no explanation for this. However, the remainder of the MLO data as well as the data from SPO show good agreement between the sets of data from both laboratories. In assessing long-term changes in $\delta^{13}\text{C}$, we have included the *Mook et al.* [1983] MLO data for 1980 and their SPO data for 1977-1980.

4.2. DISCUSSION

The results shown in Figure 3, which include data from *Mook et al.* [1983], indicate that the long-term changes in $\delta^{13}\text{C}$ are -0.012‰ yr^{-1} at MLO (1980-1989), -0.028‰ yr^{-1} at SMO (1981-1989), and -0.016‰ yr^{-1} at SPO (1977- 1989). Although the record at BRW indicated a change of $+0.006\text{‰ yr}^{-1}$ (1981-1989), the large seasonal changes in $\delta^{13}\text{C}$ at this station make this value suspect. Seasonal changes in $\delta^{13}\text{C}$ at MLO and BRW can be explained by the uptake of CO_2 by

plants during the summer, which has a delta value of approximately -27‰ .

In addition to seasonal changes in $\delta^{13}\text{C}$, we observed large changes of about -0.4‰ at MLO, SMO, and SPO that were coincident with the 1982-1983 El Niño. No such change was observed at BRW. A smaller change in $\delta^{13}\text{C}$ that may be related to the 1985 El Niño was observed in samples from SPO collected in late 1985 through early 1986. These effects of the El Niño emphasize the importance of ocean-atmosphere exchange on the CO_2 cycle.

5. REFERENCES

- Craig, H., and C.D. Keeling, The effects of atmospheric N_2O on the measured isotopic composition of atmospheric CO_2 , *Geochim. Cosmochim. Acta*, 27, 549-551, 1963.
- Mook, W.G., M. Koopmans, A.F. Carter, and C.D. Keeling, Seasonal, latitudinal, and secular variations in the abundance and isotopic ratios of atmospheric carbon dioxide, 1, Results from land stations, *J. Geophys. Res.*, 88, 10,915-10,933, 1983.

Snow Bunting Nesting Study at Barrow, Alaska

JOHN C. GEORGE, KIRSTEN BAGNE, AND MARC LEINBERGER

Department of Wildlife Management, North Slope Borough, Barrow, Alaska 99723

1. INTRODUCTION AND BACKGROUND

Snow buntings (*Plectrophenax nivalis*) are obligate cavity nesters, yet they do breed above tree line on the North Slope. They typically nest in or on artificial structures along Alaska's North Slope and in rocky crags in the Canadian Arctic [Johnson and Herter, 1989]. It would seem that such species would be "nest limited" in the Alaskan Arctic since they require manmade structures as a nesting platform.

The Department of Wildlife Management undertook the nesting project in an attempt to increase the number of nesting passerine birds in the Barrow area. The department also wanted to do a small demonstration project to show some beneficial aspects of wildlife management to the people of the North Slope. Our working hypothesis was that artificial nests would be readily used by snow buntings in the Barrow area and that their numbers would increase.

2. OBJECTIVES

The major objectives of the study were: (1) erect artificial nest boxes around the village of Barrow; (2) monitor the use of artificial nest boxes by passerine birds and gather life history data if possible, with emphasis on nesting initiation, time of hatching, numbers of eggs laid, and numbers of young fledged; and (3) increase the nesting population of snow buntings in the Barrow area.

3. METHODS

On May 2, 1989, 14 bird houses were erected near Barrow and the Northern Arctic Research Laboratory, primarily on telephone poles. We checked the houses at least once each week for bird use, and also logged sightings of other bird species during the inspections. The bird houses were 15.5 cm x 15.5 cm x 15.5 cm boxes with a 5-cm-diameter hole. They were labeled with sequential numbers from 1 to 14.

During the 1989 season, snow birds nested in 3 of the 14 boxes (numbers 2, 6, and 10) and possibly successfully fledged young in one of them. The basic results of the nest observations are summarized in Table 1. Nest building began on about May 27, and egg laying started by about June 16. Hatching began June 30 in nest number 6. The young began fledging around July 15-20.

During the 1990 season, four nest boxes were used of which two appeared to be successful. The basic results of the nest observations are summarized in Table 1. No data were gathered on nest building. Egg laying began about June 4. Eggs were noted to have hatched by June 13—somewhat earlier than in 1989. Young from two nests appeared to have successfully fledged, in particular in nest number 2.

TABLE 1. Basic Snow Bunting Nesting Study

Nest Site	Nesting Building	Egg Laying	Date Hatched	Number of Eggs	Comments
1989					
2				5	Nest failed(?)
6	May 27	June 16-23	June 30	5	Nest failed
10	<June 16	<June 23		>3	Probably successful
1990					
1		<June 15	June 18	6	Two chicks fledged(?) by July 2
2		June 4	June 11-13	7	Five fledged by June 27; two eggs failed
7		<June 25		5	
11		June 4	<July 2	6	

Dates are approximate in most cases, as nests were checked approximately once per week.

Nest building begins in late May in the Barrow area. Egg laying appears to begin by June 4, but can continue into late June. Hatching dates appear to be variable, ranging from roughly June 11 to July 2. Observations, however, were not frequent enough to determine all hatching dates with great accuracy. The females generally laid 5-7 eggs. In past years, we have noted the young remaining (and feeding) in the Barrow area until November. For both years studied, three of seven nesting attempts (43%) appeared to be successful. It is not known why other nests failed.

Initially, it seems, we can refute our hypothesis that snow buntings are nest-limited near Barrow. However, it may be the case, as for other species, that the birds take several seasons to become familiar with a nest site before they start using it (George Divoky, personal communication, 1989). Another possibility is that other factors are limiting snow bunting populations near Barrow.

Acknowledgments. We acknowledge George Divoky for assistance in nest design and Lane Franich for construction of the nest boxes. The assistance of NOAA/CMDL staff for allowing us to place nest boxes on their buildings and power poles is appreciated.

4. REFERENCE

Johnson, S., and D. Herter, *The birds of the Beaufort Sea*, BP Exploration (Alaska) Inc., Environmental and Regulatory Affairs, Anchorage, AK, 265-267, 1989.

A New Look at Optical Depth Retrieval With the Multiple Field of View Sunphotometer

PAUL F. HEIN, JOHN M. DAVIS, AND STEPHEN K. COX

Colorado State University, Department of Atmospheric Science, Fort Collins, Colorado 80523

1. INTRODUCTION

The multiple field of view (MFOV) sunphotometer was designed to infer the optical thickness of clouds from the surface by viewing the direct plus diffuse components of solar radiance. The instrument was deployed at MLO in 1987 and has been collecting data since then. Recently a new approach for retrieving the desired optical depth was developed that not only allows simpler processing of the data, but also gives new insight into limitations on the upper range of optical depths that can be measured.

2. DESCRIPTION OF THE INSTRUMENT

The MFOV sunphotometer was first built and tested at the Department of Atmospheric Science at CSU to determine the optical thickness of clouds of small to moderate optical depth, such as are common in layers of cirrus cloudiness [Raschke and Cox, 1983]. The instrument consists of five high-quality silicon photodetectors whose fields of view (fov) are coaligned and deployed so that the central line of sight tracks the solar disk (see Figure 1). The detectors have a broad response in the visible portion of the spectrum; thus the optical depth τ must be interpreted as a broadband parameter.

The instrument is mounted on an equatorial tracking device for continuous alignment throughout the day. Each fov is of different size (2, 5, 10, 20, and 28° full angle) to detect differences in the nearly forward-scattered radiative field. The initial application of the instrument relied on

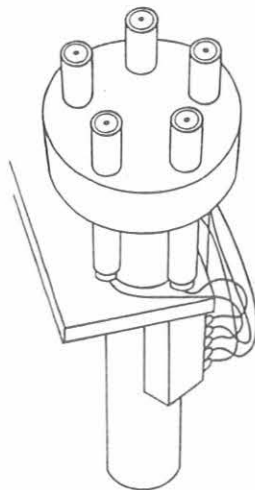


Fig. 1. Schematic of the MFOV sunphotometer.

concurrent pyrheliometric measurements to provide a direct-beam transmittance that was used to scale the output of the photometric detectors to radiometric values. The measurements in each fov were interpreted by Monte Carlo modeling of the amounts of irradiance expected at each detector viewing clouds of various optical thicknesses. A slightly different method of analyzing the data is now presented that not only is simpler, but also gives insight into the upper limit of retrievable optical depths.

3. DATA ANALYSIS

A Monte Carlo model was used to calculate the solar irradiance expected in each of the fov. The modeled irradiances were divided by the extraterrestrial irradiance to form "transmittances" for each fov. The ratios are not transmittances in the strictest sense of the definition, since scattered radiation is included in the measurements. Denoting the ratios in each fov by $T(\text{fov})$, where fov is the set (5, 10, 20, 28), other ratios were taken, namely the ratios of $T(\text{fov})/T(28)$. Doing so eliminates the need for specification of a scaling factor when the same ratios are formed from measured values; i.e., it allows the modeled and measured ratios to be used independently to infer the optical depth. Figure 2 depicts the modeled transmittance ratios as a function of fov for various optical depths, τ . The values were calculated for a solar zenith angle of 0° and a surface albedo of 0.15. A stratocumulus cloud droplet distribution was used in Mie calculations to provide the single-particle scattering parameters. The calculation was performed for the visible portion of the spectrum.

It is obvious from the convergence of the curves (Figure 2) at optical depths near 10.0 that the method will not be useful at large optical depths. Furthermore, we show as follows that the shapes of the curves have a physical interpretation related to the radiation scattered into each detector: In a monochromatic sense, the transmittance may be written simply as $T = e^{-\tau}$. If the measurement by a particular detector is denoted by

$$T(\text{fov}) = \exp \{-[\tau - \tau_s(\text{fov})]\}, \quad (1)$$

where τ_s is a parameter that accounts for the radiation scattered into the detector's fov, effectively increasing the reading, then the ratio of two such measurements, depicted in Figure 2, may be expressed as

$$\frac{T(\text{fov})}{T(28)} = \exp [\tau_s(28) - \tau_s(\text{fov})]. \quad (2)$$

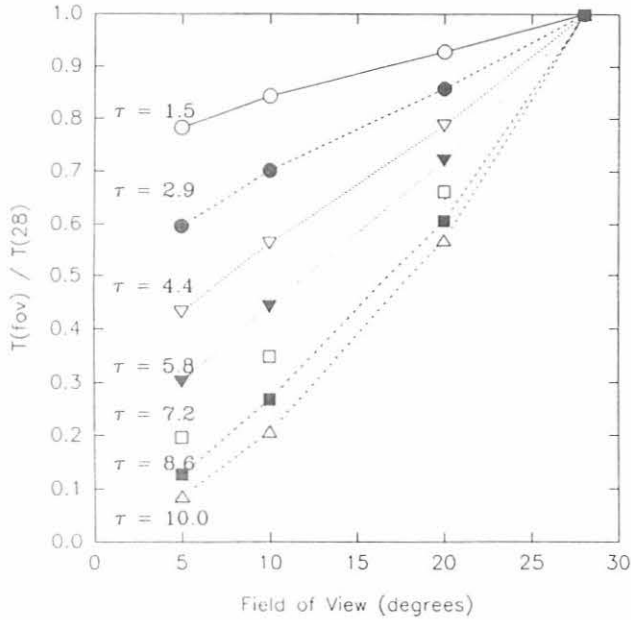


Fig. 2. Modeled transmittance ratios versus fov for various optical depths τ , a solar zenith angle of 0° , and a surface albedo of 0.15.

In (2), it is assumed that the actual transmissivity is the same for all detectors, which should be the case if the calibration is correct. Thus each curve, according to this formulation, decays exponentially in a manner related to the difference in the exponents that describe the amount of energy scattered into the detectors at each fov. For small τ , multiple scattering is small and so is the value of the exponent. The curve at $\tau = 1.5$ shows a relatively small decay as a result.

Since the exponent in (2) is expressed as the difference between the optical depths attributed to scattering into the fov, and since the volume scattering coefficient may be expressed in terms of an integral of the phase function over scattering angles, it is reasonable to expect the exponent to also be related to the difference in the angles themselves, at least in the first-order sense. If so, a reasonable guess at fitting the curves in Figure 2 would be

$$\frac{T(\text{fov})}{T(28)} = \exp[-a(\tau)(28 - \theta_{\text{fov}})], \quad (3)$$

where $a(\tau)$ is an optical depth parameter and θ_{fov} is the angular fov. When this is done and the values of $a(\tau)$ are plotted as a function of τ , a nearly linear relationship results for $\tau < 10$ (Figure 3). Thus for small optical depths, the value of $a(\tau)$ is nearly linearly related to τ . The slope of this line may change with different types of scattering functions and with solar zenith angle, and is the subject of future research; however, once the linear relationship is obtained in this form, it is a simple matter to relate the ratios of transmittances to the optical depth. For example, if the relationship in Figure 3 is expressed as $a(\tau) = m\tau + b$, where m is slope and b is intercept, then the optical depth is obtained as

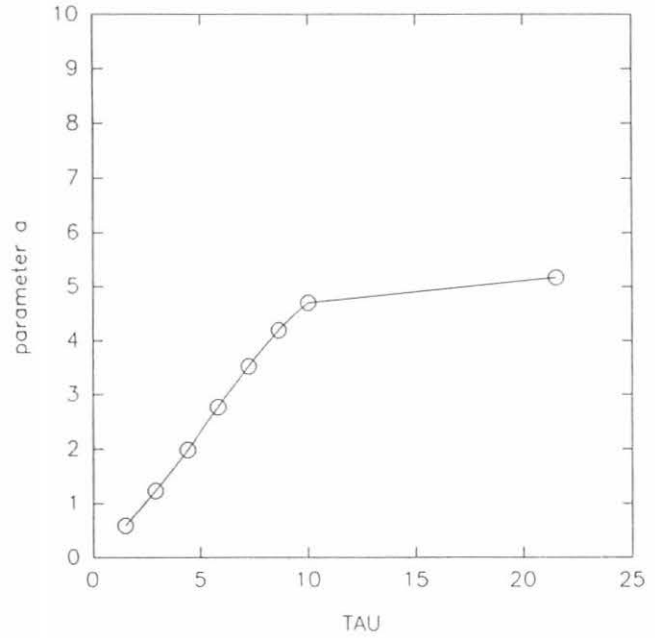


Fig. 3. The parameter $a(\tau)$ plotted as a function of τ , for a solar zenith angle of 0° .

$$\tau = -\frac{1}{m} \left\{ \frac{\ln[T(\text{fov})/T(28)]}{28 - \theta_{\text{fov}}} - b \right\} \quad (4)$$

The kink in the fit of $a(\tau)$ is exaggerated by the lack of data points for $10 < \tau < 20$. It is another indication, as seen in Figure 2, that the MFOV sunphotometer optical depth retrieval should be used for optically thinner clouds and only as a flag of thicker clouds when the inferred thickness is larger.

4. FUTURE RESEARCH

In addition to continued maintenance of the MFOV sunphotometer at MLO and ongoing data collection, a modeling effort is indicated to examine the behavior of the sensitivity of the algorithm for computing τ to changes in solar zenith angle and cloud microphysics. For example, cirrus cloud crystals may produce a significantly different value for the slope m in (4) in which case it may be necessary to search for additional information on cloud type in the MFOV sunphotometer signal. This signal may be found by incorporating phase function information into the exponent of (3). Alternately, with a more refined choice of the fov number and precision, ways may be found to extract properties of the scattering phase function and the optical depth simultaneously.

5. REFERENCE

- Raschke, R.A., and S.K. Cox, Instrumentation and technique for deducing cloud optical depth, *J. Clim. Appl. Meteorol.*, 22, 1887-1893, 1983.

Tropospheric Nitrogen Oxide Measurements During Spring at Barrow

R. E. HONRATH AND D. A. JAFFE

University of Alaska, Geophysical Institute and Department of Chemistry, Fairbanks, Alaska 99775-0800

1. INTRODUCTION

Nitrogen oxides are critical in the chemistry of the atmosphere [Crutzen, 1979]. By controlling the photochemical production of ozone and hydroxyl radicals in the troposphere, NO_x ($\text{NO} + \text{NO}_2$) plays a central role in atmospheric photochemistry. Additionally, NO_x is a precursor to nitric acid (HNO_3), a major constituent of acid rain [Galloway and Likens, 1981]. Other nitrogen oxides, such as peroxyacetyl nitrate (PAN), may have a significant part in the global distribution and lifetime of nitrogen oxides [Singh, 1987]. The concentration of total reactive nitrogen ($\text{NO}_y = \text{NO} + \text{NO}_2 + \text{HNO}_3 + \text{N}_2\text{O}_5 + \text{PAN} + \text{RONO}_2 + \text{particulate-NO}_3^- + \dots$) can be used as a surrogate for the individual species and can provide valuable information on transport and removal processes, especially in situations where measurements of individual species are limited by resources or instrument sensitivities. In addition, it is possible that unknown and/or unmeasured compounds make up a significant fraction of the total NO_y reservoir in remote areas [Singh, 1987].

The role of anthropogenic nitrogen oxides in changes in Arctic tropospheric ozone concentrations is not well understood. Surface ozone at BRW during summer has shown a 2% yr^{-1} increase since 1973 [Oltmans and Komhyr, 1986]. Industrial nitrogen oxide emissions from the Prudhoe Bay area could be responsible for the observed summer surface O_3 increase, although to date the available summer NO_y data do not support this hypothesis. Alternatively, photochemical O_3 production resulting from lower-latitude NO_x sources could also contribute to the observed O_3 increase.

2. EXPERIMENTAL PROCEDURES

NO and NO_y were measured from March 2 to April 7, 1989, using a high-sensitivity chemiluminescent detector built at the University of Alaska, Fairbanks [Honrath and Jaffe, 1990; Jaffe et al., 1990]. NO_y is detected as NO following reduction in a heated converter. The accuracy and precision of low-level NO and NO_y measurements at BRW have steadily improved. The detection limit during the spring 1989 measurements was 75 ppt for NO , and about 120 ppt for NO_y . The current detection limit for this instrument is 5 ppt for NO or NO_y , with an estimated uncertainty of $\pm 15\%$ at concentrations well above the detection limit. Since NO_x is produced in virtually all combustion processes, it is necessary to carefully screen the data to eliminate local impacts on the data. To remove any possibility of local sources affecting the measurements, we screened the data by wind direction and variability. Data shown here were obtained only when the winds were not from the direction of significant local sources and exhibited low variability.

3. RESULTS

Two types of measurement conditions were identified in the data record after screening by wind direction and ambient variability [Jaffe et al., 1990]: background periods and events. Background periods correspond to times when NO and NO_y concentrations were constant and low relative to values in the overall data record. Inspection of the raw data also revealed several events, during which ambient NO and NO_y concentrations changed smoothly and reached high values even though wind was generally from the clean sector (5° - 130°). Maximum NO_y levels exceeded 3 ppb during each event.

3.1. BACKGROUND PERIODS

Eleven background periods were identified. Concentrations varied very little during individual periods, but larger differences were observed among the periods. A histogram of all NO_y measurements during the springtime background periods ($N = 885$) is shown in Figure 1. Median NO_y levels during each of the 11 background periods ranged from 280 to 850 ppt, with an overall median of 616 ppt. NO concentrations during background periods were all below our detection limit of 75 ppt. On the basis of a photostationary-state calculation, NO_x levels must have been below 145 ppt, at least during clear midday periods [Jaffe et al., 1990].

An analysis of 850 mb back trajectories [Jaffe et al., 1990; Harris, 1982] shows that these measurements are consistent with the understanding of a generally contaminated reservoir of air over the Arctic basin during winter and spring,

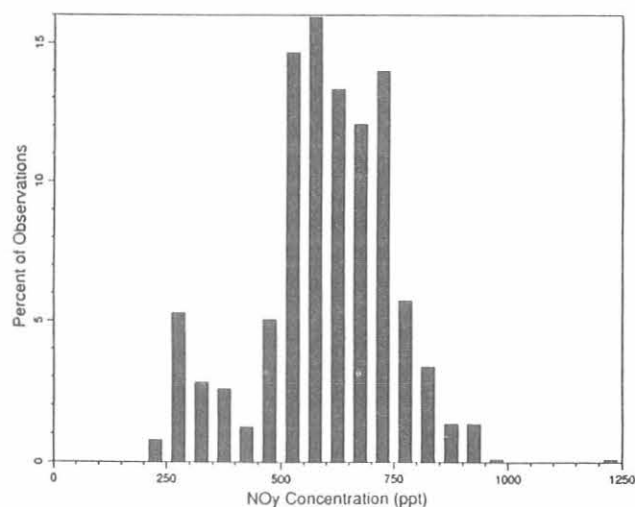


Fig. 1. Histogram of background NO_y concentrations during spring 1989 at BRW.

regenerated by episodic transport from source regions. The relatively constant and high NO_y levels during Arctic trajectories are indicative of a high- NO_y Arctic reservoir. Lower NO_y levels during periods of transport from the south are probably due to enhanced scrubbing of air by the greater frequency and amount of precipitation in those regions. Interestingly, spring concentrations were higher than summer concentrations, even during southerly flow, a finding that is consistent with the increased lifetime of NO_y reservoir compounds, such as PAN, during winter [Singh and Hanst, 1981].

3.2. EVENTS

During this campaign, four identifiable pollution events were observed, lasting from 12-60 hours each, as shown in Figure 2. For event 1, NO_y reached a peak of 16.4 ppb, while NO reached 1.4 ppb. The suddenness with which such events occur and the extremely high NO_y concentrations observed are not characteristic of arctic haze at a background site. Moreover, the relatively smooth changes in NO_y concentration during such events contrast sharply with the well-characterized high-variability signatures of local (Barrow) pollution sources [Honrath and Jaffe, 1990].

Figure 3 shows a plot of the observed NO_y concentrations during events and background periods in 1989 versus the local wind direction. The events were observed to occur when wind directions were in the range of 98° to 233° . Highest NO_y concentrations were observed when local winds were from 110° to 120° , suggesting that the nitrogen oxide source responsible for these events is in that sector. The only major NO_x source in that direction is the Prudhoe Bay oil production complex, at 111° from BRW and approximately 300 km distant. The NO_x emissions from those facilities arise from natural gas combustion and are estimated at 10,000-15,000 metric tons yr^{-1} (J. Coutts, personal communication, 1989). Other data, including estimated NO_x concentrations and SO_2 and SO_4 filter measurements, are consistent with a Prudhoe Bay source. It is interesting to note that Prudhoe Bay was first suggested as a possible influence on the BRW record by Radke *et al.* [1976], based on measurements of condensation nuclei at BRW during 1970.

Pollution episodes at BRW due to a non-local sources, having a very similar appearance, have been previously attributed to long-range transport events [Hansen *et al.*, 1989]. A comparison of these nitrogen oxide data with black carbon, CO_2 , and CH_4 data is currently under way and should prove to be very useful in characterizing these events.

4. SUMMARY

As a result of this measurement program, we have learned much about nitrogen oxides in the Arctic atmosphere. In particular we have found the following about background NO_y and NO_y events:

(1) Background NO_y . NO_y concentrations in the Arctic are significantly higher in spring than in summer. In spring,

surface NO_y levels at BRW appear to be comparable to concentrations in the free troposphere outside of Arctic haze layers [Dickerson, 1985], with haze-layer concentrations being about twice as high. In addition, springtime NO_y concentrations during southerly flow (as indicated by 850 mb trajectories) were 50-70% of the levels observed when trajectories indicated that Arctic air was being sampled at BRW. During southerly flow, springtime NO_y concentrations were higher than those in summer, providing evidence for an increased NO_y lifetime during winter. NO_x concentrations in the arctic during spring are estimated to be 0-20% of NO_y concentrations.

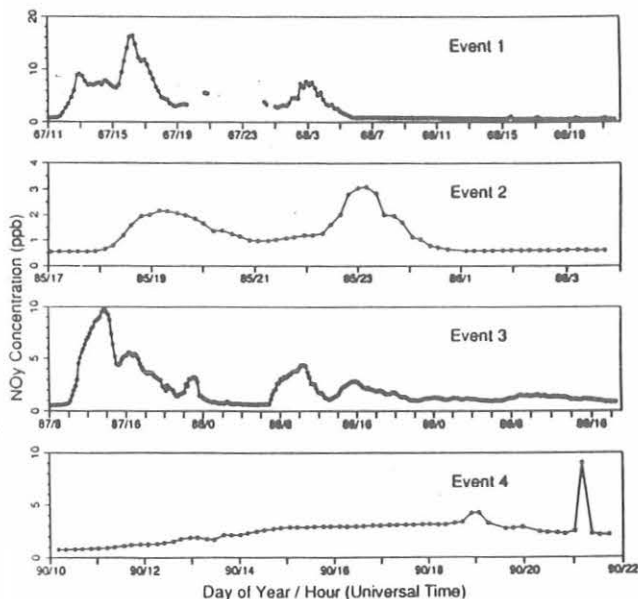


Fig. 2. NO_y concentrations during events observed in the spring of 1989 at BRW.

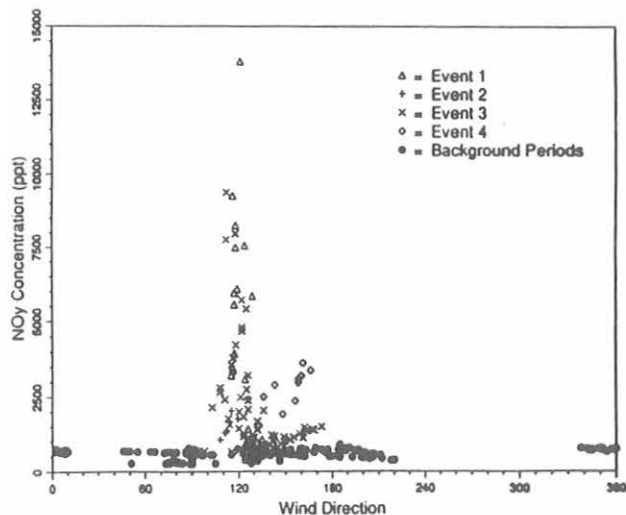


Fig. 3. NO_y concentrations during events and background periods (spring 1989) versus surface wind direction at BRW.

(2) NO_y events. Substantially elevated NO_y concentrations (to 16 ppb) were observed in the spring of 1989 during four events lasting from 12-60 hours. Substantial evidence suggests that emissions from the Prudhoe Bay industrial region were responsible: (1) slow and smooth concentration variations during the events indicated that local (Barrow) sources were not the cause; (2) the correlation with local wind direction indicated that the source was in the 110° - 120° sector, consistent with Prudhoe Bay, which lies at a 111° bearing from Barrow; (3) the ratio of NO_x : NO_y estimated for these events is very high (to 0.87), indicating that the NO_y enrichment was almost entirely due to NO_x and that very fresh NO_x emissions were responsible for the events; and (4) filter measurements of SO_4^{2-} and SO_2 did not indicate enrichment of sulfur compounds during the events. This is consistent with a source, such as Prudhoe Bay, which is rich in NO_x .

Although the CMDL site at Barrow is in a remote region, it is affected by local, regional, and global-scale pollutant sources. To differentiate between these sources, we must select data collected at such a site with great care so that measurements are representative of specific, identifiable air masses. Our data indicate that atmospheric transport processes can bring different air masses to the BRW site on a time scale of hours. Daily, weekly, or monthly means may therefore not be adequate to discriminate between different air masses. In general, measurement systems that provide high time resolution data will provide greater insight into complex atmospheric processes at a site such as BRW.

Acknowledgments. Trajectories were calculated by Joyce Harris (CMDL, Boulder, Colorado). W. T. Sturges, S.-M. Li, and the staff of BRW helped with sample collection. We are also thankful for assistance from the North Slope Borough Department of Wildlife

Management. This work was supported by NSF grant ATM 88-14518.

5. REFERENCES

- Crutzen, P.J., The role of NO and NO_2 in the chemistry of the troposphere and stratosphere, *Ann. Rev. Earth Planet. Sci.*, **7**, 443-472, 1979.
- Dickerson, R.R., Reactive nitrogen compounds in the Arctic, *J. Geophys. Res.*, **90**, 10,739-10,743, 1985.
- Galloway, J.N., and G.E. Likens, Acid precipitation: The importance of nitric acid, *Atmos. Environ.*, **15**, 1081-1085, 1981.
- Hansen, A.D.A., T.J. Conway, L.P. Steele, B.A. Bodhaine, K.W. Thoning, P. Tans, and T. Novakov, Correlations among combustion effluent species at Barrow, Alaska: Aerosol black carbon, carbon dioxide, and methane, *J. Atmos. Chem.*, **9**, 283-299, 1989.
- Harris, J.M., The GMCC atmospheric trajectory program, *NOAA Tech. Memo. ERL ARL-116*, Air Resources Laboratory, Rockville, MD, 1982.
- Honrath, R.E., and D.A. Jaffe, Measurements of nitrogen oxides in the Arctic, *Geophys. Res. Lett.*, **17**, 611-614, 1990.
- Jaffe, D.A., R.E. Honrath, J.A. Herring, and S.M. Li, Measurement of nitrogen oxides at Barrow, Alaska: Evidence for regional and northern hemispheric sources of pollution, *J. Geophys. Res.*, submitted, 1990.
- Oltmans, S., and W.P. Komhyr, Surface ozone distributions and variations from 1973-1984: Measurements at the NOAA Geophysical Monitoring for Climatic Change baseline observatories, *J. Geophys. Res.*, **91**, 5229-5236, 1986.
- Radke, L.F., P.V. Hobbs, and J.E. Pinnons, Observations of cloud condensation nuclei, sodium-containing particles, ice nuclei and the light-scattering coefficient near Barrow, Alaska, *J. Appl. Meteorol.*, **15**, 982-995, 1976.
- Singh, H.B., Reactive nitrogen in the troposphere, *Environ. Sci. Technol.*, **21**, 320-327, 1987.
- Singh, H.B., and P.L. Hanst, Peroxyacetyl nitrate (PAN) in the unpolluted atmosphere: An important reservoir for nitrogen oxides, *Geophys. Res. Lett.*, **8**, 941-944, 1981.

Chemical Analyses of Atmospheric Particulates and Gases at MLO

C. R. JENSEN, X. CAI, AND W. H. ZOLLER
University of Washington, Seattle, Washington 98195

1. INTRODUCTION

Atmospheric particulate samples have been collected continuously at MLO using the selective sampling system installed in 1979 [Parrington, 1983]. This system was originally designed to collect either upslope or downslope aerosol samples, based on wind direction, wind speed, time of day, and CN concentration. During conditions that did not fit into either upslope or downslope parameters, an interim sample was collected. In 1985 two changes were made. First, the separate upslope sampling was discontinued by setting only downslope parameters and making all other conditions interim. Second, $^7\text{LiOH}$ -treated filters were added to collect downslope gases. Downslope samples since 1985 have therefore been collected on Teflon, Nuclepore, and treated filters, while the interim samples have been collected on Nuclepore filters. We are currently working on analyzing a backlog of samples from 1985 to the present using two methods: instrumental neutron activation analysis is used to characterize particulates collected on Teflon and Nuclepore filters; ion chromatography is used to measure water-soluble ions on the Teflon and Nuclepore filters, and absorbed gases on the treated filters.

2. PRELIMINARY RESULTS AND DISCUSSION

2.1. INSTRUMENTAL NEUTRON ACTIVATION ANALYSIS RESULTS

Initial calculations for several elements collected on downslope Teflon filters show increased concentrations during the dust season (mid-February to July) as expected [Bodhaine *et al.*, 1981; Parrington *et al.*, 1983]. Figure 1 shows this trend for Mn and V in 1987; the highest concentrations are in the spring, especially April and May. Mean concentrations for several elements during 1987 clean and dust seasons, and the ratios of dust to clean averages are given in Table 1. The predominantly crustal elements Al, V, and Mn show a fivefold to ninefold increase during the dust season, while the predominantly marine elements Na, Cl, and Br show only a twofold increase.

2.2. ION CHROMATOGRAPHY ANALYSIS

Figure 2 shows initial results for SO_4^{2-} and SO_2 from April 1989 to April 1990. Only one sample was collected for the 2-wk period from the end of February to the middle of March 1990 due to a snow storm that closed the road to MLO. The SO_4^{2-} measured on downslope Teflon filters shows no distinct trends. The increase from January to April 1990 may indicate the beginning of the dust season, but more data are needed to confirm this. Unfortunately some data are missing for the spring of 1989, so that the trend in SO_4^{2-}

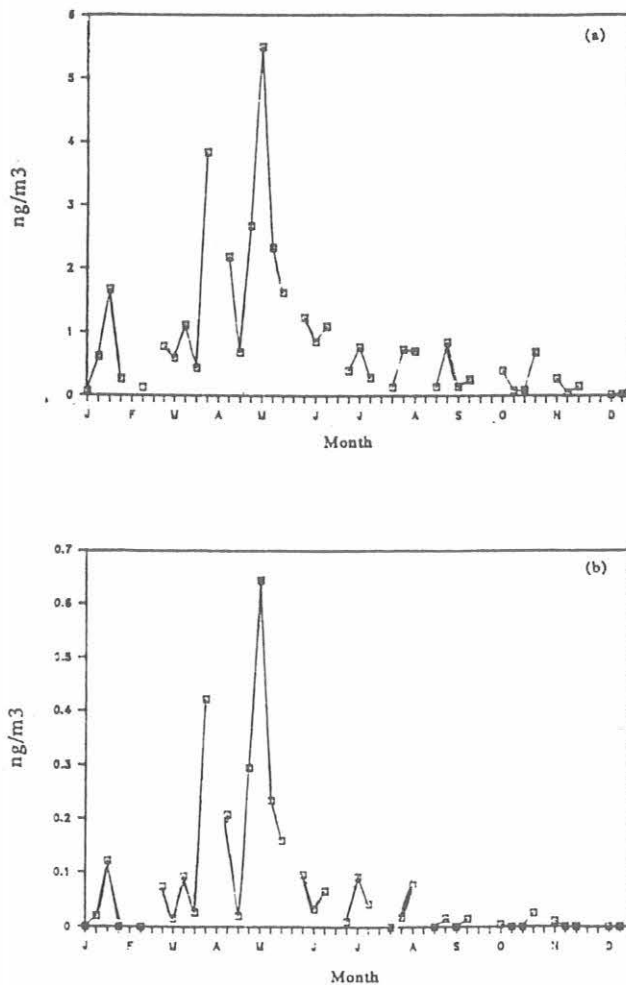


Fig. 1. Concentrations (ng m^{-3}) of (a) Mn and (b) V, 1987. Each sample is collected for 1 week.

during the 1989 dust season is difficult to discern. The SO_2 measured on downslope treated filters does not exhibit increased concentrations during dust seasons. The increase in SO_2 between September and December 1989 may be due to gaseous volcanic eruptions at Kilauea that reach the observatory when the eruptive clouds break the marine boundary layer and enter the free troposphere.

Because downslope samples are simultaneously collected on Teflon and Nuclepore filters, we can compare the collection efficiencies of the two types of filter. Figure 3 shows a comparison of the 1989-1990 monthly averages for SO_4^{2-} on Teflon and Nuclepore filters. Both types of filters have about the same collection efficiency for SO_4^{2-} .

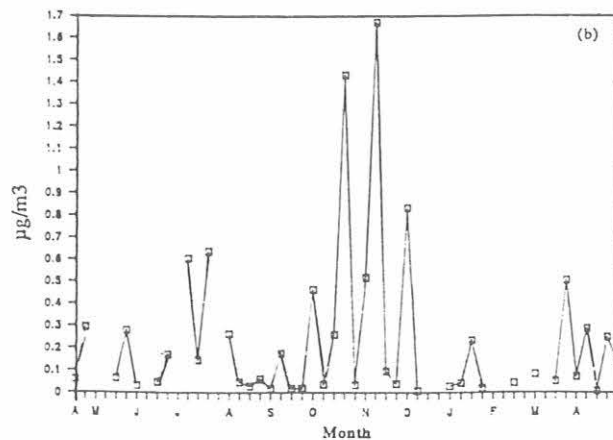
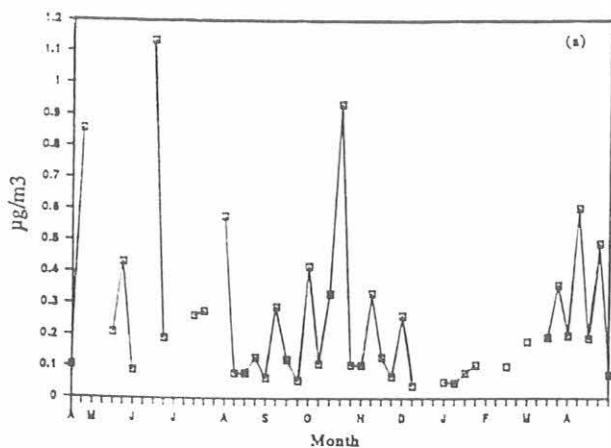


Fig. 2. Concentrations ($\mu\text{g m}^{-3}$) of (a) SO_4^{2-} and (b) SO_2 , 1989-1990. Each sample is collected for 1 week.

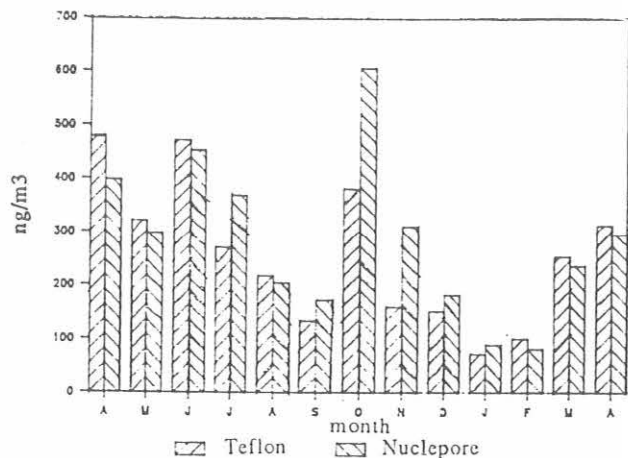


Fig. 3. Comparison of SO_4^{2-} collection efficiencies of Teflon and Nuclepore filters at MLO during 1989-1990. Monthly averages (ng m^{-3}) are compared.

3. ONGOING RESEARCH

Samples are still being collected continuously using the system started in 1985. We are currently analyzing all the samples collected since 1985 and doing additional data analysis. All data from 1979 to the present will be combined to give a 12-yr record of atmospheric particulates and a 6-yr record of atmospheric gases at MLO. To obtain more

TABLE 1. Mean Concentrations of Several Elements During 1987 Clean and Dust Seasons

Element	Mean Concentration, ng m^{-3}		Dust/Clean Ratio
	Clean	Dust	
Al	23.3	122.3	5.2
V	0.0186	0.1604	8.6
Mn	0.37	1.69	4.6
Na	22.0	49.5	2.3
Cl	2.4	6.5	2.7
Br	0.61	0.98	1.6

information, we also plan to use inductively coupled plasma analysis on the samples from 1985 to the present to measure additional elements.

Acknowledgments. Support for the research was supplied in part by NSF grant 62632. We also thank the NOAA/CMDL staff at MLO for the collection of air filter samples and the staff at Los Alamos National Laboratory for assistance with instrumental neutron activation analysis.

REFERENCES

- Bodhaine, B.A., B.G. Mendonca, J.M. Harris, and J.M. Miller, Seasonal variations in aerosols and atmospheric transmission at Mauna Loa Observatory, *J. Geophys. Res.*, **86**, 7395-7398, 1981.
- Parrington, J.R., The chemistry of background atmospheric particles collected at Mauna Loa Observatory, Hawaii, Ph.D. thesis, University of Maryland, 1983.
- Parrington, J.R., W.H. Zoller, and N.K. Aras, Asian dust: Seasonal transport to the Hawaiian Islands, *Science*, **220**, 195-197, 1983.

A Temperature Inversion Climatology for Barrow: 1976-1985

JONATHAN D. KAHL

University of Wisconsin, Department of Geosciences, Milwaukee, Wisconsin 53201

1. INTRODUCTION

The tropospheric temperature inversion is an ubiquitous feature of the high-latitude climate. In the Arctic, the inversion is a complicated phenomenon involving interactions between surface radiative cooling, subsidence, and warm-air advection [Vowinckel and Orvig, 1970; Busch *et al.*, 1982]. Multiple inversion layers are frequently found in Arctic temperature soundings [Belmont, 1957]. The inversion layer nearest the surface, the low-level temperature inversion, is primarily driven by a deficit of solar radiation at the earth's surface. The low-level inversion inhibits the mixing of surface-level air with air of the overlying "free" troposphere and thus plays an important role in the dynamics of the Arctic planetary boundary layer.

The low-level temperature inversion has been linked to topics of current interest in Arctic research, including the occurrence and transport of Arctic haze [Bridgman *et al.*, 1989] and the destruction of boundary layer ozone at the onset of polar sunrise [Barrie *et al.*, 1988]. In addition, knowledge of inversion characteristics is needed to model the movement of sea ice [Overland, 1985] and to estimate the fluxes of heat and moisture through leads and polynyas [Barry and Miles, 1988].

This paper describes the climatological characteristics of the low-level temperature inversion at BRW, the site of a background atmospheric chemistry monitoring station in continuous operation since 1972 [Bodhaine, 1983]. The results should assist research on current problems in Arctic meteorology, air chemistry, and oceanography.

2. RESULTS

Twice-daily rawinsonde ascents for 1976-1985 were analyzed in this study; only 6.5% of the soundings were missing. The rawinsonde data were supplemented with 3-hourly surface observations to compute cloud-cover statistics (Section 2.2). An inversion-detection algorithm was developed to identify low-level inversion characteristics objectively. This algorithm is described by Kahl [1990].

2.1. INVERSION CHARACTERISTICS

Three fundamental inversion characteristics are determined for each sounding throughout the 10-yr analysis period: height of inversion base, inversion depth, and temperature difference across the inversion. The monthly distributions of these characteristics are shown in Figures 1-3. The data are displayed as "box and whisker" diagrams, showing the 5th, 25th, 50th (median), 75th, and 95th percentiles (thus 90% of the distribution occurs within the extent of the whiskers). Numerical summaries of these distributions are given in Table 1.

During the entire 1976-1985 analysis period, the inversion base (Figure 1) was situated at the surface over 39% of the time at BRW. The inversion was surface-based at least 25% of the time during all months but May, June, and September. Surface-based inversions occurred more than half the time from November through February. Perhaps more interesting is the observation that the inversion was frequently based above the surface, even during the winter months. Thus, the commonly-used term "surface temperature inversion" is a misnomer; "low-level temperature inversion" is more appropriate.

Monthly distributions of inversion depth for 1976-1985 are shown in Figure 2. The median depths were greatest in March (~850 m) and smallest in September (~250 m). The largest monthly variations in inversion depth occurred during the coldest months, November through April, with interquartile ranges of 700-800 m.

Distributions of temperature difference across the inversion for 1976-1985 are shown in Figure 3. These data exhibit the same seasonal trends as do inversion depth data (Figure 2); a median maximum of 11°C occurred in February and a minimum of 2°C in September.

2.2. RELATIONSHIP OF THE INVERSION TO CLOUD COVER

The inversion characteristics shown in Figures 1-3 do not exhibit a simple annual cycle of deeper, surface-based inversions in the coldest months followed by shallower, elevated inversions in the warmer months. Rather, a temporary plateau is reached in the months of June, July, and August whereby the median inversion base retreats toward the surface, while the median depth and temperature difference decrease less rapidly or even remain constant. This pattern is investigated further by comparing the median inversion depths with mean cloud cover statistics. The cloud cover is analyzed in the form of total sky cover (including fog) recorded in the 3-hourly surface observations for the period 1976-1985.

The sky-cover data are shown in Figure 4, along with the median inversion depths of Figure 2. The most notable feature of the sky-cover climatology is the extreme cloudiness at the Alaskan coastal stations, particularly during May-October, having mean values in excess of 70%. This is primarily due to the prevailing easterly wind off the Beaufort Sea. Also prominent is the plateau from May to July when the springtime sky-cover increase is halted at about 75%. In August the increase resumes, and the sky cover reaches a peak of about 90% in September. The inversion depth closely follows the annual cycle of clear-sky percentages; the middle-year plateau in inversion depth corresponds to the plateau in the sky-cover climatology.

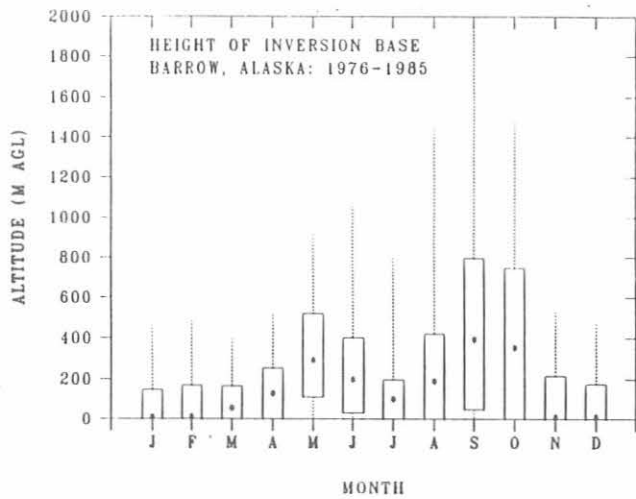


Fig. 1. Monthly distributions of height of inversion base at BRW, 1976-1985. The box and whisker diagrams show upper and lower quartiles (top and bottom of box), median (asterisk), and 5th and 95th percentiles (outer extent of whiskers).

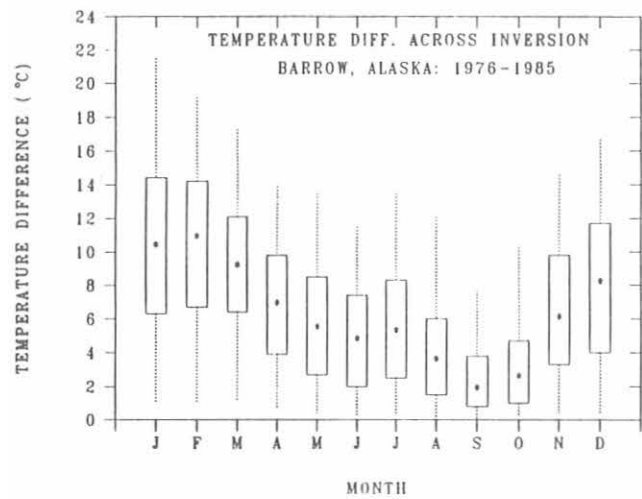


Fig. 3. Monthly distributions of temperature difference across the inversion at BRW, 1976-1985. The box and whisker diagrams show upper and lower quartiles (top and bottom of box), median (asterisk), and 5th and 95th percentiles (outer extent of whiskers).

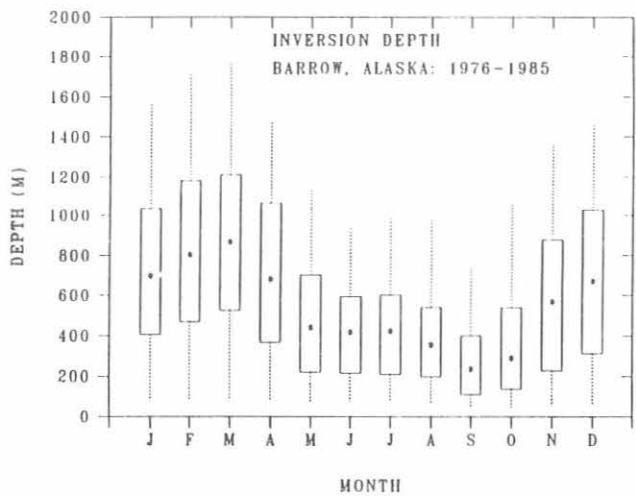


Fig. 2. Monthly distributions of inversion depth at BRW, 1976-1985. The box and whisker diagrams show upper and lower quartiles (top and bottom of box), median (asterisk), and 5th and 95th percentiles (outer extent of whiskers).

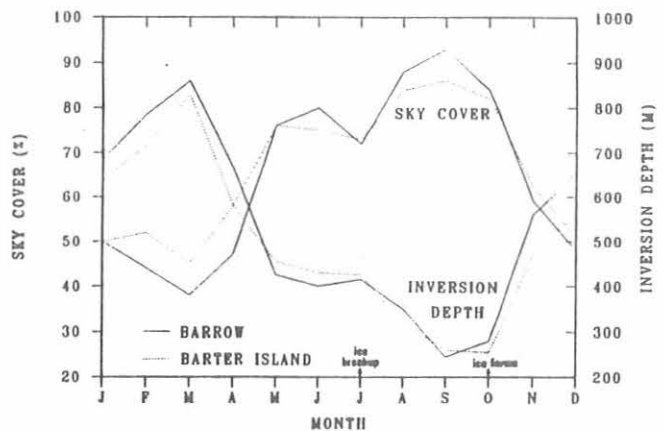


Fig. 4. Mean monthly sky cover, in percent, from 3-hourly surface observations at BRW and at Barter Island, Alaska. Also shown is the monthly median inversion depth from Figure 2 and approximate breakup and formation dates of the land-fast sea ice [after Barry *et al.*, 1979].

3. DISCUSSION

The climatic features of inversions and cloud cover along the Alaskan Arctic coast are part of the complex interactions between radiative forcings [Maykut and Church, 1973], synoptic activity [Serreze and Barry, 1988], and sea-ice dynamics [Barry *et al.*, 1979]. During the winter, the large radiation deficit at the surface fosters the development and maintenance of strong inversions, primarily based on the surface. Synoptic activity in the Alaskan Arctic basin at that time is dominated by anticyclones, and the coastal waters are covered with continuous land-fast ice.

Beginning in March, the radiation deficit is reduced by a rapid increase in solar irradiance combined with a relatively high frequency of clear skies. Throughout the spring the surface temperature rises, accelerating ablation and decreasing the thermal stability near the surface. A mixed layer forms above the surface, elevating the inversion. At this time the cloudiness also increases, weakening the inversion through the increased longwave radiative flux to the surface. Synoptic activity continues to be dominated by anticyclones, while the coastal ice remains stable. The increase in cloudiness and decrease in inversion depth continues until May when a plateau is reached.

TABLE 1. Cumulative Frequency Distributions of Inversion Characteristics at BRW, 1976-1985

Percentile*	Jan.	Feb.	March	April	May	June	July	August	Sept.	Oct.	Nov.	Dec.	All
<i>Height of Inversion Base (m AGL)</i>													
5	0	0	0	0	0	0	0	0	0	0	0	0	0
10	0	0	0	0	0	0	0	0	0	0	0	0	0
25	0	0	0	0	111	31	0	0	49	0	0	0	0
50	0	0	44	117	282	187	89	179	382	343	0	0	116
75	147	169	166	254	521	401	197	420	797	747	216	177	329
90	326	337	287	401	736	730	452	922	1489	1185	413	331	653
95	464	485	397	515	916	1076	799	1453	2415	1490	532	471	977
<i>Inversion Depth (m)</i>													
5	80	82	86	83	68	76	82	63	41	50	58	58	65
10	150	176	213	126	113	120	114	98	59	71	94	103	100
25	405	469	525	366	220	215	209	197	111	137	227	311	232
50	686	791	855	668	429	405	410	342	222	277	555	657	492
75	1032	1183	1212	1066	702	594	601	538	399	538	876	1026	833
90	1330	1490	1516	1359	941	791	856	782	590	826	1200	1294	1203
95	1563	1711	1765	1472	1134	935	982	976	737	1058	1354	1459	1395
<i>Temperature Difference Across Inversion (°C)</i>													
5	1.0	1.0	1.2	0.7	0.4	0.3	0.3	0.2	0.1	0.3	0.4	0.4	0.3
10	2.6	3.4	3.5	1.9	0.9	0.7	0.7	0.4	0.3	0.5	1.1	1.4	0.8
25	6.3	6.7	6.4	3.9	2.7	2.0	2.5	1.5	0.8	1.0	3.3	4.0	2.6
50	10.3	10.8	9.1	6.8	5.4	4.7	5.2	3.5	1.8	2.5	6.0	8.1	5.8
75	14.4	14.2	12.1	9.8	8.5	7.4	8.3	6.0	3.8	4.7	9.8	11.7	9.9
90	18.8	17.4	15.3	12.4	11.1	10.3	11.9	9.1	6.2	7.3	12.6	14.7	13.6
95	21.5	19.2	17.3	13.9	13.5	11.5	13.5	12.1	7.7	10.3	14.6	16.7	15.9

*The value corresponding to the nth percentile indicates that n% of the distribution is less than or equal to that value.

In describing the radiation climate of BRW, *Maykut, and Church* [1973] note that 70% of the annual radiative flux to the surface occurs as longwave radiation. This is consistent with the observed relationship between inversion depth and cloud cover (Figure 4). However, the surface radiation budget fails to explain the late summer peak in cloud cover and the associated weakening of the inversion. A more likely explanation is that the apparent equilibrium between the mean radiative and cloud forcings, established in May, breaks down in July with the breakup of the land-fast sea ice [Barry *et al.*, 1979]. Large areas of open water, combined with prevailing easterly winds [Harris and Herbert, 1980] and the summer peak in the frequency of cyclone activity [Serreze and Barry, 1988], result in nearly continuous sky cover from August until October. Longwave radiation from this enhanced cloud cover further weakens the inversion until October when the coastal waters begin to freeze.

4. REFERENCES

- Barrie, L.A., J.W. Bottenheim, R.C. Schnell, P.J. Crutzen, and R.A. Rasmussen, Ozone destruction and photochemical reactions at polar sunrise in the lower Arctic atmosphere, *Nature*, 334, 138-141, 1988.
- Barry, R.G., and M.W. Miles, Lead patterns in Arctic sea ice from remote sensing data: Characteristics, controls and atmospheric interactions, *Extended Abstracts Volume, Second Conference on Polar Meteorology and Oceanography*, Madison, WI, March 29-31, 1988, pp. 40-43, American Meteorological Society, Boston, 1988.
- Barry, R.G., R.E. Moritz, and J.C. Rogers, The fast ice regimes of the Beaufort and Chukchi Sea coasts, Alaska, *Cold Regions Sci. Technol.*, 1, 129-152, 1979.
- Belmont, A.D., Lower tropospheric inversions at ice island T-3, *J. Atmos. Terr. Phys.*, Special Supplement, Part 1, 215-284, 1957.
- Bodhaine, B.A., Aerosol measurements at four background sites, *J. Geophys. Res.*, 88, 10,753-10,768, 1983.
- Bridgman, H., R.C. Schnell, J.D. Kahl, G.A. Herbert, and E. Joranger, A major haze event near Point Barrow, Alaska during AGASP-II, 2-3 April 1986: Analysis of probable source regions and transport pathways, *Atmos. Environ.*, 23, 2537-2549, 1989.
- Busch, N., U. Ebel, H. Kraus, and E. Schaller, The structure of the subpolar inversion-capped ABL, *Arch. Meteorol. Geophys. Bioclim.*, 31A, 1-18, 1982.
- Harris, J.M., and G.A. Herbert, Carbon dioxide, condensation nuclei and wind climatology of the Barrow GMCC Observatory (1973-1979), *NOAA Data Report ERL ARL-2*, Air Resources Laboratory, Silver Spring, MD, 112 pp., 1980.
- Kahl, J.D., Characteristics of the low-level temperature along the Alaskan Arctic coast, *J. Climatol.*, in press, 1990.
- Maykut, G.A., and P.E. Church, Radiation climate of Barrow, Alaska, 1962-1966, *J. Appl. Meteorol.*, 12, 620-628, 1973.
- Overland, J.E., Atmospheric boundary layer structure and drag coefficients over sea ice, *J. Geophys. Res.*, 90, 9029-9049, 1985.
- Serreze, M.C., and R.G. Barry, Synoptic activity in the Arctic basin, 1979-1985, *J. Climate*, 1, 1276-1295, 1988.
- Vowinkel, E., and S. Orvig, The climate of the North Polar Basin, in *World Survey of Climatology, Vol. 14: Climates of the Polar Regions*, edited by S. Orvig, pp. 129-226, Elsevier, Amsterdam, 1970.

The Global Precipitation Chemistry Project

WILLIAM C. KEENE AND JAMES N. GALLOWAY
University of Virginia, Charlottesville, Virginia 22903

GENE E. LIKENS
Institute of Ecosystem Studies, Cary Arboretum, Millbrook, New York 12545

JOHN M. MILLER
NOAA, Air Resources Laboratory, Silver Spring, Maryland 20910

1. INTRODUCTION

Anthropogenic emissions of SO_2 and NO_x have resulted in widespread acidification of precipitation and subsequent environmental damage in eastern North America and northern Europe. Of numerous research questions posed by this phenomenon, two are of special interest: (1) What was the composition of precipitation prior to the advent of fossil-fuel combustion, and (2) To what degree does the long-distance transport of sulfur and nitrogen species influence the composition of the remote troposphere? The GPCP was initiated in 1979 to address these questions. Principal objectives are to measure the chemical composition of precipitation in remote areas of the world and to determine major processes controlling measured composition. Earlier reports of the GPCP compare the composition of precipitation in remote and impacted regions [Galloway *et al.*, 1982, 1984, 1987]; quantify the importance of, evaluate sources of, and intercompare measurement techniques for carboxylic acids in the atmosphere [Keene *et al.*, 1983, 1989; Keene and Galloway, 1984a, b, 1985, 1986, 1988]; evaluate the cycling of amine compounds in the atmosphere [Gorzelska and Galloway, 1990]; assess factors controlling the chemical composition of precipitation at remote locations [Jickells *et al.*, 1982; Church *et al.*, 1982; Galloway and Gaudry, 1984; Dayan *et al.*, 1985; Likens *et al.*, 1987; Keene *et al.*, 1990]; and present objective methods for differentiating seasalt and non-seasalt constituents in marine precipitation and aerosols [Keene *et al.*, 1986; Hawley *et al.*, 1988]. This report summarizes results of a study made to determine processes controlling the composition of precipitation on Amsterdam Island, Indian Ocean, and describes experiments conducted with formicine ants in order to arrive at a preliminary estimate of the contribution of formic acid by the ants to the global formic acid budget of the atmosphere. On-going research is briefly summarized.

2. MATERIALS AND METHODS

Samples of precipitation were collected by event in scrupulously washed polyethylene containers. Immediately after collection, pH was measured, samples were treated with CHCl_3 to prevent biological activity, and aliquots were sent to the University of Virginia for analyses for major organic and inorganic chemical constituents. To date, we have analyzed samples of precipitation collected at 14 land-based sites during 10 oceanic cruises.

Three colonies each from three different species of formicine ants were collected in central Virginia. Each colony was placed in a $61 \times 20 \times 20$ cm Teflon-lined plexiglass enclosure swept with 16 L min^{-1} of ambient air. Formic acid (HCOOH) in the inlet and outlet air streams was sampled with mist chambers, and concentrations were measured by ion chromatography. Emissions of HCOOH from each colony were determined from differences in HCOOH concentrations in the inlet and outlet air streams. To assess the representativeness of data generated by this procedure, emissions were also measured in the field by inverting the enclosure over an undisturbed ant colony and operating it as above. The colony was subsequently collected and placed inside the enclosure. Emissions from the enclosed colony were then measured. An average detection limit of $3.8 \text{ nmol per colony hour}$ ($0.0054 \text{ nmol per ant hour}$) was calculated from 10 replicate 1-h enclosure blanks.

3. RESULTS AND DISCUSSION

3.1. PROCESSES CONTROLLING THE CHEMICAL COMPOSITION OF PRECIPITATION ON AMSTERDAM ISLAND, INDIAN OCEAN

Samples of precipitation were collected on an event basis at Amsterdam Island in the central Indian Ocean from May 1980 through January 1987 [Moody *et al.*, 1990]. The quality-assured data set corresponded to 179 samples analyzed for major inorganic ions, and a subset of 142 samples analyzed for major carboxylic species. Back trajectories and ^{222}Rn data were used to identify source regions for air masses generating precipitation at the site. The technique of cluster analysis was applied to determine the influence of source region and transport velocity on the chemical composition of precipitation. The most important source regions in terms of ion deposition were Madagascar and/or southeast Africa, and the oceanic region north and east of Amsterdam Island. Several processes were found to influence variability in the chemical composition of precipitation. These include seasonality in the source strength of biogenic precursors for non-seasalt SO_4^{2-} and carboxylic acids, seasonality in continental influences, variations in source region driven by daily changes in meteorology, and seasonal and interannual differences in transport and removal patterns. Interannual differences in non-seasalt SO_4^{2-} concentrations, in particular, suggest a

relationship with changes in large-scale atmospheric circulation patterns, defined by the Southern Oscillation phenomenon.

3.2. ATMOSPHERIC FORMIC ACID FROM FORMICINE ANTS

Comparisons between emissions of HCOOH from undisturbed and enclosed colonies of formicine ants indicate that representative data were generated by the experimental technique [Donoghue, 1990]. The average rate of HCOOH emission from the nine colonies tested was 0.43 ± 0.16 nmol per ant hour. A marked diel periodicity was observed; 70% of the HCOOH was emitted during the day between 0900 and 1700 LST. The emission rate exhibited a significant positive correlation with temperature. Assuming instantaneous vertical mixing to 1000 m, a 1-day atmospheric lifetime, and population densities reported in the literature, we estimate that formicine ants contribute approximately 4% of ambient HCOOH concentrations during the growing season in central Virginia. On the basis of estimated source strengths for HCOOH and ant population densities from the literature, we estimate that formicine ants contribute 24% of HCOOH in the atmosphere over the world's continents.

4. ONGOING RESEARCH

Research efforts currently under way within the GPCP include analysis of a 15-year data record for precipitation chemistry at MLO; assessment of processes controlling the chemical composition of precipitation at Cape Point, South Africa; Torres del Paine, Chile; and Lijiang, China; evaluation of linkages between the cycling of sulfur and nitrogen in the remote atmosphere; and interpretation of atmospheric transport patterns in north central Siberia.

5. REFERENCES

- Church, T.M., J.N. Galloway, T.D. Jickells, and A.H. Knap, The chemistry of western Atlantic precipitation at the mid-Atlantic coast and on Bermuda, *J. Geophys. Res.*, **87**, 11,013-11,018, 1982.
- Dayan, U., J.M. Miller, W.C. Keene, and J.N. Galloway, A meteorological analysis of precipitation chemistry data from Alaska, *Atmos. Environ.*, **19**, 651-657, 1985.
- Donoghue, C., Atmospheric formic acid from formicine ants, M. S. thesis, University of Virginia, unpublished, 1990.
- Galloway, J.N., and A. Gaudry, The chemistry of precipitation on Amsterdam Island, Indian Ocean, *Atmos. Environ.*, **18**, 2649-2656, 1984.
- Galloway, J.N., G.E. Likens, W.C. Keene, and J.M. Miller, The composition of precipitation in remote areas of the world, *J. Geophys. Res.*, **87**, 8771-8786, 1982.
- Galloway, J.N., G.E. Likens, and M.E. Hawley, Acid precipitation: Natural versus anthropogenic compounds, *Science*, **226**, 829-830, 1984.
- Galloway, J.N., D. Zhao, J. Xiong, and G.E. Likens, Acid rain: China, United States and a remote area, *Science*, **236**, 1559-1562, 1987.
- Gorzelska, K., and J. N. Galloway, Amine nitrogen in the atmospheric environment over the North Atlantic Ocean, *Global Biogeochem. Cycles*, submitted, 1990.
- Hawley, M.E., J.N. Galloway, and W.C. Keene, Standard error calculations for non-sea-salt constituents in marine precipitation, *Water Air Soil Pollut.*, **42**, 87-102, 1988.
- Jickells, T.C., A.H. Knap, T.M. Church, J.N. Galloway, and J.M. Miller, Acid precipitation on Bermuda, *Nature*, **297**, 55-56, 1982.
- Keene, W.C., and J.N. Galloway, A note on acid rain in an Amazon rainforest, *Tellus*, **36B**, 137-138, 1984a.
- Keene, W.C., and J.N. Galloway, Organic acidity in precipitation of North America, *Atmos. Environ.*, **18**, 2491-2497, 1984b.
- Keene, W.C., and J.N. Galloway, Gran's titrations: Inherent errors in measuring the acidity of precipitation, *Atmos. Environ.*, **19**, 199-202, 1985.
- Keene, W.C., and J.N. Galloway, Considerations regarding sources for formic and acetic acids in the troposphere, *J. Geophys. Res.*, **91**, 14,466-14,474, 1986.
- Keene, W.C., and J.N. Galloway, The biogeochemical cycling of formic and acetic acids through the troposphere: An overview of current understanding, *Tellus*, **40B**, 322-334, 1988.
- Keene, W.C., J.N. Galloway, and D.H. Holden, Jr., Measurement of weak organic acidity in precipitation from remote areas of the world, *J. Geophys. Res.*, **88**, 5122-5130, 1983.
- Keene, W.C., A.A.P. Pszenny, J.N. Galloway, and M.E. Hawley, Sea-salt corrections and interpretation of constituent ratios in marine precipitation, *J. Geophys. Res.*, **91**, 6647-6658, 1986.
- Keene, W.C., R.W. Talbot, M.O. Andreae, K. Beecher, H. Berresheim, M. Castro, J.C. Farmer, J.N. Galloway, M.R. Hoffmann, S.-M. Li, J.R. Maben, J.W. Munger, R.B. Norton, A.A.P. Pszenny, H. Puxbaum, H. Westberg, and W. Winiwarter, An intercomparison of measurement systems for vapor and particulate phase concentrations of formic and acetic acids, *J. Geophys. Res.*, **94**, 6457-6471, 1989.
- Keene, W.C., G. Wu, R.S. Artz, J.N. Galloway, J. Liu, J.M. Harris, and J.M. Miller, Processes controlling the chemical composition of precipitation at a remote temperate continental site in south-central China, *Proc. of the International Conferences on Global and Regional Environmental Atmospheric Chemistry*, edited by C.S. Kiang, Beijing, PRC, in press, 1990.
- Likens, G.E., W.C. Keene, J.M. Miller, and J.N. Galloway, The chemistry of precipitation from a remote, terrestrial site in Australia, *J. Geophys. Res.*, **92**, 13,299-13,314, 1987.
- Moody, J.L., A.A.P. Pszenny, A. Gaudry, J.N. Galloway, W.C. Keene, and G. Polian, Precipitation composition and its variability in the southern Indian Ocean, 1980-1987, *J. Geophys. Res.*, submitted, 1990.

Radioactivity in the Surface Air at BRW, MLO, SMO, and SPO

RICHARD LARSEN AND COLIN SANDERSON

U.S. Department of Energy, Environmental Measurements Laboratory, New York, New York 10014-3621

1. INTRODUCTION

Air filter samples are routinely collected by CMDL personnel at BRW, MLO, SMO, and SPO for EML's Surface Air Sampling Program (SASP). The primary objective of this program is to study the temporal and spatial distribution of specific natural and anthropogenic radionuclides in the surface air. Of the radionuclides that are analyzed by gamma-ray spectrometry, only the naturally occurring radioisotopes ^7Be and ^{210}Pb are still readily measured in most of the filter samples. ^7Be (half-life 53.2 days) is produced by cosmic-ray interactions in the upper troposphere and the stratosphere. ^{210}Pb (half-life 21 years) is a decay product of ^{222}Rn , which is a natural radioisotope emitted from soils. Because of their distinctly different source

regions, these radioisotopes serve as tracers for upper and lower tropospheric sources and transport processes.

2. MATERIALS AND METHODS

High-volume air filter samples are continuously collected on approximately a weekly basis using Microdon filter material. The air samplers move $\sim 1700\text{ m}^3$ of air per day through a 20-cm diameter filter.

The weekly filter samples collected at BRW and MLO are analyzed by compressing a section of each filter into a 1-2 cm^3 cylinder, which is analyzed by gamma-ray spectrometry using a high-purity germanium (HPGe) detector with a 1.5-cm diameter well. For each site, one-half of each of the weekly filter samples are added together to form a monthly

TABLE 1. Monthly Surface Air Concentrations of Radionuclides at BRW, MLO, SMO, and SPO During 1989

Site	Nuclide	Jan.	Feb.	March	April	May	June	July	Aug.	Sept.	Oct.	Nov.	Dec.
BRW	Gamma (cpm m^{-3})	*	*	*	*	*	<0.01	<0.01	<0.01	<0.01	<0.01	<0.01	<0.01
MLO	Gamma (cpm m^{-3})	<0.01	<0.01	<0.01	<0.01	<0.01	<0.01	<0.01	<0.01	<0.01	<0.01	<0.01	<0.01
SMO	Gamma (cpm m^{-3})	<0.01	<0.01	<0.01	<0.01	<0.01	<0.01	<0.01	<0.01	<0.01	<0.01	<0.01	<0.01
SPO	Gamma (cpm m^{-3})	<0.01	<0.01	<0.01	<0.01	<0.01	<0.01	<0.01	<0.01	<0.01	*	<0.01	<0.01
BRW	^7Be (mBq m^{-3})	*	*	*	*	*	0.2	0.5	0.6	0.6	1.1	1.4	1.5
MLO	^7Be (mBq m^{-3})	5.8	6.1	6.7	5.4	4.9	5.7	4.2	5.0	5.4	3.3	5.9	5.1
SMO	^7Be (mBq m^{-3})	1.7	1.8	1.7	1.3	1.9	2.3	3.0	3.7	3.5	1.9	1.9	2.1
SPO	^7Be (mBq m^{-3})	3.6	4.7	3.2†	1.4	1.4†	1.6	1.8	1.7	1.5	*	1.2	3.0
BRW	^{95}Zr ($\mu\text{Bq m}^{-3}$)	*	*	*	*	*	<4.8	<2.2	<4.5	<2.2	<6.4	<4.0	<3.0
MLO	^{95}Zr ($\mu\text{Bq m}^{-3}$)	<10.6	<8.7	<20.5	<4.9	<12.0	<7.2	<4.8	<7.0	<5.7	<9.4	<4.1	<11.1
SMO	^{95}Zr ($\mu\text{Bq m}^{-3}$)	<6.5	<6.2	<2.9	<3.7	<3.1	<10.3	<2.9	<3.1	<2.6	<2.0	<7.3	<1.6
SPO	^{95}Zr ($\mu\text{Bq m}^{-3}$)	<4.0	<70.8	<67.5	<31.0	<48.4	<8.6	<11.1	<14.9	<18.4	*	33.1	<10.7
BRW	^{137}Cs ($\mu\text{Bq m}^{-3}$)	*	*	*	*	*	<1.0	<0.8	<1.2	<0.7	<1.2	<0.9	<0.9
MLO	^{137}Cs ($\mu\text{Bq m}^{-3}$)	<4.5	<3.5	<3.0	<2.2	<3.7	<2.5	<2.1	<2.1	<2.1	<2.2	<1.3	<4.0
SMO	^{137}Cs ($\mu\text{Bq m}^{-3}$)	<1.6	<2.1	<1.4	<1.1	<1.3	<3.2	<1.0	<0.9	<1.1	<1.6	<1.7	<1.8
SPO	^{137}Cs ($\mu\text{Bq m}^{-3}$)	<1.7	<1.8	<1.3	<1.4	<1.7	<0.8	<1.4	<2.0	<2.5	*	<4.1	<1.7
BRW	^{144}Ce ($\mu\text{Bq m}^{-3}$)	*	*	*	*	*	<3.3	<2.8	<5.1	<2.0	<5.0	<2.9	<3.1
MLO	^{144}Ce ($\mu\text{Bq m}^{-3}$)	<18.4	<14.1	<13.4	<7.6	<15.7	<10.7	<7.5	<8.6	<8.6	<9.2	<5.3	<16.6
SMO	^{144}Ce ($\mu\text{Bq m}^{-3}$)	<6.4	<6.1	<5.5	<4.5	<5.2	<15.2	<4.6	<4.8	<5.1	<2.5	<8.6	<2.4
SPO	^{144}Ce ($\mu\text{Bq m}^{-3}$)	<6.9	<11.5	<8.2	<8.6	<10.2	<3.9	<6.8	<7.4	<11.4	*	<16.4	<7.6
BRW	^{210}Pb (mBq m^{-3})	*	*	*	*	*	0.02	0.06	0.10	0.10	0.25	0.87	0.97
MLO	^{210}Pb (mBq m^{-3})	0.15	0.25	0.34	0.28	0.31	0.26	0.27	0.19	0.27	0.16	0.29	0.20
SMO	^{210}Pb (mBq m^{-3})	*	*	*	*	*	*	*	*	*	*	*	*
SPO	^{210}Pb (mBq m^{-3})	0.03	0.05	0.01	0.03	0.01	0.04	0.03	0.02†	0.03	*	<0.01	0.04

*No data

†Uncertainty is between 20% and 100%; uncertainty for all other concentrations is <20%.

composite sample. These composite samples are compressed into a 45-cm³ plastic planchet, and are routinely analyzed for several gamma-ray-emitting radionuclides using either HPGe n-type low-energy coaxial or Ge(Li) or HPGe p-type coaxial high-resolution germanium detectors. Detailed information on SASP is periodically published [Larsen and Sanderson, 1990].

3. RESULTS

The results of the analyses of several radionuclides and the total gamma-ray activities for the monthly composite samples from filters collected at BRW, MLO, SMO, and SPO during 1989 are reported in Table 1. The total gamma-ray activities are reported in units of counts per minute (cpm) per standard cubic meter (15°C, 1 atm) of sampled air. The surface air concentrations of ⁷Be and ²¹⁰Pb are reported in millibecquerels (mBq) per standard cubic meter of air, and ⁹⁵Zr, ¹³⁷Cs, and ¹⁴⁴Ce are reported in microbecquerels (μBq) per standard cubic meter of air. The concentrations are reported as corrected for radioactive decay to the midpoint of the month of collection. The results

of the analyses on the weekly samples from BRW and MLO are being prepared for publication as an EML report.

4. DISCUSSION

There were no announced atmospheric nuclear weapons tests or other reported significant releases of radioactive materials into the atmosphere during 1989, and the concentrations of fission products such as ⁹⁵Zr, ¹³⁷Cs, and ¹⁴⁴Ce were at or below the lower limits of detection for the analytical and sampling techniques that we currently use to measure them.

Monthly mean concentrations continue to show a seasonal cycle for ⁷Be at all CMDL sites, and a seasonal cycle for ²¹⁰Pb at BRW and MLO.

Acknowledgment. We thank the NOAA/CMDL staff at BRW, MLO, SMO, and SPO for the collection of air filter samples for the SASP.

5. REFERENCE

Larsen, R.J., and C.G. Sanderson, Annual report of the surface air sampling program, *EML-524*, 120 pp., U.S. Department of Energy Environmental Measurements Laboratory, New York, 1990.

Total Nitrate Variations at Mauna Loa

G. LEE AND B. J. HUEBERT

University of Rhode Island, Graduate School of Oceanography, Narragansett, Rhode Island 02882-1197

1. INTRODUCTION

Much of the NO and NO_2 that is emitted into the atmosphere is converted to nitric acid vapor or aerosol nitrate before it is removed by dry or wet deposition. This conversion to nitrate is largely complete within a few days of the odd-nitrogen's emission; therefore, in remote areas such as MLO, the total nitrate concentration (nitric acid vapor and aerosol nitrate) represents a fair estimate of the total odd-nitrogen concentration [Galasyn *et al.*, 1987a, b; Robinson and Harris, 1987].

With support from NSF, we have measured nitrate concentrations at MLO for several years to help identify the important sources of odd-nitrogen compounds in remote parts of the globe. Since August 1988, in collaboration with the MLO staff, we have been measuring total nitrate every night.

2. MATERIALS AND METHODS

Initially, one nylon filter was exposed each night from 2000 to 0800 LST to collect the total nitrate. During the summers of 1988 and 1989, a Teflon/nylon filter pack method, which entails the separate collection and measurement of nitric acid vapor and nitrate aerosol, was used. We began using this method exclusively in March 1990 in an attempt to ascertain the causes of the spring and summer increases in total nitrate from changes in its composition with time. Filters are returned to our URI laboratory for extraction and analysis by ion chromatography. Our final data are sorted using three criteria (wind direction, humidity, and CN count) to eliminate those samples that were influenced by local sources on the island.

3. RESULTS AND DISCUSSION

3.1. SHORT-TERM VARIATIONS

Figure 1 shows the total nitrate variation from August 1988 to July 1990. All samples measured at MLO have been included. No period of steady (less than a 50% change) concentration lasting more than 10 days was measured. Total nitrate concentrations fluctuated unpredictably from day to day. Some of the short-term decreases in total nitrate appear, however, to be related to approaching frontal zones and rain storms. It is most likely, also, that some of the positive spikes in the total nitrate reflect local island sources. Generally, the magnitude of total nitrate short-term variation during spring and summer is much larger than that of fall and winter. Extensive synoptic and dynamic analyses are required to examine closely the details of these short-term variations.

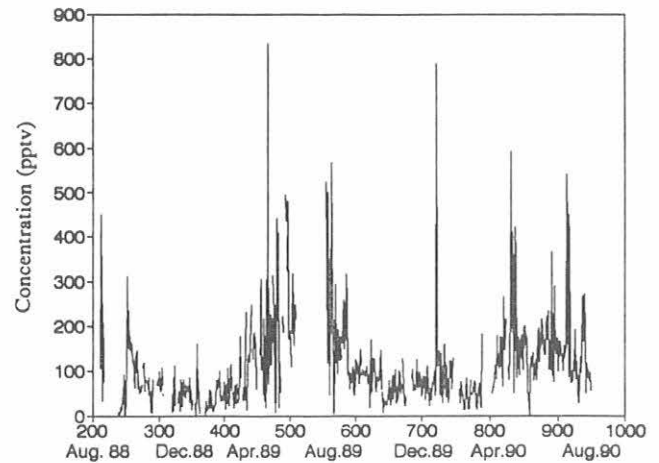


Fig. 1. Total nitrate versus time at MLO, August 1988-July 1990.

3.2. LONGER-TERM VARIATIONS

The most apparent feature of the longer-term variations in total nitrate at MLO is the concentration increase during spring and summer months (Figure 2). This annual variation has been observed every year. Total nitrate in 1989 was higher and more variable than that of 1990. It is unknown whether the causes of the springtime high concentrations are fundamentally different from those in summer. In 1990 a slight concentration dip is evident in May. Because samples were not measured during June 1989, the details of spring and summer total nitrate variations are still unclear.

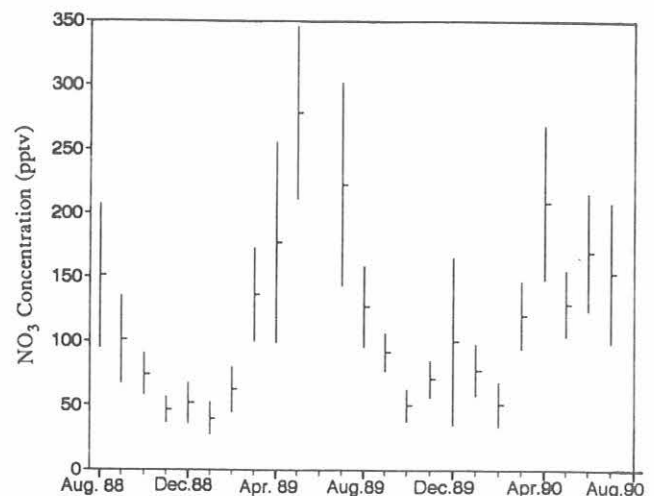


Fig. 2. Monthly mean total nitrate concentrations at MLO with standard deviations.

The averages and standard deviations of total nitrate concentration in winter are small. Compared with data obtained in past years, the large concentrations of total nitrate in December 1989, which lasted about a week, were unusual.

4. ONGOING RESEARCH

We are continuing our nightly sampling from the tower with the help of the MLO staff. Although equipment failures and bad weather (which prevents filter changes on the tower) have occasionally caused brief lapses in the data, a very interesting record is emerging. We hope to identify and

confirm both the frequency and source of high nitrate events during the next year.

5. REFERENCES

- Galasyn, J.F., K.L. Tschudy, and B.J. Huebert, Seasonal and diurnal variability of nitric acid vapor and ionic aerosol species in the remote free troposphere at Mauna Loa, Hawaii, *J. Geophys. Res.*, 92, 3105-3133, 1987a.
- Galasyn, J.F., K.L. Tschudy, and B.J. Huebert, Authors' Reply to the Comment of Robinson and Harris, *J. Geophys. Res.*, 92, 14,868, 1987b.
- Robinson, E., and J. Harris, Comment on "Seasonal and diurnal variability of nitric acid vapor and ionic aerosol species in the remote free troposphere at Mauna Loa, Hawaii," by Galasyn, Tschudy, & Huebert, *J. Geophys. Res.*, 92, 14,865-14,867, 1987.

Seasonal and Latitudinal Trends in the $^{13}\text{C}/^{12}\text{C}$ Ratio of Methane

PAUL QUAY, STAGG KING, JOHN STUTSMAN, AND DAVID WILBUR

University of Washington, School of Oceanography WB-10, Seattle, Washington 98195

1. INTRODUCTION

The isotopic composition of methane (CH_4) can be used to distinguish between various CH_4 sources [e.g., *Stevens and Engelkemeir*, 1988; *Wahlen et al.*, 1989; *Quay et al.*, 1990]. CH_4 released from natural gas and biomass burning sources has a distinctly higher $^{13}\text{C}/^{12}\text{C}$ ratio than does CH_4 microbially produced in anoxic environments like rice paddies, wetlands, and ruminants. Our research at the CMDL sites has focused on measuring the seasonal and latitudinal trends in the $^{13}\text{C}/^{12}\text{C}$ ratio of CH_4 . We intend to use the measured trends in $^{13}\text{CH}_4$ to constrain the spatial and temporal variability in the release rate of CH_4 from wetlands and biomass burning sources. Results of these measurements are discussed in *Quay et al.* [1990].

2. SAMPLING AND ANALYSIS

We have been collecting CH_4 samples for isotopic analysis from the CMDL sites at BRW and MLO, and at a site on the Washington coast (48°N , 126°W) since 1987. In 1989 we initiated a similar sampling program at SMO. We also have had samples collected at Cape Grim (41°S , 144°E) by CSIRO. We ship a pre-evacuated 35- or 15-L flask to the sampling site, where the flask is simply opened, allowed to fill to atmospheric pressure, and then returned to our laboratory. The CH_4 concentration at time of collection is provided by CMDL. Air samples are collected approximately biweekly, except at Cape Grim where collection is bimonthly. CH_4 in the air sample is extracted, purified, and combusted to CO_2 under high vacuum following the procedure developed by *Stevens and Rust* [1982]. The CO_2 is measured for its $^{13}\text{C}/^{12}\text{C}$ ratio using a Finnigan MAT251 mass spectrometer. This procedure yields a CO_2 sample volume of $\sim 30 \mu\text{L}$ for mass spectrometric analysis.

$^{13}\text{C}/^{12}\text{C}$ of the atmospheric CH_4 is reported relative to $^{13}\text{C}/^{12}\text{C}$ of a standard (PDB) using the δ notation (δ):

$$\delta^{13}\text{C} (\text{‰}) = \left[\left(\frac{^{13}\text{C}}{^{12}\text{C}} \right)_{\text{sam}} / \left(\frac{^{13}\text{C}}{^{12}\text{C}} \right)_{\text{std}} - 1 \right] * 1000$$

where sam is the sample and std is the standard. The precision of our $\delta^{13}\text{C}$ measurement is about $\pm 0.04\text{‰}$, based on standards analyzed over the last year.

3. RESULTS AND DISCUSSION

The results of our $^{13}\text{CH}_4$ measurements at our three northern hemisphere sampling sites are presented in Figure 1. The $^{13}\text{CH}_4$ data at BRW and the Olympic Peninsula do not show a significant interannual change; at MLO there appears to be a slight increase in $^{13}\text{CH}_4$ with time. The

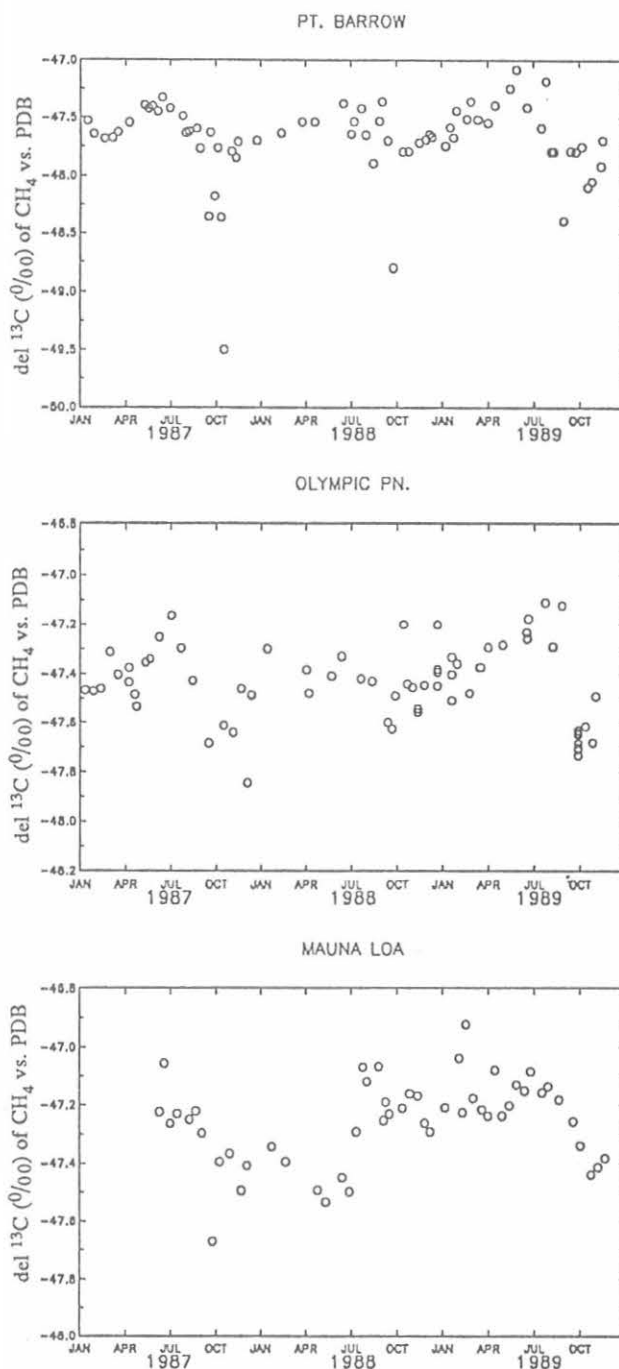


Fig. 1. Time series for the $\delta^{13}\text{C}$ of atmospheric CH_4 at three clean-air sites in the northern hemisphere.

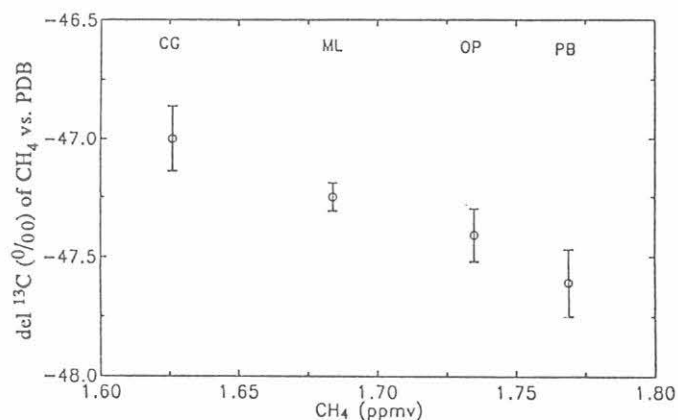


Fig. 2. Relationship between the mean annual $\delta^{13}\text{C}$ and concentration of atmospheric CH_4 at Cape Grim (CG; 41°S, 144°E), MLO (ML; 19°N, 155°W), Olympic Peninsula (OP; 48°W, 126°W), and BRW (PB; 71°N, 156°W).

annual mean $^{13}\text{CH}_4$ values increase southward from an annual mean value of -47.6‰ at BRW to -47.0‰ at Cape Grim, Figure 2. There is an inverse correlation between annual mean CH_4 concentration and $^{13}\text{CH}_4$ (Figure 2). This trend is expected because of the isotopic fractionation during OH oxidation of CH_4 when $^{12}\text{CH}_4$ is oxidized at a slightly faster rate than $^{13}\text{CH}_4$ [e.g., Davidson *et al.*, 1987]. On the basis of the inverse correlation between $^{13}\text{CH}_4$ and CH_4

concentration, we estimate a kinetic isotope effect during CH_4 oxidation (i.e., k_{13}/k_{12}) of 0.993 [Quay *et al.*, 1990].

Our measured global mean average $\delta^{13}\text{C}$ of -47.2‰ , when coupled with a kinetic fractional effect of 0.993, yields a value of -53.3‰ for the $\delta^{13}\text{C}$ of the global CH_4 source. An estimate of the CH_4 released from biomass burning can be derived from the $\delta^{13}\text{C}$ of the global source [e.g. Stevens and Engelkemeir, 1988]. We estimate that biomass burning contributes $\sim 11\%$ of the total CH_4 source strength or $\sim 60 \text{ Tg yr}^{-1}$ based on a total source strength of $\sim 550 \text{ Tg yr}^{-1}$ [Quay *et al.*, 1990].

4. REFERENCES

- Davidson, J.A., C. A. Cantrell, S.C. Tyler, R.E. Shetter, R.J. Cicerone, and J.G. Calvert, Carbon kinetic isotope effect in the reaction of CH_4 with OH, *J. Geophys. Res.*, **92**, 2195-2199, 1987.
- Quay, P.D., S.L. King, J. Stutsman, D.O. Wilbur, L.P. Steele, I. Fung, R.H. Gammon, T.A. Brown, G.W. Farwell, P.M. Grootes, and F.H. Schmidt, Carbon isotopic composition of atmospheric CH_4 : Fossil and biomass burning source strengths, *Global Biogeochem. Cycles*, in press, 1990.
- Stevens, C.M., and A. Engelkemeir, Stable carbon isotopic composition of methane from some natural and anthropogenic sources, *J. Geophys. Res.*, **93**, 725-733, 1988.
- Stevens, C.M., and F.E. Rust, The carbon isotopic composition of atmospheric methane, *J. Geophys. Res.*, **87**, 4879-4882, 1982.
- Wahlen, M., N. Tanaka, R. Henry, B. Deck, J. Zeglen, J.S. Vogel, J. Southon, A. Shemish, R. Fairbanks, and W. Broecker, Carbon-14 in methane sources and in atmospheric methane: Contribution from fossil carbon, *Science*, **245**, 286-290, 1989.

Aerosol Constituents at American Samoa, November 1989

DENNIS L. SAVOIE AND JOSEPH M. PROSPERO

*University of Miami, Rosenstiel School of Marine and Atmospheric Science, Division of Marine and Atmospheric Chemistry
Miami, Florida 33149-1098*

RICHARD ARIMOTO AND ROBERT A. DUCE

*University of Rhode Island, Graduate School of Oceanography, Center for Atmospheric Chemistry Studies
Narragansett, Rhode Island 02882-1197*

1. INTRODUCTION

A major goal of our cooperative work at SMO is to define more rigorously the sources, atmospheric pathways, and fluxes of particulate nitrogen and sulfur species in the remote marine atmosphere. Toward this end, we continue to collect weekly bulk aerosol samples at SMO where past studies [e.g., *Arimoto et al.*, 1987] indicate that the transport of soil material and pollutants from continental sources is extremely low. In addition, daily aerosol samples were collected throughout November 1989, as part of our support for the First Survey Flight of the NASA, GLOBE. The objective of GLOBE is to assess the feasibility of a space-based lidar system that could provide vertical profiles of winds over a substantial portion of the earth. Our task in this endeavor was to place the period of the flight within a climatological framework by comparing the November 1989 results with those from our long-term record. We also used this opportunity to make our first measurements of ammonium and to investigate further the relationship between MSA and nss sulfate at remote sites.

As with our normal weekly samples, the daily samples were collected from onshore winds by drawing air through 20×25 cm Whatman 41 filters at a flow rate of $1.1 \text{ m}^3 \text{ min}^{-1}$. Nitrate, sulfate, and MSA in aqueous extracts of the filters were determined by ion chromatography, ammonium by automated colorimetry, and sodium by flame atomic absorption at the University of Miami; aluminum concentrations were measured by neutron activation analysis at the University of Rhode Island. Mineral aerosol was estimated from aluminum, which constitutes about 8% of the mineral aerosol mass. Nss sulfate was estimated as total sulfate minus sodium times 0.2517, the sulfate to sodium mass ratio in seawater.

2. MEAN CONCENTRATIONS

Samples included in this study were collected from October 31 through November 30, 1989. The wind was out-of-sector more than 80% of the time during the collection of the last sample of the series and therefore the results from that sample are not considered here. For the other samples, the nitrate, sulfate, sodium, and MSA concentrations in the samples were all well above their detection limits; concentrations on the filters were at least 10 times higher than in the blanks, and the net concentrations (total-blank) were always at least 50 times higher than the

standard deviation of the blank. In contrast, the ammonium and aluminum blanks accounted for a major fraction of the total concentrations of these species in most of the samples. Gross ammonium concentrations in the samples were usually only a factor of 2 higher than the blanks, and most net concentrations were only factors of 3-4 higher than the standard deviation of the blank. For aluminum, the gross sample concentrations were frequently within the range of the blanks and were never more than a factor of 3 higher than the average blank. Because the reported sample concentrations are based on the net sample concentration (gross minus average blank), calculated negative concentrations frequently result when the atmospheric concentrations are extremely low, as is the case for aluminum. Though the results clearly attest to the very low concentrations of ammonium and mineral dust at the site, the high relative errors for these constituents make it difficult to assess the real day-to-day variations in their concentrations.

Four of the samples were collected over 2-day (as opposed to 1-day) periods. In calculating the statistical parameters for the data set, we assigned each day of these 2-day periods the same set of concentrations, i.e., the mean concentrations for the 2-day period. The statistics calculated on this basis are presented in Table 1 along with other comparative data. The levels of most of the various constituents are roughly equivalent to those from the complete long-term data set and to those from all previous Novembers. Moreover, the similarity of the SMO and Rarotonga ($21^{\circ}15'S$, $159^{\circ}45'W$) data indicate that the SMO concentrations may apply to a broad region of the tropical South Pacific. There are, however, some temporal and geographical differences that are significant and may prove to be important.

The mean nitrate concentration at SMO during November 1989 is about 35% higher than the long-term (1983-1987) November mean and 55% higher than the overall 1983-1987 mean. Although the various means at Rarotonga exhibit a similar trend, the differences are not as dramatic. Also, while the overall long-term means at SMO and Rarotonga are essentially identical, the November 1989 mean at SMO is about 25% higher than that at Rarotonga.

The mean nss sulfate concentration during November 1989 is identical to the 1983-1987 November mean and also does not differ significantly from the overall 1983-1987 mean. As with nitrate, the November 1989 mean nss sulfate at SMO is significantly higher than that at Rarotonga by about 30%.

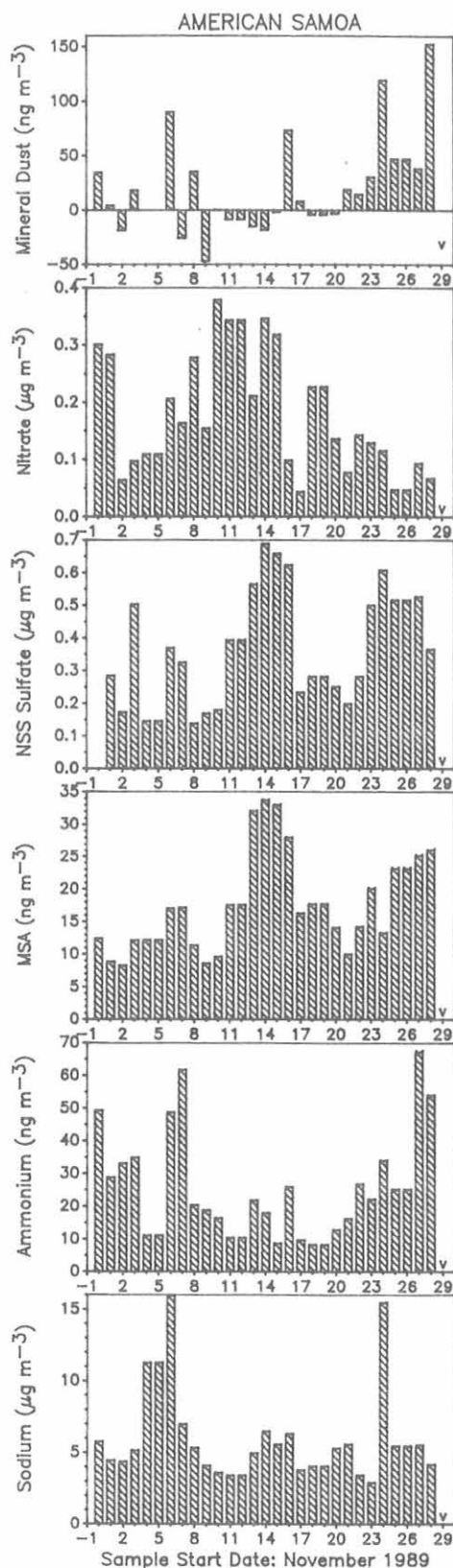


Fig. 1. Daily-average concentrations of chemical species in atmospheric particulates at SMO during November 1989.

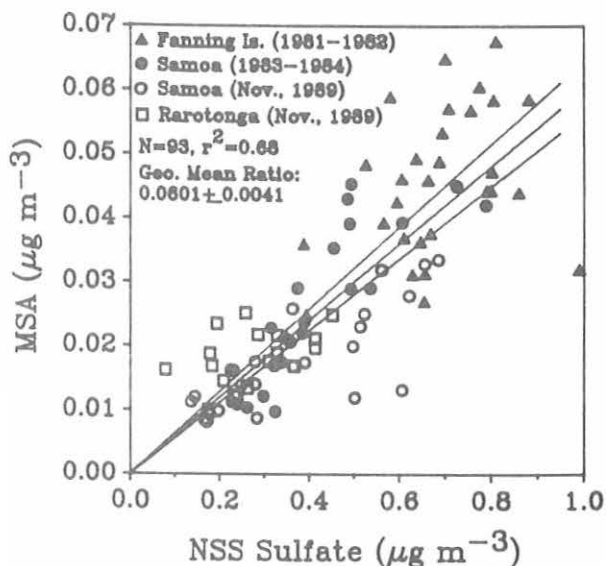


Fig. 2. MSA versus nss sulfate at SMO, Fanning Island, and Rarotonga for various time periods.

Acknowledgments. We thank T. Snowdon, R. Nees, Huang F., Huang T., and M. Izaguirre (all of the University of Miami) and J.D. Cullen (University of Rhode Island) for their technical assistance. We also thank C. Farmer and E. Wilson-Godinet (NOAA/CMDL/SMO) for maintaining and operating our sampling systems. We gratefully acknowledge the cooperation of B. Mendonca and NOAA/CMDL Boulder for allowing us to continue our program at SMO. This work was supported under NASA contract NAG 8-621.

5. REFERENCES

- Arimoto, R., R.A. Duce, B.J. Ray, A.D. Hewitt, and J. Williams, Trace elements in the atmosphere of American Samoa: Concentrations and deposition to the tropical South Pacific, *J. Geophys. Res.*, **92**, 8465-8479, 1987.
- Prospero, J.M., and D.L. Savoie, Effect of continental sources on nitrate concentrations over the Pacific Ocean, *Nature*, **339**, 687-689, 1989.
- Prospero, J.M., M. Uematsu, and D.L. Savoie, Mineral aerosol transport to the Pacific Ocean, in *Chemical Oceanography*, vol. 10, edited by J.P. Riley, R. Chester, and R.A. Duce, pp. 188-218, Academic, London, 1989.
- Quinn, P.K., R.J. Charlson, and T.S. Bates, Simultaneous observations of ammonia in the atmosphere and ocean, *Nature*, **335**, 336-338, 1988.
- Saltzman, E.S., D.L. Savoie, J.M. Prospero, and R.G. Zika, Atmospheric methanesulfonic acid and non-seasalt sulfate at Fanning and American Samoa, *Geophys. Res. Lett.*, **12**, 437-440, 1985.
- Saltzman, E.S., D.L. Savoie, J.M. Prospero, and R.G. Zika, Methanesulfonic acid and non-sea-salt sulfate in Pacific air: Regional and seasonal variations, *J. Atmos. Chem.*, **4**, 227-240, 1986.
- Savoie, D.L., J.M. Prospero, and E.S. Saltzman, Nitrate, non-seasalt sulfate and methanesulfonate over the Pacific Ocean, in *Chemical Oceanography*, vol. 10, edited by J.P. Riley, R. Chester, and R.A. Duce, pp. 219-250, Academic, London, 1989a.
- Savoie, D.L., J.M. Prospero, J.T. Merrill, and M. Uematsu, Nitrate in the atmospheric boundary layer of the tropical South Pacific: Implications regarding sources and transport, *J. Atmos. Chem.*, **8**, 391-415, 1989b.
- Savoie, D.L., J.M. Prospero, R. Larsen, and E.S. Saltzman, Nitrogen and sulfur species in aerosols at Mawson, Antarctica, and their relationship to natural radionuclides, *J. Atmos. Chem.*, in preparation, 1990.

Update on the O-Ring Bias as Determined from MLO Precipitation Chemistry Samples

G. J. STENSLAND

Illinois State Water Survey, Atmospheric Science Division, Champaign, Illinois 61820

In a cooperative study with the CMDL staff at MLO, special precipitation samples were collected to evaluate the bias (contamination) introduced into the chemical results by the O-ring in the lid of the collection/shipping container. This O-ring bias may be important for other data sets because the majority of precipitation chemistry networks in the United States have used this collection/shipping container since 1978. Sample collection in this cooperative project began in February 1984, and by December 1987, 73 sample sets had been collected. A summary of the O-ring effect on pH for these first 73 samples was presented in the *Geophysical Monitoring for Climatic Change, No. 17: Summary Report 1988* [Elkins and Rosson, 1989].

Sample collection continued through October 1989. The complete sample set (117 samples) has now been analyzed and quality assured. The research in progress consists of a final interpretation of these 117 sample sets to determine the O-ring bias on pH, SO_4^- , NO_3^- , NH_4^+ , CA^{++} , MG^+ , NA^+ , and K^+ . Results will be compared with results from measurements obtained at a Pennsylvania site and a Baltimore site that should be published next year.

REFERENCE

- Elkins, J.W., and R.M. Rosson (Eds.), *Geophysical Monitoring for Climatic Change, No. 17: Summary Report 1988*, 130 pp., NOAA Air Resources Laboratory, Boulder, CO, 1989.

Trends of the Carbon Isotopic Composition of Atmospheric Methane in the Southern Hemisphere

C. M. STEVENS AND A. ENGELKEMEIR

Argonne National Laboratory, Chemical Technology Division, Argonne, Illinois 60439

The long-term trend of the stable carbon isotopic composition of atmospheric CH₄ in the southern hemisphere was investigated using air samples collected at SMO. The objective of this program is to apply the results to understanding the causes of the increasing global concentration of atmospheric CH₄. The interpretations of the results to date, including those of the only air samples collected in 1989, were summarized by *Stevens and Engelkemeir* [1989]. These results show ¹³CH₄ increasing in both hemispheres, but with a greater rate of increase in the southern hemisphere. Increasing fluxes of isotopically heavy CH₄ from biomass burning in the southern hemisphere during the past decade

are calculated to be 3-4 Tg yr⁻² (Tg = 10¹² g), which is 50% of the increasing concentration of atmospheric CH₄ and hence a major cause of atmospheric CH₄ increase. A detailed analysis of the isotopic results will be given in a forthcoming paper.

REFERENCES

- Stevens, C.M., and A. Engelkemeir, Trends of the carbon isotopic composition of atmospheric methane, in *Geophysical Monitoring for Climatic Change, No. 17: Summary Report 1988*, edited by J. W. Elkins, pp. 131-132 NOAA Air Resources Laboratory, Boulder, CO, 1989.

Bromine and Surface Ozone Atmospheric Chemistry at Barrow, Alaska, During Spring 1989

W. T. STURGES AND R. C. SCHNELL

Cooperative Institute for Research in Environmental Sciences, University of Colorado, Boulder, Colorado 80309-0216

S. J. OLTMANS

NOAA, Climate Monitoring and Diagnostics Laboratory, Boulder, Colorado 80303-3328

S. LANDSBERGER

University of Illinois, Department of Nuclear Engineering, Urbana, Illinois 61801

S.-M. LI

Atmospheric Environment Service, Downsview, Ontario M3H 5T4, Canada

1. INTRODUCTION

Surface ozone and particulate and gaseous bromine were measured at BRW during March and April 1989 to examine the causes of surface ozone destruction during the Arctic spring. A simple photochemical experiment was performed to investigate the rate of particulate bromine formation.

2. METHODOLOGY

Samples were collected during 12-h periods, with change-over at about 1000 and 2220 LST. Particulate bromine was collected on PTFE or Nuclepore membranes. Organic halogen gases were collected by absorption in Tenax GC chromatography absorbent in 4-mm-inside-diameter glass tubes. Inorganic bromine gases were collected on KOH-impregnated cellulose filters downstream of either a PTFE filter or an MgO denuder and filter combination. Ozone data, consisting of consecutive hourly average concentrations, were obtained from routine measurements at BRW by CMDL staff, as were meteorological data.

PTFE filter samples were analyzed by neutron activation analysis (NAA). Nuclepore filters were water extracted for bromide ion analysis by ion chromatography. Tenax tubes were thermally desorbed into a gas chromatograph, and organic halogenated species were measured with an electron capture detector.

A simple experiment was performed at BRW to determine if filterable bromine formation could be induced in the ambient nighttime atmosphere by illumination with long-wavelength UV (actinic) light. Air drawn into the building was split through two identical Pyrex glass tube chambers, one of which was surrounded by actinic fluorescent tubes that simulate the actinic spectrum of midday solar radiation at BRW at that time of year. The other chamber was blacked out and acted as a control for the illuminated chamber results. Both chambers were connected to filter packs. Experiments were conducted during the hours of total darkness and only when the air was flowing off the Arctic Ocean so that the key bromine species would be present, but not at times when

ozone was already almost completely removed so as to prohibit further reactions.

3. RESULTS AND DISCUSSION

The surface ozone record for the study period is shown in the top panel of Figure 1. Several large negative excursions in ozone are numbered 1-5. Episodes with concentrations more typical of a well-mixed and nondepleted troposphere are identified by the letters A-C. These high-ozone periods occurred during either incursions of Pacific air or downslope air off the Brooks Range mountains. There was no consistent evidence for an impact on ozone during airflow from local combustion sources, taken as occurring when winds were from 215-320° (a less stringent definition than normal of the clean-air sector is required in considering ozone chemistry).

Particulate total bromine (f-Br) amounts measured by NAA are shown in the center panel of Figure 1. The major ozone depletion events occurred during times of elevated f-Br, although the f-Br record is incomplete during several of these events due to difficulties in access to the station.

Bromoform concentrations are plotted in the lower panel of Figure 1. Dibromochloromethane and bromodichloromethane concentrations (not shown in the figure) were strongly correlated to bromoform, but at about an order of magnitude lower levels [Sturges *et al.*, 1990a], suggesting a common origin, which we believe to be Arctic sea ice microalgae [Sturges *et al.*, 1990b]. Bromoform peaked at about the same time as f-Br, approximately coinciding with ozone depletion events 1 and 2.

Inorganic gaseous bromine is discussed by Sturges *et al.* [1990a]. It was found to be a relatively minor component of total atmospheric bromine, and was not strongly correlated to ozone depletion.

Figure 2 shows the amount of f-Br formed in the illuminated chamber in excess of that measured in the (dark) control chamber. The gradient of the line implies a rate of formation of f-Br of 7.9 ng Br m⁻³ min⁻¹; i.e., it would take on the order of minutes to form the ambient f-Br concentrations observed in this study. A study of air mass trajectories and satellite

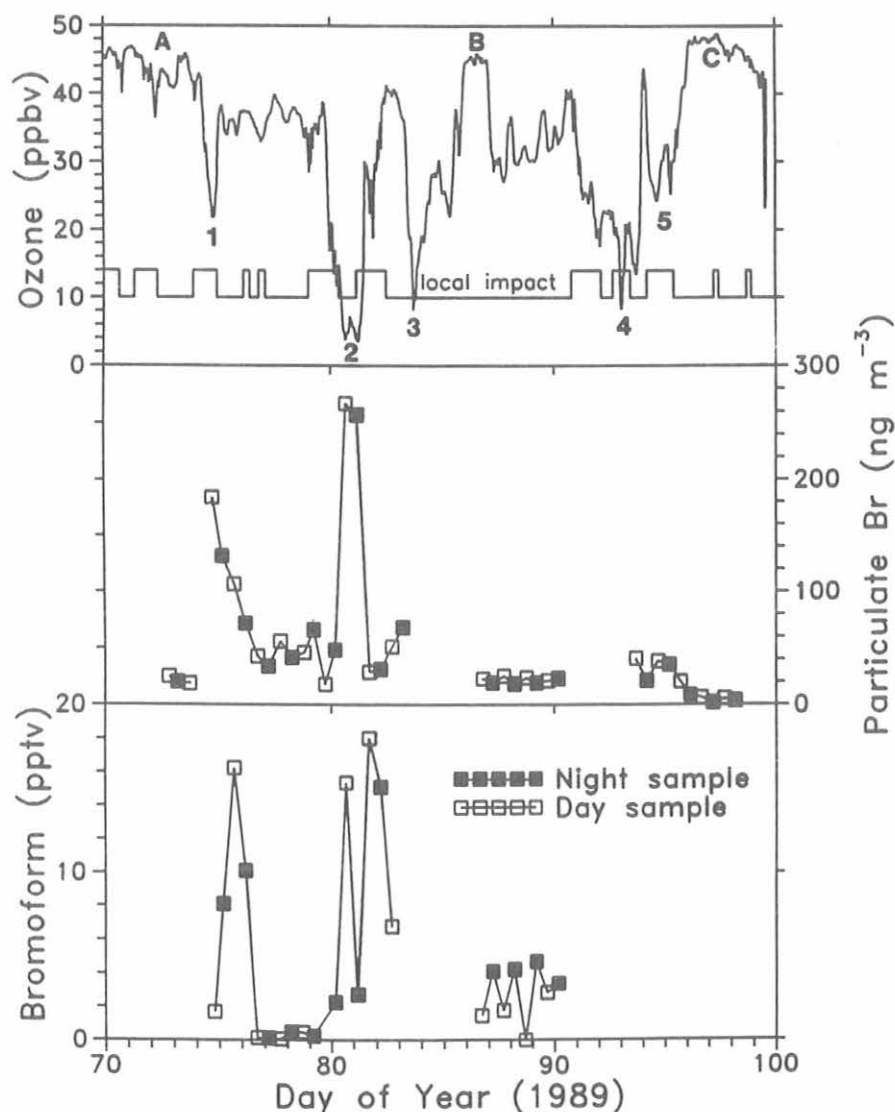


Fig. 1. Ozone, particulate bromine (f-Br), and bromoform gas measurements from March 11 to April 10 (LST), 1989, at BRW. Open symbols are day samples; filled symbols are night samples. In the top panel, numbers 1-5 refer to ozone depletion events, and letters A-C refer to high-ozone periods.

images during this period [Sturges *et al.*, 1990a] indicated that ozone depletion was associated with transport from open leads in the Arctic Ocean, at most 1 or 2 days upwind. This also indicates that the reaction rates of bromine-ozone photochemistry are rapid.

Such rapid photochemistry disagrees with a model of ozone destruction involving gas-phase photolysis of bromoform [Barrie *et al.*, 1988]. Can the two sets of observations be reconciled? One clue comes from a comparison of the NAA and IC results (Figure 3). Total bromine was invariably higher than bromide ion, and the greatest discrepancy was at night. We propose that organic bromine-rich particles undergo reactions to produce more readily photolyzable forms of bromine with an accompanying conversion to inorganic bromine in the particle.

Independent evidence for the existence of such particles has been recently shown (P. J. Sheridan, personal communication, AGASP III mission). Leads may be a possible source of these particles.

4. CONCLUSIONS

Dramatic surface ozone destruction events at BRW in the spring are accompanied by elevated levels of filterable bromine (f-Br) and organic bromine gases. Photochemical experiments showed a rapid formation potential for f-Br in the Arctic spring atmosphere; there is also evidence that ozone depletion is a rapid process. Simple gas-phase photolysis of bromoform is evidently too slow to account for such fast reactions, but there is evidence that organic

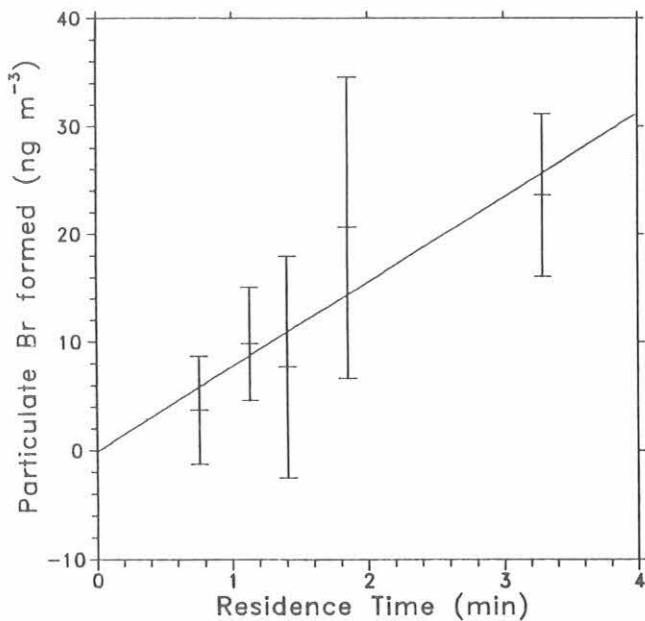


Fig. 2. Excess f-Br formed in the photochemical chamber. The error bars are analytical uncertainty (1 sigma).

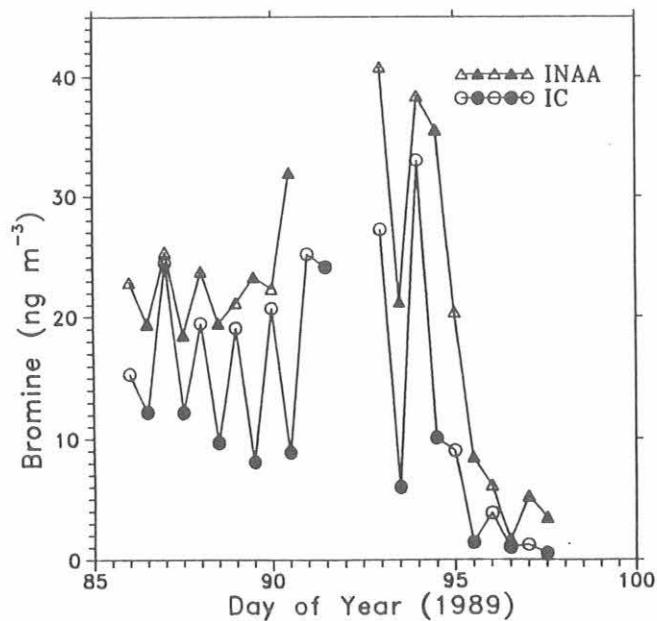


Fig. 3. Comparison of analyses of total elemental bromine by NAA and of bromide ion by IC. Open symbols are day samples, filled symbols are night samples.

bromines in the particulate phase may take part in fast photolytic processes.

Acknowledgments. We acknowledge support and assistance from the National Research Council, NOAA/CMDL, the BRW staff, and the North Slope Borough.

REFERENCES

Barrie, L.A., J.W. Bottenheim, R.C. Schnell, P.J. Crutzen, and R.A.

- Rasmussen, Ozone destruction and photochemical reactions at polar sunrise in the lower Arctic atmosphere, *Nature*, 334, 138-141, 1988.
- Sturges, W.T., R.C. Schnell, S. Landsberger, S.J. Oltmans, J.M. Harris, and S.-M. Li, Chemical and meteorological influences on surface ozone destruction at Barrow, Alaska, during spring 1989, *Atmos. Environ.*, submitted, 1990a.
- Sturges, W.T., C.W. Sullivan, R.C. Schnell, L.E. Heidt, and W.H. Pollack, Bromine production by Antarctic ice algae: The source of ozone-depleting bromine radicals in the polar troposphere?, *Nature*, submitted, 1990b.

USGS Barrow Observatory

JACK TOWNSHEND

U.S. Geological Survey, College Observatory, Fairbanks, Alaska 99775-5160

The USGS Barrow observatory is the northernmost of this agency's 12 continuously recording, digital magnetic observatories. As such, it serves as a singularly important site in a global network of observing stations whose combined data define the planetary magnetic field and track its secular change. Ground stations such as that at Barrow are controls for field modeling by harmonic analysis, essential reference stations for airborne and satellite surveys, and absolute calibration locations for field survey instrumentation. The observatory is operated from the USGS College Observatory at the University of Alaska in Fairbanks, as a satellite station. Staff scientists from the College Observatory visit the site bimonthly to make absolute observations, perform routine equipment maintenance, and retrieve data on magnetic tape. Staff from NOAA CMDL make weekly visits to the site to check equipment operation and occasionally perform emergency service when problems occur and a staff

person is not available from the College Observatory to make repairs.

The primary equipment used to acquire the magnetic data is an EDA FM-100BR Triaxial fluxgate magnetometer, an EDA PPM-105 proton free-precession magnetometer, an observatory magnetometer interface system, and several pier-mounted instruments for absolute control of observations. Data are retrieved by telephone periodically through a computer modem by the USGS office in Golden, Colorado.

A seismograph is operated on site in a vault 6.1 m beneath the ground surface. Access to the vault is down a ladder through a 76.2-cm-diameter vertical tunnel. The present seismic program is operated in cooperation with the Geophysical Institute at the University of Alaska, Fairbanks.

The USGS Barrow observatory has been in continuous operation since 1949.

Radon from Distant Continents Detected at the Mauna Loa Observatory

S. WHITTLESTONE

Australian Nuclear Science and Technology Organization, PMB 1, Menai, NSW, 2037 Australia

1. INTRODUCTION

Radon is widely used as a tracer for air masses that have passed over land within the last few days, because radon is an inert gas unaffected by chemical interactions in transit and because land emits about 100 times more radon per square meter than does the ocean [Wilkening and Clements, 1975].

Previous continuous observations of maritime radon have been at sea level [Lambert *et al.*, 1970; Whittlestone, 1985a; Downey *et al.*, 1989; Pereira *et al.*, 1988]. At a station on the coast at sea level, the direct contribution of local land to the radon concentration in onshore winds is negligible. Events in which radon is transported from distant continents are clearly defined. For example, at Macquarie Island, about 2000 km south of Australia in the Southern Ocean, radon concentrations are generally below 100 mBq m⁻³ but can rise to more than 1000 mBq m⁻³ when the air is from Australia [Downey *et al.*, 1989]. Air mass trajectory calculations confirmed the continental origin of the air at times of enhanced radon concentrations. Radon measurements at such sites provide evidence of continental contamination of baseline air samples, an indication of dilution of the continental air during its trajectory, and accurate timing of air mass transport for assessment of air transport models.

MLO is located on the north-northeast slope of the Mauna Loa volcano at an altitude of 3397 m. This is above the trade wind inversion at some times and below it at others. Air influenced by the island is most likely to reach the observatory when sun warms the mountain, causing convective "upslope" winds. Radon measurements at this site could certainly provide evidence of contamination of baseline air, but it was not clear prior to this study whether the knowledge gained would contribute significantly to that obtained from several other parameters already used at MLO to characterize the air mass. Some preliminary measurements by Hutter *et al.* [1989] have shown that there is a substantial difference between the radon concentrations during episodes when the wind is from the island (upslope winds) compared with concentrations in free-tropospheric air.

Only long-term observations could determine the concentrations in the boundary layer, in the free troposphere, or from the island under a range of air mass transport conditions. This study presents preliminary data from continuous measurement of radon at MLO during August-December 1989. Meteorological data were correlated with the radon concentrations. A number of particular events were singled out to demonstrate the range of radon concentrations from local and distant sources.

2. INSTRUMENTATION

The radon detector was modeled on that described by Whittlestone [1985b]. The sensitivity was 0.189 counts s⁻¹ for a concentration of 1 Bq m⁻³. A 30% statistical error from a 1-h count was obtained at a concentration of 15 mBq m⁻³. The background count rate of the detector was difficult to evaluate. An upper limit was set by the median of the 10 lowest concentrations measured during the 5-month period, that is 30 mBq m⁻³. The detector response time was 90 minutes to 50% of maximum.

3. RESULTS

Figure 1 shows five typical summer days in August, having a strong diurnal cycle in all parameters. The maximum radon and particle concentrations occurred during periods of upslope (northerly) winds. A high dew point during these periods confirms the presence of moist boundary layer air. The initial impression from Figure 1, that radon is strongly correlated with particles, does not hold in general. On August 28, there was a strong radon signal, but few particles. This most likely arose because the radon source was broadly distributed, whereas particles generally come from human habitations. The upslope winds inevitably brought radon, but brought many particles only when the trajectory was over a town or some other source of particles.

A more detailed analysis of data for the whole month of August showed that radon levels were low even for moist air, except when the wind was upslope, bringing radon from the island. Such radon concentrations indicated, therefore, that the air in both the free troposphere and the boundary layer had not contacted land for a period long compared with the 4-day half-life of radon.

In November, the weather conditions were different, having predominantly southerly local winds (Figure 2) and low dewpoint. The radon levels were much higher, having peaks up to 700 mBq m⁻³ on a background of 250 mBq m⁻³, compared with peaks of about 250 mBq m⁻³ on a background of 70 mBq m⁻³ in August. There was no positive correlation with particles, and no systematic increase during upslope wind directions. In fact, close examination of the data shows that the highest radon concentrations generally occurred when the air was sampled from the free troposphere, i.e., when dewpoint and particle concentrations were lowest. Radon concentrations in the boundary layer were low, and most of what was measured could be attributed to local sources. From the radon measurements, then, it appears that air from a distant continent had been mixed into the free

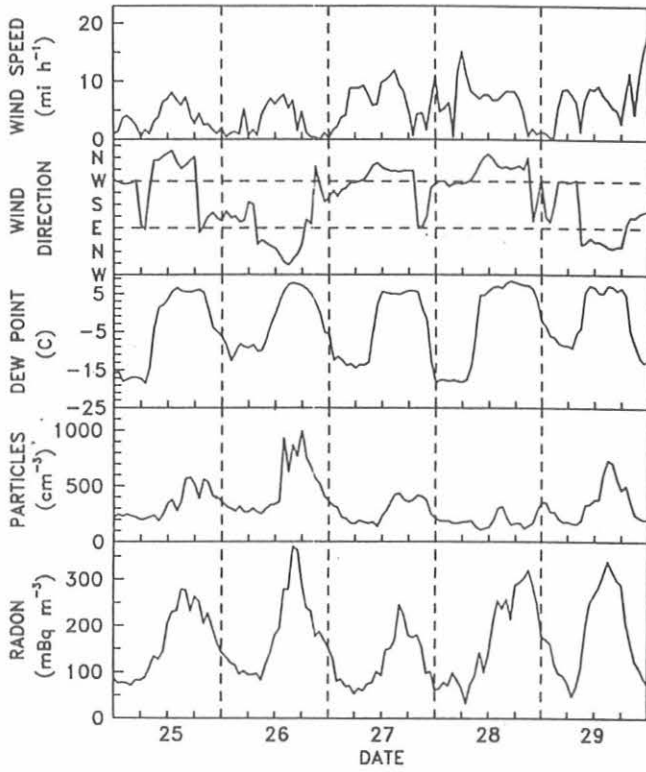


Fig. 1. Meteorological data, particle counts, and radon concentrations at MLO in August 1989.

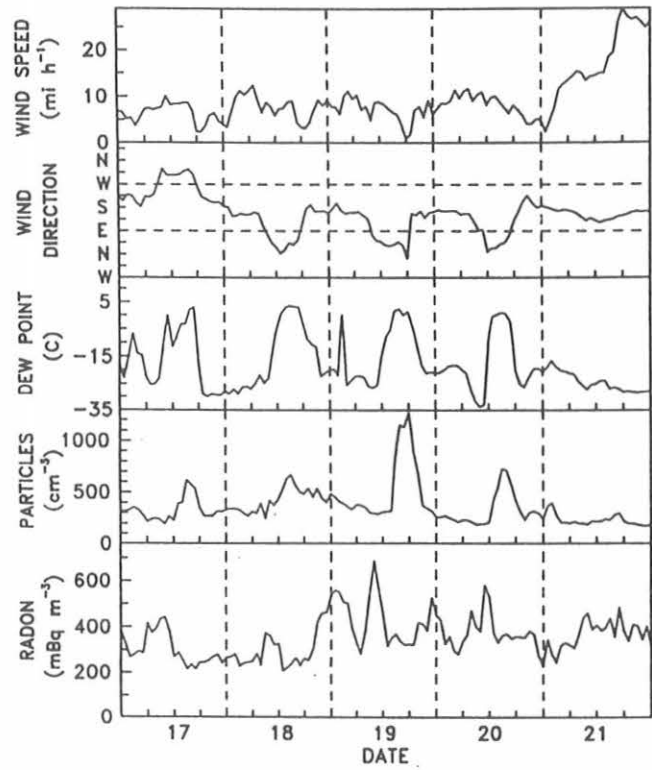


Fig. 2. Meteorological data, particle counts, and radon concentrations at MLO in November 1989.

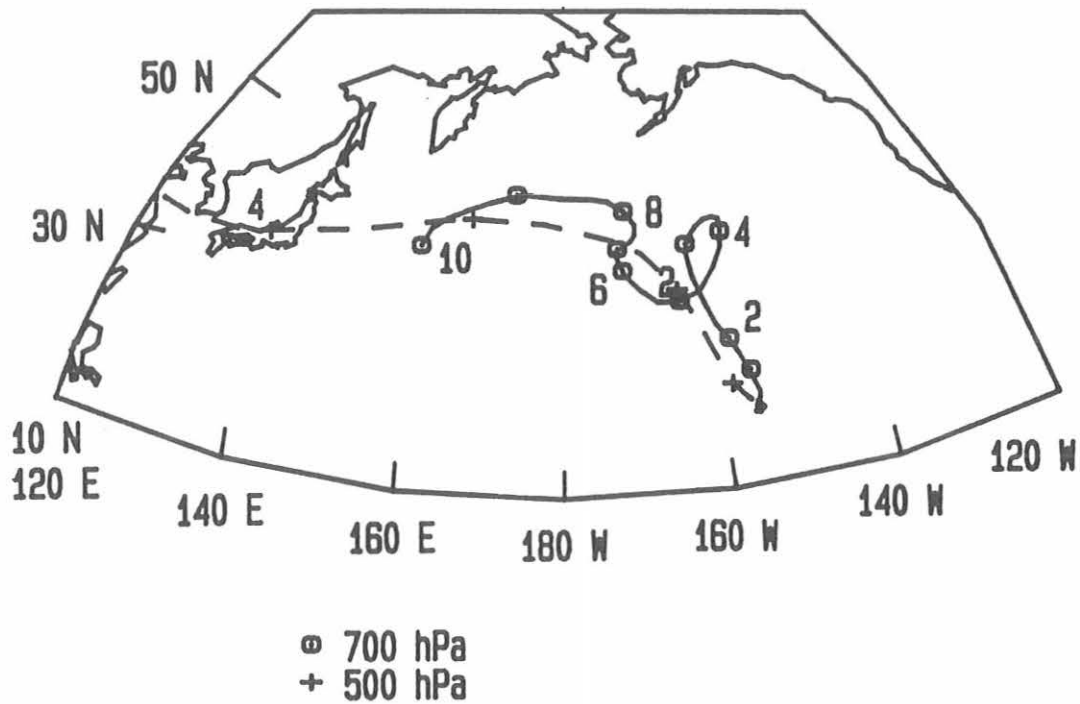


Fig. 3. Back trajectory calculations ending at MLO at 0200 on November 19, 1989.

troposphere and transported to the observatory with relatively little mixing to the boundary layer.

This interpretation of the radon results was confirmed by back trajectory calculations. Figure 3 shows a typical trajectory for the boundary layer (700 hPa) and the free troposphere (500 hPa) for the period shown in Figure 2. Symbols are plotted for each day of the trajectory. The free-tropospheric air (dashed line) had come from Asia in about 5 days. Transport was much slower in the boundary layer and had not passed near land during the 10 days before reaching the observatory.

4. CONCLUSIONS

Radon measured at MLO with a limit of detection of 15 mBq m⁻³ has provided unequivocal real-time proof that the air contacted land during the few weeks before it reached MLO. This applies equally to boundary layer and free-tropospheric air. Radon is therefore a valuable addition to the other parameters such as wind speed, wind direction, and dew point used to characterize the air sampled at MLO.

The absolute values of the radon concentrations at MLO are similar to those of another remote location, Macquarie Island, ranging from about 20 to more than 1000 mBq m⁻³. The maximum concentrations of radon in the lower boundary layer and the free troposphere are also very similar. This indicates that long range transport of a non-reactive gas can

be just as efficient via the free troposphere as transport in the boundary layer.

Acknowledgments. The author is grateful to CMDL for providing the laboratory space and technical support for this work. Particular thanks are due to Elmer Robinson for his assistance during installation and S. Ryan for his skilled maintenance and operation of the detector.

5. REFERENCES

- Hutter, A.R., A.C. George, M.L. Maiello, I.M. Fisenne, R.J. Larsen, H.L. Beck, and F.C. Wilson, ²²²Rn, ²²²Rn progeny and ²²⁰Rn progeny as atmospheric tracers of air mass at the Mauna Loa Observatory, 26 pp., Internal report of the Environmental Measurements Laboratory, U.S. Department of Energy, New York, NY, 1989.
- Downey, A., J.D. Jasper, J. Gras, and S. Whittlestone, Lower tropospheric transport over the Southern Ocean, *J. Atmos. Chem.*, in press, 1989.
- Lambert, G., G. Polian, and D. Taupin, Existence of periodicity in radon concentrations and in the large-scale circulation at lower altitudes between 40° and 70° south, *J. Geophys. Res.*, 75, 2341-2345, 1970.
- Pereira, E.B., A.W. Setzer, and I.F.A. Cavalcanti, ²²²Rn in the Antarctic Peninsula during 1986, *Radiat. Prot. Dosim.*, 24(14), 85-88, 1988.
- Whittlestone, S., Radon measurements as an aid to the interpretation of atmospheric monitoring, *J. Atmos. Chem.*, 3, 187-201, 1985a.
- Whittlestone, S., A high sensitivity Rn detector incorporating a particle generator, *Health Phys.*, 49 (5), 847-852, 1985b.
- Wilkening, M.H., and W.E. Clements, Radon-222 from the ocean surface, *J. Geophys. Res.*, 80, 3828-3831, 1975.

11. International Activities, 1989

CMDL continued cooperative flask air sampling agreements with Australia (Cape Grim), Barbados (Ragged Point), Canada (Alert and Mould Bay), France (Amsterdam Island), Japan (Syowa Station, Antarctica), Norway (Station M), and the United Kingdom (Halley Bay, Antarctica, and South Georgia Island). Sampling was begun in Bermuda in cooperation with the AEROCE program.

P. Tans, J. Peterson, and K. Thoning attended the Third International Carbon Dioxide Conference on Analysis and Evaluation of Atmospheric CO₂ Data Present and Past, held October 16-20 in Hinterzarten, Federal Republic of Germany.

P. Tans visited CSIRO, Division of Atmospheric Research, in Melbourne, Australia, on June 19-July 22, to work with R. Francey on CO₂ stable isotopes.

L. Waterman and representatives of the Chevron Shipping and Chevron Research Companies met in San Francisco to discuss the collection of shipboard air samples aboard Chevron vessels. Since emphasis will be on investigation of continental sources of CH₄, vessel routes near Asia were examined. One such route runs between Singapore and Hong Kong in the South China Sea. The suitability of the route and the vessel will be tested using an NDIR analyzer to make continuous measurements of CO₂ simultaneously with flask sampling on the first voyage. It is planned to have the flasks shipped via Singapore.

A public service commendation plaque was presented in San Francisco by L. Waterman to Captain M. McGilvary of the *MV Southland Star* to recognize the collection of the 1000th atmospheric sample by the vessel's deck officers. Operation Pacific Air was begun in 1986 to collect air samples on the ship's route between the U.S. West Coast and Auckland, New Zealand.

L. Waterman visited Palmer Station, operated by NSF, on January 10. The regular air sampling site was inspected, and a set of samples was collected by a U.S. Navy volunteer. Strategies for collecting samples when the wind was coming from directions other than the clean air sector and for expediting the return of samples to Boulder on both research and cruise ship calls were discussed. L. Waterman also visited the British Antarctic Survey station on Bird Island, South Georgia, on January 26. He made direct contacts with the BAS winter-over staff. They were provided with instructions on the use of the P³ air sampler and given a short-form manual and equipment diagrams. Nine cases of flasks accumulated from previous years of unsuccessful attempts to initiate the program were returned to Boulder. During February, as part of the return trip from Antarctica, L. Waterman visited flask sampling sites at Barbados, at the West Indies Laboratory (Teague Bay), and at St. Croix (U.S. Virgin Islands). A seminar was given for the West Indies Laboratory staff on the flask network CO₂ and CH₄ results. Finally, new sites were selected at St. David's Head and Southampton, Bermuda.

During March, T. Conway participated in the AGASP-III project based in Bodo, Norway. One-hundred eighty-six flask air samples were collected on six flights in the Arctic.

The samples were analyzed in Boulder for CO₂, CH₄, and CO. G. Herbert also participated in the AGASP-III project. He served as operations meteorologist for the Arctic haze sampling phase of this program.

E. Dutton traveled to Kwajalein in the Marshall Islands in March to establish a surface radiation monitoring site. He presented a paper entitled "An extraordinary site for surface radiation budget/satellite ground-truth studies" at the IAMAP 89 Fifth Scientific Assembly of the International Association of Meteorology and Atmospheric Physics, in Reading, England, held July 31-August 12.

The NOAA reference absolute cavity radiometer was taken to Ensenada, Mexico, in April by D. Nelson for a WMO-sanctioned regional comparison of pyrhelimeters. The NOAA instrument was one of a contingent of 10 U.S. cavity radiometers that participated. While at the comparison, he gave a short presentation on the current status of the U.S. Solar Radiation Network and the development and operation of the new Eppley automatic solar trackers.

B. Bodhaine participated in the International Conference on Global and Regional Environmental Atmospheric Chemistry in Beijing, China, May 2-11, and presented a paper entitled "Aerosol monitoring at Mauna Loa Observatory."

As part of U.S./U.S.S.R. Working Group VIII (Influence of Environmental Changes on Climate), B. Bodhaine, J. DeLuisi (U.S. Organizer), and D. Gillette participated in the First Soviet-American Symposium on Atmospheric Aerosols and Climate at the Institute of Experimental Meteorology, in Obninsk, U.S.S.R., held August 28-September 1. The purpose of this symposium was to formulate recommendations concerning what aerosol measurements should be made to help understand the effects of aerosols on climate. The meeting was attended by nine American scientists and numerous Soviet scientists. At the symposium, J. DeLuisi presented a paper entitled "Aerosol optical thickness measurements for climate modeling," and B. Bodhaine presented a paper entitled, "Background aerosol measurements at CMDL stations."

Following the Obninsk symposium, B. Bodhaine and D. Gillette traveled to Dushanbe, Tadzhikistan, U.S.S.R., to participate in the U.S.S.R./U.S. Desert Aerosol Experiment on September 3-9. This experiment was designed to study dust storms and desertification in southern U.S.S.R. Nine American and many Soviet scientists participated in the study.

At a Geneva meeting held October 19-21, 1988, the Joint Scientific Committee Working Group on Radiative Fluxes recommended that the World Climate Research Program (WCRP) establish a global baseline network of surface stations to measure the solar and terrestrial longwave fluxes to help meet the requirements for long-term data sets on global surface radiation balance components. The mission of this network would be to monitor long-term trends in radiation fluxes at the surface and to provide validation data for satellite determinations of the surface radiation budget.

The network would consist of 10-20 strategically located sites and would take advantage of existing national sites that meet established criteria. The WCRP requested J. DeLuisi's assistance to organize the network. At the WCRP Workshop on Surface Radiation Budget held at Wurzburg, Germany, October 30-November 3, 1989, a special session, chaired by J. DeLuisi, was held to establish the guidelines for a Baseline Surface Radiation Network (BSRN). A report containing the workshop's recommendations was written and circulated. It became the basis of the BSRN plan, which was issued later.

J. Elkins attended the Intergovernmental Panel on Climate Change (IPCC) meeting sponsored by the WMO and the United Nations Environment Program in Cambridge, Massachusetts, on October 19. He wrote the N₂O section for the IPCC report and was acknowledged as a contributor to *Climate Change, The IPCC Scientific Assessment*, Cambridge University Press, 1990.

Total ozone and Umkehr observations continued to be made with automated Dobson ozone spectrophotometers at the CMDL-foreign cooperative stations of Haute Provence, France; Lauder, New Zealand; and Perth, Australia. Similar observations were made with a manually operated Dobson instrument at Huancayo, Peru.

R. Evans traveled to MLO during the summer to set up a program for checking the state of calibration of World Standard Dobson Spectrophotometer no. 83 and to calibrate Japanese secondary Standard Dobson instrument no. 116.

During the summer of 1989, R. Grass optically aligned, electronically revamped, and calibrated Pretoria, South Africa, Dobson instrument no. 89. He also provided training to M. Zunkel of the South African Weather Bureau on the operation, maintenance, and calibration of Dobson instruments.

Surface ozone measurements began at a new AEROCE site,

Mace Head, Ireland. Similar observations continued in Barbados and Bermuda.

In July, B. Mendonca traveled to Budapest, Hungary, at the request of the Hungarian Government, to consult with the WMO on the development of a background air pollution monitoring network for Hungary. In December, he consulted with the Costa Rican Government and the WMO in San Jose, Costa Rica, about setting up baseline climate observatories.

At the invitation of the WMO, J. Peterson attended a working meeting in Geneva, Switzerland, May 19-26, to finalize publication of the World Climate Data Program Review of the Global Climate System for 1986-1988. During October 20-24, he presented a paper at a meeting on Monitoring and Assessment of Changing Composition of the Troposphere in Sofia, Bulgaria. He traveled to Taipei, Taiwan, to present an invited paper at the U.S.-Taiwan Bilateral Workshop on Long-Term Air Quality Changes and Their Climatic Impact, held November 18-19.

On February 4-April 20, members of the Nitrous Oxide and Halocarbons Group participated in the RITS 1989 cruise aboard the NOAA *R/V Discoverer* traveling across the central and eastern Pacific Ocean. The purpose of this international expedition was to measure N₂O, CFC-11, CFC-12, CFC-113, CH₃CCl₃, and CCl₄ in air and surface sea water, to measure N₂O at depth, and to collect flask samples for analysis of LEAPS gases between Seattle and the edge of the ice cap near Antarctica, and return. The cruise was divided into three major legs. T. Thompson helped install the equipment on the ship before the first leg. J. Butler and B. Halter ran the instruments on the first leg from Seattle to Easter Island. B. Halter continued on the second leg from Easter Island to Tahiti. C. Brunson joined the ship in Tahiti for the third and final leg of the cruise back to Seattle.

12. Publications and Presentations by CMDL Staff, 1989

- Anderson, S.M., A.C. Delany, F.C. Fehsenfeld, P.D. Goldan, C.E. Kolb, B.A. Ridley, and L.P. Steele, Status of chemical sensors for flux measurements, in *Global Tropospheric Chemistry, Chemical Fluxes in the Global Atmosphere*, edited by D.H. Lenschow and B.B. Hicks, pp. 47-68, National Center for Atmospheric Research, Boulder, CO, 1989.
- Andreae, M., A.C. Delany, S. Liu, J. Logan, L.P. Steele, H. Westberg, and R. Zika, Key aspects of species related to global biogeochemical cycles, in *Global Tropospheric Chemistry, Chemical Fluxes in the Global Atmosphere*, edited by D.H. Lenschow and B.B. Hicks, pp. 9-29, National Center for Atmospheric Research, Boulder, CO, 1989.
- Bodhaine, B.A., Aerosol monitoring at Mauna Loa Observatory, paper GII-8 presented at the International Conference on Global and Regional Environmental Atmospheric Chemistry, Beijing, China, May 3-10, 1989.
- Bodhaine, B.A., Background aerosol measurements at GMCC stations, paper presented at the First Soviet-American Symposium on Aerosols and Climate, Obninsk, U.S.S.R., August 28-September 1, 1989.
- Bodhaine, B.A., Barrow surface aerosol: 1976-1986, *Atmos. Environ.*, 23, 2357-2369, 1989.
- Bodhaine, B.A., South Pole aerosol measurements, *Ant. J. U. S.*, 24, 233-235, 1989.
- Bodhaine, B.A., N.C. Ahlquist, and R.C. Schnell, Three-wavelength nephelometer suitable for aircraft measurements of background aerosol scattering extinction coefficient, paper 3P.20 presented at the 1989 Annual Meeting of the American Association for Aerosol Research, Reno, NV, October 9-13, 1989.
- Bodhaine, B.A., E.G. Dutton, J.J. DeLuisi, G.A. Herbert, G.E. Shaw, and A.D.A. Hansen, Surface aerosol measurements at Barrow during AGASP II, *J. Atmos. Chem.*, 9, 213-224, 1989.
- Bridgman, H.A., R.C. Schnell, G.A. Herbert, B.A. Bodhaine, and S.J. Oltmans, Meteorology and haze structure during AGASP II, Part 2, Canadian Arctic flights, 13-16 April 1986, *J. Atmos. Chem.*, 9, 49-70, 1989.
- Butler, J.H., and J.W. Elkins, An automated headspace technique for the measurement of N_2O in water and sea water, paper presented at the Oceanography Society Inaugural Meeting, Monterey, CA, August 27-30, 1989.
- Butler, J.H., J.W. Elkins, T.M. Thompson, and K.B. Egan, Tropospheric and dissolved N_2O of the west Pacific and east Indian Oceans during the El Niño Southern Oscillation event of 1987, *J. Geophys. Res.*, 94(D12), 14,865-14,877, 1989.
- Conway, T.J., and L.P. Steele, Carbon dioxide and methane in the Arctic atmosphere, *J. Atmos. Chem.*, 9, 81-99, 1989.
- DeLuisi, J., Aerosol optical thickness measurements for climate modeling, paper presented at the First Soviet-American Symposium on Atmospheric Aerosols and Climate, Obninsk, U.S.S.R., August 28-September 1, 1989.
- DeLuisi, J.J., E.G. Dutton, G.L. Koenig, U.U. Longenecker, and P.J. Reddy, Zenith-sky cloud detection for automated Dobson Umkehr measurements, in *Ozone in the Atmosphere, Proceedings, Quadrennial Ozone Symposium 1988 and Tropospheric Ozone Workshop, Halkidiki, Greece*, edited by R.D. Bojkov and P. Fabian, pp. 736-738, A. Deepak, Hampton, VA, 1989.
- DeLuisi, J.J., D.U. Longenecker, C.L. Mateer, and D.J. Wuebbles, An analysis of northern middle-latitude Umkehr measurements corrected for stratospheric aerosols for 1979-1986, *J. Geophys. Res.*, 94(D7), 9837-9846, 1989.
- Dutton, E.G., J.J. DeLuisi, and R.D. Cess, An extraordinary site for surface radiation budget/satellite ground-truth studies, paper presented at the IAMAP 89 Fifth Scientific Assembly of the International Association of Meteorology and Atmospheric Physics, Reading, England, July 31-August 12, 1989.
- Dutton, E.G., J.J. DeLuisi, and G. Herbert, Shortwave aerosol optical depth measured on board the NOAA WP-3D, AGASP-II, April 1986, *J. Atmos. Chem.*, 9, 71-79, 1989.
- Dutton, E.G., R.S. Stone, and J.J. DeLuisi, South Pole surface radiation balance measurements April 1986 to February 1988, *NOAA Data Rep. ERL ARL-17*, 49 pp., NOAA Air Resources Laboratory, Boulder, CO, 1989.
- Elkins, J.W., Nitrous oxide and the ozone layer, paper presented at the University of Virginia, Department of Environmental Sciences, Charlottesville, VA, October 25, 1989.
- Elkins, J.W., Recent developments and controversies in atmospheric trace gas standards, presented at the Center for Analytical Chemistry Colloquium Series, NIST, Gaithersburg, MD, October 24, 1989.
- Elkins, J.W., Referee's report (ATLAS-WAS stratospheric nitrous oxide intercomparison), presented at the NASA Summer Science Meeting, Lake Tahoe, CA, July 17, 1989.
- Elkins, J.W., Sources and sinks for atmospheric nitrous oxide, paper presented at NASA Ames Research Center, Moffett Field, CA, August 15, 1989.
- Elkins, J.W., The state of the research for atmospheric nitrous oxide, presented at the Intergovernmental Panel for Climatic Change (IPCC), Cambridge, MA, October 19, 1989.
- Elkins, J.W., Techniques for the preparation of gas standards for atmospheric CCl_4 , paper presented at the NOAA/ARL Idaho Springs Laboratory, Idaho Falls, ID, April 20, 1989.
- Elkins, J.W., Trends and distributions of atmospheric nitrous oxide, presented at the Atmospheric Chemistry Seminar, Harvard University, Department of Earth and Planetary Sciences, Cambridge, MA, October 20, 1989.
- Elkins, J.W., and T.M. Thompson, Measurements of nitrous oxide (N_2O), trichlorofluoromethane (CFC-11), and dichlorodifluoromethane (CFC-12) at Niwot Ridge, Colorado, since 1977, paper presented at the Front Range Branch AGU Conference, Colorado School of Mines, Golden, CO, February 12-14, 1989.
- Elkins, J.W., T.M. Thompson, B. Hall, K.B. Egan, and J.H. Butler, NOAA/GMCC halocarbons and nitrous oxide measurements at the South Pole, *Ant. J. U. S.*, 23(5), 176-177, 1988.
- Evans, R.D., G.L. Koenig, W.D. Komhyr, J. Easson, and P. Marché, Umkehr observations at five automated Dobson spectrophotometer stations in 1986 and 1987, in *Ozone in the Atmosphere, Proceedings, Quadrennial Ozone Symposium 1988 and Tropospheric Ozone Workshop, Halkidiki, Greece*, edited by R.D. Bojkov and P. Fabian, pp. 151-154, A. Deepak, Hampton, VA, 1989.
- Fiocco, G., W.D. Komhyr, and D. Fuá, Is ozone destroyed during the Antarctic polar night in the presence of polar stratospheric clouds? *Nature*, 341(6241), 426-427, 1989.
- Franchois, P.R., G. Koenig, R.D. Evans, and W.D. Komhyr, Comparison of ECC ozonesonde and Umkehr profiles at Boulder, Colorado, 1985-1987, and Mauna Loa, Hawaii, 1985-1987, in *Ozone in the Atmosphere, Proceedings, Quadrennial Ozone Symposium 1988 and Tropospheric Ozone Workshop, Halkidiki, Greece*, edited by R.D. Bojkov and P. Fabian, pp. 155-159, A. Deepak, Hampton, VA, 1989.
- Grass, R.D., and W.D. Komhyr, Traveling standard lamp calibration checks of Dobson ozone spectrophotometers during 1985-1987, in *Ozone in the Atmosphere, Proceedings, Quadrennial Ozone Symposium 1988 and Tropospheric Ozone Workshop, Halkidiki, Greece*, edited by R.D. Bojkov and P. Fabian, pp. 144-146, A. Deepak, Hampton, VA, 1989.
- Hansen, A.D.A., B.A. Bodhaine, T.J. Conway, and J.D. Kahl, Long-range transport of combustion plumes across the Arctic: Preservation of signature ratios of aerosol black carbon, CO_2 ,

- and CH₄, paper 4D.3 presented at the 1989 Annual Meeting of the American Association for Aerosol Research, Reno, NV, October 9-13, 1989.
- Hansen, A.D.A., T.J. Conway, L.P. Steele, B.A. Bodhaine, K.W. Thoning, P. Tans, and T. Novakov, Correlations among combustion effluent species at Barrow, Alaska: Aerosol black carbon, carbon dioxide, and methane, *J. Atmos. Chem.*, 9, 283-299, 1989.
- Herbert, G.A., J.M. Harris, and B.A. Bodhaine, Atmospheric transport during AGASP-II: The Alaskan flights (April 2-10, 1986), *Atmos. Environ.*, 23(11), 2521-2535, 1989.
- Herbert, G.A., R.C. Schnell, H.A. Bridgman, B.A. Bodhaine, S.J. Oltmans, and G.E. Shaw, Meteorology and haze structure during AGASP-II, Part 1, Alaskan Arctic flights, 2-10 April 1986, *J. Atmos. Chem.*, 9, 17-48, 1989.
- Kahl, J.D., J.M. Harris, G.A. Herbert, and M.P. Olson, Intercomparison of three long-range trajectory models applied to Arctic haze, *Tellus*, 41b, 524-536, 1989.
- Kolb, C.E., F.C. Fehsenfeld, L.P. Steele, and P.D. Goldan, Flux measurement program plan, in *Global Tropospheric Chemistry, Chemical Fluxes in the Global Atmosphere*, edited by D.H. Lenschow and B.B. Hicks, pp. 69-82, National Center for Atmospheric Research, Boulder, CO, 1989.
- Komhyr, W.D., R.D. Grass, R.D. Evans, and R.K. Leonard, Results of international Dobson spectrophotometer and Brewer spectrometer intercomparisons, Arosa, Switzerland, 1986, in *Ozone in the Atmosphere, Proceedings, Quadrennial Ozone Symposium 1988 and Tropospheric Ozone Workshop*, Halkidiki, Greece, edited by R.D. Bojkov and P. Fabian, pp. 776-779, A. Deepak, Hampton, VA, 1989.
- Komhyr, W.D., R.D. Grass, and R.K. Leonard, Calibration of primary standard Dobson spectrophotometer no. 83 and total ozone trends at Mauna Loa Observatory, Hawaii, and American Samoa, South Pacific, in *Ozone in the Atmosphere, Proceedings, Quadrennial Ozone Symposium 1988 and Tropospheric Ozone Workshop*, Halkidiki, Greece, edited by R.D. Bojkov and P. Fabian, pp. 85-87, A. Deepak, Hampton, VA, 1989.
- Komhyr, W.D., R.D. Grass, and R.K. Leonard, Dobson spectrophotometer 83: A standard for total ozone measurements, 1962-1987, *J. Geophys. Res.*, 94(D7), 9847-9861, 1989.
- Komhyr, W.D., R.D. Grass, P.J. Reitelbach, S.E. Kuester, P.R. Franchois, and M.L. Fanning, Total ozone, ozone vertical distributions, and stratospheric temperature at South Pole, Antarctica, in 1986 and 1987, *J. Geophys. Res.*, 94(D9), 11,429-11,436, 1989.
- Komhyr, W.D., T.B. Harris, L.S. Waterman, J.F.S. Chin, and K.W. Thoning, Atmospheric carbon dioxide at Mauna Loa Observatory, 1, NOAA Global Monitoring for Climatic Change measurements with a nondispersive infrared analyzer, 1974-1985, *J. Geophys. Res.*, 94, 8533-8547, 1989.
- Komhyr, W.D., J.A. Lathrop, V.N. Arbutova, V.V. Khatatov, P.G. Nureyev, V.V. Rudakov, and I.V. Zamyshlyev, ECC ozonesonde observations at Mirny, Antarctica in 1988, *NOAA Data Rep. ERL ARL-19*, 125 pp., NOAA Air Resources Laboratory, Silver Spring, MD, 1989.
- Komhyr, W.D., J.A. Lathrop, R.W. Poston, and T.O. Mullen, ECC ozonesonde observations at South Pole, Antarctica, during 1988, *NOAA Data Rep. ERL ARL-18*, 277 pp., NOAA Air Resources Laboratory, Silver Spring, MD, 1989.
- Komhyr, W.D., S.J. Oltmans, P.R. Franchois, W.F. Evans, and W.A. Matthews, The latitudinal distribution of ozone to 35 km altitude from ECC ozonesonde observations, *Ozone in the Atmosphere, Proceedings, Quadrennial Ozone Symposium 1988 and Tropospheric Ozone Workshop*, edited by R.D. Bojkov and P. Fabian, pp. 147-150, A. Deepak, Hampton, VA, 1989.
- Komhyr, W.D., S.J. Oltmans, R.D. Grass, P.R. Franchois, and R.K. Leonard, Changes in total ozone and ozone vertical distributions at South Pole, Antarctica, 1962-1987, *Ozone in the Atmosphere, Proceedings, Quadrennial Ozone Symposium 1988 and Tropospheric Ozone Workshop*, edited by R.D. Bojkov and P. Fabian, pp. 28-31, A. Deepak, Hampton, VA, 1989.
- Lowe, D.C., C. Brenninkmeijer, M. Manning, S.C. Tyler, E. Dlugokencky, P. Steele, and P. Lang, Carbon isotopic composition of atmospheric methane, paper A21A-4 presented at the Fall AGU Meeting, San Francisco, CA, December 4-8, *EOS*, 70(43), 1017, 1989.
- Margitan, J.J., G.A. Brothers, E.V. Browell, D. Cariolle, M.T. Coffey, J.C. Farman, C.B. Farmer, G.L. Gregory, J.W. Harder, D.J. Hofmann, W. Hypes, S. Ismail, R.O. Jakoubek, W. Komhyr, S. Kooi, A.J. Krueger, J.C. Larsen, W. Mankin, M.P. McCormick, G.H. Mount, M.H. Proffitt, A.R. Ravishankara, A.L. Schmeltekopf, W.L. Starr, G.C. Toon, A. Torres, A.F. Tuck, A. Wahner, and I. Watterson, Intercomparison of ozone measurements over Antarctica, *J. Geophys. Res.*, 94(D14), 16,557-16,569, 1989.
- Matthews, W.A., W.D. Komhyr, and P.R. Franchois, Vertical distribution and variation in atmospheric ozone over Lauder, New Zealand, in *Ozone in the Atmosphere, Proceedings, Quadrennial Ozone Symposium 1988 and Tropospheric Ozone Workshop*, edited by R.D. Bojkov and P. Fabian, pp. 85-87, A. Deepak, Hampton, VA, 1989.
- McPeters, R.D., and W.D. Komhyr, Long-term changes in SBUV/TOMS relative to the world primary standard Dobson instrument, in *Ozone in the Atmosphere, Proceedings, Quadrennial Ozone Symposium 1988 and Tropospheric Ozone Workshop*, edited by R.D. Bojkov and P. Fabian, pp. 265-267, A. Deepak, Hampton, VA, 1989.
- Oltmans, S.J., W.D. Komhyr, P.R. Franchois, and W.A. Matthews, Tropospheric ozone: Variations from surface and ECC ozonesonde observations, in *Ozone in the Atmosphere, Proceedings, Quadrennial Ozone Symposium 1988 and Tropospheric Ozone Workshop*, edited by R.D. Bojkov and P. Fabian, pp. 539-543, A. Deepak, Hampton, VA, 1989.
- Oltmans, S.J., W.E. Raatz, and W.D. Komhyr, On the transfer of stratospheric ozone into the troposphere near the North Pole, *J. Atmos. Chem.*, 9, 245-254, 1989.
- Oltmans, S.J., R.C. Schnell, P.J. Sheridan, R.E. Peterson, S.M. Li, J.W. Winchester, P.P. Tans, W.T. Sturges, J.D. Kahl, and L.A. Barrie, Seasonal surface ozone and filterable bromine relationship in the high Arctic, *Atmos. Environ.*, 23(11), 2431-2441, 1989.
- Oltmans, S.J., P.J. Sheridan, R.C. Schnell, R.E. Peterson, J.W. Winchester, L.A. Barrie, J.D. Kahl, and W.D. Komhyr, Springtime ozone fluctuations at high Arctic latitudes and their possible relationship to atmospheric bromine, in *Ozone in the Atmosphere, Proceedings, Quadrennial Ozone Symposium 1988 and Tropospheric Ozone Workshop*, edited by R.D. Bojkov and P. Fabian, pp. 498-501, A. Deepak, Hampton, VA, 1989.
- Peterson, J.T., NOAA long-term trace gas monitoring, paper presented at the U.S.-Taiwan Bilateral Workshop on Long-Term Air Quality Changes and Their Climatic Impact, Taipei, Taiwan, November 18-19, 1989.
- Sachse, G.W., K.B. Bartlett, R.C. Harriss, G.F. Hill L.O. Wade, L.G. Burney, J.E. Collins, Jr., and L.P. Steele, Airborne measurements of methane and carbon monoxide during ABLE-3A, paper A11A-04 presented at the Spring AGU Meeting, Baltimore, MD, May 7-23, *EOS*, 70(15), 282, 1989.
- Schnell, R.C., and B.A. Bodhaine, The Arctic basin atmospheric chemistry report, paper 2D.1 presented at the 1989 Annual Meeting of the American Association for Aerosol Research, Reno, NV, October 9-13, 1989.
- Schnell, R.C., T.B. Watson, and B.A. Bodhaine, NOAA WP-3D instrumentation and flight operations on AGASP-II, *J. Atmos. Chem.*, 9, 1-16, 1989.
- Steele, L.P., T.J. Conway, L.S. Waterman, and P.M. Lang, The NOAA/GMCC measurements of CH₄ and CO₂ from air samples collected at Cape Grim, in *Baseline 1987*, edited by B.W. Forgan and G.P. Ayers, pp. 48-50, Department of Administrative Services,

- Bureau of Meteorology, in cooperation with CSIRO, Division of Atmospheric Research, Aspendale, Australia, 1989.
- Tans, P.P., T.J. Conway, and T. Nakazawa, Latitudinal distribution of the sources and sinks of atmospheric carbon dioxide derived from surface observations and an atmospheric transport model, *J. Geophys. Res.*, *94*, 5151-5172, 1989.
- Thoning, K.W., T.J. Conway, P.P. Tans, and J.T. Peterson, Recent atmospheric CO₂ growth rates, Third International Conference on Analysis and Evaluation of Atmospheric CO₂ Data Present and Past, Hinterzarten, Federal Republic of Germany, October 16-20, 1989, *WMO Environmental Pollution Monitoring and Research Progress Report No. 59*, p. 237, World Meteorological Organization, Geneva, Switzerland, 1989.
- Thoning, K.W., P.P. Tans, and W.D. Komhyr, Atmospheric carbon dioxide at Mauna Loa Observatory, 2, Analysis of NOAA GMCC Data, 1974-1985, *J. Geophys. Res.*, *94(D6)*, 8549-8565, 1989.
- Thoning, K.W., P.P. Tans, T.J. Conway, and L.S. Waterman, Indication of a decrease in the amplitude of the CO₂ seasonal cycle, Third International Conference on Analysis and Evaluation of Atmospheric CO₂ Data Present and Past, Hinterzarten, Federal Republic of Germany, October 16-20, 1989, *WMO Environmental Pollution Monitoring and Research Progress Report No. 59*, p. 236, World Meteorological Organization, Geneva, Switzerland, 1989.
- Waterman, L.S., D.W. Nelson, W.D. Komhyr, T.B. Harris, K.W. Thoning, and P.P. Tans, Atmospheric carbon dioxide measurements at Cape Matatula, American Samoa, 1976-1987, *J. Geophys. Res.*, *94(D12)*, 14817-14829, 1989.

13. Acronyms and Abbreviations

ACR	active cavity radiometer
ADVR	Advanced Very-High-Resolution Radiometer
AEM	analytical electron microscope
AEROCE	Atmosphere/Ocean Chemistry Experiment
AES	Atmospheric Environment Service, Canada
AGASP	Arctic Gas and Aerosol Sampling Program
AGL	above ground level
AGU	American Geophysical Union
ALIVE	Atmospheric Lidar Validation Experiment
ALT	Alert Observatory, Canada
ANL	Argonne National Laboratory
ANSTO	Australian Nuclear Science and Technology Organization
AOML	Atlantic Oceanographic and Meteorological Laboratory, Miami, Florida (ERL)
AQG	Air Quality Group, Boulder, Colorado (ARL)
ARL	Air Resources Laboratory, Silver Spring, Maryland (ERL)
ARM	Aerosols and Radiation Monitoring Group, Boulder, Colorado (CMDL)
ASCS	Alaska Soil Conservation Service
ASL	above sea level
ATS	Application Technology Satellite
BAO	Boulder Atmospheric Observatory
BAS	British Antarctic Survey
BRW	Barrow Observatory, Barrow, Alaska (CMDL)
CAF	Clean Air Facility
CAMS	Control and Monitoring System
CFC	chlorofluorocarbon
CFC-11	trichlorofluoromethane
CFC-12	dichlorodifluoromethane
CIRES	Cooperative Institute for Research in Environmental Sciences, University of Colorado, Boulder, Colorado
CMDL	Climate Monitoring and Diagnostics Laboratory, Boulder, Colorado (ERL) (formerly GMCC)
CN	condensation nuclei
CNC	condensation nucleus counter
COR	correlation coefficient
CSI	Columbia Scientific, Inc.
CSIRO/DAR	Commonwealth Scientific and Industrial Research Organization/Division of Atmospheric Research, Australia
CSU	Colorado State University
DB	direct-beam [irradiance]
DEW	distant early warning
DMS	dimethyl sulfide
DNA	Deoxyribonucleic acid
DOT	Department of Transportation
EPA	Environmental Protection Agency
DSIR	Department of Scientific and Industrial Research, New Zealand
DU	Dobson units
ECC	electrochemical concentration cell
ECD	electron capture detector
EC-GC	electron capture-gas chromatograph
ECMWF	European Centre for Medium Range Weather Forecasts
EKTO	[a commercial name for a prefabricated building]
EML	Environmental Measurements Laboratory
ENSO	El Niño/Southern Oscillation
EPA	Environmental Protection Agency
ERBE	Earth Radiation Budget Experiment
ERL	Environmental Research Laboratories, Boulder, Colorado (NOAA)
FAST	forward alpha scattering techniques
FID	flame ionization detector

FS	Forest Service
FTIR	Fourier transform infrared (spectroscopy)
GC	gas chromatograph
G.E.	General Electric
GSFC	Goddard Space Flight Center
GLOBE	Global Backscatter Experiment
GMCC	Geophysical Monitoring for Climatic Change, Boulder, Colorado (ARL) (now CMDL)
HASL	Health and Safety Laboratory
HP	Hewlett-Packard
HST	Hawaii standard time
IBM	International Business Machines
IC	ion chromatography
IMPROVE	Interagency Monitoring of Protected Visual Environments
IR	infrared
ISWS	Illinois State Water Survey
JPL	Jet Propulsion Laboratory
LEAPS	Low Electron Attachment Potential Species
LST	local standard time
LW	longwave
LWD	longwave downward irradiance
LWRF	longwave radiative forcing
MLO	Mauna Loa Observatory, Hawaii (CMDL)
MLOPEX	MLO Photochemical Experiment
MSL	mean sea level
NADP	National Atmospheric Deposition Program
NASA	National Aeronautics and Space Administration
NCAR	National Center for Atmospheric Research
NCS	Navigation Consulting Services
NDIR	non-dispersive infrared analyzer
NIH	National Institutes of Health
NIP	normal incidence pyrheliometer
NIST	National Institute for Standards and Technology (formerly NBS)
NMC	National Meteorological Center
NOAA	National Oceanic and Atmospheric Administration
NOAH	Nitrous Oxide And Halocarbons Group, Boulder, Colorado (CMDL)
NPS	National Park Service
NRBS	non-Rayleigh backscatter
NSF	National Science Foundation
NSO	National Solar Observatory
NWR	Niwot Ridge, Colorado
NWS	National Weather Service
OGC	Oregon Graduate Center (now OGIST)
OGIST	Oregon Graduate Institute of Science and Technology (formerly OGC)
PBL	planetary boundary layer
PC	personal computer
PDB	pee dee belemnite
PESA	proton elastic scattering analysis
PIXE	Proton-Induced X-ray Emission
PMEL	Pacific Marine Environmental Laboratory, Seattle, Washington (ERL)
PMOD	Physikalisch-Meteorologisches Observatorium Davos [World Radiation Center]
PMT	photomultiplier tube
PRC	People's Republic of China
PSC	Polar stratospheric cloud
PSI	Paul Scherrer Institute, Switzerland
PTFE	polytetrafluoroethylene (Teflon)
P ³	Portable Pressurizer Pack (air sampler)
RITS	Radiatively Important Trace Species
RSD	residual standard deviation

SAGE	Stratospheric Aerosol and Gas Experiment
SASP	Surface Air Sampling Program
SBUV	solar backscattered ultraviolet (satellite ozone instrument)
SC	sky cover
SEAREX	Sea-Air Exchange Experiment
SEASPAN	SEAREX South Pacific Aerosol Network
SERI	Solar Energy Research Institute
SIO	Scripps Institution of Oceanography
SMO	Samoa Observatory, American Samoa (CMDL)
SOI	Southern Oscillation Index
SOLRAD	Solar Radiation
SPO	South Pole Observatory, Antarctica (CMDL)
SRF	Solar Radiation Facility (CMDL)
SRM	standard reference material
SUNYA	State University of New York at Albany
TECO	Thermal Electron Company
TEM	transmission electron microscope
TOMS	Total Ozone Mapping Spectrometer
TSI	Thermo Systems Incorporated
TSL	Technical Services Laboratory
TSP	total suspended particulate
UCI	University of California, Irvine
URAS	[a commercial CO ₂ analyzer]
URI	University of Rhode Island
USDA	United States Department of Agriculture
USGS	United States Geological Survey
UT	universal time
UV	ultraviolet
UVB	ultraviolet B band
WCRP	World Climate Research Program
WMO	World Meteorological Organization
WPL	Wave Propagation Laboratory, Boulder, Colorado (ERL)

